Newcastle University

Institute for Cell and Molecular Biosciences

Characterization of the Cell Division Factor ZapB of *Escherichia coli*

Elisa Galli

A thesis submitted for the degree of Doctor of Philosophy

August 2011

Abstract

Bacterial cell division relies on the formation and contraction of the Z-ring, coordinated and regulated by a dynamic protein complex called divisome.

Here, we show that ZapB, a newly identified cell division factor in *Escherichia coli*, is recruited to the division site in the early stages of Z-ring assembly by ZapA. Inactivation or overproduction of ZapA caused ZapB delocalization and diffusion. Bacterial two-hybrid and *in vitro* assays showed that ZapB interacts directly with ZapA and, through it, with FtsZ and that the three proteins together can form a high-molecular-weight complex.

Furthermore, during the cell cycle ZapB closely followed FtsZ dynamic localization but interestingly, using high-resolution 3D reconstruction microscopy, we found that it formed a ring located on the inside of the Z-ring, consistently in all cells in consecutive cell division events. Only in the absence of the bacterial actin homologue MreB, ZapB was not able to constrict ahead of FtsZ and instead co-localized seemingly perfectly with the Z-ring.

Morphological analysis of cells carrying a *zapB* deletion and the *ftsZ84* allele exhibited a synthetic detrimental phenotype and cell division defects. A model in which ZapB further increases the lateral association of FtsZ filaments by cross-linking ZapA molecules bound to adjacent FtsZ filaments is supported by light scattering assays and analysis of structures formed by FtsZ-ZapA-ZapB using electron microscopy.

Surprisingly, ZapB seemed to be active in cell division in the absence of ZapA raising the possibility that ZapB might have a secondary ZapA-independent function.

Acknowledgements

First, I would like to thank my supervisor, Professor Kenn Gerdes, for his support, guidance and enthusiasm.

I would also like to thank all the people I've met in Newcastle, coming and going from the lab during the last four years. I've learnt something from each one of you.

Then, how can I forget my support group of papere! We live in different continents and barely see each other once a year, but I always felt you beside me, just a click away. Thanks.

Infine, vorrei ringraziare la mia famiglia per aver sempre sostenuto le mie scelte ed essermi stata vicina durante questo lungo cammino.

Table of Contents

Abbreviations

aa, amino acids

Amp, ampicillin

Ara, arabinose

aTc, anhydrotetracycline

AU, arbitrary unit

B. pertussis, *Bordetella pertussis*

BSA, bovine serum albumin

B. subtilis, *Bacillus subtilis*

BTH, bacterial two-hybrid

C. crescentus, *Caulobacter crescentus*

CAA, casamino acids

Cml, chloramphenicol

DAPI, 4,6-diamidino-2-phenylindole

dH_2O, deionised water

DNA, deoxyribonucleic acid

dNTP, deoxyribonucleotide triphosphate

DTT, dithiothreitol

E. coli, *Escherichia coli*

ECT, electron cryotomography

EDTA, ethylenediaminetetraacetic acid

e.g., *exempli gratia* (for example)

et al., *et alii* (and others)

FP, fluorescent protein

FPALM, fluorescence photoactivation localization microscopy

FRAP, fluorescence recovery after photobleaching

fts, filament-forming temperature-sensitive

GFP, green fluorescent protein

GDP, guanosine diphosphate

GTP, guanosine triphosphate

HEPES, 4-(2-Hydroxyethyl)piperazine-1-ethanesulfonic acid

HMW, high molecular weight

IPTG, isopropyl-β-D-1-thiogalactopyranoside

Kan, kanamycin

kDa, kilo Dalton

LB, Luria-Bertani broth

min, minute

MM, minimal medium

M. tuberculosis, *Mycobacterium tuberculosis*

MW, molecular weight

n, number

NA, nutrient agar

ND, no data

NO, nucleoid occlusion

OD_{450}, optical density measured at a wavelength of 450 nm

oxyTc, oxytetracycline

P. aeruginosa, *Pseudomonas aeruginosa*

PAGE, polyacrylamide gel electrophoresis

PALM, photoactivated localization microscopy

PBP, penicillin-binding protein

PBS, phosphate buffered saline solution

PCR, polymerase chain reaction

P_i, inorganic phosphate

PIPES, piperazine-N,N'-bis(ethanesulfonic acid)

RNA, ribonucleic acid

rpm, revolutions per minute

SAP, Shrimp Alkaline Phosphatase

SDS, sodium dodecyl sulfate

sec, second

S. aureus, *Staphylococcus aureus*

S. elongatus, Synechococcus elongatus

S. flexneri, *Shigella flexneri*

S. pneumoniae, *Streptococcus pneumoniae*

STED, stimulated emission depletion

STORM, stochastic optical reconstruction microscopy

TAE, Tris-acetate-EDTA

Tc, tetracycline

TEM, transmission electron microscopy

tol, m-toluic acid

Tris-HCl, tris(hydroxymethyl)aminomethane hydrochloride

ts, temperature sensitive

U, unit

UV, ultraviolet

vs, versus

wt, wild-type

X-Gal, 5-bromo-4-chloro-3-indolyl-β-D-galactopyranoside

YFP, yellow fluorescent protein

3D, three-dimensional

Chapter 1

Introduction

1.1 Bacterial cell division

Cell division is a highly regulated morphological process involving topological and temporal coordination of cell elongation, chromosome replication and segregation, selection of the division site and cell constriction, culminating in the production of two equal-sized daughter cells.

In bacteria, such as *Escherichia coli*, cell division is achieved by a macromolecular machinery, called the divisome, containing at least 12 proteins (Vicente and Rico, 2006; Adams and Errington, 2009). This dynamic protein complex is composed of cytoplasmic, inner membrane and periplasmic proteins that localize into a ring at the division site in a regulated and concerted manner (Goehring and Beckwith, 2005; Vicente and Rico, 2006). Conditional mutants unable to septate at non-permissive conditions (usually high temperature) have been employed to identify genes involved in cell division, these mutations were called *fts*, for filament-forming temperature-sensitive (Hirota *et al.*, 1968). At first, FtsZ polymerizes in a ring-like structure, known as Z-ring, underneath the cytoplasmic membrane at the division site (Bi and Lutkenhaus, 1991). In *E. coli*, FtsZ polymers are stabilized and tethered to the membrane by FtsA and ZipA (Pichoff and Lutkenhaus, 2002). After the formation of the Z-ring the downstream proteins, involved in the dynamics and maturation of the Z-ring and in the late stages of cell division and constriction, are recruited into the septal ring in an almost linear pathway (FtsZ>FtsA/ZipA/ZapA/ZapC>FtsE/FtsX>FtsK>FtsQ>FtsL/FtsB>FtsW>FtsI>FtN> AmiC>EnvC) (Aarsman *et al.*, 2005; Goehring and Beckwith, 2005). Ten of these proteins are essential (FtsZ, A, B, I, K, L, N, Q, W and ZipA) (de Boer, 2010) and cells deprived of one of them fail to septate forming long filaments.

Bacteria share a common division machinery and the core of the division apparatus is well conserved among all of them (Vicente *et al.*, 2006). Hereafter, the *E. coli* cell division components are discussed, with a focus on FtsZ, the early cell division proteins and those involved in division site selection, with particular attention paid to the negative and positive regulators of FtsZ assembly. The late cell division components of the *E. coli* division machinery and cell division regulators are also briefly presented. A parallel with the Gram-positive *Bacillus subtilis* has been outlined where possible.

1.2 FtsZ and the Z-ring

FtsZ is the most important factor in bacterial cell division: it is highly conserved in the major groups of Bacteria and is also present in a subset of Archaea and in chloroplasts and mitochondria of primitive eukaryotes (Margolin, 2005; Adams and Errington, 2009).

FtsZ is the first division protein to localize at mid-cell where it forms a ring-like structure that acts as a scaffold for the recruitment of subsequent division factors and the assembly of the divisome (Bi and Lutkenhaus, 1991; Addinall and Lutkenhaus, 1996; Adams and Errington, 2009).

The tertiary structure of FtsZ (Fig. 1.1A) has been solved: it consists of two globular domains divided by a highly conserved central core helix that makes it very similar to the three-dimensional structure of tubulin (Lowe and Amos, 1998; Adams and Errington, 2009). The N-terminal globular domain contains a variable N-terminal segment, a nucleotide-binding site and a glycine-rich loop, GGGTGTG, which is known as the tubulin signature motif. The C-terminal globular domain contains the catalytic T7 loop and a C-terminal peptide essential for interactions with several division proteins, such as FtsA and ZipA (Lowe and Amos, 1998; Margolin, 2005; Adams and Errington, 2009). Like tubulin, FtsZ is a self-activating GTPase (de Boer *et al.*, 1992; RayChaudhuri and Park, 1992; Mukherjee *et al.*, 1993). When it assembles in a protofilament, the C-terminal globular domain of an FtsZ monomer binds to the N-terminal globular domain of the subunit below, bringing the T7 loop of the new subunit into contact with the GTP pocket of the subunit beneath, leading to activation of the GTPase activity. Therefore, FtsZ GTPase activity depends on the head-to-tail association of FtsZ monomers in linear polymers (Fig. 1.1B) (Mukherjee and Lutkenhaus, 1994; Scheffers *et al.*, 2002; Oliva *et al.*, 2004; Adams and Errington, 2009; Erickson *et al.*, 2010).

In *E. coli*, FtsZ single-stranded protofilaments can associate laterally forming bundles or sheets and their assembly can be induced by Ca^{2+} (Yu and Margolin, 1997; Lowe and Amos, 1999; Jaiswal and Panda, 2009) or molecular crowding agents (Gonzalez *et al.*, 2003; Popp *et al.*, 2009) or other cell division factors such as ZipA (RayChaudhuri, 1999), ZapA (Gueiros-Filho and Losick, 2002; Low *et al.*, 2004; Small *et al.*, 2007; Mohammadi *et al.*, 2009) and ZapC (Durand-Heredia *et al.*, 2011; Hale *et al.*, 2011).

FtsZ polymerization depends on GTP binding and, accordingly, FtsZ protofilaments disassemble *in vitro* in the absence of available GTP (Mukherjee and Lutkenhaus, 1994; Mukherjee and Lutkenhaus, 1998), even though after hydrolysis GDP allows the formation of curved filaments (Lu *et al.*, 2000; Huecas and Andreu, 2003). *In vitro* studies have shown that in steady state FtsZ protofilaments are mainly bound to GTP (Romberg and Mitchison, 2004) and the abundance of GTP in the cytoplasm as well as the fact that the nucleotide-binding pocket is accessible to the cytoplasm suggest that GTP hydrolysis, and not GTP binding, is the rate-limiting step in the FtsZ protofilament assembly cycle (Oliva *et al.*, 2004; Adams and Errington, 2009).

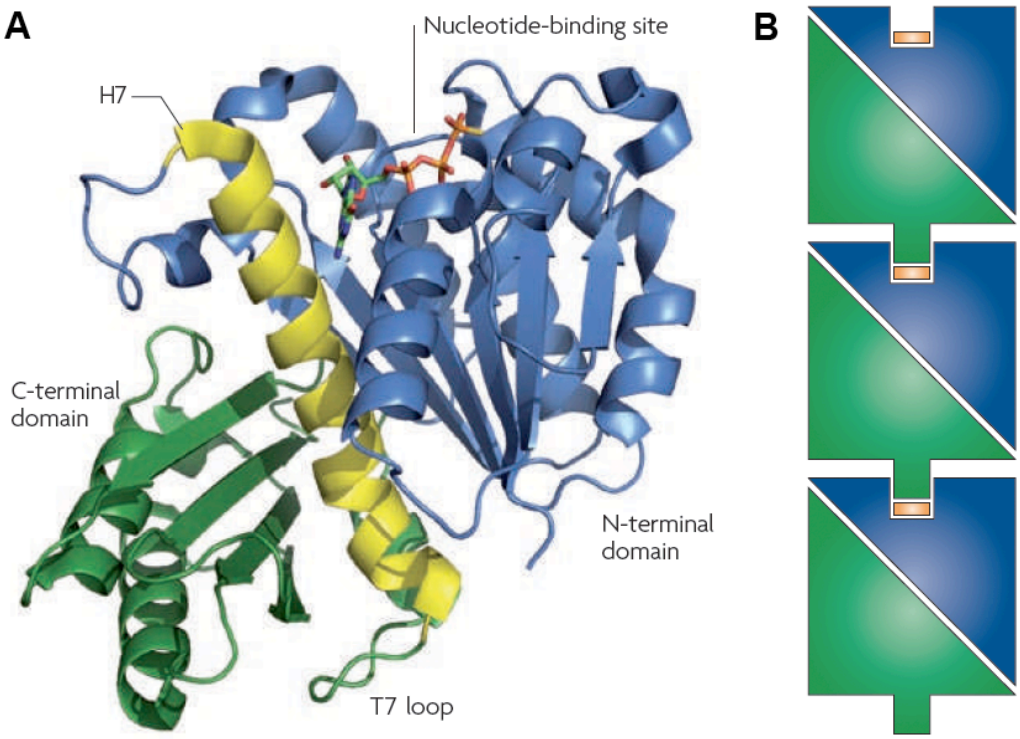

Fig. 1.1 FtsZ structure

A. The crystal structure of a *B. subtilis* FtsZ monomer bound to GTP-γS. **B.** Head-to-tail association of FtsZ monomers in linear polymers. In orange the nucleotide-binding site (Adams and Errington, 2009).

GTP hydrolysis is not required for protofilament formation (Mukherjee and Lutkenhaus, 1998; Chen and Erickson, 2005), but it promotes polymer disassembly and a constant exchange of FtsZ subunits (Chen and Erickson, 2005). Indeed, the Z-

ring is a highly dynamic structure and *in vivo* subunit turnover in a protofilament at steady state is very fast, with a half-time in the order of ~8 seconds (Stricker *et al.*, 2002; Anderson *et al.*, 2004). In a cell, only ~30% of the total FtsZ molecules are found in the Z-ring (Stricker *et al.*, 2002; Anderson *et al.*, 2004), the remaining molecules forming a dynamic helical-like structure along the cell (Thanedar and Margolin, 2004; Peters *et al.*, 2007). Once a subunit in the protofilaments has hydrolyzed its GTP, it dissociates from the polymer and is rejuvenated in the cytoplasm to its active state by binding GTP (Chen and Erickson, 2009; Erickson *et al.*, 2010). FRET analyses suggested that there are two mechanisms responsible for subunit exchange in polymers and contribute equally to the subunit turnover: one requires GTP hydrolysis and exchange of FtsZ-GDP subunits with FtsZ-GTP in the cytoplasm and the other replacement of FtsZ-GTP monomers from the extremities of protofilaments without GTP hydrolysis (Chen and Erickson, 2009; Erickson *et al.*, 2010).

Interestingly, even if FtsZ protofilaments are only one subunit thick, they display cooperative assembly (Romberg *et al.*, 2001; Caplan and Erickson, 2003; Chen and Erickson, 2005) and it has been suggested that a monomer isomerization step could be the conformational change producing cooperativity (Huecas *et al.*, 2008; Miraldi *et al.*, 2008; Adams and Errington, 2009).

1.3 Selection of the division site

The selection of the correct division site at mid-cell between two segregated chromosomes must be tightly regulated to prevent aberrant septation. Therefore, Z-ring positioning is coordinated by the combination of two negative regulatory systems: the Min system and the nucleoid occlusion (NO) (Fig. 1.2) (Errington *et al.*, 2003; Barak and Wilkinson, 2007; Bramkamp and van Baarle, 2009).

Cells remain viable in the absence of only one of these two systems, whereas inactivation of both of them is synthetically lethal. Indeed, in *E. coli*, the nucleoid occlusion factor SlmA was identified in a screening for factors synthetically lethal with a defective Min system (Bernhardt and de Boer, 2005).

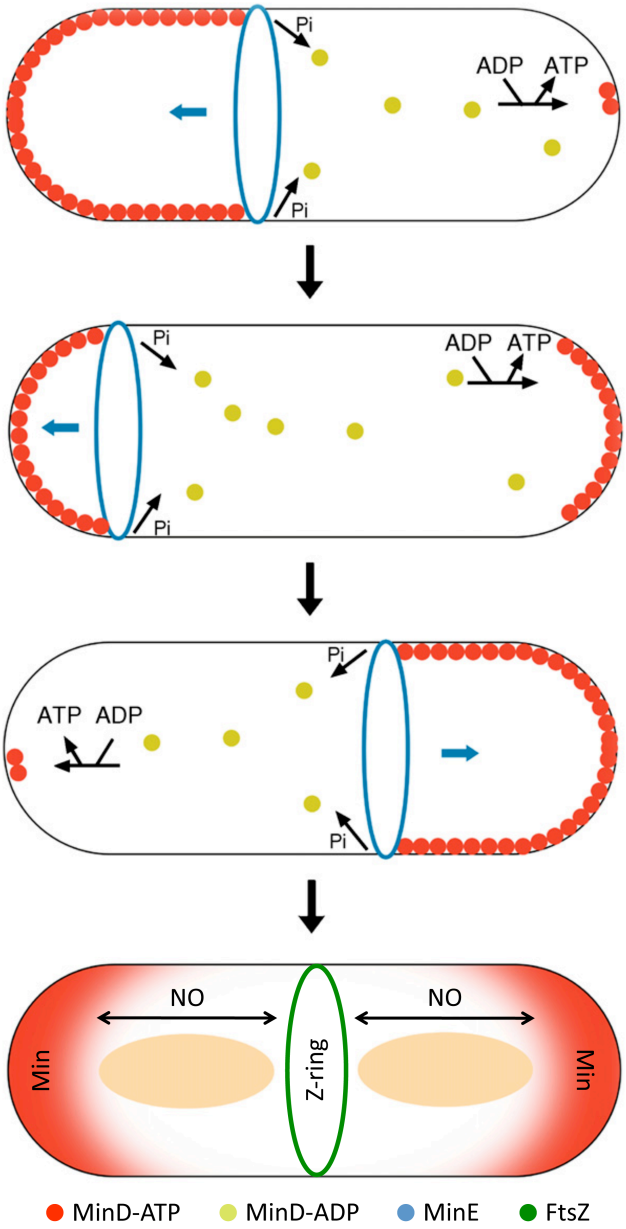

Fig. 1.2 Division site selection

In *E. coli* the selection of the division site is regulated by the Min and the nucleoid occlusion system (modified from Bramkamp and van Baarle, 2009). FtsZ (green ellipse) assembles in a Z-ring at mid-cell, where the concentration of the two negative regulators is lower. The Min system inhibits Z-ring formation at the cell poles. MinD-ATP (red spheres) binds to the membrane and recruits MinC (not shown), the inhibitor of FtsZ assembly. MinE (blue ellipse) displaces MinCD from the membrane activating MinD ATPase. MinD-ADP (yellow spheres) undergoes nucleotide exchange in the cytoplasm and migrates towards the opposite pole where it recruits MinC. MinCD oscillation creates a gradient (red shading) with the highest concentration at the poles and the lowest one at mid-cell. SlmA binds asymmetrically over the nucleoids inhibiting Z-ring assembly on the chromosomes.

The Min system specifically regulates the lateral positioning of the Z-ring preventing aberrant division at the cell poles. In the absence of a functional Min system, Z-rings can assemble at places other than mid-cell leading to division events near the cell poles and, consequently, generation of anucleate minicells and increased average length of the cells containing DNA (de Boer *et al.*, 1989; Lutkenhaus, 2007; Bramkamp and van Baarle, 2009).

In *E. coli*, the Min system is composed of three proteins: MinC, MinD and MinE. MinC is the factor responsible for blocking Z-ring formation, MinD is the activator of MinC and MinE is the topological regulator of MinCD (Lutkenhaus, 2007).

Specific inhibition at the cell poles is achieved through a regulated oscillation of the Min proteins between the cell poles. MinD, an ATPase, binds to the membrane in its ATP-bound form and recruits MinC forming a MinCD complex. Meanwhile, MinE stimulates MinD ATPase activity and the release, following ATP hydrolysis, of MinD-ADP and MinC from the membrane. MinD and MinC then migrate towards the opposite pole where, after nucleotide exchange in the cytosol, MinD-ATP re-associates with the membrane and the MinCD complex can reform in the opposite cell half, where MinE is not yet present (Hu and Lutkenhaus, 2001; Lutkenhaus, 2007; Bramkamp and van Baarle, 2009). In dividing cells MinE oscillates in a ring-like structure from side to side of the cell inducing MinCD migration from pole to pole. MinCD oscillation, driven by MinE, results in a higher concentration of the inhibitor MinC at the cell poles and a lower one at mid-cell, which mediates the specific inhibition of Z-ring assembly at the cell poles but not at mid-cell (Raskin and de Boer, 1999; Fu *et al.*, 2001; Loose *et al.*, 2011). MinC inhibits Z-ring formation preventing lateral interactions of FtsZ filaments and, accordingly, this inhibitory effect can be antagonized by ZapA: a positive cross-linking and bundling factor of FtsZ filaments (Dajkovic *et al.*, 2008a; Scheffers, 2008).

In *B. subtilis*, MinC and MinD are conserved, but the topological regulator MinE is absent and the polar localization of MinCD is regulated by a factor called DivIVA through the adaptor protein MinJ (Bramkamp *et al.*, 2008; Patrick and Kearns, 2008; Bramkamp and van Baarle, 2009). Furthermore, whereas in *E. coli* the MinCD complex oscillates from pole to pole, following cell division in *B. subtilis*, the MinCD complex dynamically relocalizes from the old pole towards the new cell

division sites at mid-cell, preventing Z-ring assembly close to sites of recent septation (Gregory *et al.*, 2008).

The second regulatory mechanism, the nucleoid occlusion system, prevents formation of Z-rings in close vicinity of nucleoids (Errington *et al.*, 2003). When initiation of replication is blocked in a nucleoid occlusion mutant, Z-rings can form over the segregated chromosomes, effectively guillotining them (Lutkenhaus, 2007). The NO effectors, Noc in *B. subtilis* (Wu and Errington, 2004) and SlmA in *E. coli* (Bernhardt and de Boer, 2005), are DNA-binding proteins. The overproduction of either of them leads to cell elongation and delay in cell division. Recently, it has been shown that both Noc and SlmA are asymmetrically distributed over the nucleoid, binding specific DNA sequences located near the replication origin region of the chromosome and essentially absent from the replication terminus region (Wu *et al.*, 2009; Cho *et al.*, 2011; Tonthat *et al.*, 2011). Recruitment of SlmA and Noc to specific regions on the chromosome may provide a mechanism for the coordination of cell division and chromosome segregation, allowing a spatiotemporal regulation of Z-ring assembly (Wu *et al.*, 2009; Cho *et al.*, 2011; Tonthat *et al.*, 2011). Indeed, artificial recruitment of Noc into the replication terminus region leads to a delay in cell division (Wu *et al.*, 2009). So far, the mechanism with which Noc inhibits Z-ring formation is still unknown. Instead, it has been shown that SlmA directly interacts with FtsZ, leading to the proposition that following dimerization (or oligomerization) induced by DNA binding, SlmA dimers could alter FtsZ polymer assembly by disrupting FtsZ-FtsZ interactions (Cho *et al.*, 2011; Tonthat *et al.*, 2011).

Mutants defective both in the Min and in the NO system fail to divide and form filaments, but interestingly, along the length of the resultant filamentous cells, FtsZ is still able to form non-productive rings that are preferentially located between the nucleoids (Wu and Errington, 2004; Bernhardt and de Boer, 2005). Hence, it is speculated that there could be at least a third system involved in the spatial regulation of Z-ring assembly (Lutkenhaus, 2007).

1.4 The SOS response: SulA

In addition to the spatiotemporal regulation of Z-ring formation, coordinated by the Min and the NO systems, Z-ring assembly can also be modulated in response to DNA damage by induction of the SOS response (Gottesman, 1981). In *E. coli*, SulA is the SOS factor responsible for the inhibition of cell division (Huisman *et al.*, 1984). It is induced following damages to DNA and it persists, blocking FtsZ polymerization (Mukherjee *et al.*, 1998; Trusca *et al.*, 1998), until the DNA has been repaired. At that point, SulA is rapidly degraded by the Lon protease (Mizusawa and Gottesman, 1983). In contrast to MinC, which inhibits the formation of FtsZ higher-order structures (Dajkovic *et al.*, 2008a), SulA binds to the T7 loop of FtsZ (Cordell *et al.*, 2003), blocking its dimerization and polymerization (Dajkovic *et al.*, 2008b). SulA sequesters FtsZ monomers in SulA-FtsZ complexes, reducing the amount of FtsZ able to polymerize. Only after degradation of SulA, FtsZ is free to participate in Z-ring assembly and cell division can proceed (Dajkovic *et al.*, 2008b).

In *B. subtilis*, the SOS-induced division inhibitor is YneA (Kawai *et al.*, 2003). As opposed to SulA, YneA seems to target not FtsZ but later stages of cell division, such as daughter cell separation and septum formation (Kawai *et al.*, 2003; Kawai and Ogasawara, 2006; Mo and Burkholder, 2010).

1.5 Anchoring FtsZ to the membrane: ZipA and FtsA

All models for FtsZ ring assembly and constriction require FtsZ association to the membrane (Errington *et al.*, 2003; Adams and Errington, 2009). Moreover, this is believed to be necessary to coordinate the invagination at the septum with the synthesis of new septal peptidoglycan (Errington *et al.*, 2003; Adams and Errington, 2009). FtsZ has no affinity for the membrane and in *E. coli* two membrane-associated proteins, ZipA and FtsA, interacting with its C-terminal peptide, anchor FtsZ to the membrane (Hale and de Boer, 1997; Pichoff and Lutkenhaus, 2002).

FtsA and ZipA are recruited independently to the Z-ring by FtsZ. Although they are both essential for cell division, FtsZ is able to assemble in non-functional Z-rings between the segregated chromosomes along the cell filaments that are formed in

the absence of either one of them, whereas when they are both inactivated Z-rings cannot form (Hale and de Boer, 1999; Pichoff and Lutkenhaus, 2002; Adams and Errington, 2009). The cellular levels of FtsZ, FtsA and ZipA are very important, consequently overproduction of any of them abolishes cell division leading to the formation of cell filaments, but what is actually more important is the balance of FtsZ and FtsA levels and those of FtsZ and ZipA (Dai and Lutkenhaus, 1992; Dewar *et al.*, 1992; Hale and de Boer, 1997).

ZipA is a bitopic protein that binds to the membrane through an N-terminal transmembrane domain and interacts with FtsZ through a C-terminal globular domain (Hale and de Boer, 1997; Mosyak *et al.*, 2000; Moy *et al.*, 2000). Probably, in *E. coli*, cell division failure to proceed in the absence of ZipA is due to its role in the recruitment of FtsK, another essential division factor, into the divisome (Hale and de Boer, 2002). *In vitro*, it has been shown that the ZipA C-terminal domain has the ability to induce FtsZ protofilament bundling and lateral alignment (RayChaudhuri, 1999; Hale *et al.*, 2000), although the molecular mechanism is still unknown. ZipA's positive role in FtsZ filaments stabilization and bundling is supported by the suppression of the *ftsZ84* mutant defective phenotype at the non-permissive temperature when ZipA levels are increased two-fold (RayChaudhuri, 1999).

ZipA is present mainly in the γ-proteobacteria (Hale and de Boer, 1997) as opposed to the second FtsZ tethering protein, FtsA, which is widely conserved (Pichoff and Lutkenhaus, 2005). Furthermore, a gain-of-function point mutation in FtsA, called FtsA*, overcomes lack of ZipA (Geissler *et al.*, 2003) suggesting a redundant role for ZipA and making FtsA the primary tether to the membrane in Bacteria (Geissler *et al.*, 2003; Adams and Errington, 2009).

FtsA is an ATPase belonging to the actin superfamily (Bork *et al.*, 1992; van den Ent and Lowe, 2000). It binds peripherally to the membrane through a C-terminal peptide that forms an amphipathic helix (Pichoff and Lutkenhaus, 2005) and it is able to interact with both itself and FtsZ (Yan *et al.*, 2000; Yim *et al.*, 2000; Pichoff and Lutkenhaus, 2007a; Shiomi and Margolin, 2007). Biochemical studies of *E. coli* FtsA have been hampered by the low activity of the purified protein (de Boer, 2010). Instead, purified FtsA from *B. subtilis* has been reported to be able to dimerize and to bind and hydrolyze ATP (Feucht *et al.*, 2001). Interestingly, FtsA from *Streptococcus pneumoniae* can reversibly form polymers that are highly stable in the presence of ATP and less stable with ADP (Lara *et al.*, 2005). The importance of ATP binding is

also underlined by the loss of FtsA ability to interact with itself and with FtsZ when residues involved in ATP binding are mutated (Pichoff and Lutkenhaus, 2007a).

In *E. coli*, in addition to its role in tethering FtsZ to the membrane and assisting Z-ring formation (Pichoff and Lutkenhaus, 2007a), FtsA is also essential for the maturation of the Z-ring, recruiting downstream proteins such as FtsN and FtsI into the divisome (Corbin *et al.*, 2004; Rico *et al.*, 2004).

In *B. subtilis*, by contrast, FtsA is not essential, even though cells depleted of the protein are filamentous (Beall and Lutkenhaus, 1992), and it is believed that FtsA is not necessary for the recruitment of late-division proteins (Jensen *et al.*, 2005). In this organism it is still unknown how FtsZ can be anchored to the membrane in the absence of FtsA and ZipA.

1.6 Modulating Z-ring assembly and dynamics

In vivo the Z-ring has been shown to consist of short overlapping FtsZ protofilaments (Li *et al.*, 2007; Fu *et al.*, 2010) and many, often non-essential, proteins are suspected to modulate their formation and interaction, hence regulating Z-ring dynamics (Adams and Errington, 2009). Such Z-ring positive and negative modulating factors that appear to be phylogenetically unrelated are present among bacterial phyla (Hale *et al.*, 2011). So far, proteins postulated to regulate Z-ring assembly are ZapA, widely conserved in eubacteria (Gueiros-Filho and Losick, 2002; Low *et al.*, 2004; Small *et al.*, 2007; Mohammadi *et al.*, 2009; Dajkovic *et al.*, 2010); ClpX conserved in eubacteria and archaea (Flynn *et al.*, 2003; Weart *et al.*, 2005; Camberg *et al.*, 2009; Dziedzic *et al.*, 2010); ZapC, restricted to the γ-proteobacteria (Durand-Heredia *et al.*, 2011; Hale *et al.*, 2011); SepF, present in Gram-positives and cyanobacteria (Miyagishima *et al.*, 2005; Hamoen *et al.*, 2006; Ishikawa *et al.*, 2006; Singh *et al.*, 2008; Gundogdu *et al.*, 2011); EzrA, found in *B. subtilis* and related Gram-positives (Haeusser *et al.*, 2004; Chung *et al.*, 2007; Singh *et al.*, 2007; Steele *et al.*, 2011); ZipN (Mazouni *et al.*, 2004) and ZipS (Marbouty *et al.*, 2009) in cyanobacteria; FzlA (Goley *et al.*, 2010) and KidO (Radhakrishnan *et al.*, 2010) in *Caulobacter crescentus*; and FipA in mycobacteria (Sureka *et al.*, 2010). The

characterization of a new *E. coli* Z-ring modulating factor, ZapB, is the object of this work and it has been discussed in detail in the following chapters.

Although a unique modulating factor is not widely conserved and they are often not required for Z-ring assembly, regulation of Z-ring dynamics is likely to be beneficial enough that different organisms have evolved a variety of factors modulating Z-ring structure (Hale *et al.*, 2011).

Hereafter, the positive and negative regulators of Z-ring assembly reported in *E. coli*, *B. subtilis* and *C. crescentus* are described (Fig. 1.3).

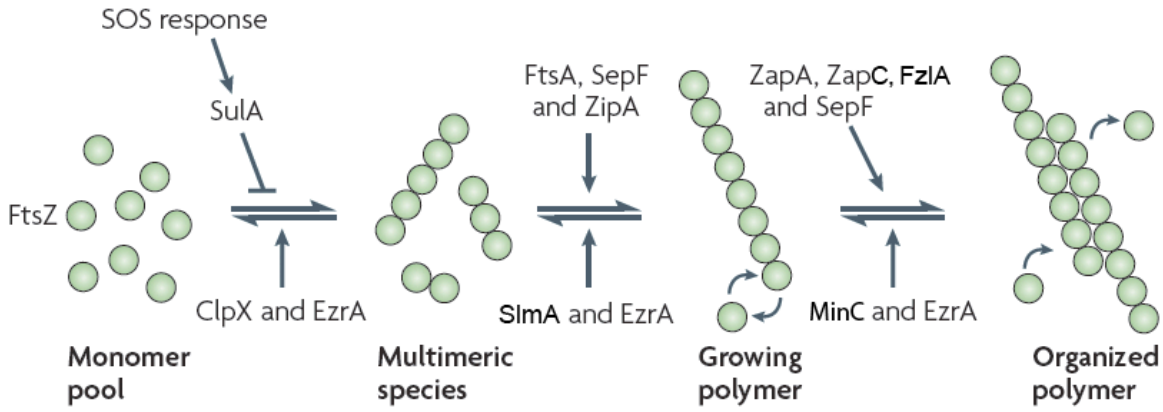

Fig. 1.3 Positive and negative regulators of Z-ring assembly

FtsZ monomers polymerize in linear protofilaments that can associate laterally forming higher order structures. Different proteins modulate FtsZ polymerization and Z-ring assembly acting as positive (FtsA, ZipA, ZapA, ZapC, SepF and FzlA) or negative (SulA, ClpX, EzrA, SlmA and MinC) regulators (modified from Adams and Errington, 2009).

ZapA was first identified in *B. subtilis* while screening for genes whose overexpression could counteract the effects of MinD overproduction (Gueiros-Filho and Losick, 2002). In *B. subtilis*, cells lacking ZapA do not show any morphological phenotype but, when ZapA inactivation is combined with the absence of the division protein EzrA or the division-site-selection protein DivIVA or with lowered levels of FtsZ, it causes a block in cell division (Gueiros-Filho and Losick, 2002). In *E. coli*, *zapA* null mutants grown in rich medium have an average cell length longer than wild-type cells (Mohammadi *et al.*, 2009; Dajkovic *et al.*, 2010) and the Z-rings are structurally looser and often fail to coalesce into coherent rings (Dajkovic *et al.*,

2010). Interacting directly with FtsZ, ZapA is recruited early into the divisome (Gueiros-Filho and Losick, 2002), where it increases FtsZ protofilament association and Z-ring stability (Gueiros-Filho and Losick, 2002; Low *et al.*, 2004; Small *et al.*, 2007; Mohammadi *et al.*, 2009; Dajkovic *et al.*, 2010). The structure of the small protein ZapA has been solved in *Pseudomonas aeruginosa*: a ZapA monomer consists of an N-terminal globular domain and a long C-terminal coiled-coil domain; in solution it exists in a dimer/tetramer equilibrium where higher ZapA concentrations shift the equilibrium towards the tetramer conformation. ZapA monomers dimerize, interacting between the N termini of the coiled-coil domains (the globular domain of one subunit could stabilize the dimer interacting with the coiled-coil domain of the second subunit) and two dimers form an anti-parallel tetramer, extensively associating along the coiled-coil protrusion. Its globular domain is postulated to mediate the interaction with FtsZ (Low *et al.*, 2004). Probably, *in vivo*, ZapA forms a dimer, but it is possible that the local concentration of ZapA at the division-site, where it likely interacts stoichiometrically with FtsZ, may be sufficient to induce a tetrameric conformation (Low *et al.*, 2004). Particularly in *E. coli*, ZapA-induced bundling and cross-linking of FtsZ protofilaments has been extensively investigated *in vitro* (Small *et al.*, 2007; Mohammadi *et al.*, 2009; Dajkovic *et al.*, 2010). Small *et al*. (2007) identified a conformational change in the FtsZ bound nucleotide upon binding with ZapA that would make it less favorable to hydrolysis and therefore render FtsZ polymers more stable. Mohammadi *et al*. (2009) proposed that ZapA stabilizes FtsZ assembly simply by enhancing FtsZ protofilaments association and, from careful analyses of EM pictures, suggested that ZapA tetramers would bind in between and probably on top of parallel double FtsZ filaments. Recently, Dajkovic *et al*. (2010), using quantitative rheometry, further proved that ZapA not only bundles but also cross-links FtsZ polymers. They also showed that ZapA is able to stabilize longitudinal bonds between FtsZ monomers in a filament, counteracting the inhibitory effects of SulA, known to destabilize FtsZ longitudinal interactions (Dajkovic *et al.*, 2008b).

ZapC is a small cytoplasmic protein, conserved in a subset of γ-proteobacteria, which has recently been characterized as an FtsZ bundling agent. ZapC was identified in a screening for proteins that localize at the division site in an

FtsZ-dependent manner (Durand-Heredia *et al.*, 2011) and by another group in a screen for genes whose inactivation is detrimental in cells with a non functional Min system (Hale *et al.*, 2011). Cells lacking or overproducing ZapC are slightly elongated and filamentation is aggravated by the absence of ZapA, furthermore when ZapC levels are altered, FtsZ forms aberrant structures. Reminiscent of ZapA, ZapC localizes early at the division-site, protects against MinC overproduction and, *in vitro*, it has been shown to directly interact with FtsZ and to promote bundling and lateral association of FtsZ protofilaments (Durand-Heredia *et al.*, 2011; Hale *et al.*, 2011). ZapC and ZapA seem to be functionally redundant with overlapping biochemical activities that synergistically promote Z-ring assembly (Durand-Heredia *et al.*, 2011; Hale *et al.*, 2011).

SepF is a cytoplasmic protein conserved in Gram-positives and cyanobacteria (Adams and Errington, 2009). The absence of SepF is lethal in *Synechococcus elongatus* (Miyagishima *et al.*, 2005), a cyanobacterium seemingly without an FtsA homologue, and results in abnormal cell morphology in *S. pneumoniae* (Fadda *et al.*, 2003) and in slightly elongated cells with abnormal septa in *B. subtilis* (Hamoen *et al.*, 2006; Ishikawa *et al.*, 2006). SepF has been further characterized in *B. subtilis*: an *ftsA*-null mutant phenotype can be suppressed by SepF overproduction and simultaneous inactivation of SepF and FtsA is synthetic lethal (Ishikawa *et al.*, 2006), as it is synthetic lethal the combination of *ezrA*, a postulated negative regulator of Z-ring formation (Levin *et al.*, 1999), and *sepF* null mutants (Hamoen *et al.*, 2006). SepF localizes at the division site in an FtsZ-dependent manner. It is not required for assembly of the divisome and it is able to directly interact with itself and with FtsZ (Hamoen *et al.*, 2006; Ishikawa *et al.*, 2006). Interestingly, the aberrant FtsZ localization pattern observed in the long filaments formed in the absence of both SepF and FtsA is very similar to the defective FtsZ structures formed in the absence of both ZipA and FtsA in *E. coli* (Ishikawa *et al.*, 2006). *In vitro*, SepF, binding the C-terminal tail of FtsZ, was found to induce the assembly and bundling of FtsZ filaments and to stabilize the Z-ring (Singh *et al.*, 2008; Gundogdu *et al.*, 2011). Strikingly, purified SepF assembles into large regular rings able to bundle FtsZ filaments into long tubular structures (Gundogdu *et al.*, 2011). The formation of poorly assembled Z-rings in the absence of SepF could cause the observed

morphological defects in septa during constriction (Gundogdu *et al.*, 2011). Furthermore, bioinformatic analysis of SepF amino acid sequence revealed the presence of a membrane anchor motif at its N-terminus (Singh *et al.*, 2008).

EzrA, a protein conserved throughout the low-GC-content Gram-positive bacteria, was first identified as an inhibitor of FtsZ ring formation in *B. subtilis* in a screen for extragenic suppressors of a temperature-sensitive allele of *ftsZ*-GFP (Levin *et al.*, 1999). *ezrA*-null mutants result in elongated cells and formation of multiple Z-rings along the cells and at the cell poles. Furthermore, in the absence of EzrA, the concentration of FtsZ necessary for Z-ring formation as well as the ability of MinCD overproduction to destabilize the Z-ring are reduced. (Levin *et al.*, 1999; Levin *et al.*, 2001; Geissler *et al.*, 2003; Kawai and Ogasawara, 2006). It was also reported that as little as a two-fold overproduction of EzrA impairs Z-ring formation in a strain carrying a temperature sensitive *ftsZ* allele (Haeusser *et al.*, 2004). EzrA is an integral membrane protein that anchors to the membrane with an N-terminal transmembrane domain. In pre-divisional cells EzrA localizes to the membrane and later, interacting directly through a C-terminal cytoplasmic domain with FtsZ, is recruited to the septal site in an FtsZ-dependent manner (Levin *et al.*, 1999; Haeusser *et al.*, 2004; Haeusser *et al.*, 2007).

In vitro, EzrA likely binds FtsZ in a 1:1 stoichiometry and inhibits the assembly of FtsZ polymers by decreasing FtsZ GTP-binding ability and enhancing the rate of FtsZ GTP hydrolysis, it is suggested that EzrA accomplishes its function by inducing a conformational change in FtsZ upon binding (Chung *et al.*, 2007). It is still unclear if EzrA is able to disassemble preformed FtsZ polymers (Haeusser *et al.*, 2004; Singh *et al.*, 2007). Probably, EzrA is able both to prevent the formation of Z-ring assemblies at the cell poles and to regulate FtsZ polymer dynamics at mid-cell (Haeusser *et al.*, 2007). Fine-tuning of FtsZ dynamics seems very important for the assembly and localization of functional Z-rings and it is possible that a defective regulation renders a strain lacking both the negative regulator EzrA and a positive regulator, such as SepF or ZapA, unable to successfully complete cytokinesis (Singh *et al.*, 2008). The existence has also been reported of a protease, CodWX, capable of degrading EzrA and hence regulating cell division (Kang *et al.*, 2003).

Recently, it has been shown in *B. subtilis* (Claessen *et al.*, 2008) and in

Staphylococcus aureus (Steele *et al.*, 2011) that EzrA has an additional role, not related to the regulation of Z-ring assembly, in coordinating cell elongation and division.

ClpX was first identified in *B. subtilis* as a negative regulator of Z-ring formation while screening for genes that could suppress the heat sensitivity of an *ftsZ* temperature sensitive allele (Weart *et al.*, 2005), as similarly done for *ezrA* (Levin *et al.*, 1999; and described above). ClpX is a member of the AAA^+ family of ATPases and is the substrate recognition subunit of the ClpXP protease (Sauer *et al.*, 2004; Weart *et al.*, 2005). *In vivo*, a modest overproduction of ClpX increases cell length and overcomes the absence of a functional MinCD (Weart *et al.*, 2005), further increase of ClpX levels leads to cell filamentation and aberrant FtsZ localization (Camberg *et al.*, 2009; Dziedzic *et al.*, 2010; Sugimoto *et al.*, 2010). Accordingly, the absence of ClpX suppresses the block in cell division induced by MinCD overproduction (Weart *et al.*, 2005). ClpX colocalizes with FtsZ (Dziedzic *et al.*, 2010) and interacts directly with FtsZ through an N-terminal zinc-binding domain, the C-terminal domain of FtsZ seems to be important for FtsZ-ClpX interaction in *E. coli*, even though it is not essential for the inhibition of FtsZ polymerization (Camberg *et al.*, 2009; Dziedzic *et al.*, 2010; Sugimoto *et al.*, 2010).

Working *in vitro* with purified proteins, different groups have reported that in *B. subtilis*, *E. coli* and *Mycobacterium tuberculosis* ClpX inhibits FtsZ assembly in a concentration-dependent manner, through a mechanism that is ClpP-independent and that does not require ATP hydrolysis. ClpX would interfere with FtsZ assembly simply by sequestering FtsZ monomers and small oligomers. Hence, by blocking the recycle of FtsZ subunits, ClpX would modulate FtsZ reassembly and dynamics (Weart *et al.*, 2005; Haeusser *et al.*, 2009; Dziedzic *et al.*, 2010; Sugimoto *et al.*, 2010). In *E. coli*, conflicting results were reported by Camberg *et al*. (2009): they showed that ClpXP, via an ATP-dependent mechanism, degrades FtsZ polymers and protomers with a higher affinity for polymerized FtsZ compared to monomers, even though ATP and ClpP were not required for ClpX to bind FtsZ. They suggest that ClpX could modulate FtsZ subunit turnover and recycling, regulating the polymer-monomer dynamics (Camberg *et al.*, 2009; Camberg *et al.*, 2011). Moreover, it has been proposed that ClpX may regulate through degradation not only FtsZ, but also

other cell division components (Camberg *et al.*, 2011). Interestingly, in *C. crescentus*, ClpXP regulates cell division by degrading the cell cycle regulator CtrA, thereby indirectly modulating the levels of cell division genes (Jenal and Fuchs, 1998; Chien *et al.*, 2007; Camberg *et al.*, 2009).

FzlA is a cytoplasmic protein conserved in α-proteobacteria that was recently identified in *C. crescentus* in a microscopy-based screening for proteins interacting directly with FtsZ (Goley *et al.*, 2010). Goley and colleagues have characterized FzlA *in vivo* and *in vitro*. They reported that it is essential for cytokinesis and that in its absence cells form long aseptate filaments. FzlA division-site localization and abundance are cell cycle regulated at the transcript and protein level, with the highest level, compared to that of FtsZ, at the beginning of the cell cycle, before and concurrently with Z-ring assembly. Analysing FtsZ localization patterns in cells overproducing or depleted of FzlA, they showed that the Z-ring is still able to form in the absence of FzlA whereas when its levels are artificially increased FtsZ is less dynamic and forms aberrant structures. *In vitro*, FzlA induces formation of stable higher-order FtsZ structures that are resistant to MipZ, an inhibitor of FtsZ polymerization (Thanbichler and Shapiro, 2006; Goley *et al.*, 2010). Interestingly, if the FtsZ-regulatory proteins previously described modulate Z-ring dynamics by promoting or destabilizing FtsZ ability to polymerize and associate in sheets or bundles, the analysis of the structures formed by purified FzlA and FtsZ suggested that FzlA may act on the bending of FtsZ filaments (Goley *et al.*, 2010). Indeed, FzlA induces the formation of regular helical right-handed bundles composed of three filaments and Goley *et al*. (2010) suggested that the two external filaments are composed of FtsZ and the inner filament of FzlA.

1.7 Late cell division proteins

The so-called late division proteins are recruited to the division site after the assembly of the Z-ring and are involved in the coordination of cell division with chromosome segregation (FtsK), in the synthesis of the peptidoglycan cell wall (FtsI, FtsW) and in the separation of the two daughter cells (AmiC, EnvC). Despite the great

advances made in the last years, it is still unclear the precise role many factors have in cell division and it is likely that new proteins, especially non-essential ones, are awaiting discovery (Weiss, 2004).

A brief description of the remaining cell division proteins is presented below, following the proposed, largely linear, pathway of recruitment to the division site (Fig. 1.4) (Aarsman *et al.*, 2005; Goehring and Beckwith, 2005).

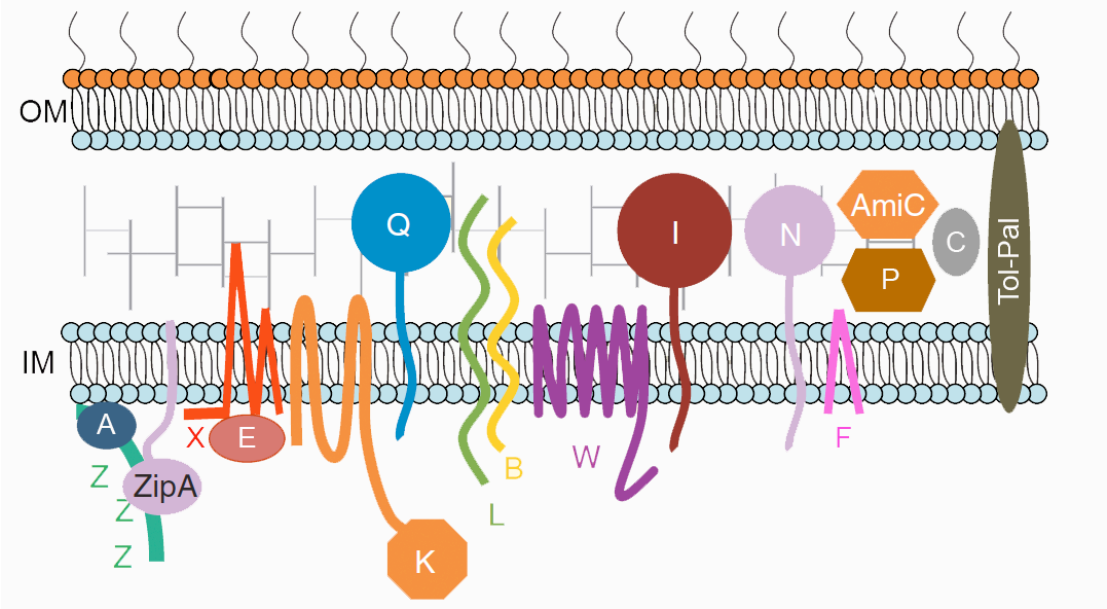

Fig. 1.4 The divisome in *E. coli*

Schematic representation of the *E. coli* cell division proteins following the order in which are recruited into the divisome, from left to right in the scheme (modified from Goehring and Beckwith, 2005). The two Z-ring associated proteins ZapA and ZapC are not included. OM, outer membrane; IM, inner membrane; Z, FtsZ; A, FtsA; X, FtsX; E, FtsE; K, FtsK; Q, FtsQ; L, FtsL; B, FtsB; W, FtsW; I, FtsI; N, FtsN; F, YmgF; P, FtsP; C, EnvC.

FtsE and **FtsX** are widely conserved among bacteria and form a complex homologous to the ATP-binding cassette (ABC)-type transporter (de Leeuw *et al.*, 1999; Schmidt *et al.*, 2004). FtsE is an ATP-binding protein with a tendency to dimerize and FtsX is the integral membrane protein that associates FtsE to the cytoplasmic side of the inner membrane (Gill *et al.*, 1986; Gill and Salmond, 1987; de Leeuw *et al.*, 1999; Schmidt *et al.*, 2004). Artificial enhancement of FtsX levels leads to growth inhibition, cell filamentation and death: defects that are partially mitigated by the concurrent overproduction of FtsE (de Leeuw *et al.*, 1999). FtsE is a conditional essential protein and an *ftsE* null mutant can grow in medium containing

high salt levels or having high osmolarity (de Leeuw *et al.*, 1999; Schmidt *et al.*, 2004; Reddy, 2007). *ftsEX* null mutant lethality can also be overcome by increasing FtsQAZ or FtsP cellular levels (Reddy, 2007). Both FtsE and FtsX localize to the division-site in an FtsZ-dependent manner (Schmidt *et al.*, 2004), but it is not clear which of the two proteins targets the FtsEX complex to the Z-ring or if they are able to localize independently from each other, since it has been shown that FtsE can interact with FtsZ independently of FtsX (Corbin *et al.*, 2004) and that FtsX is recruited to the septal site in cells lacking FtsE (Arends *et al.*, 2009).

It is suggested that FtsEX could play a role in the assembly and stability of the divisome, especially in the absence of the optimal osmotic conditions, when the protein-protein interactions necessary for the correct folding of the divisome might be destabilized (Schmidt *et al.*, 2004; Reddy, 2007).

Interestingly, in *B. subtilis*, FtsEX seems involved in the initiation of spore formation (Garti-Levi *et al.*, 2008).

FtsK, a dsDNA-dependent AAA^+ ATPase, is a widely conserved protein across bacterial species and is essential in *E. coli* (Crozat and Grainge, 2010). The multifunctional and multidomain protein couples chromosome segregation with cell division, localizing at the division site where it acts as a double-stranded DNA translocase (Bigot *et al.*, 2007; Wu, 2009; Crozat and Grainge, 2010). The N-terminal domain, containing four membrane-spanning segments, interacts with FtsZ. It is responsible for FtsK recruitment to the division-site and is required for cell division. Accordingly, its absence induces formation of cell filaments with no septum constriction. FtsK N-terminal domain is also involved in the recruitment of downstream cell-division components into the divisome and probably stabilizes the divisome before septation (Bigot *et al.*, 2007; Wu, 2009; Crozat and Grainge, 2010). The cytoplasmic C-terminal ATPase domain of FtsK is the translocation motor: it forms a hexameric ring with a central channel for dsDNA that is involved in chromosome segregation. In the last stage of chromosome segregation it ensures the resolution of intercatenation links and chromosome dimers, respectively mediated by Topoisomerase IV and XerCD (Bigot *et al.*, 2007; Wu, 2009; Crozat and Grainge, 2010). The DNA translocase is loaded onto DNA in a specific orientation by binding to polarised chromosomal sequences, called KOPS, such that the translocation is

always towards the chromosome terminus (Bigot *et al.*, 2007; Wu, 2009; Crozat and Grainge, 2010).

In *B. subtilis*, two FtsK-like proteins have been identified: SpoIIIE and SftA. These two DNA translocases guarantee fidelity in chromosome segregation during vegetative growth acting at two different stages: SftA in the course of septum synthesis and constriction and SpoIIIE specifically upon chromosome entrapment (Wu, 2009). SpoIIIE is essential for spore development, translocating chromosomal DNA from the mother cell into the prespore (Wu *et al.*, 1995; Wu and Errington, 1997).

FtsQ, a bitopic protein highly conserved in bacteria with a cell wall (van den Ent *et al.*, 2008), has a small cytoplasmic N-terminal domain and a large C-terminal periplasmic domain (Carson *et al.*, 1991) carrying a polypeptide transport-associated (POTRA) domain that is usually involved in protein interactions or chaperone-like functions (D'Ulisse *et al.*, 2007). In *E. coli*, FtsQ overproduction induces formation of multiseptate filaments (Carson *et al.*, 1991) and filamentation becomes extensive in strains carrying a mutant *ftsA*, *ftsI* or *ftsZ* allele (Dai and Lutkenhaus, 1992). Conversely, FtsN overproduction partially suppresses *ftsQ*(ts) phenotype (Chen *et al.*, 1999). If FtsQ is essential in *E. coli* (Carson *et al.*, 1991), its counterpart in *B. subtilis*, DivIB, is not required for vegetative growth at low temperatures (Beall and Lutkenhaus, 1989; Wadsworth *et al.*, 2008), even though it is still essential for sporulation (Thompson *et al.*, 2006). Another significant difference between the two organisms is the intracellular level of FtsQ, present in only 25-50 copies per cell in *E. coli* (Carson *et al.*, 1991; Buddelmeijer *et al.*, 1998), and DivIB, with 5,000-13,000 copies per cell in *B. subtilis* (Katis *et al.*, 1997; Rowland *et al.*, 1997).

FtsQ localizes to the division site in an FtsZ-, FtsA-, ZipA- and FtsK-dependent manner and, in turn, recruits into the divisome FtsL, FtsB, FtsW, FtsI and FtsN (Chen *et al.*, 1999; Chen and Beckwith, 2001). In bacterial two-hybrid analyses FtsQ interacts with itself and with a great number of cell division factors: FtsA, FtsK, FtsX, FtsL, FtsB, FtsW, FtsI, FtsN and YmgF (Di Lallo *et al.*, 2003; D'Ulisse *et al.*, 2007; Karimova *et al.*, 2009). Interestingly, FtsQ is able to form a stable independent trimeric complex with FtsL and FtsB (Buddelmeijer and Beckwith, 2004). The high number of interaction partners suggests that FtsQ may provide a structural link

between the early cytoplasmic and late periplasmic division proteins (Di Lallo *et al.*, 2003; D'Ulisse *et al.*, 2007) or have a role in the regulation of the divisome assembly (Piette *et al.*, 2004). It has also been hypothesized that FtsQ might play a part in cell wall synthesis (Piette *et al.*, 2004; van den Ent *et al.*, 2008).

FtsL, a bitopic protein with a small N-terminal cytoplasmic domain and a major C-terminal periplasmic domain, is a division factor essential in most eubacteria (Guzman *et al.*, 1992; Bramkamp *et al.*, 2006). FtsL localization to the division site depends upon FtsZ, FtsA and FtsQ (Ghigo *et al.*, 1999) and is co-dependent on FtsB with which it is able to form a subcomplex that, in the absence of FtsQ, can interact with FtsW and FtsI (Goehring *et al.*, 2006). It is suggested that in *E. coli* the subcomplex FtsL/FtsB could act as a scaffold during divisome assembly (Gonzalez *et al.*, 2010).

Interestingly, in *B. subtilis*, FtsL is highly unstable (Daniel and Errington, 2000) and the intramembrane protease RasP (YluC), targeting the cytoplasmic domain of FtsL, has been identified as the factor responsible for FtsL degradation (Bramkamp *et al.*, 2006; Wadenpohl and Bramkamp, 2010). Furthermore, FtsL stabilizes DivIC (FtsB analogue in *B. subtilis*) that in its absence is degraded (Daniel and Errington, 2000) and likewise DivIC stabilizes FtsL against RasP cleavage (Wadenpohl and Bramkamp, 2010). DivIB is also able to stabilize FtsL and, in turn, FtsL overproduction overcomes a *divIB* null mutant phenotype (Daniel and Errington, 2000). These data suggest that, in *B. subtilis*, FtsL would play a role in regulation of division (Bramkamp *et al.*, 2006). In *E. coli*, so far, no stability effects have been reported for FtsL (Daniel *et al.*, 2006).

FtsB was first identified in a bioinformatic screen for proteins interacting with FtsL in *E. coli* and in a transposon screen for essential genes in *Vibrio cholerae* (Buddelmeijer *et al.*, 2002). Like FtsL, FtsB is a small bitopic protein with a small N-terminal cytoplasmic domain and a large C-terminal periplasmic domain (Buddelmeijer *et al.*, 2002). The presence of the complex formed by FtsQ/FtsL/FtsB appears to be evolutionarily conserved (Gonzalez *et al.*, 2010). FtsL and FtsB are codependent for septal localization and the subcomplex FtsL/FtsB is recruited to mid-cell by FtsQ (Gonzalez and Beckwith, 2009; Gonzalez *et al.*, 2010). In the absence of

FtsQ or FtsL, FtsB is partially degraded (Gonzalez and Beckwith, 2009), likewise to FtsB counterpart in *B. subtilis*, DivIC, that is destabilized by the absence of FtsL (Daniel and Errington, 2000). The proteases responsible for FtsB or DivIC degradation have not yet been identified.

Together with FtsL, it is suggested that FtsB acts as a scaffold for divisome assembly (Gonzalez and Beckwith, 2009).

FtsW is an essential *E. coli* integral membrane protein, characterized by 10 transmembrane segments (Lara and Ayala, 2002). It is a member of a large family of proteins called SEDS (for shape, elongation, division and sporulation) and it appears to be present in all bacteria with a peptidoglycan cell wall (Ikeda *et al.*, 1989; Joris *et al.*, 1990; Henriques *et al.*, 1998; Mohammadi *et al.*, 2011). Each member of the SEDS family appears to be specifically coupled to a penicillin-binding protein of class B (Matsuhashi *et al.*, 1990): FtsW is paired with FtsI (also known as PBP3), a transpeptidase specific for septal peptidoglycan synthesis (Spratt, 1977; Khattar *et al.*, 1994; Margolin, 2000; Mercer and Weiss, 2002). FtsW is recruited late into the divisome where it is required for the localization of its cognate transpeptidase FtsI (Mercer and Weiss, 2002; Fraipont *et al.*, 2011). Peptidoglycan synthesis is a multistep process that requires the translocation of a cell wall precursor, called Lipid II, from the cytoplasm to the periplasm and recently it has been shown that FtsW is a flippase that can transport lipid-linked peptidoglycan precursors to the outer side of the cytoplasmic membrane (Mohammadi *et al.*, 2011). Interestingly, in mycobacteria, FtsZ, FtsW and PBP3 form a ternary complex and it is suggested that FtsZ may regulate septal peptidoglycan synthesis modulating the interaction between FtsW and PBP3 (Datta *et al.*, 2006).

FtsI, also known as PBP3 (PBP 2B in *B. subtilis*), is an essential transpeptidase specifically involved in the synthesis of septal peptidoglycan (Botta and Park, 1981; Wientjes and Nanninga, 1991). FtsI is a bitopic membrane protein consisting of a small N-terminal cytoplasmic region connected through a single trans-membrane domain to a large periplasmic domain (Adam *et al.*, 1997; Nguyen-Disteche *et al.*, 1998; Weiss *et al.*, 1999; Piette *et al.*, 2004). In the absence of FtsI, cell division is blocked and filamentous cells with visible septal indentations are

formed (Botta and Park, 1981). FtsI localizes to the division site in an FtsZ-, FtsA-, FtsQ-, FtsL- and FtsW-dependent manner, FtsI membrane anchor domain seems involved in its recruitment to mid-cell (Weiss *et al.*, 1997; Weiss *et al.*, 1999; Mercer and Weiss, 2002) and, in turn, the non-catalytic region of FtsI periplasmic domain is required for FtsN recruitment (Wissel and Weiss, 2004).

FtsN, as previously seen for FtsQ, FtsL and FtsB, is a bitopic protein with a small N-terminal cytoplasmic domain and a large C-terminal periplasmic domain. The periplasmic domain can be divided into three regions: the region close to the membrane comprises three short helices and is connected to a C-terminal globular SPOR domain through an unstructured glutamine-rich linker (Dai *et al.*, 1996; Yang *et al.*, 2004; Gerding *et al.*, 2009). The SPOR domain might recognize specifically the septal peptidoglycan present during constriction (Gerding *et al.*, 2009). Interestingly, the other three *E. coli* proteins containing a C-terminal SPOR domain, DamX, DedR and RlpA, accumulate at the division site and they might be putative non-essential division proteins (Gerding *et al.*, 2009). DamX and DedR are two bitopic inner membrane proteins whereas RlpA is an outer membrane lipoprotein (Gerding *et al.*, 2009).

At first thought to be restricted to the enteric bacteria, FtsN-like proteins have recently been identified in *C. crescentus*, β- and δ-proteobacteria, even though highly different at the sequence level (Moll and Thanbichler, 2009). FtsN was first identified in *E. coli* in a screening as a multicopy suppressor of an *ftsA*(ts) mutant (Dai *et al.*, 1993) and it was later shown that FtsN overproduction could partially suppress the phenotype of temperature-sensitive mutants in *ftsQ*, *ftsI* (Dai *et al.*, 1993; Goehring *et al.*, 2007) and *ftsK* (Draper *et al.*, 1998; Goehring *et al.*, 2007). An *ftsA* mutant allele able to overcome the block in division induced by FtsN absence has been isolated and the same *ftsA* mutant can partially suppress the effects of *zipA* and *ftsK* deletion or MinC overproduction, likely increasing Z-ring integrity (Bernard *et al.*, 2007).

FtsN localizes to the septum in an FtsA- and FtsQ-dependent manner (Rico *et al.*, 2010) and interacts with the cell division factors FtsA, FtsQ and FtsW and the peptidoglycan synthases PBP1b and PBP3 (Karimova *et al.*, 2005; Muller *et al.*, 2007). FtsN has been shown to stimulate the peptidoglycan synthesis activities of

PBP1b *in vitro* (Muller *et al.*, 2007) and Muller *et al*. (2007) suggested that FtsN might activate PBP1b, by inducing its dimerization and/or increasing its processivity.

The overall data suggest that FtsN may be involved in the stability of the divisome and/or in the coordination of peptidoglycan synthases, acting as a trigger for septation (Lutkenhaus, 2009).

FtsP (also known as SufI) is a periplasmic protein, conserved only in the orders *Enterobacteriales* and *Pasteurellales* of the γ-proteobacteria (Samaluru *et al.*, 2007; Tarry *et al.*, 2009), which localizes to the division-site in an FtsN-dependent manner (Tarry *et al.*, 2009). *ftsP* is synthetic lethal with an *ftsEX* null mutant grown in conditions of high osmotic strength (Reddy, 2007) and is essential for the viability of cells grown under conditions of stress, such as oxidative stress and DNA damage (Samaluru *et al.*, 2007). Multiple copies of *ftsP* are able to overcome the phenotypes of an *ftsEX* null mutant or of mutants carrying the *ftsI123*, *ftsA12*, *ftsQ1* or *ftsK44* allele. Furthermore, the presence of the *ftsA** allele or overproduction of FtsQAZ or FtsN can suppress the phenotypes of *ftsP* mutants (Samaluru *et al.*, 2007). Samaluru *et al*. (2007) suggested that FtsP might stabilize or protect the divisome under various stress conditions.

YmgF is an integral membrane protein characterized by two transmembrane segments and present only in *E. coli* strains and in *Shigella flexneri* (Karimova *et al.*, 2009). It was identified in a bacterial two-hybrid-based screen looking for proteins interacting with FtsL and was shown to localize at the division-site in an FtsZ-, FtsA-, FtsQ-, and FtsN-dependent manner (Karimova *et al.*, 2009). No clear phenotypes are originated by YmgF absence or overproduction, although the latter does suppress the thermosensitivity phenotype of the *ftsQ1* temperature-sensitive allele under non-permissive conditions (Karimova *et al.*, 2009). It is suggested that under specific conditions YmgF could stabilize the divisome (Karimova *et al.*, 2009).

AmiC is an N-acetylmuramyl-L-alanine amidase involved in the cleavage of septal peptidoglycan during cell division (Heidrich *et al.*, 2001). Two other amidases, named AmiA and AmiB, are postulated to be involved in septal peptidoglycan

splitting, but only AmiC has been shown to localize to the septum of constricting cells (Heidrich *et al.*, 2001; Bernhardt and de Boer, 2003). AmiC is a non-essential periplasmic protein and, accordingly to its role in cell separation, *amiC* null mutants form cell chains. The absence of AmiA and AmiB further aggravates the cell chain phenotype of *amiC* mutants (Heidrich *et al.*, 2001). AmiC recruitment to the septum is via its N-terminal non-amidase region and it is FtsN-dependent (Bernhardt and de Boer, 2003).

EnvC is a periplasmic peptidoglycan hydrolase that localizes to the division-site where it participates in septal peptidoglycan cleavage (Bernhardt and de Boer, 2004; Uehara *et al.*, 2009; Uehara *et al.*, 2010). EnvC has been shown to activate the amidases AmiA and AmiB, probably regulating the two cell wall hydrolases spatially and temporally (Uehara *et al.*, 2010). Even though EnvC is not essential, *envC* null mutants show a cell chain phenotype (Hara *et al.*, 2002; Uehara *et al.*, 2009) and, in combination with the inactivation of the Min system, are synthetic lethal (Bernhardt and de Boer, 2004). Furthermore, *envC* overexpression induces inhibition of cell growth (Hara *et al.*, 2002). It is likely that in the absence of the Min system the maturation of the divisome is compromised, since the components of the septal ring form multiple structures along the cell filaments, and further inactivation of EnvC could cause the formation of septal rings unable to complete division (Bernhardt and de Boer, 2004).

Tol-Pal is a complex of at least five proteins, widely conserved across the Gram-negative bacteria (Sturgis, 2001) and required for the invagination of the outer-membrane (Gerding *et al.*, 2007). The known proteins forming the Tol-Pal complex are the inner membrane TolA, TolQ and TolR, the periplasmic TolB and the peptidoglycan-associated lipoprotein Pal in the outer membrane. All of the components localize to the constriction site in an FtsN-dependent manner (Gerding *et al.*, 2007). Specific interactions between the proteins in the system connect the inner and outer membrane, coordinating the invagination of the envelope layers (Gerding *et al.*, 2007). *E. coli* mutants with a defective Tol-Pal system contain large outer-membrane blebs at the septa and at the poles and show a delay in the invagination of the outer-membrane (Gerding *et al.*, 2007).

1.8 The penicillin-binding proteins

In Gram-negative bacteria the cell envelope comprises the cytoplasmic inner membrane, the peptidoglycan wall and the outer membrane that during division must all grow and divide in a coordinated manner (Weiss, 2004). The main function of the peptidoglycan layer is to resist the turgor pressure of the cell and to confer and maintain a defined cell shape (Weidel *et al*., 1960; Schwarz and Leutgeb, 1971; Holtje, 1998; Nanninga, 1998; Sauvage *et al.*, 2008; Vollmer *et al.*, 2008).

During each cell-cycle a cell goes through an elongation and a division process that end with the formation of two equal-sized daughter cells. During these events the penicillin-binding proteins (PBPs) are involved in peptidoglycan synthesis and maturation (Sauvage *et al.*, 2008). Peptidoglycan (PG) consists of linear glycan strands of alternating *N*-acetylglucosamine (Glc*N*Ac) and *N*-acetylmuramic acid (Mur*N*AC) cross-linked by short-peptides attached to the Mur*N*AC. The glycan strands are formed by oligomerization of monomeric disaccharide peptide units (lipid II) through transglycosylation reactions (Ghuysen, 1968; Schleifer and Kandler, 1972; Glauner and Holtje, 1990; Harz *et al*., 1990; Vollmer *et al.*, 2008).

PBPs direct PG synthesis catalyzing polymerization of the glycan strands (transglycosylation reaction) and cross-linking between glycan chains (transpeptidation reaction) (Sauvage *et al.*, 2008). The large family of PBPs has been subdivided into two main groups, high-molecular-weight (HMW) and low-molecular-weight (LMW) PBPs. The HMW PBPs, characterized by a cytoplasmic domain, a transmembrane segment and two periplasmic domains, are multi-modular proteins involved in PG polymerization and insertion into pre-existing cell wall (Goffin and Ghuysen, 1998; Born *et al.*, 2006; Sauvage *et al.*, 2008) and they can be further divided into class A or class B PBPs on the basis of their N-terminal domain structure and catalytic activity (Sauvage *et al.*, 2008).

In *E. coli* there are 12 different PBPs: three belonging to class A PBPs (PBP1a, PBP1b and PBP1c), two to class B (PBP2 and PBP3) and seven are LMW PBPs (PBP4, PBP5, PBP6, PBP6b, PBP7, PBP4b and AmpH) (Sauvage *et al.*, 2008).

PBP1a and PBP1b are the major bifunctional PG synthases and the loss of both of them is lethal (Denome *et al.*, 1999). Recently, it has been shown that two outer membrane lipoproteins, LpoA and LpoB, are responsible for the function, respectively, of PBP1a and PBP1b, probably stimulating the transpeptidase activity of

their specific cognate PBP (Typas *et al.*, 2010). The role of PBP1c is still unclear (Schiffer and Holtje, 1999; Sauvage *et al.*, 2008).

PBP2 and PBP3 (also known as FtsI) are monofunctional transpeptidases essential, respectively, for lateral wall synthesis and septal peptidoglycan synthesis. PBP2 is required for cell elongation and cell-shape maintenance whereas PBP3 for cell division (Weiss *et al*., 1997; den Blaauwen *et al*., 2003; Osborn and Rothfield, 2007; Sauvage *et al.*, 2008). If PBP3 is coupled with FtsW, as it was previously described, PBP2 seems to be connected to RodA, a protein sharing high homology with FtsW (Henriques *et al.*, 1998; de Pedro *et al.*, 2001; Osborn and Rothfield, 2007). FtsW and RodA flip the peptidoglycan precursors across the membrane and interact with their specific cognate PBP (Henriques *et al*., 1998; de Pedro *et al*., 2001; Mercer and Weiss, 2002; Osborn and Rothfield, 2007; Mohammadi *et al.*, 2011).

The LMW PBPs comprise two endopeptidases (PBP4 and PBP7), three carboxypeptidase (PBP5, PBP6 and PBP6b), AmpH, which is likely associated with peptidoglycan remodeling (Gonzalez-Leiza *et al*., 2011), and PBP4b, of which the function is still unknown (Vega and Ayala, 2006; Sauvage *et al.*, 2008).

1.9 The morphogenetic factors MreBCD and RodZ

Cell wall peptidoglycan is necessary but not sufficient to determine and maintain a rod cell-shape; cytoskeletal elements are required as well to coordinate peptidoglycan synthesis along the length of the cell (Fig. 1.5). In *E. coli* it is now clear that the proteins MreB, MreC and MreD, encoded by the *mre* operon, are involved in cell shape determination (Wachi *et al*., 1987; Iwai *et al*., 2002; Kruse *et al*., 2005; Osborn and Rothfield, 2007; Pichoff and Lutkenhaus, 2007b). Inactivation of PBP2 or RodA originates round cells (de Pedro *et al.*, 2001) and, consistently, lack of any one of the Mre proteins results in spherical cells very similar to those formed in the absence of cell elongation factors (Wachi *et al.*, 1987; Kruse *et al.*, 2005). MreB has been shown to localize in a dynamic helical-like pattern along the cell and to accumulate at the constriction site prior to cytokinesis in *E. coli* and *C. crescentus*, whereas in *B. subtilis* the helical structure is predominant during the whole cell cycle (Carballido-Lopez and Errington, 2003; Figge *et al.*, 2004; Gitai *et al.*, 2004; Vats and Rothfield, 2007). An

analogous helical localization was observed for MreC (Divakaruni *et al.*, 2005; Dye *et al.*, 2005; Leaver and Errington, 2005; van den Ent *et al.*, 2006), even though MreC helical structures seemed to alternate and not colocalize with the ones formed by MreB (Dye *et al.*, 2005). Recently, it has been shown that MreB might not form a helical structure but patches moving perpendicularly to the cell axis (Dominguez-Escobar *et al*., 2011; Garner *et al*., 2011; van Teeffelen *et al*., 2011). In support of a role for MreBCD as shape determinants, in *C. crescentus*, *B. subtilis* and *E. coli*, insertion of newly synthesized peptidoglycan precursors into pre-existing cell wall appears to be organized in a similar helical pattern (Daniel and Errington, 2003; Tiyanont *et al.*, 2006; Divakaruni *et al.*, 2007; Varma *et al.*, 2007).

MreB is a structural homologue of actin, widely present in non-spherical bacteria (Daniel and Errington, 2003) and able to polymerize in a nucleotide-dependent manner underneath the cytoplasmic membrane (van den Ent *et al.*, 2001; Esue *et al.*, 2005a). Beside its role as morphogenetic factor, it has also been suggested that MreB migh play a role in chromosome segregation (Kruse *et al.*, 2003; Kruse *et al.*, 2006; Madabhushi and Marians, 2009), even though other groups showed that it is not directly involved in chromosome segregation (Formstone and Errington, 2005; Karczmarek *et al*., 2007).

The widely conserved MreC and MreD are, respectively, a bitopic and a polytopic inner membrane protein (Wachi *et al.*, 1989; van den Ent *et al.*, 2006). It has been shown that MreC interacts with MreB, MreD and several PBPs, including PBP2, raising the possibility that it could form a complex with MreB and MreD involved in the spatial and temporal control of cell wall synthesis (Divakaruni *et al.*, 2005; Kruse *et al.*, 2005; van den Ent *et al.*, 2006; Cabeen and Jacobs-Wagner, 2010).

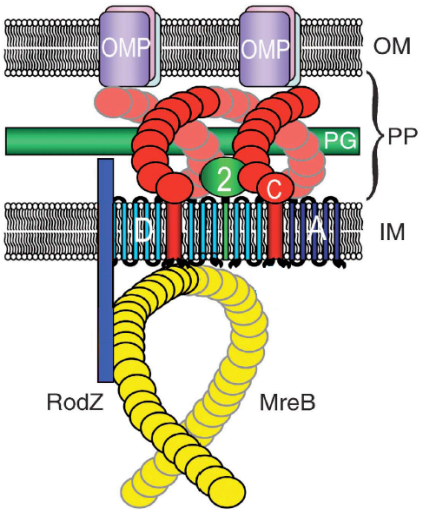

Fig. 1.5 *E. coli* morphogenetic factors

Schematic representation of *E. coli* morphogenetic factors (modified from Gerdes, 2009). OM, outer membrane; IM, inner membrane; PP, periplasm; PG, peptidoglycan layer; OMP, outer membrane protein; 2, PBP2; C, MreC; D, MreD; A, RodA.

Recently, a new morphogenetic factor has been identified: a conserved bitopic inner membrane protein called RodZ (Shiomi *et al.*, 2008; Alyahya *et al.*, 2009; Bendezu *et al.*, 2009). Consistent with its role in cell shape determination and maintenance, lack of RodZ induces formation of spherical cells and reduction of growth rate (Shiomi *et al.*, 2008; Alyahya *et al.*, 2009; Bendezu *et al.*, 2009). Furthermore, RodZ and MreB have been shown to form interdependent helical structures and a proper MreB:RodZ ratio seems crucial to maintain the bacterial rod-shape (Alyahya *et al.*, 2009; Bendezu *et al.*, 2009), even though Shiomi *et al.* (2008) data suggest that the two proteins can assemble into filaments independently from each other. van den Ent *et al.* (2010) showed that RodZ interacts directly with MreB and mutations affecting their association impair RodZ localization and cell shape maintenance.

It is suggested that RodZ, together with MreBCD, controls the peptidoglycan synthesis machinery. More precisely, MreBCD would be involved in cell width regulation and RodZ in cell length (Shiomi *et al.*, 2008; Alyahya *et al.*, 2009; Bendezu *et al.*, 2009).

1.10 FtsZ and the force of cell constriction

Different models have been suggested to explain how FtsZ could mediate cell constriction (Li *et al.*, 2007; Erickson *et al.*, 2010): the first model hypothesizes the presence of motor proteins bound to different FtsZ filaments able to make them slide past each other and, in doing so, induce septal constriction, but so far no myosin-like motor molecules have been identified in bacteria; the second model envisages the peptidoglycan-synthetic machinery as the key player in cell constriction with FtsZ only acting as a scaffold for its positioning; the third model postulates that FtsZ by itself is able to generate the constriction force.

The model based on the peptidoglycan-synthetic machinery as the generator of constriction force seems to be unlikely since there are Mycoplasma species lacking completely peptidoglycan but carrying a copy of *ftsZ* (Wang and Lutkenhaus, 1996). Furthermore, *E. coli* mutant strains that are able to divide without peptidoglycan synthesis have been constructed (Heidrich *et al*., 2002) and a mutant *B. subtilis* FtsZ carrying the C-terminal domain of the *E. coli* protein can replace the wt protein during division in *E. coli* (Osawa and Erickson, 2006).

Recent papers (Osawa *et al.*, 2008; Osawa *et al.*, 2009; Osawa and Erickson, 2011) support the Z-centric model showing that FtsZ, if artificially tethered to the membrane and able to polymerize in filaments, can generate the constriction force all by itself.

How FtsZ could generate this force has been the subject of much speculation and the models arisen can be divided into two main categories (Erickson, 2009): the first (Fig. 1.6A) is based on the conformational change of FtsZ filaments from straight to curved upon GTP hydrolysis (Lu *et al.*, 2000; Li *et al.*, 2007; Allard and Cytrynbaum, 2009); the second (Fig. 1.6B) is based on the alignment of long continuous FtsZ polymers that sliding onto each other form multiple lateral bonds, decreasing Z-ring diameter in the process (Horger *et al.*, 2008; Lan *et al.*, 2009).

Recent experiments support the FtsZ filament bending model in which short FtsZ filaments, going through a conformational change cycle from straight to curved, pinch inwards the membrane they are tethered to. A continuous constriction would be driven by regular GTP hydrolysis and exchange of subunits within the FtsZ filaments (Li *et al.*, 2007; Osawa *et al.*, 2009; Osawa and Erickson, 2011).

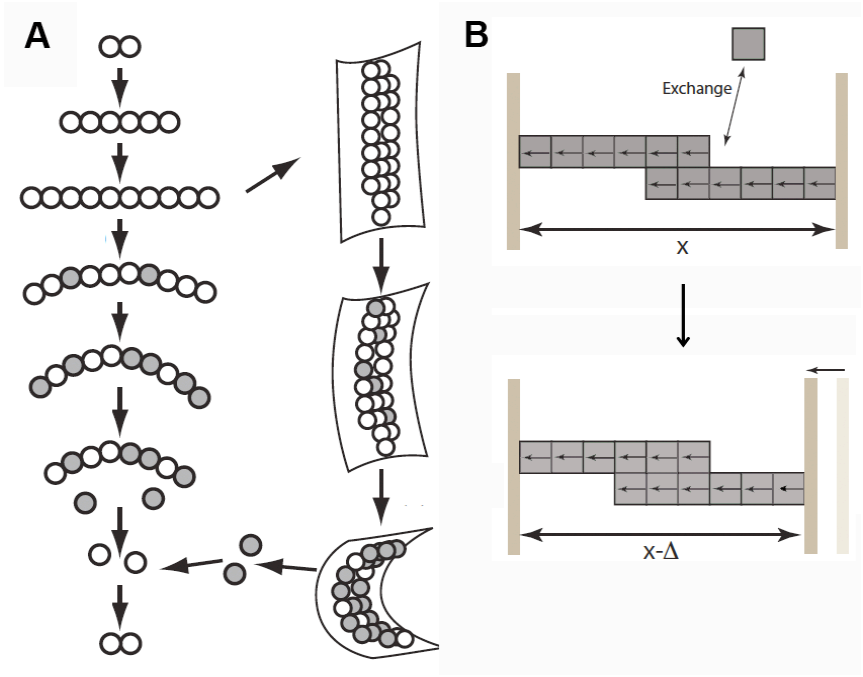

Fig. 1.6 Constriction force generation

Schematic representation of the two models proposed to explain how FtsZ could generate constriction force. **A.** FtsZ protofilaments after GTP hydrolysis (white spheres, FtsZ-GTP; grey spheres, FtsZ-GDP) go through a conformational change, from a straight to a curved conformation, pinching the membrane inwards (modified from Allard and Cytrynbaum, 2009). **B.** FtsZ filaments slide onto each other to increase the number of lateral bonds and in the process induce contraction (modified from Lan *et al*., 2009).

FtsZ protofilaments would be able to constrict the membrane to a diameter between ~50 and ~250 nm but not to complete scission (Erickson *et al.*, 2010). Different models have been proposed on how the final steps of cell constriction could be accomplished (Erickson *et al.*, 2010): one possibility is that the cell wall could actively complete septation; a second model postulates that the transmembrane proteins of the peptidoglycan synthesis machinery could regulate constriction; a third alternative, supported by work done in L-forms (Leaver *et al.*, 2009) and in cell shape defective mutants (Bendezu *et al.*, 2009), suggests that the final step in the separation of two daughter cells could be accomplished through natural membrane fluctuations.

Chapter 2

Materials and Methods

2.1 Solutions, buffers and media

In appendix A is listed the chemical composition of all the solutions, buffers and media used in this study.

2.2 Strains and Plasmids

Bacterial strains and plasmids constructed and used in this study are listed in table 2.1 and 2.2, respectively. The required antibiotics were added at the final concentration reported in the tables.

TABLE 2.1 Strains used in this study

Strains	**Genotype**	**Resistance**	**Source**
AB1157	*thr-1 leuB6 hisG4 proA2 argE3 thi-1 lacy1 galK2 ara-14 xyl-5 mtl-1 tsx-33 supE44 rpsL3*		(Bachmann, 1972)
AB1157Z84	AB1157 carrying the *ftsZ84* mutation	Tc	Gift from David J. Sherratt
AX655	F-, *thr-1*, *araC14*, *leuB6*(Am), *ftsI2158*(ts), Δ*(gpt-proA)62*, *lacY1*, *tsx-33*, *qsr'-0*, *glnV44*(AS), *galK2*(Oc), *λ*¯, *Rac-0*, *hisG4*(Oc), *rfbC1*, *mgl-50*?, *rpsL31*(strR), *kdgK51*, *xylA5*, *mtl-1*, *argE3*(Oc), *thi-1*		(Walker *et al*., 1975)
AX655Δ*zapB*	AX655 *zapB::kan*	Kan	This work
BL21A1	Arabinose-inducible gene expression from T7 promoter		Invitrogen
BL21DE3	IPTG-inducible gene expression from T7 promoter		Invitrogen
BTH101	F-*, cya99, araD139, galE15, galK16, rpsL1, hsdR2, mrA1, mrB1*		(Karimova *et al.*, 1998)
BTH101 *zapA::kan*	BTH101 *zapA::kan*	Kan	This work
BTH101Δ*zapA*	BTH101Δ*zapA*		This work
BTH101ΔzapA *zapB::kan*	BTH101Δ*zapA zapB::kan*	Kan	This work
BTH101Δ*zapA*Δ*zapB*	BTH101Δ*zapA*Δ*zapB*		This work
BTH101 *zapB::kan*	BTH101 *zapB::kan*	Kan	This work
BTH101Δ*zapB*	BTH101Δ*zapB*		This work
C41	F-, *ompT, hsdSB, (rB- mB-), gal, dcm*		Laboratory collection

DH5α	F-, *φ80lacZΔM15*, *Δ(lacZYAargF)U196*, *recA1*, *endA1*, *hsdR17*, *(rK- , mK+)*, *phoA*, *supE44*, *λ-*, *thi-1*, *gyrA96*, *relA1*		Invitrogen
KG22	C600 *lacI^q lacZΔM15*		Laboratory collection
KG22Δ*zapB*	KG22 in which the *zapB* gene is deleted		(Ebersbach *et al.*, 2008)
KG22Z84	KG22 carrying the *ftsZ84* mutation	Tc	(Ebersbach *et al.*, 2008)
KG22Z84Δ*zapB*	KG22 carrying the *ftsZ84* mutation, in which the *zapB* gene is deleted	Tc	This work
MC1000	*Δ(ara-leu), Δlac, rpsL150*		(Casadaban and Cohen, 1980)
MC1000Z84	MC1000 carrying the *ftsZ84* mutation	Tc	This work
MC1000Z84Δ*zapA*	MC1000Δ*zapA* carrying the *ftsZ84* mutation	Tc	This work
MC1000Z84Δ*zapB*	MC1000Δ*zapB* carrying the *ftsZ84* mutation	Tc	This work
MC1000Δ*minCD*	MC1000 *minCD::kan*	Kan	(Ebersbach *et al.*, 2008)
MC1000 *slmA::cml*	MC1000 *slmA::cml*	Cml	(Ebersbach *et al.*, 2008)
MC1000Δ*slmA*	MC1000Δ*slmA*		This work
MC1000 *sulA::kan*	MC1000 *sulA::kan*	Kan	This work
MC1000Δ*sulA*Δ*zapB*	MC1000Δ*zapB sulA::kan*	Kan	This work
MC1000 *zapA::cml*	MC1000 *zapA::cml*	Cml	(Ebersbach *et al.*, 2008)
MC1000Δ*zapA*	MC1000Δ*zapA*		This work
MC1000Δ*zapB*	MC1000Δ*zapB*		(Ebersbach *et al.*, 2008)
MC1000Δ*zapC*	MC1000 *zapC::kan*	Kan	This work
MC1000Δ*minCD*Δ*zapB*	MC1000Δ*zapB minCD::kan*	Kan	(Ebersbach *et al.*, 2008)
MC1000Δ*slmA*Δ*zapB*	MC1000Δ*zapB slmA::cml*	Cml	(Ebersbach *et al.*, 2008)
MC1000Δ*zapB zapA::cml*	MC1000Δ*zapB zapA::cml*	Cml	(Ebersbach *et al.*, 2008)
MC1000Δ*zapA*Δ*zapB*	MC1000Δ*zapA*Δ*zapB*		This work
MC1000Δ*minCD zapA::cml*	MC1000 *zapA::cml minCD::kan*	Kan, Cml	This work
MC1000Δ*zapA*Δ*minCD*	MC1000Δ*zapA minCD::kan*	Kan	This work
MC1000Δ*slmA zapA::cml*	MC1000Δ*slmA zapA::cml*	Cml	This work
MC1000Δ*zapA*Δ*slmA*	MC1000Δ*zapA*Δ*slmA*		This work
MC1000Δ*zapA*Δ*zapB*Δ*slmA*	MC1000Δ*zapA*Δ*zapB slmA::cml*	Cml	This work

MC1000Δ*zapB*Δ*minCD zapA::cml*	MC1000Δ*zapB zapA::cml minCD::kan*	Cml, Kan	This work
MC1000Δ*zapA*Δ*zapB*Δ*minCD*	MC1000Δ*zapA*Δ*zapB minCD::kan*	Kan	This work
MG1655			Laboratory collection
TB28	MG1655 Δ*lacIZYA*		Laboratory collection
TB28 *zapA::kan*	TB28 *zapA::kan*	Kan	This work
TB28Δ*zapA*	TB28Δ*zapA*		This work
TB28Δ*zapA*Δ*minCD*	TB28Δ*zapA minCD::kan*	Kan	This work
TB28Δ*zapA zapB::kan*	TB28Δ*zapA zapB::kan*	Kan	This work
TB28 *zapB::kan*	TB28 *zapB::kan*	Kan	This work
TB28Δ*zapB*	TB28Δ*zapB*		This work
TB28Δ*zapB*Δ*minCD*	TB28Δ*zapB minCD::kan*	Kan	This work
TB28Δ*zapA*Δ*zapB*	TB28Δ*zapA*Δ*zapB*		This work
TB28Δ*zapA*Δ*zapB*Δ*minCD*	TB28Δ*zapA*Δ*zapB minCD::kan*	Kan	This work
W3110	wild type		(Pichoff and Lutkenhaus, 2002)
PS223	W3110 *zipA1*		(Pichoff and Lutkenhaus, 2002)
PS223Δ*zapB*	PS223 *zapB::kan*	Kan	This work
PS236	W3110 *ftsA12 leu::Tn10*	Tc	(Pichoff and Lutkenhaus, 2002)
PS236Δ*zapB*	PS236 *zapB::kan*	Kan	This work
PS234	W3110 *zipA1 ftsA12 leu::Tn10*	Tc	(Pichoff and Lutkenhaus, 2002)

Cml, 30 μg/ml chloramphenicol; Kan, 30 μg/ml kanamycin; Tc, 10 μg/ml tetracycline

TABLE 2.2 Plasmids used in this study

Plasmids	**Relevant Features**	**Resistance**	**Source**
pASK75	Cloning vector	Amp	(Skerra, 1994)
pBAD24	Cloning vector	Amp	(Guzman *et al.*, 1995)
pBAD33	Cloning vector	Cml	(Guzman *et al.*, 1995)
pCA24N	Cloning vector	Cml	(Kitagawa *et al.*, 2005)
pCP20	*repA*(ts), FLP helper plasmid	Amp	(Datsenko and

			Wanner, 2000)
pEGFP	*egfp* fusion vector	Amp	Clonetech
pEG3a	P_{BAD}*::zapB::gfp*	Cml	This work
pEG4	P_{BAD}*::ftsZ::mCherry*	Cml	This work
pEG6	P_{lac}*::zapB::mCherry*	Amp	This work
pEG7	P_{lac}*::ftsZ::gfp*	Amp	This work
pEG9	P_{BAD}*::zapB::mCherry*	Cml	This work
pEG12	P_{lac}*::ftsZ::gfp*	Amp	This work
pEG28	P_{oxyTc}*::zapA*	Amp	This work
pEG37	P_{T7}*::Δ10zapB::*his_6	Amp	This work
pEG43	P_{lac}*::*his_6*::zapA*	Amp	This work
pEG47	P_{lac}*::*his_{12}*::zapA*	Amp	This work
pEG49	P_{T7}*::zapB*^{S4L5AA}*::*his_6	Amp	This work
pEG58	P_{lac}*::zapA*	Amp	This work
pEG59	P_{BAD}*::zapA*	Cml	This work
pEG60	P_{tol}*::zapB::mCherry*	Tc	This work
pEG82	P_{zapB}*::zapB, zapA*	Amp	This work
pEG82b	P_{zapB}*::zapB*	Amp	This work
pEG83	P_{zapA}*::zapA*	Amp	This work
pEG84	P_{zapB}*::Δ10zapB*	Amp	This work
pEG86	P_{zapB}*::zapB::gfp*	Amp	This work
pEG88	P_{zapB}*::zapB::*his_6	Amp	This work
pEG89	P_{zapA}*::*his_6*::zapA*	Amp	This work
pEG90	P_{zapB}*::zapB::mCherry*	Amp	This work
pFX158	P_{BAD}*::gfp::ftsK*	Amp	(Dubarry and Barre, 2010)
pGE604	P_{BAD}*::zapB*	Cml	(Ebersbach *et al.*, 2008)
pGE620	P_{lac}*::zapB::gfp*	Amp	(Ebersbach *et al.*, 2008)
pHis17	Cloning vector	Amp	(van den Ent and Lowe, 2000)
pKT25N-ZapA-1	P_{lac}*::zapA*(aa 1-20)*::T25*	Kan	This work
pKT25N-ZapA-2	P_{lac}*::zapA*(aa 1-47)*::T25*	Kan	This work
pKT25	T25 fusion vector	Kan	(Karimova *et al.*, 1998)
pKT25N	T25 fusion vector	Kan	(Karimova *et al.*, 1998)
pKT25-FtsA	P_{lac}*::T25::ftsA*	Kan	(Ebersbach *et al.*, 2008)

pKT25-FtsZ	P_{lac}*::T25::ftsZ*	Kan	(Ebersbach *et al.*, 2008)
pKT25-ZapA	P_{lac}*::T25::zapA*	Kan	This work
pKT25-ZapA-3	P_{lac}*::T25::zapA*(aa 21-109)	Kan	This work
pKT25-ZapA-4	P_{lac}*::T25::zapA*(aa 48-109)	Kan	This work
pKT25-ZapB	P_{lac}*::T25::zapB*	Kan	This work
pJB866	Cloning vector	Tc	(Blatny *et al.*, 1997)
pMFV56	P_{T7}*::ftsZ*	Kan	(Rivas *et al.*, 2000)
pMG25	Cloning vector	Amp	Laboratory collection
pNDM220	Cloning vector	Amp	(Gotfredsen and Gerdes, 1998)
pNG53	P_{lac}*::yfp::zapA*	Amp	(Goehring *et al.*, 2005)
pOU82	Cloning vector	Amp	Laboratory collection
pQE30	Cloning vector	Amp	Qiagen
pQW58	*rfp* fusion vector	Amp	(Ebersbach *et al.*, 2008)
pQW59	P_{lac}*::ftsZ::mCherry*	Amp	(Ebersbach *et al.*, 2008)
pUT18C	T18 fusion vector	Amp	(Karimova *et al.*, 1998)
pUT18C-ZapA	P_{lac}*::T18::zapA*	Amp	This work
pUT18C-ZapB	P_{lac}*::T18::zapB*	Amp	(Ebersbach *et al.*, 2008)
pUT18C-ZapB-1	P_{lac}*::T18::zapB* (aa 11-81)	Amp	This work
pUT18C-ZapB-2	P_{lac}*::T18::zapB* (aa 21-81)	Amp	This work
pUT18C-ZapB-3	P_{lac}*::T18::zapB* (aa 31-81)	Amp	This work
pUT18C-ZapB-4	P_{lac}*::T18::zapB* (aa 41-81)	Amp	This work
pUT18C-ZapB-5	P_{lac}*::T18::zapB* (aa 1-70)	Amp	This work
pUT18C-ZapB-6	P_{lac}*::T18::zapB* (aa 1-60)	Amp	This work
pUT18C-ZapB-7	P_{lac}*::T18::zapB* (aa 1-50)	Amp	This work
pUT18C-ZapB-8	P_{lac}*::T18::zapB* (aa 1-40)	Amp	This work
pUT18C-ZapB-b	P_{lac}*::T18::zapB*^{S4L5AA}	Amp	This work
pUT18C-ZapB-c	P_{lac}*::T18::zapB*^{E6V7AA}	Amp	This work
pUT18C-ZapB-d	P_{lac}*::T18::zapB*^{F8E9AA}	Amp	This work
pUT18C-ZapB-e	P_{lac}*::T18::zapB*^{K10L11AA}	Amp	This work
pZapBHis	P_{T7}*::zapB::his*$_6$	Amp	(Ebersbach *et al.*, 2008)

Amp, 30 µg/ml or 100 µg/ml ampicillin; Cml, 30 µg/ml chloramphenicol; Kan, 30 µg/ml kanamycin; Tc, 10 µg/ml tetracycline

2.3 Oligonucleotides

DNA oligonucleotide sequences of primers used in this study for PCR reactions are listed in appendix B.

2.4 DNA methods

2.4.1 Polymerase chain reaction (PCR)

The Phusion DNA polymerase (Finnzymes) was used for cloning purposes; instead the GoTaq Flexi DNA Polymerase (Promega) was chosen when a high-fidelity polymerase was not necessary, for example for colony PCRs or for controlling chromosomal gene deletions. In a typical PCR reaction were mixed 10 ng of DNA template, the Reverse and Forward oligonucleotides at a final concentration of 0.3 μM, a mixture of the four dNTPs at a final concentration of 200 μM and the reaction buffer and the polymerase were added at the final concentration suggested by the company selling the Polymerase in use. The thermal cycling protocol followed the indications given by the Company selling the enzymes.

2.4.2 Colony PCR

Colony PCR was used for screening of correct clones after transformation of a ligation reaction. It was performed using one primer that anneals on the backbone of the plasmid and a second primer annealing on the DNA sequence we wished to clone in the plasmid. Oligonucleotides, dNTPs, buffer and polymerase concentrations were the same used for standard PCR reactions.

The colonies were picked up using sterile plastic tips, streaked on a selective plate (in order to be able to recover the clones giving the positive products in the PCR reaction) and twirled in a tube containing the PCR reaction mix.

2.4.3 Plasmid DNA purification

A 5 ml LB culture of *E. coli* was incubated over-night at 37°C shaking. The

plasmid DNA was purified from the over-night culture using the QIAminiprep (Qiagen) kit, following the supplied instructions.

2.4.4 Restriction enzyme digestion of DNA

The restriction enzymes and the buffers used were from Roche, New England Biolabs or Promega. DNA was usually incubated with the restriction enzymes for 1 or 2 hours, the temperature at which the enzymes are active and the condition for their inactivation (if possible) are stated by the supplier companies.

2.4.5 Purification of DNA fragments

PCR products or digested DNA samples were purified using the QIAquick PCR purification kit (Qiagen), following the supplied instructions.

2.4.6 Blunt-end production from DNA 3' and 5' overhangs

T4 DNA polymerase (New England Biolabs) was used to remove DNA 3' overhangs and fill-in DNA 5' overhangs, producing DNA blunt-ends. 100 μM dNTPs, the T4 buffer and BSA were added to restriction enzyme reactions containing the DNA template. The reaction was incubated for 15 minutes at 12°C with 1U of T4 DNA polymerase and then the enzyme inactivated by addition of 10 mM EDTA and incubation at 75°C for 20 minutes.

2.4.7 DNA dephosphorilation reaction

Dephosphorilation of linearized plasmid DNA (to prevent religation of a digested plasmid during a ligation reaction) was performed using Shrimp Alkaline Phosphatase (SAP, Usb). After the DNA had been digested with the endonucleases, the SAP enzyme was added directly to the restriction enzymatic reaction (1 unit of SAP for every 1 pmol of DNA ends) and incubated at 37°C for 30-60 minutes. The SAP enzyme could be inactivated incubating the reaction at 65°C for 15 minutes.

2.4.8 DNA ligation reaction

T4 DNA ligase (Roche) was used to ligate double-stranded DNA molecules with cohesive or blunt ends. A typical ligation reaction contained digested plasmids and DNA fragments, the T4 ligase buffer and 1 U of T4 DNA ligase. The ligation reaction was incubated for 1 hour at room temperature.

2.4.9 Agarose gel electrophoresis

Agarose gels (usually 1%) were made melting agarose powder in 1x TAE buffer, the agarose solution was allowed to cool to ~55°C and ethidium bromide added to a final concentration of 0.75 μg/ml. DNA samples were mixed with loading dye, loaded in the solidified gels and then run in 1x TAE buffer at a constant voltage of 120 V. Pictures of the gels were taken using a UV transilluminator attached to a Lumenera USB 2.0 camera.

2.4.10 Extraction of DNA fragments from agarose gels

DNA fragments were purified from agarose gels using the QIAquick (Qiagen) Gel Extraction kit, following the supplied instructions.

2.4.11 DNA sequencing

The correct sequence of new constructs, made using DNA fragments produced by PCR reactions, was ascertained by DNA sequencing. All the constructs made in this study were sequenced by the sequencing facility of the University of Dundee.

2.4.12 Preparation of *E. coli* competent cells

An over-night culture was diluted 100x in 10 ml of LB and grown at 37°C until the OD_{450} reached ~0.5, then cells harvested by centrifugation. The cell pellet was first washed by centrifugation with 5 ml of ice-cold 50 mM $CaCl_2$, then resuspended in 800 μl ice-cold 50 mM $CaCl_2$ and incubated on ice for 30-60 minutes. The cells were then competent and ready to use for transformation.

2.4.13 Transformation of *E. coli* competent cells

1 µl of supercoiled plasmid DNA or 10 µl of a ligation reaction were added to one aliquot (50-100 µl) of competent cells. The cells and the DNA were incubated on ice for 30 minutes, heat-shocked for 2 minutes at 42°C and then left on ice for 5-10 minutes. 500 µl of LB were then added and the cells incubated shaking at 37°C for 1 hour. 100-200 µl from each transformation were plated on selective plates.

2.4.14 Purification of *E. coli* chromosomal DNA

Chromosomal DNA was purified from an over-night culture using the MasterPure Complete DNA Purification kit (Epicentre), following the supplied instructions.

2.4.15 P1 phage transduction

Making P1 phage lysate: an over-night culture (10 ml) was diluted 40 times in LB and incubated at 37°C until the optical density (OD_{450}) reached ~0.5. From this culture 1 ml was diluted in 10 ml LB containing 10 mM $MgCl_2$ and 5 mM $CaCl_2$, 100 µl of phage stock were added and the culture left to grow at 37°C until lysis occured (1-4 hours). The culture was then transferred to a tube, 200 µl of chloroform were added and the culture spun down for 10 minutes at 3,500 rpm. The supernatant was transferred to a new tube and the chloroform extraction repeated a second time. The P1 phage lysate could then be stored at 4°C.

Making P1 transduction: an over-night culture was diluted 20 times in LB and grown at 37°C for 4 hours. Cells were harvested, resuspended in ½ volume of 10 mM $MgCl_2$ and 5 mM $CaCl_2$ and centrifuged at 3,500 rpm for 10 minutes. This step was repeated a second time. 100 µl of cells were mixed with 5-100 µl of P1 phage lysate and incubated at 30°C for 30 minutes. 1 ml of LB + 10 mM NaCitrate were added to the cells, after incubation at 37°C for 1-2 hours everything was plated on selective plates.

2.5 RNA methods

2.5.1 Extraction of RNA from cells

Over-night cultures were diluted in M9 minimal medium supplemented with 0.2% glucose and incubated at 37°C. At an OD_{450} ~0.5 the cultures were diluted 100x in fresh medium and left to grow until OD_{450} ~0.3, when 3 ml of each culture were collected in tubes, immersed in liquid N_2 and centrifuged for 10 minutes at 5,000 rpm at 4°C. The pellet was stored at −80°C over-night and the next day RNA extraction was performed using the RNeasy Mini Kit (Qiagen), following the supplied instructions. To assess the quality of the purified RNA, an aliquot from each sample was incubated for 5 minutes at 70°C and then loaded on an agarose gel.

2.5.2 Reverse transcription qPCR

2 µg of each purified RNA were digested by DNaseI for 10 minutes at 37°C in a 20 µl reaction volume and the enzyme was then inactivated by adding 5 µl of a 7.5 mM EDTA solution and incubating the reaction at 65°C for 15 minutes. The cDNA was synthesized using a high-capacity cDNA reverse transcription kit (Applied Biosystems), following the supplied instructions. A qPCR reaction was assembled mixing 10 ng cDNA, 0.3 µM of both the primers and 10 µl of 2x PCR Master Mix for Sybr green kit (Eurogentec). For each sample two qPCR reactions were run in parallel on a LightCycler 480 real-time PCR system (Roche). *rpsA* and *rpoB* were chosen as reference genes. The primers used were: *rpsA*: rpsAqPCR-f + rpsAqPCR-r; *rpoB*: rpoBqPCR-f + rpoBqPCR-r; *zapA*: zapAqPCR-f + zapAqPCR-r; *zapB*: zapBqPCR-f + zapBqPCR-r. The relative folds of expression between the different strains were calculated using the qBase software (Hellemans *et al.*, 2007).

2.6 Protein methods

2.6.1 Protein concentration determination

The concentration of the purified proteins was determined or by using the direct absorbance at 280 nm on a NanoVue Plus Spectrophotometer (GE Healthcare) or by using the Bradford colorimetric assay (Bradford, 1976).

2.6.2 SDS-polyacrylamide gel electrophoresis (SDS-PAGE)

Proteins were separated by size and visualized on gel using SDS-polyacrylamide gel electrophoresis. The NuPAGE LDS Sample Buffer (Invitrogen) and the NuPAGE Sample Reducing Agent were added to the proteins in solution, the samples were then incubated at 80°C for 10 minutes before being loaded on a gel. The gels used for electrophoresis were Precast Novex Midi Gels 4-12% Bis-Tris (Invitrogen), the electrophoresis chamber was filled with 1x MES buffer (Invitrogen) and usually, to see the proteins analysed in this study clearly separated, gels were run for 40 minutes at 200 V.

2.6.3 Colloidal Coomassie staining of NuPAGE Bis-Tris gels

To visualize the proteins the gels were immersed for 1 hour in a Coomassie staining solution (50% methanol, 10% acetic acid, 40% water, 10 mg/l Coomassie R-250) and subsequently in a destaining solution (50% methanol, 10% acetic acid, 40% water) for 1-2 hours.

2.6.4 Western blotting

The protein samples were run on a SDS-PAGE and then transferred to a PVDF membrane (GE Healthcare) using a semi-dry transfer blotting cassette (Hoefer Scientific). In the cassette were placed on top of each other 6 sheets of filter paper soaked in transfer buffer, a PVDF membrane soaked in methanol and equilibrated for 10 minutes in transfer buffer (see appendix), the gel soaked in transfer buffer and other 6 sheets of filter paper soaked in transfer buffer. Possible bubbles between the

gel and the PVDF membrane were eliminated by rolling a glass tube on the filter papers at the top. The transfer was performed at 115 mA for 60 minutes. After the transfer, the membrane sandwich was disassembled and the PVDF membrane rinsed in PBST (PBS + 0.1% Tween 20) and incubated shaking over-night in blocking buffer (PBST + 5% milk powder). The morning after, the membrane was rinsed in PBST and then immersed in blocking buffer with the addition of the primary antibody (usually diluted 5,000 or 10,000 times) for 1 hour, washed 3 times for 20 minutes in PBST, incubated for 1 hour in blocking buffer with the addition of the secondary antibody (1:10,000 dilution of anti rabbit horseradish-peroxidase (Sigma)) and washed again 3 times in PBST. The proteins of interest were visualized using the ECL Plus Western Blotting Detection System (GE Healthcare), following the supplied instructions.

2.6.5 Purification of FtsZ

The protocol for the purification of FtsZ was adapted from Rivas *et al*. (2000). FtsZ was overproduced in *E. coli* BL21DE3 (Invitrogen) transformed with the plasmid pMFV56. The over-night culture was diluted 1:400 in 400 ml LB and incubated shaking at 37°C, at mid-exponential growth gene expression was induced by the addition of 1 mM IPTG. After 3 hours of induction, cells were harvested, resuspended in 4 ml PEM buffer (50 mM PIPES pH 6.5; 5 mM $MgCl_2$; 1 mM EDTA) and lysed by sonication on ice. The lysate was centrifuged for 40 minutes at 15,000 rpm at 4°C and the supernatant saved. Then the 1st purification cycle was initiated: FtsZ polymerization was induced by adding 1 mM GTP and 20 mM $CaCl_2$ to the supernatant and incubating the sample for 15 minutes at 30°C. FtsZ polymers were then pelleted by centrifugation (15 minutes at 13,000 rpm) and resuspended in 4 ml of PEM buffer. The sample was again incubated for 15 minutes at 30°C and centrifuged for 15 minutes at 13,000 rpm, but this time the supernatant was saved and used in the 2nd purification cycle, which was an absolute repetition of cycle one. The final supernatant was loaded onto a 1 ml HiTrap Q HP ion exchange column (Amersham) and the protein eluted in a salt gradient of PEM buffer containing NaCl from 0 to 1 M. Purified FtsZ was dialysed into FtsZ storage buffer (50 mM Tris, pH 7.5; 1 mM EDTA; 250 mM NaCl; 10% glycerol), concentrated, snap-frozen in liquid nitrogen and stored at −80°C.

2.6.6 Purification of ZapB-His

ZapB-His_6 was overproduced from plasmid pZapBHis in *E. coli* BL21AI cells (Invitrogen) grown at 37°C in 2xTY medium supplemented with 0.2% glucose. At mid-exponential growth gene expression was induced by addition of 0.4% arabinose. After 6 hours of induction, cells were harvested, resuspended in buffer A (50 mM Tris-HCl, pH 5.0; 300 mM NaCl; 15 mM imidazole) containing 5 μg/ml DNaseI and 1 mg/ml lysozyme, and lysed by sonication. The lysate was cleared by centrifugation for 30 minutes at 20,000 rpm. The cleared lysate was loaded onto a 1 ml HisTrap column (GE Healthcare) and the protein was eluted with stepwise increments of buffer B (buffer A + 2 M imidazole). Purified ZapB-His_6 was dialysed into ZapB storage buffer (20 mM Tris-HCl pH 7.0; 1 mM EDTA; 10% glycerol), concentrated, snap-frozen in liquid nitrogen and stored at −80°C. ZapB-His_6 mutants were purified using the same protocol.

2.6.7 Purification of His-ZapA

His_6-ZapA was overproduced from plasmid pCA24N-*zapA*$^+$ in *E. coli* C41 cells grown at 37°C in 2xTY medium. At mid-exponential growth gene expression was induced by the addition of 1 mM IPTG. After 5 hours of induction, cells were harvested, resuspended in buffer A (50 mM Tris-HCl pH 7.0; 300 mM NaCl; 15 mM imidazole) containing 5 μg/ml DNaseI and 1 mg/ml lysozyme, and lysed by sonication. The lysate was cleared by centrifugation for 30 minutes at 20,000 rpm. The cleared lysate was loaded onto a 1 ml HisTrap column (GE Healthcare) and the protein eluted in a buffer B (buffer A + 1 M imidazole) gradient. Purified His_6-ZapA was dialysed into buffer C (20 mM Tris-HCl pH 7.0; 10% glycerol), concentrated, snap-frozen in liquid nitrogen and stored at −80°C.

2.6.8 Purification of ZapA

His_{12}-ZapA (containing the Xa cleavage site between the His_{12}-tag and ZapA) was overproduced from plasmid pEG47 in *E. coli* C41 cells grown at 25°C in LB medium. At mid-exponential growth gene expression was induced by addition of 1 mM IPTG. After 20 hours of induction, cells were harvested, resuspended in buffer A

(20 mM Tris-HCl, pH 8.0; 200 mM NaCl; 15 mM imidazole) containing 5 μg/ml DNaseI and 1 mg/ml lysozyme, and lysed by sonication. The lysate was cleared by centrifugation for 30 minutes at 20,000 rpm. The cleared lysate was loaded onto a 1 ml HisTrap column (GE Healthcare) and the protein eluted in a buffer B (buffer A + 1 M imidazole) gradient. Purified His_{12}-ZapA was dialysed into Xa reaction buffer (20 mM Tris-HCl, pH 8.0; 100 mM NaCl; 2 mM $CaCl_2$) and incubated at room temperature with factor Xa for 20 hours (10 μg of factor Xa for a reaction containing 3 mg of purified protein). The complete cleavage was confirmed by SDS-PAGE. ZapA was then dialysed into buffer C (20 mM Tris-HCl pH 7.0; 10% glycerol) and concentrated by centrifugation through a 10-kDa cut-off filter that removed the His-tag. Aliquots were snap-frozen in liquid nitrogen and stored at −80°C. Xa cleavage resulted in a ZapA with no extra amino acids at its N-terminal.

2.6.9 Sucrose Gradient Centrifugation

For interaction studies between His-ZapA, ZapB-His and FtsZ a step gradient of 10, 20, 30, 40, 50 and 60% sucrose was used. Purified proteins (10-15 μg each) were mixed in the presence of BSA (the absence of BSA did not change the sedimentation patterns) in a 50 mM PIPES pH 6.5 buffer and incubated for 30 minutes at room-temperature before being loaded on sucrose gradients (the sucrose stock solutions were buffered in 50 mM PIPES pH 6.5 buffer).

Protein samples were spun down for 2 h (25,000 rpm, 4°C) in a Beckman Rotor SW50.1/55 using 0.8 ml tubes (5 x 41 mm) and suitable adapters. After centrifugation, sample fractions of 100 μl were collected and analysed by SDS-PAGE and Coomassie staining.

2.6.10 Ni^{2+}–NTA-agarose affinity chromatography

0.2 mg/ml of FtsZ or/and ZapA were added to 100 μl of PEM buffer in the presence of either His_6-ZapA (0.1 mg/ml) or ZapB-His_6 (0.1 mg/ml) or $ZapB^{S4L5AA}$-His_6 (0.1 mg/ml) and the reactions were incubated at room temperature for 15 minutes, slowly shaking. 20 μl of Ni^{2+}–NTA-agarose (equilibrated in PEM buffer) were then added to each tube and the reactions incubated at room temperature for 5 minutes to allow the binding of the His-tagged proteins to the agarose beads. The

resin was separated from the reaction solution by centrifugation (2 minutes at 3,000 rpm) and washed twice in 100 µl of PEM buffer supplemented with 10 mM imidazole. The proteins bound to the resin were then eluted washing the resin twice in 20 µl of PEM buffer supplemented with 500 mM imidazole. The final eluted fractions were 2.5 times more concentrated than the initial sample and the intermediate fractions. Equal volumes from each fraction were analysed by SDS-PAGE and Coomassie staining or by immunoblotting.

2.6.11 Far-Western Blotting

2 µg of each protein were spotted on a Hybond-C membrane (Amersham Biosciences) and left to dry for 30 minutes at room temperature. The membrane was incubated slowly shaking in PEM buffer + 5% milk powder and, after 30 minutes, 10 µg of the second protein (the probe) were added into the solution. After 1 hour, the membrane was washed 4 times for 5 minutes in PEM buffer + 5% milk powder. From now on the Western-blot protocol previously described was followed, using an antibody against the probe protein as the primary one.

2.6.12 GTPase activity assay

FtsZ GTPase activity was assayed using Malachite green assay to quantify the released phosphate (Lanzetta *et al.*, 1979). Two different polymerization buffers were used: Buffer 1 (50 mM PIPES pH 6.5, 50 mM KCl, 10 mM $MgCl_2$) and Buffer 2 (50 mM HEPES pH 7.5, 50 mM KCl, 10 mM $MgCl_2$). To the polymerization buffers were added 5 µM of FtsZ, ZapA and ZapB-His and 1 mM GTP (the GTP stock solutions were buffered in the 2 different polymerization buffers) in a total volume of 100 µl. The reactions were incubated at 30°C and 10 µl samples were withdrawn at different time points during a 30 minutes period. Standard curves with known concentrations of phosphate were used to determine the amount of phosphate released.

2.6.13 90° Angle Light Scattering assay

Light scattering experiments were based on the method described by

Mukherjee and Lutkenhaus (1999), using a Varian Cary Eclipse fluorescence spectrophotometer and a quartz cuvette (1 cm light path) maintained at 30°C. Excitation and emission wavelengths were set to 350 nm with slit widths of 2.5 nm and the photomultiplier tube at 600 V. Proteins (concentrations as indicated in the text) were incubated in 50 µl of polymerization buffer (Buffer 1 and Buffer 2 as described for the GTPase activity assay) in the cuvette and, after establishing a baseline for 5 minutes, polymerization was induced by addition of 0.5 or 1 mM GTP. The light scattering was recorded for a total of 15 or 30 minutes. In the graphs is reported AU or ΔAU vs. time, where the ΔAU was calculated by subtracting the baseline values from the AU registered by the machine after GTP addition.

2.6.14 Sedimentation assay

Reactions containing FtsZ, ZapA and ZapB-His (concentrations as indicated in the text) were incubated for 5 minutes at 30°C in polymerization Buffer 1 (as described for the GTPase activity assay). 0.5 or 1 mM GTP (or GDP) was then added to initiate FtsZ polymerization and samples incubated for 5 minutes at 30°C before ultracentrifugation (80,000 rpm for 10 minutes at 25°C). The Supernatant was removed and an equal volume of SDS-PAGE sample buffer was used to resuspend the Pellet. An equal volume from each fraction was analysed by SDS-PAGE and Coomassie staining.

2.6.15 Negative stain electron microscopy

Polymerization reactions were prepared as done for the sedimentation assays. 30 seconds after the addition of GTP, 5 µl of each polymerization reaction were placed on a carbon-coated copper grid (Newcastle Biomedical EM Unit) and the liquid in excess blotted off. The grid was then stained with 100 µl of a 2% uranyl-acetate solution and again blotted off. Grids were examined using a Philips CM100 Compustage Transmission Electron Microscope (FEI) with an AMT CCD camera (Deben).

2.6.16 Bacterial two-hybrid analysis

Bacterial two-hybrid analysis was performed as described by Karimova *et al*. (1998). Strain BTH101 (or derivatives) was co-transformed with pKT25 and pUT18C derived plasmids and, from each co-transformation reaction, a 15 µl aliquot was spotted onto nutrient agar plates supplemented with 100 µg/ml ampicillin, 50 µg/ml kanamycin, 0.1 mM IPTG and 0.004% X-Gal. The plates were incubated at 30°C and pictures taken after 48 hours. 0.1 mM IPTG probably induces the production of high amounts of the tagged proteins, especially if compared to the short pulse of transcription needed to avoid inclusion bodies formation when using a ZapB-GFP fusion. We don't know why using the BTH assay the tagged ZapB is still able to interact with ZapA and does not precipitate in inclusion bodies.

2.7 Microscopy

2.7.1 Microscopic imaging

For phase-contrast and fluorescence microscopy 1–3 µl of a culture sample were placed on a microscope slide coated with a thin agarose (1%) layer and covered with a coverslip. For DNA staining a 10 µl culture sample was mixed with 1 µl of DAPI (Sigma) solution (1 µg/ml). Images were acquired with a Sony Cool-Snap HQ cooled CCD camera (Roper Scientific) attached to a Zeiss Axiovert 200 M microscope. The images were acquired and analysed with METAMORPH version 6 software. Final image preparation was performed in Adobe Photoshop 6.0 (Adobe Systems Incorporated). For the Z-stacks and 3D reconstruction, images were acquired with a Deltavision microscope (Applied Precision). The images in the Z series were recorded with step size of 0.2 µm and deconvolved using software softWoRx version 3.5.1. The 3D models were rendered using software softWoRx version 3.5.1.

2.7.2 Cell fixation

500 µl of cells, grown in M9 minimal medium or in LB medium, were mixed with an equal volume of Fixative solution (see appendix) and incubated first at room

temperature for 20 minutes and then shifted on ice for 40 minutes. The fixated cells were washed 3 times in PBS and finally resuspended in 100 µl of PBS. Cells were stored at 4°C for up to 48 hours before microscopy.

2.7.3 Fluorescent fusion protein expression and localization

Cells were grown at 30°C or 37°C in M9 minimal medium supplemented with 1 µg/ml thiamine, 0.1% casamino acids, 0.2% glucose and the specific antibiotics. ZapB-GFP induction and localization from pEG3a: at an OD_{450} value of about 0.2, a cell sample was harvested by centrifugation and resuspended in pre-heated medium without glucose, gene expression was induced by adding 0.2% arabinose. After 5 minutes, induction was stopped by adding 0.2% glucose. ZapB-GFP induction and localization from pGE620: exponentially growing cultures were induced with 50-200 µM IPTG for 60 minutes before samples were collected for microscopy. FtsZ-mCherry from pEG4: at an OD_{450} value of about 0.2, a cell sample was harvested by centrifugation and resuspended in pre-heated medium without glucose, gene expression was induced by adding 0.2% arabinose. After 1 minute, induction was stopped by adding 0.2% glucose. ZapB-mCherry from pEG9 and GFP-FtsK from pFX158: at an OD_{450} value of about 0.2, a cell sample was harvested by centrifugation and resuspended in pre-heated medium without glucose, gene expression was induced by adding 0.2% arabinose. After 25 minutes induction was stopped by adding 0.2% glucose. YFP-ZapA from pNG53 and FtsZ-mCherry from pQW59: the leakiness of the promoter was sufficient for localization studies. FtsZ-GFP from pEG12: at an OD_{450} value of about 0.2 FtsZ-GFP was induced by 200 µM IPTG. ZapB-mCherry from pEG60: at an OD_{450} value of about 0.2 ZapB-mCherry was induced by 3 mM Tol. After induction, cells were left to grow for at least another 30 minutes before samples were collected and analysed at the microscope. If not differently specified, all the localization analyses were performed using fusions expressed from a plasmid in addition to the native untagged copy on the chromosome.

2.7.4 ZapB-GFP localization in an *ftsZ84* strain with and without cephalexin treatment

Cells carrying pEG3a (P_{BAD}*::zapB::gfp*) were grown at the permissive temperature (30°C) in M9 minimal medium supplemented with 1 μg/ml thiamine, 0.2% glucose, 0.1% casamino acids and 30 μg/ml chloramphenicol. ZapB-GFP expression from pEG3a was induced as previously described. Each culture was then split in two and cephalexin was added to a final concentration of 10 μg/ml to one half. The other half of each culture was allowed to grow for another 60 minutes at 30°C before being diluted 2 folds and again divided in two: one half was left growing at 30°C and the other half incubated at the non-permissive temperature (42°C). Samples were collected from KG22/pEG3a and KG22Z84/pEG3a cultures both at 30°C and 42°C after 45 minutes, whereas from the cephalexin-treated cultures samples were taken after 90 minutes. Samples of KG22/pEG3a and KG22Z84/pEG3a at 30°C and 42°C were immediately fixed, as previously described.

2.7.5 ZapB-GFP localization in PS223, PS234, PS236 strains

Cells of strains PS223, PS234 and PS236 carrying the ZapB-GFP expression plasmid pEG3a (P_{BAD}*::zapB::gfp*) were grown at the permissive temperature (30°C) in LB medium. ZapB-GFP expression from pEG3a was induced as previously described. 60 minutes after induction each culture was split in two and diluted two folds: one half was left to grow at 30°C and the other half incubated at 42°C, the non-permissive temperature. Samples from all the cultures were collected after 60 minutes and cells immediately fixed, before being analysed at the microscope.

2.7.6 Nucleoid analysis in KG22 and KG22Δ*zapB* strains

Cells of strains KG22 and KG22Δ*zapB* were grown at 30°C in LB medium. At an OD_{450} value of about 0.2, cephalexin was added to a final concentration of 10 μg/ml and the cultures left to grow for 90 minutes. Nucleoids were stained with 1 μg/ml DAPI and cells visualized at the microscope.

2.7.7 Live/Dead staining of MC1000Δ*zapB* cells

Cells of strain MC1000Δ*zapB* were grown at 37°C in LB medium. A sample of cells in mid-exponential growth phase was collected and stained with the LIVE/DEAD BacLight Bacterial Viability Kit (Invitrogen) before analysis at the microscope.

2.7.8 ZapA, YFP-ZapA, ZapB and ZapB-mCherry overproduction

Overproduction of ZapB and ZapB-mCherry: cells of strain KG22/pGE604 (P_{BAD}*::zapB*) and KG22/pEG6 (P_{lac}*::zapB::mCherry*) were grown in LB at 37°C, at an OD_{450} value of about 0.2 gene expression was induced respectively with 0.2% arabinose and 1 mM IPTG. Cells of strains KG22/pEG12 (P_{lac}*::ftsZ::gfp*)/pGE604 (P_{BAD}*::zapB*) and KG22/pEG6 (P_{lac}*::zapB::mCherry*) were analysed at the microscope 2 hours after induction.

Overproduction of ZapA and YFP-ZapA: cells of strain MC1000/pEG58 (P_{lac}*::zapA*), MC1000/pEG59 (P_{BAD}*::zapA*) and MC1000/pNG53 (P_{lac}*::yfp::zapA*) were grown in M9 minimal medium supplemented with 10% glycerol and the specific antibiotics at 30°C. At an OD_{450} value of about 0.2, cultures were induced respectively with 500 µM or 1 mM IPTG, 0.2% arabinose and 200 µM, 500 µM or 1 mM IPTG.

Cells of strain MC1000 / pEG12 (P_{lac}*::ftsZ::gfp*) / pEG59 (P_{BAD}*::zapA*), MC1000/pEG3a (P_{BAD}*::zapB::gfp*)/pEG58 (P_{lac}*::zapA*) and DH5α/pEG12 (P_{lac}*::ftsZ::gfp*)/pEG59 (P_{BAD}*::zapA*)/pEG60 (P_{tol}*::zapB::mCherry*) were analysed at the microscope 2 hours after induction.

2.7.9 Growth and cell length analysis

The growth of all deletion and *wt* strains was performed in LB at 30°C and in M9 minimal medium and LB at 37°C. Cultures were grown over-night and in the morning diluted ~500 folds into fresh medium, the optical density OD_{450} was measured every 30-60 minutes during cell growth. Cell samples for cell length measurements were collected at an OD_{450} value of about 0.4.

2.7.10 Transmission electron microscopy (TEM) of *wt* and Δ*zapB* cells

Cultures of MC1000 and MC1000Δ*zapB* were grown in LB at 37°C and at mid-exponential phase cell samples were collected and fixed by adding glutaraldehyde (2.5% final concentration). After centrifugation the cell pellet was washed in 2.5% glutaraldehyde and incubated over-night at 4°C. TEM samples were prepared for analysis by the Electron Microscopy Research Facility (University of Newcastle) and examined with a Philips CM100 Compustage Transmission Electron Microscope (FEI) with an AMT CCD camera (Deben).

2.8 Construction of plasmids

Purified MG1655 chromosomal DNA was used as template for PCR reactions, if not differently specified. Plasmid pEG3a carries *zapB::gfp* downstream of the arabinose inducible P_{BAD} promoter of vector pBAD33. The *Psi*I-*Stu*I fragment carrying *zapB::gfp* from pGE620 was inserted into the unique *Sma*I site of pBAD33 in a clockwise orientation, thus creating pEG3a. Plasmid pEG4 carries *ftsZ::mCherry* downstream of the arabinose inducible P_{BAD} promoter of vector pBAD33. A *Bam*HI(blunted)-*Hind*III fragment from pQW59 carrying *ftsZ::mCherry* was inserted into *Sma*I-*Hind*III sites of pBAD33. Plasmid pEG6 carries *zapB::mCherry* downstream of the IPTG inducible P_{lac} promoter of vector pQW58. *zapB* was amplified by PCR with primers: ForZapB-RFP + RevZapB-RFP. The PCR fragment was cut with restriction enzymes *Bam*HI and *Sac*I and cloned into the corresponding sites of pQW58. Subsequently, an *Eco*RI(blunted)-*Hind*III fragment carrying *zapB::mCherry* was inserted into the *Sma*I-*Hind*III sites of pBAD33, creating pEG9. Plasmid pEG7 carries *ftsZ::gfp* downstream of the IPTG inducible P_{lac} promoter of vector pEGFP. *ftsZ* was amplified by PCR with primers: ForFtsZ-GFP + RevFtsZ-GFP. The PCR fragment was cut with restriction enzymes *Sma*I and *Nco*I and cloned into the corresponding sites of pEGFP. Subsequently, a *Bam*HI-*Stu*I fragment carrying *ftsZ::gfp* was inserted into *Bam*HI-*Pml*I sites of pNDM220, creating pEG12. Plasmid pEG28 is a pASK75 derivative that carries *zapA* downstream of the oxyTc

inducible promoter. *zapA* was amplified by PCR with primers: zapA-3 + zapA-4. The PCR product was cut with *Bam*HI and *Hind*III and cloned into the same sites of pASK75. Plasmid pEG37 is a pHis17 derivative that carries Δ*10zapB::his*$_6$ (deletion of the first 10 N-terminal aa) downstream of the T7 inducible promoter. Δ*10zapB* was amplified by PCR with primers: ZapB-H17 + ZapB-H17R. The PCR product was cut with *Nde*I and *Bam*HI and cloned into the same sites of pHis17. Plasmid pEG43 is a pQE30 derivative that carries *his*$_6$*::zapA* downstream of the P$_{lac}$ promoter. *his*$_6$*::zapA* was amplified by PCR with primers: Xa-zapA + zapA-4. The PCR product was cut with *Bam*HI and *Hind*III and cloned into the same sites of pQE30. Plasmid pEG47 carries *his*$_{12}$*::zapA* downstream of the IPTG inducible P$_{lac}$ promoter of vector pMG25. *his*$_{12}$*::zapA* was amplified from plasmid pEG43 by PCR with primers: EG47-For + zapA-4. The PCR fragment was cut with restriction enzymes *Nco*I and *Hind*III and cloned into the corresponding sites of pMG25. Plasmid pEG49 is a pHis17 derivative that carries *zapB*^{S4L5AA}*::his*$_6$ downstream of the T7 inducible promoter. *zapB*^{S4L5AA} was amplified by PCR with primers: mut41 + ZapB-H17R. The PCR product was cut with *Nde*I and *Bam*HI and cloned into the same sites of pHis17. Plasmid pEG58 is a pMG25 derivative that carries *zapA* downstream of the P$_{lac}$ inducible promoter. The *Bam*HI-*Hind*III fragment carrying *zapA* from pEG28 was inserted into the *Bam*HI-*Hind*III sites of pMG25. Plasmid pEG59 is a pBAD33 derivative that carries *zapA* downstream of the P$_{BAD}$ inducible promoter. The *Sac*I-*Hind*III fragment carrying *zapA* from pEG28 was inserted into the *Sac*I-*Hind*III sites of pBAD33. Plasmid pEG60 carries *zapB::mCherry* downstream of the m-toluic acid inducible P$_{tol}$ promoter of vector pJB866. The *Kpn*I-*Hind*III fragment carrying *zapB::mCherry* from pEG9 was inserted into the corresponding sites of pJB866. Plasmids pEG82b, pEG83, pEG84, pEG86, pEG88, pEG89 and pEG90 are derivatives of pOU82. Plasmid pEG82b carries *zapB* under its own native promoter. *zapB* was amplified by PCR with primers: zapB-82 + zapB-83. The PCR fragment was cut with restriction enzymes *Eco*RI and *Bam*HI and cloned into the corresponding sites of pOU82. Plasmid pEG83 carries *zapA* under its own native promoter. *zapA* was amplified by PCR with primers: pEG83-For + pEG83-Rev. The PCR fragment was cut with restriction enzymes *Eco*RI and *Bam*HI and cloned into the corresponding sites of pOU82. Plasmid pEG84 carries *Δ10zapB* under its own native promoter. *Δ10zapB* was amplified by PCR: a first PCR reaction was performed using primers zapB-82 + zapB-84F and a second PCR using primers zapB-84R + zapB-83, the two PCR products were mixed and used

as a template for the final PCR product amplified using primers zapB-82 + zapB-83. The PCR fragment was cut with restriction enzymes *Eco*RI and *Bam*HI and cloned into the corresponding sites of pOU82. Plasmid pEG86 carries *zapB::gfp* under *zapB* native promoter. *zapB::gfp* was amplified by PCR: a first PCR reaction was performed on pEG82b using primers zapB-82 + zapB-86F and a second PCR reaction on pEG3a using primers zapB-86R + zapB-86, the two PCR products were mixed and used as a template for the final PCR product amplified using primers zapB-82 + zapB-86. The PCR fragment was cut with restriction enzymes *Eco*RI and *Bam*HI and cloned into the corresponding sites of pOU82. Plasmid pEG88 carries *zapB::his*$_6$ under *zapB* native promoter. *zapB::his*$_6$ was amplified by PCR: a first PCR reaction was performed on pEG82b using primers zapB-82 + zapB-86F and a second PCR reaction on pZapBHis using primers zapB-86R + zapB-88, the two PCR products were mixed and used as a template for the final PCR product amplified using primers zapB-82 + zapB-88. The PCR fragment was cut with restriction enzymes *Eco*RI and *Stu*I and cloned into the *Eco*RI-*Bam*HI(blunted) sites of pOU82. Plasmid pEG89 carries *his*$_6$*::zapA* under *zapA* native promoter. *his*$_6$*::zapA* was amplified by PCR: a first PCR reaction was performed on pEG83 using primers pEG83-For + zapA-89R and a second PCR reaction on pCA24N-*zapA*$^+$ using primers zapA-89F + zapA-89, the two PCR products were mixed and used as a template for the final PCR product amplified using primers pEG83-For + zapA-89. The PCR fragment was cut with restriction enzyme *Pvu*II and cloned into the *Bam*HI(blunted) site of pOU82 in a counter-clockwise orientation. Plasmid pEG90 carries *zapB::mCherry* under *zapB* native promoter. *zapB::mCherry* was amplified by PCR: a first PCR reaction was performed on pEG82b using primers zapB-82 + zapB-86F and a second PCR reaction on pEG9 using primers zapB-86R + zapB-90, the two PCR products were mixed and used as a template for the final PCR product amplified using primers zapB-82 + zapB-90. The PCR fragment was cut with restriction enzymes *Eco*RI and *Bam*HI and cloned into the corresponding sites of pOU82. Plasmid pEG82 is a derivative of pEG82b, *zapA* was cloned immediately after *zapB*. *zapA* was amplified by PCR with primers: zapA-82 + zapA-83. The PCR fragment was cut with restriction enzymes *Asp*718 and *Bam*HI and cloned into the corresponding sites of pEG82b. Plasmids used in the bacterial two-hybrid system: fragments T18 and T25 of the catalytic domain of the *Bordetella pertussis* adenylate cyclase were fused to the N-termini (vectors pUT18C and pKT25) of *zapA* and *zapB* or the C-terminus of *zapA* (vector pKT25N).

zapA and *zapB* were amplified by PCR with the following primers: *zapA*: zapA-1 + zapA-2, *zapA-1*: zapA-N1 + zapA-N2, *zapA-2*: zapA-N1 + zapA-N3, *zapA-3*: zapA-12 + zapA-2, *zapA-4*: zapA-13 + zapA-2, *zapB-1*: zapB-61 + zapB-7, *zapB-2*: zapB-62 + zapB-7, *zapB-3*: zapB-63 + zapB-7, *zapB-4*: zapB-64 + zapB-7, *zapB-5*: zapB-6 + zapB-71, *zapB-6*: zapB-6 + zapB-72, *zapB-7*: zapB-6 + zapB-73, *zapB-8*: zapB-6 + zapB-74, *zapB-b*: zapB-6b + zapB-7, *zapB-c*: zapB-6c + zapB-7, *zapB-d*: zapB-6d + zapB-7, *zapB-e*: zapB-6e + zapB-7. The PCR fragments were cloned between the *Sal*I + *Kpn*I sites of pUT18C, between the *Bam*HI and *Kpn*I sites of pKT25 and between the sites *Hind*III and *Bam*HI of pKT25N.

2.9 Construction of mutant strains

zapA::kan, *zapB::kan*, *zapC::kan*, *slmA::cml*, *minCD::kan* and *sulA::kan* were introduced into the receiver strains by P1 transduction. Colonies were tested for insertion of the resistance gene by using colony-PCR with primers: zapA-up + zapA-down, zapB-up + zapB-down, zapC-up + zapC-down, slmA-up + slmA-down, minC-up + minD-down and sulA-up + sulA-down, respectively for *zapA*, *zapB*, *zapC*, *slmA*, *minCD* and *sulA*. The temperature sensitive helper plasmid pCP20, encoding the FLP recombinase, was used to eliminate the resistance genes, as described by Datsenko and Wanner (2000). It was not possible to eliminate the kanamycin resistance gene from the strains carrying *minCD::kan*.

The *ftsZ84* allele was introduced in KG22 and MC1000 by P1 phage transduction using AB1157Z84 as donor. Transductants were selected on plates containing 10 μg/ml tetracycline and subsequently *ftsZ84* mutants were isolated screening for transductants not able to grow at the non-permissive temperature (42°C).

Chapter 3

The cell division factor ZapB

3.1 Introduction

ZapB is a small cytoplasmic protein conserved in a subset of γ-proteobacteria, including *Salmonella typhimurium*, *Haemophilus influenzae* and *Vibrio cholerae* (Ebersbach *et al.*, 2008). It was identified by screening an *E. coli* chromosomal library for factors that, when present in high-copy number, would destabilize the partitioning mechanism of plasmid pB171 (Ebersbach *et al.*, 2008). At first, it was mistakenly believed to specifically impair the function of the *par2* locus of plasmid pB171, encoding the oscillating ATPase ParA, the centromere binding protein ParB and two centromer-like sites (Gerdes *et al.*, 2000; Ebersbach and Gerdes, 2001; Ebersbach *et al.*, 2008), and only by revisiting ZapB was its involvement in cell division investigated.

Overproduction of ZapB induced formation of highly compacted nucleoids, often abnormally located at the cell poles, as well as defects in cell division: like the presence of filaments and very small cells among the cell population (Ebersbach *et al.*, 2008). On the other hand, inactivation of *zapB* caused an increase in the average cell length and, besides slightly longer cells, filaments with no septal constriction were present (Ebersbach *et al.*, 2008). FtsZ, in the absence of ZapB, formed aberrant structures such as multiple bands or spirals, in a few cases mislocated over the nucleoid (Ebersbach *et al.*, 2008).

A bacterial two-hybrid assay showed that ZapB could interact with both itself and the cell division factors FtsZ and FtsA (Ebersbach *et al.*, 2008).

ZapB crystallographic structure was solved and consists of a unique coiled-coil domain, it was suggested that ZapB could dimerize and polymerize through interactions between the coiled-coil end regions (Ebersbach *et al.*, 2008).

Furthermore, ZapB is a relatively abundant protein, present in ~13,000 copies per cell, an amount comparable to or higher than FtsZ, quantified to be between 3,200 and 15,000 molecules per cell in *E. coli* B/r cells (Lu *et al.*, 1998; Rueda *et al.*, 2003; Ebersbach *et al.*, 2008). Mohammadi *et al*. (2009) determined the amount of ZapA and FtsZ in *E. coli* cells grown in the same conditions and found ZapA to be ~6,100 molecules per cell and FtsZ ~4,800 molecules for cell, indicating that ZapA and FtsZ are approximately in a 1:1 stoichiometry (Mohammadi *et al*., 2009).

3.2 Aim of this chapter

The preliminary data collected by Dr. Gitte Ebersbach, a former PhD student in Prof. K. Gerdes laboratory, such as the interaction between ZapB and FtsZ in a BTH assay and the morphological defects and the aberrant Z-ring assembly in a *zapB* mutant strain, strongly suggested an involvement of ZapB in the cell division process, particularly in the early stages of Z-ring formation (Ebersbach *et al.*, 2008).

The aim of this chapter is to characterize the novel cell division factor ZapB, investigating its localization pattern and dynamics during cell division in order to gain further knowledge on how it could affect the process of cytokinesis.

3.3 Results

3.3.1 ZapB localizes at mid-cell in a dynamic FtsZ-like pattern

Initially, ZapB subcellular localization analysis was attempted using a plasmid carrying a P_{lac}*::zapB::gfp* (pGE620) fusion, however the protein precipitated in inclusion bodies near the cell poles (Gitte Ebersbach and Kenn Gerdes personal communication).

To avoid production of inclusion bodies, we decided to use the tightly regulated expression system of plasmid vectors carrying the P_{BAD} promoter, inducible by arabinose and repressed by glucose (Guzman *et al.*, 1995).

The plasmid carrying the *zapB::gfp* fusion under the arabinose-inducible promoter (pEG3a) was used to study the localization pattern of ZapB in the wt strain MC1000. After a short pulse (5 minutes) of transcription, almost all cells (96%) of MC1000/pEG3a showed a fluorescent signal located at the division site (Fig. 3.1A). Longer pulses of transcription from pEG3a resulted in formation of inclusion bodies, as previously reported using the IPTG inducible plasmid pGE620 (data not shown).

In a time-lapse microscopy experiment ZapB-GFP localization was followed in individual cells through a cell cycle (in a time lapse-experiment the cell generation time was ~60 minutes) (Fig. 3.1B). ZapB localized at the cell division plane of newly formed cells as two small dots or a band, as the pre-divisional cell became longer the transverse band condensed into a central dot (0' to 35'). Between 35′ and 40′, the central dot disappeared and new transverse bands formed at quarter-cell positions, corresponding to the mid-cell positions of the new daughter cells. In order to visualize ZapB-GFP localization during the course of an entire cell-cycle, we used short exposure times to avoid bleaching of the fluorescent signal over-time, in turn decreasing the resolution of the images and making impossible to detect the transition of ZapB to the division sites of the daughter cells. Nevertheless, using longer exposure times without following the entire cell division process, in a few cases, we were able to capture a ZapB-GFP helical signal connecting the old localization site at mid-cell with the new bands at quarter-cell positions (Fig. 3.1C).

Thus, the subcellular localization of ZapB highly resembled that described for FtsZ (Addinall *et al.*, 1996).

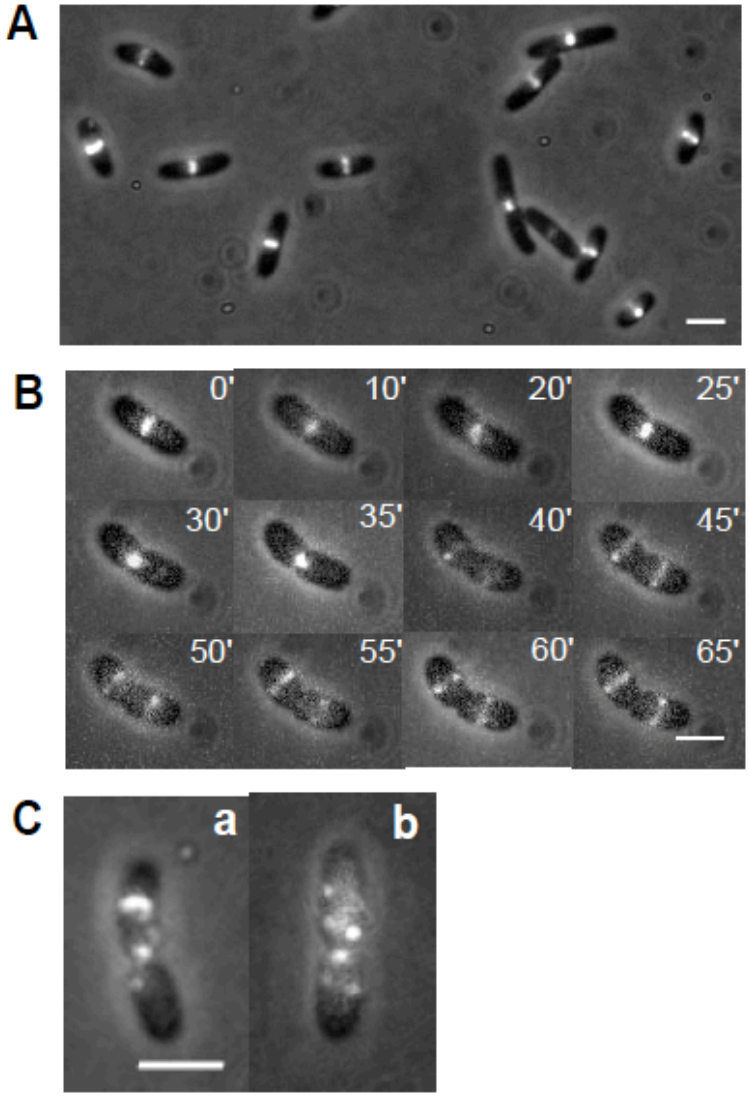

Fig. 3.1 Dynamic subcellular localization of ZapB

Combined phase-contrast and fluorescence microscopy images showing the localization of ZapB-GFP in living cells of strain MC1000 (Ebersbach *et al.*, 2008). Cells were grown at 37°C in M9 minimal medium supplemented with glucose and casamino acids. Expression of ZapB-GFP from plasmid pEG3a was induced by addition of arabinose as described in *Materials and Methods*. Fluorescence images using a GFP filter were taken immediately after mounting the cells on a microscope slide. **A.** ZapB-GFP localization. **B.** Time-lapse series. Fluorescence images were taken every 5 minutes. **C.** ZapB-GFP signal connecting the old dot at mid-cell with the new bands at quarter-cell positions. Scale bars = 2 µm. The different cell morphologies in A and B were due to differences in growth conditions (growth in liquid vs. solid medium).

3.3.2 Formation of ring-like ZapB structures at mid-cell depends on the Z-ring but not FtsA, ZipA or FtsI

To understand if ZapB recruitment at the division site required the previous localization of early cell division proteins such as FtsZ, FtsA and ZipA, we made use of strains carrying temperature-sensitive alleles. In these strains, at the non-permissive temperature of 42°C, the mutant proteins are not able to localize at the division site whereas at the permissive temperature of 30°C their localization pattern is unaffected and Z-ring formation and cell division can proceed as in the wild-type strain.

The strain KG22Z84, carrying the temperature-sensitive *ftsZ84* mutation, was chosen to investigate ZapB localization in the absence of a functional FtsZ. In a Z84 mutant strain, upon shift at 42°C, Z-rings disassemble, leading to a block in cell division and formation of cell filaments (Addinall *et al.*, 1997). ZapB-GFP localization in the wt (KG22) strain at 30°C and at 42°C (Fig. 3.2A, a-d) showed the typical localization pattern described above, a similar localization pattern was seen in the *ftsZ84* strain at 30°C (Fig. 3.2B, a-c). However, in the latter strain, at the non-permissive temperature, cells became filamentous and the GFP signal appeared diffuse in the elongated cells (Fig. 3.2B, d). This showed that ZapB-GFP localization at mid-cell depended on a functional FtsZ protein.

To further confirm that ring-like ZapB structures at the division site were able to form only if the Z-ring was present, we studied ZapB-GFP localization in temperature sensitive strains that carried mutations in *ftsA* (*ftsA12*, PS236) or in *zipA* (*zipA1*, PS223) or in both of them (PS234). It is known that either one of FtsA or ZipA alone is sufficient for the formation of the Z-ring, even if with a lower frequency compared to the wt. However, when they are both inactivated FtsZ is unable to assemble into a Z-ring (Pichoff and Lutkenhaus, 2002). Inactivation of FtsA did not affect the formation of ZapB-GFP bands along the filamentous cells (Fig. 3.2C, a-b). Similarly, inactivation of ZipA only slightly reduced the number of ZapB-GFP bands (Fig. 3.2D, a-b), also excluding ZipA as a crucial factor for ZapB recruitment. By contrast, simultaneous inactivation of FtsA and ZipA prevented ZapB-GFP localization (Fig. 3.2E, a-b).

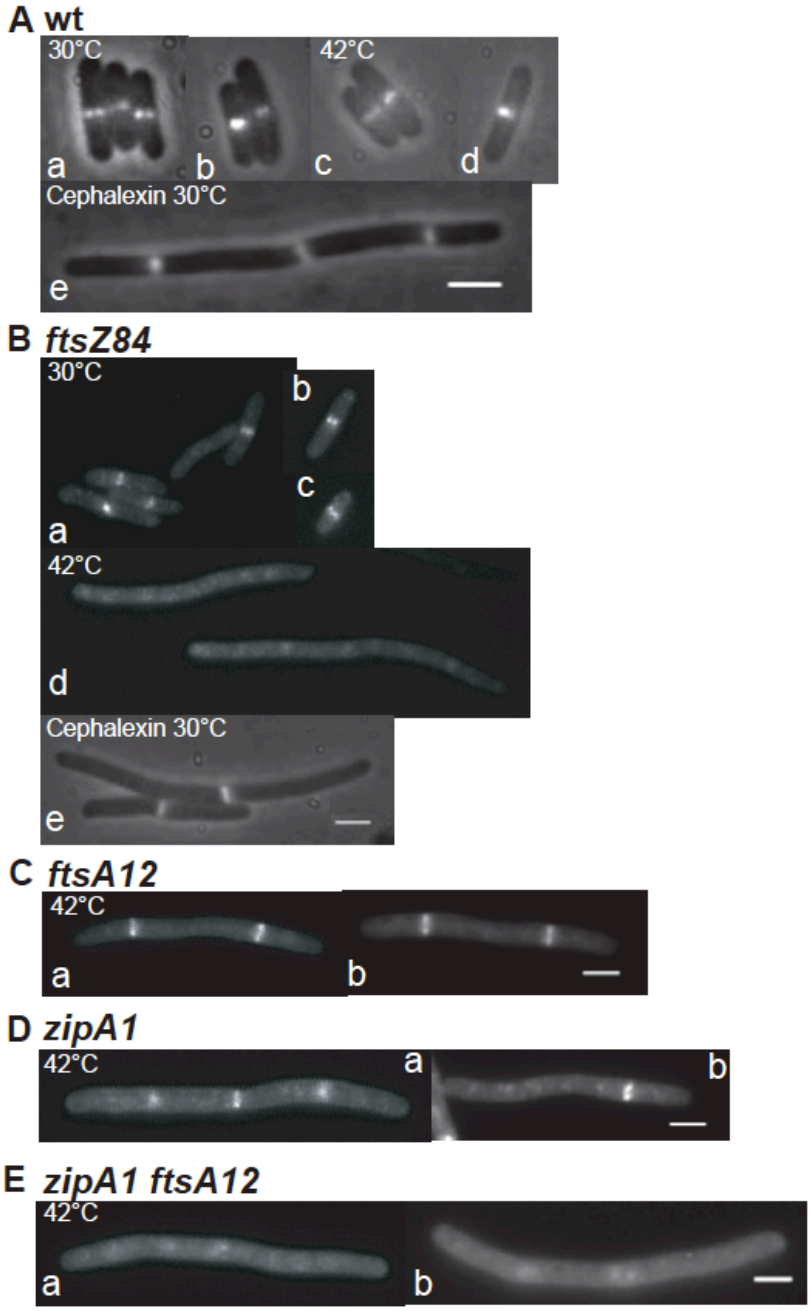

Fig. 3.2 Localization of ZapB depends on FtsZ but not FtsA, ZipA or FtsI

Fluorescence microscopy images showing the localization of ZapB-GFP in living cells of strains (A) KG22 (wt) and (B, e) KG22Z84 (*ftsZ84*), and in fixed cells of strains (B, a-d) KG22Z84, (C, a-b) PS236 (*ftsA12*), (D, a-b) PS223 (*zipA1*) and (E, a-b) PS234 (*zipA1 ftsA12*) (Ebersbach *et al.*, 2008). Cells were grown at 30°C in M9 minimal medium supplemented with glucose and casamino acids (A and B) or in LB medium (C, D and E). Expression of ZapB-GFP from plasmid pEG3a was induced by the addition of arabinose as described in *Materials and Methods*. 1.5 h after induction, exponentially growing cultures were diluted into fresh medium pre-heated to the non-permissive temperature (42°C). Samples were collected 45 minutes (A and B) or 60 minutes (C, D and E) after the shift to 42°C. The cultures in C, D and E had a normal morphology and localization of ZapB-GFP at 30°C (data not shown). In the cells in (A, e) and (B, e), cell division was inhibited by treatment with 10 µg/ml cephalexin, at 30°C. Scale bars = 2 µm.

These results confirmed that the presence of a functional Z-ring is essential for a proper ZapB recruitment to the division site.

To exclude the involvement of late cell division proteins in recruitment or stabilization of ZapB into the divisome, we analysed ZapB-GFP localization in KG22 and KG22Z84 cells treated with cephalexin, an inhibitor of the late cell division protein FtsI (Hedge and Spratt, 1985). Following FtsI inactivation, ZapB-GFP maintained the ability to be recruited at the division site both in KG22 and KG22Z84 cells, even though in the presence of the *ftsZ84* allele ZapB-GFP localized only once at mid-cell whereas in wt cells it was regularly distributed along the filamentous cells (Fig. 3.2A, e and Fig. 3.2B, e). Since cephalexin treatment delays Z-ring formation at future but not nascent division sites (Pogliano *et al.*, 1997), a plausible explanation could be that cells carrying *ftsZ84* have a reduced number of nascent division sites.

As FtsI inhibition did not affect ZapB localization, the late cell division proteins are very likely not involved in the formation or stabilization of ZapB structures at the division site.

3.3.3 ZapB co-localizes with FtsZ and ZapA

Since ZapB recruitment at the division site seemingly only requires FtsZ and not ZipA, FtsA or late cell division factors such as FtsI, we compared, at the same time and in the same cell, the localization of ZapB to the one of FtsZ and ZapA, an early cell division protein that requires only FtsZ in order to be recruited into the Z-ring (Gueiros-Filho and Losick, 2002; Goehring *et al.*, 2005). To investigate the localization of two proteins at the same time in the same cell we used double fluorescence labelling: FtsZ and ZapB were fused to mCherry and GFP, respectively, whereas for the ZapA and ZapB pair we used YFP-ZapA and ZapB-mCherry fusions. All cells with a visible FtsZ-mCherry signal at mid-cell exhibited a co-localizing ZapB-GFP signal (n = 2000) (Fig. 3.3A) and the same result was obtained with the ZapA-ZapB pair, for all cells observed (n = 2000) ZapB and ZapA invariably co-localized (Fig. 3.3B).

To further investigate the timing of ZapB recruitment to the Z-ring, we performed a time-lapse experiment looking at the localization pattern of both ZapB and FtsZ during a cell cycle. Throughout the entire cell division process ZapB and

FtsZ co-localized (Fig. 3.4), even more interestingly ZapB was associated with FtsZ during the transition from a helical structure into a ring (Fig. 3.4, 0'-5' and 55'-70') and the two proteins localized simultaneously at the new division sites of the daughter cells.

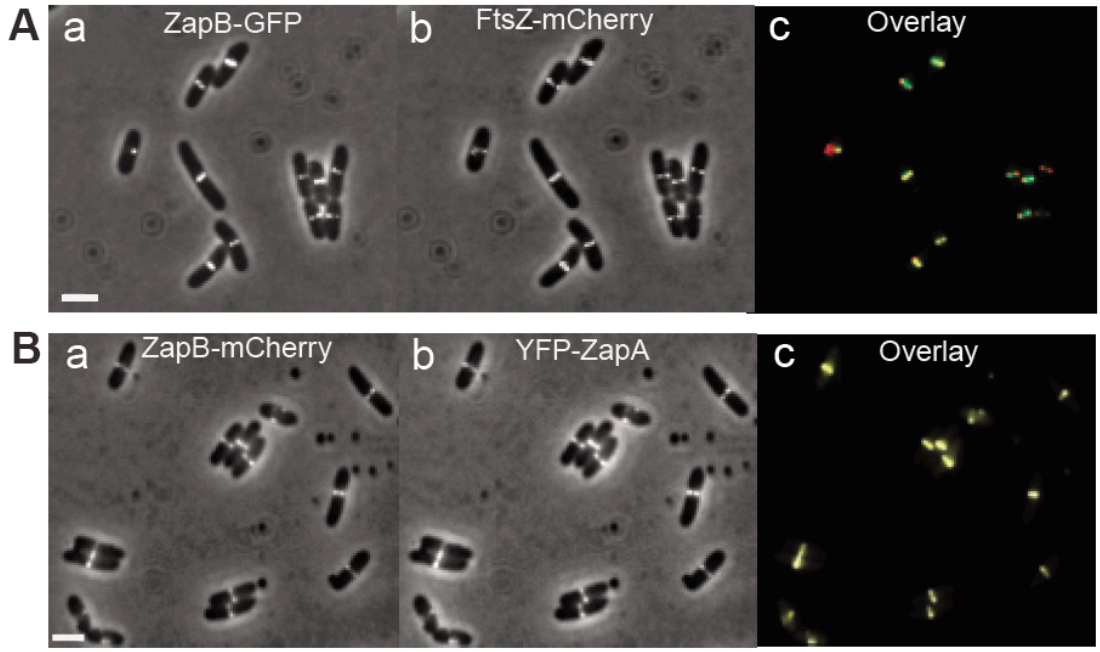

Fig. 3.3 ZapB co-localizes with FtsZ and ZapA

Cells were grown at 30°C in M9 minimal medium supplemented with glucose and casamino acids (Galli and Gerdes, 2010). Cells were visualized by combined phase-contrast and fluorescence microscopy. For the P_{lac} fusions, the leakiness of the P_{lac} promoter resulted in a sufficient level of expression while the P_{BAD} fusions required a pulse of transcription (0.2% arabinose was added for 5 minutes for pEG3a and 25 minutes for pEG9). The experiment is described in further detail in *Materials and Methods*.
A. MC1000 / pEG3a (P_{BAD}*::zapB::gfp*) / pQW59 (P_{lac}*::ftsZ::mCherry*).
B. MC1000 / pEG9 (P_{BAD}*::zapB::mCherry*) / pNG53 (P_{lac}*::yfp::zapA*).
Scale bars = 2 µm.

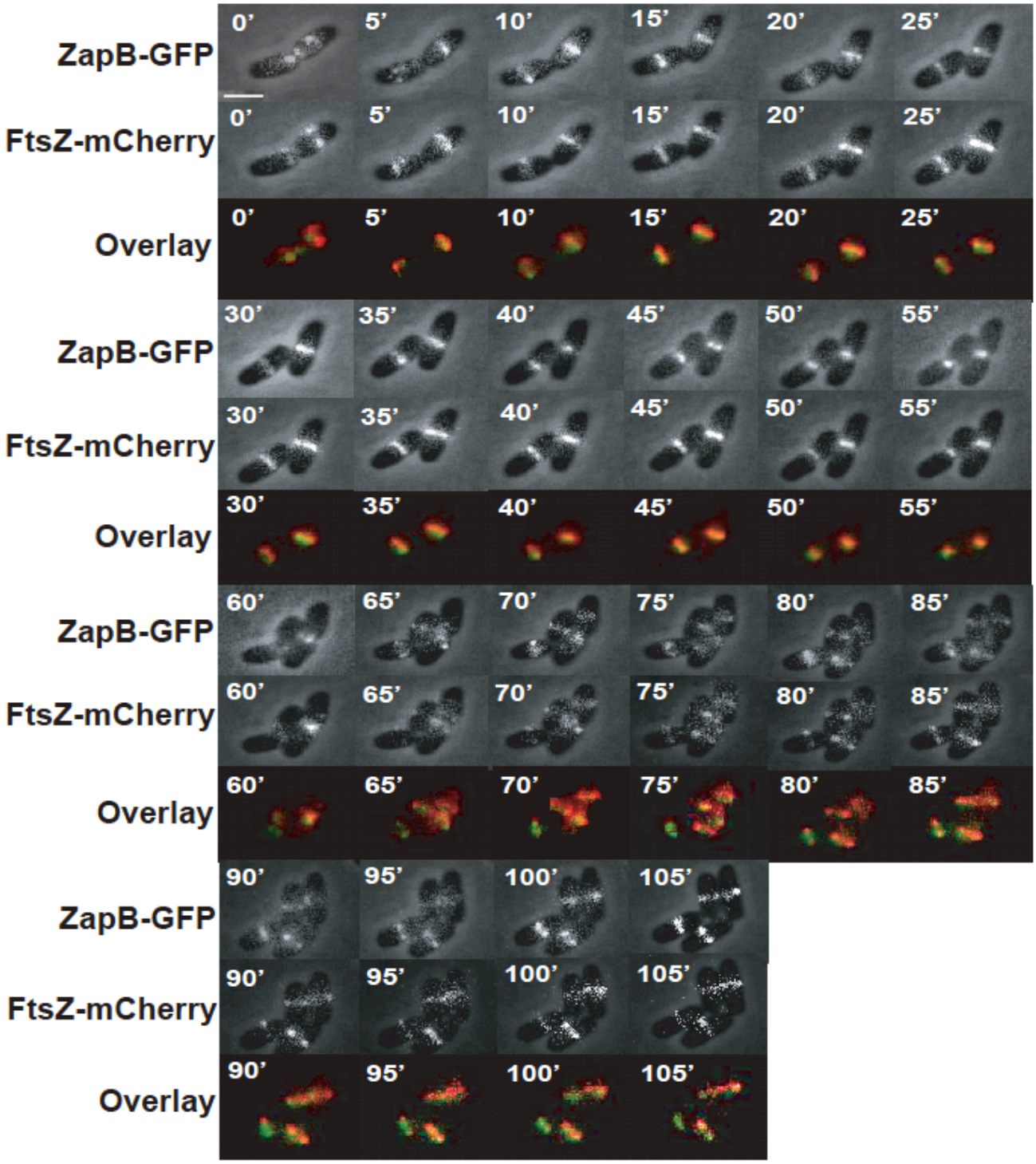

Fig. 3.4 Time-lapse of ZapB-GFP and FtsZ-mCherry

Combined phase-contrast and fluorescence microscopy images showing the localization of ZapB-GFP and FtsZ-mCherry in living cells of strain MC1000 / pEG3a (P_{BAD}*::zapB::gfp*) /pQW59 (P_{lac}*::ftsZ::mCherry*) (Galli and Gerdes, 2010). Cells were grown at 37°C in M9 minimal medium supplemented with glucose and casamino acids. Expression of ZapB-GFP from plasmid pEG3a was induced by addition of arabinose as described in *Materials and Methods*. Fluorescence images were taken every 5 minutes using a GFP filter set with 1 sec exposure and a RFP filter set with 0.8 sec exposure. Scale bar = 2 µm.

3.3.4 ZapB is recruited early into the divisome

FtsK and ZapB co-localization analysis was investigated to confirm that ZapB belongs to the class of early cell division proteins, since FtsK is recruited to the division site after the formation of the Z-ring and before or together with the arrival of the late division factors (Chen and Beckwith, 2001; Vicente and Rico, 2006; Kennedy *et al*., 2008).

To study simultaneously the localization of ZapB and FtsK, we used the fusion proteins ZapB-mCherry and GFP-FtsK. In this case it was not possible to obtain informative time-lapse series because of the limited signal emitted by the GFP-FtsK fusion protein. However, from static images arranged as a pseudo-time-lapse (Fig. 3.5), it was evident that the ZapB-mCherry signal condensed from ring-like structures (Fig. 3.5A) to dots (Fig. 3.5B) and moved to new cell division sites (Fig. 3.5C–E) before the GFP-FtsK signal (Fig. 3.5A′–E′). ZapB-mCherry, as previously seen with ZapB-GFP, exhibited helical localization patterns when moving to the new cell division sites whereas these structures were not visible with GFP-FtsK, even though we can not exclude that failing to see FtsK helical structures was due to limits in GFP-FtsK signal detection. This suggests that ZapB localizes at the cell division site before FtsK and it strengthens the conclusion that ZapB is recruited early into the divisome.

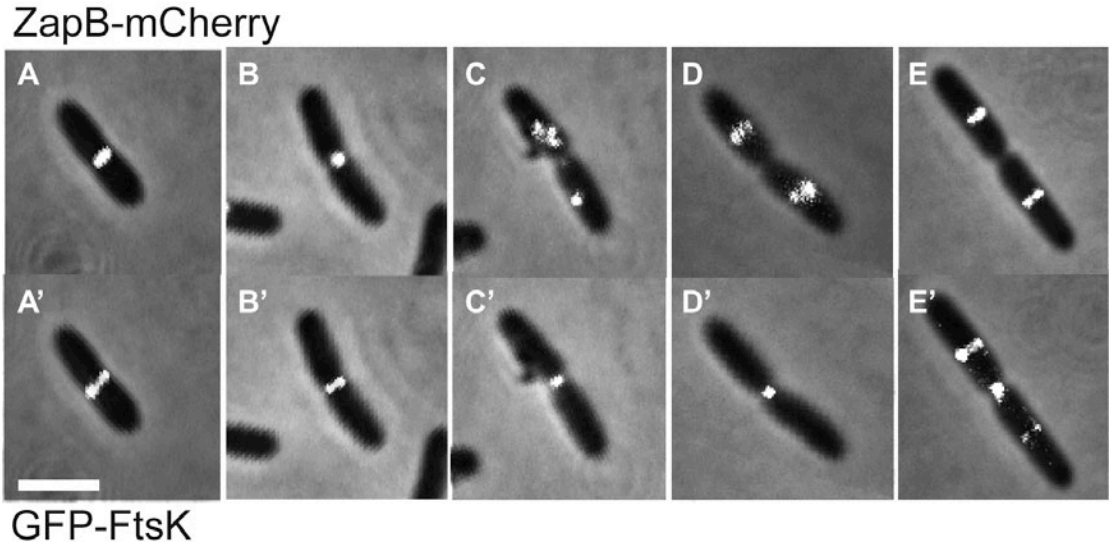

Fig. 3.5 ZapB is recruited to the divisome before FtsK

Combined phase-contrast and fluorescence microscopy images showing ZapB-mCherry and GFP-FtsK localization (Galli and Gerdes, 2010).
MC1000/pEG9 (P_{BAD}*::zapB::mCherry*)/pFX158 (P_{BAD}*::gfp::ftsK*) cells were grown in M9 minimal medium supplemented with glucose and casamino acids at 30°C. Expression of both fusion proteins was induced with a 25 minutes pulse of 0.2% arabinose as described in further detail in *Materials and Methods*. Representative cells were sampled from liquid culture to generate a pseudo-time-lapse series. (A–E): ZapB-mCherry localization; (A′–E′): GFP-FtsK localization. Scale bar = 2 μm.

3.3.5 ZapA is required for the recruitment of ZapB to the divisome

ZapB dynamic localization pattern and the results of a bacterial two-hybrid assay (Ebersbach *et al.*, 2008) suggested that ZapB could interact directly with FtsZ. However, *in vitro*, the two purified proteins did not interact in any of the assays performed (pull down assays, pelletting assays and co-immunoprecipitations) (Jakob Møller-Jensen personal communication).

In these assays the FtsZ associated protein ZapA always interacted with FtsZ. For example, using an affinity chromatography assay His-ZapA was able to interact with the purified FtsZ and the two proteins co-eluted, whereas ZapB-His did not interact with FtsZ under these conditions and hence was not retained by the column (Fig. 3.6).

The absence of interaction between FtsZ and ZapB *in vitro* indicated that ZapB differs from ZapA in how it becomes part of the Z-ring, a plausible explanation was that ZapB does not interact directly with FtsZ and that the interaction between the two proteins is mediated by a third factor, essential for recruiting ZapB at the division site.

To address this possibility we investigated ZapB-GFP localization in cell-division mutant strains, reasoning that ZapB-GFP localization pattern might be perturbed in a strain in which the factor recruiting ZapB to the septum is absent. The previously reported results indicated that ZapB localizes early at the division site and that neither FtsA nor ZipA affected ZapB localization (Fig. 3.2). Therefore, we started testing ZapB-GFP localization in strains lacking known cell-division genes such as *zapA*, *minCD* and *slmA*. Using these three strain backgrounds we were able to investigate the effects that an early Z-ring associated factor (ZapA) or proteins involved in the selection of the division site (MinCD) or the NO system (SlmA) had on ZapB recruitment at mid-cell.

Interestingly, the previously described ZapB septal localization was maintained in cells lacking *minCD* or *slmA*, but it was completely lost in the absence of *zapA* (Fig. 3.7A). Western-blot analyses showed that the ZapB-GFP fusion was not destabilized in cells lacking ZapA (Fig. 3.7D). We showed above that ZapB structures at mid-cell depend on FtsZ. To confirm that ZapB-GFP diffusion in the Δ*zapA* background was not due to an unexpected localization defect of FtsZ, we investigated FtsZ and ZapB co-localization in the same Δ*zapA* strain. Indeed, the Z-ring was able to form in Δ*zapA* cells whereas ZapB, requiring the presence of ZapA to be recruited into the ring, was diffuse in the cytoplasm (Fig. 3.7B). Finally, we tested if ZapB-GFP localization could be restored in Δ*zapA* cells by ectopic production of ZapA from a plasmid. Positively, *zapA* expressed *in trans* in Δ*zapA* cells resulted in the recovery of ZapB localization pattern, now indistinguishable from that of wt cells (Fig. 3.7C).

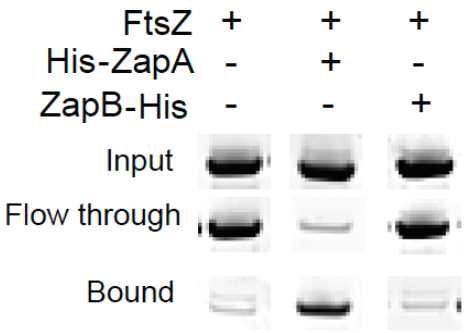

Fig. 3.6 ZapA but not ZapB binds directly to FtsZ

Ni^{2+}–NTA affinity chromatography of FtsZ in the presence or absence of His_6-ZapA or ZapB-His_6 (Galli and Gerdes, 2010). Bands correspond to FtsZ in the input, flow through or output fractions and are from a Coomassie stained SDS-PAGE.

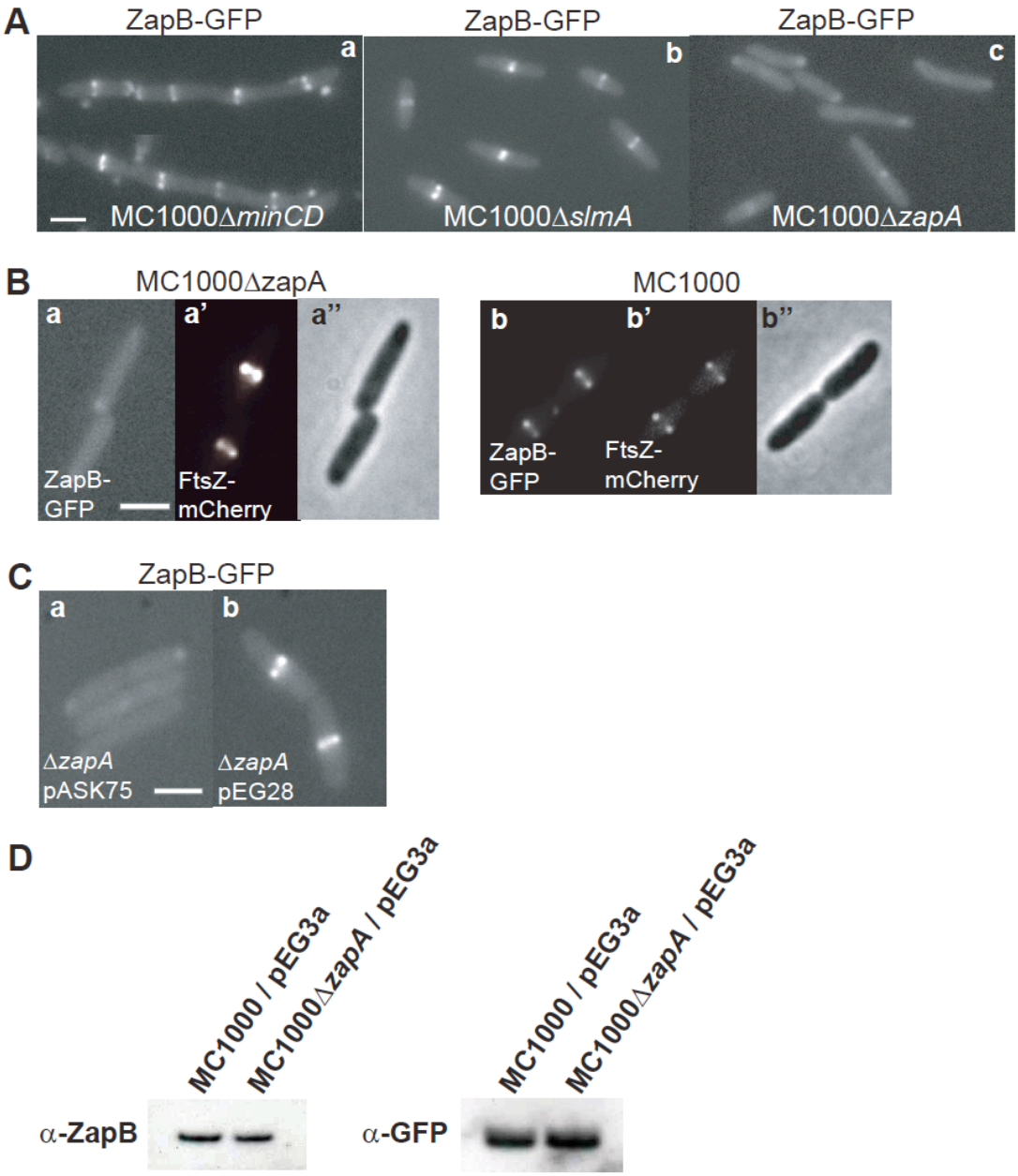

Fig. 3.7 ZapA recruits ZapB to the Z-ring

Phase-contrast and fluorescence microscopy images showing the localization of ZapB-GFP in living cells of strain MC1000 and MC1000Δ*zapA* (Galli and Gerdes, 2010). Cells were grown at 30°C in M9 minimal medium supplemented with glucose and casamino acids. Expression of ZapB-GFP from plasmid pEG3a, FtsZ-mCherry from plasmid pQW59 and ZapA from plasmid pEG28 was induced as described in *Materials and Methods*. **A.** ZapB-GFP localization in (a) MC1000Δ*minCD*, (b) MC1000Δ*slmA* and (c) MC1000Δ*zapA*. **B.** Localization of (a-b) ZapB-GFP, (a′-b′) FtsZ-mCherry and (a″-b″) phase-contrast in living cells of strain MC1000Δ*zapA* (a, a′ and a″) and MC1000 (b, b′ and b″). **C.** Localization of ZapB-GFP in (a) MC1000Δ*zapA*/pEG3a (P_{BAD}*::zapB::gfp*) /pASK75 (empty plasmid) and (b) MC1000Δ*zapA*/pEG3a (P_{BAD}*::zapB::gfp*)/pEG28 (P_{oxyTc}*::zapA*). **D.** Immuno-blotting analyses of ZapB-GFP expression in MC1000/pEG3a (P_{BAD}*::zapB::gfp*) and MC1000Δ*zapA*/pEG3a (P_{BAD}*::zapB::gfp*). ZapB-GFP was expressed as described in *Materials and Methods*, samples were collected and a Western-blot performed using α-ZapB and α-GFP antibodies.
Scale bars = 2 µm.

These results indicated that ZapA is the protein mediating the recruitment of ZapB into the Z-ring, acting as a bridging factor between FtsZ and ZapB.

We also investigated whether the absence of ZapB had an effect on the recruitment of ZapA into the Z-ring, but ZapB seemed to have no role in stabilizing ZapA-FtsZ interaction and YFP-ZapA co-localized as expected with FtsZ in a Δ*zapB* background (Fig. 3.8).

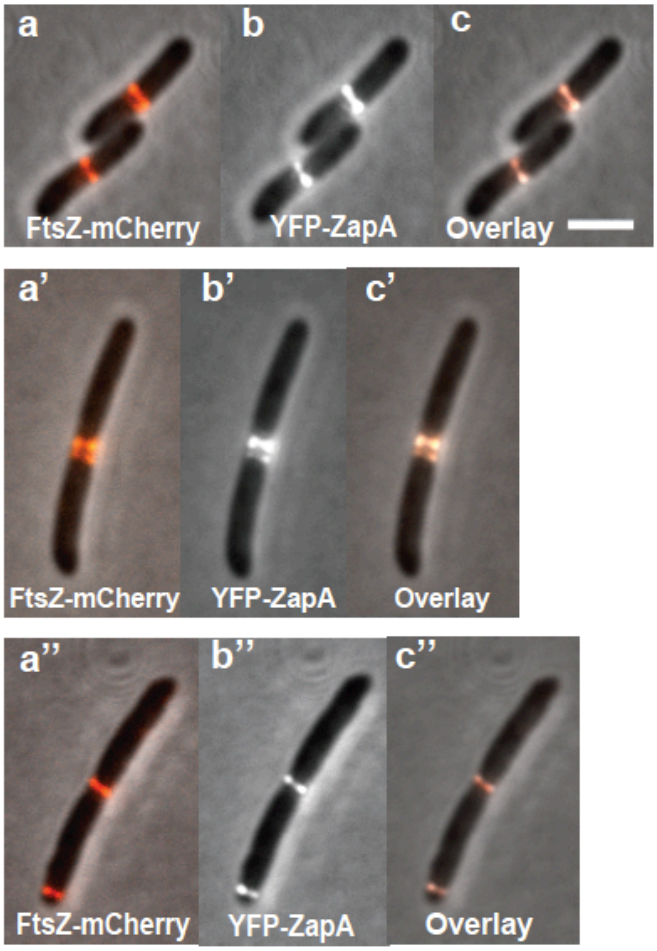

Fig. 3.8 ZapB is not necessary for ZapA localization

Localization of YFP-ZapA and FtsZ-mCherry in living cells of strain MC1000Δ*zapB* (Galli and Gerdes, 2010). Cells were grown at 30°C in M9 minimal medium supplemented with glucose and casamino acids. Expression of YFP-ZapA from plasmid pNG53 (P_{lac}*::yfp::zapA*) and FtsZ-mCherry from plasmid pEG4 (P_{BAD}*::ftsZ::mCherry*) was induced as described in *Materials and Methods*. a, a', a'': FtsZ-mCherry; b, b', b'': YFP-ZapA; c, c', c'': overlay of YFP-ZapA and FtsZ-mCherry. Scale bar = 2 μm.

3.3.6 Overproduction of ZapA delocalizes ZapB

Since ZapA was now a key player in the study of ZapB and its role in cell division, we investigated the effects of ZapA overproduction on cell growth and morphology.

Overproduction of ZapA in MC1000 resulted in the formation of elongated cells. Occasionally such elongated cells appeared twisted with bends at sites expected to have a pre-divisional constriction (Fig. 3.9A). Very similar morphological defects were seen with two different ZapA overproducing constructs. Overproduction of ZapA did not affect the growth-rate of the cultures (data not shown).

We then analysed how elevated levels of ZapA affected the localization of FtsZ and ZapB. During these experiments, ZapA was overproduced 7 to 12 folds as determined by Western-blotting (data not shown). In the absence of inducer, normal Z-rings were formed, as expected. After induction, FtsZ formed helical structures or spirals at the division site or along the undivided short filaments (Fig. 3.9B). Indeed, the formation of short filaments and what seemed to be cells with a twisted septum were indicative of defects in the formation of a functional Z-ring.

Next, we inspected ZapB localization in the presence of an increased level of ZapA. In the absence of the inducer, ZapB-GFP localized at the division site as expected. Increasing amounts of IPTG reduced the septal GFP signal (Fig. 3.9C).

To be able to visualize both ZapB and FtsZ while overproducing ZapA we employed an expression system compatible with both the standard IPTG and arabinose regulated promoters. We decided to use an expression vector based on the RK2 replicon and inducible by toluic acid (Blatny *et al.*, 1997). For reasons still unknown to us, the expression levels from the P_{tol} promoter were very low in the MC1000 strain, the wt strain chosen for our localization analyses. However, in the DH5α background, it was possible to obtain sufficient expression of ZapA from a P_{BAD} promoter and at the same time visualize FtsZ-GFP (from an IPTG inducible plasmid) and ZapB-mCherry (from the TOL inducible plasmid). In the absence of ZapA inducer, ZapB-mCherry and FtsZ-GFP formed co-localizing bands at the division sites, as previously described. By contrast, in the presence of elevated levels of ZapA, FtsZ-GFP formed aberrant structures whereas ZapB-mCherry was diffuse in the cytoplasm (Fig. 3.9D).

We also overproduced YFP-ZapA. As expected, YFP-ZapA signal became diffuse in the cells and the YFP signal in the cytoplasm increased to such a high level that the YFP-ZapA bands at mid-cell became barely visible (Fig. 3.9E).

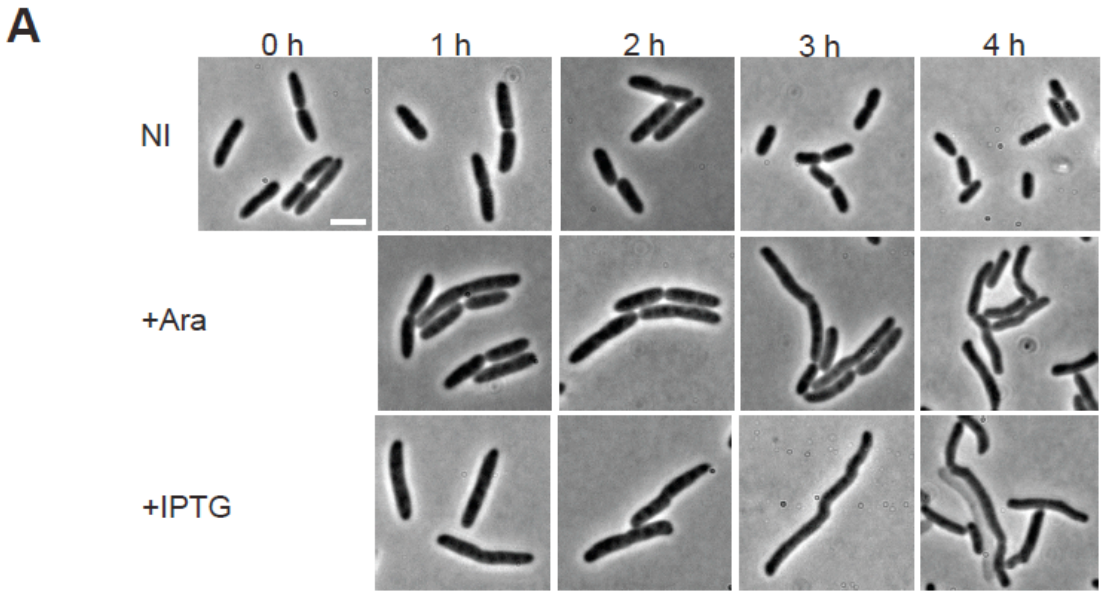

Fig. 3.9A ZapA overproduction delocalizes ZapB

Combined phase-contrast and fluorescence microscopy images showing the localization of ZapB and FtsZ when ZapA is overproduced. Cells were grown at 30°C in M9 minimal medium supplemented with glucose (or glycerol) and casamino acids. Expression of ZapB-GFP from plasmid pEG3a, ZapB-mCherry from plasmid pEG60, FtsZ-GFP from plasmid pEG12 and ZapA from plasmid pEG58 and pEG59 was induced as described in *Materials and Methods*. **A.** Phase-contrast of living cells of strain MC1000/pEG58 (P_{lac}*::zapA*) (+IPTG) and MC1000 / pEG59 (P_{BAD}*::zapA*) (+Ara) over time. Scale bar = 2 µm.

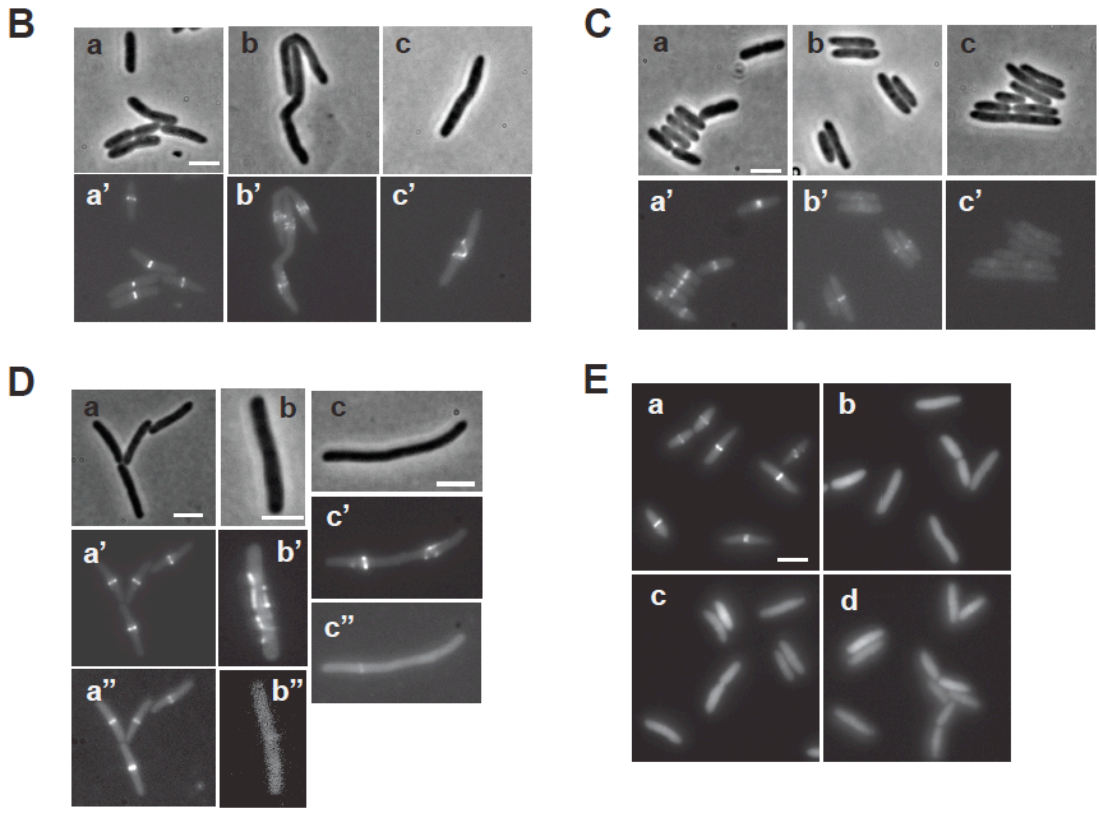

Fig. 3.9BCDE ZapA overproduction delocalizes ZapB

Combined phase-contrast and fluorescence microscopy images showing the localization of ZapB and FtsZ when ZapA is overproduced. Cells were grown at 30°C in M9 minimal medium supplemented with glucose (or glycerol) and casamino acids. Expression of ZapB-GFP from plasmid pEG3a, ZapB-mCherry from plasmid pEG60, FtsZ-GFP from plasmid pEG12 and ZapA from plasmid pEG58 and pEG59 was induced as described in *Materials and Methods*. **B.** Phase-contrast image (a, b and c) and FtsZ-GFP localization (a', b' and c') in living cells of strain MC1000/pEG59 (P_{BAD}*::zapA*) /pEG12 (P_{lac}*::ftsZ::gfp*) 2 hours after ZapA induction with 0.2% Ara (b and c) or without the inducer (a). ZapA levels are 8 fold higher than in wt conditions. **C.** Phase-contrast (a, b and c) and ZapB-GFP localization (a', b' and c') in living cells of strain MC1000/pEG58 (P_{lac}*::zapA*) /pEG3a (P_{BAD}*::zapB::gfp*) 2 hours after ZapA induction with 500 µM IPTG (b), 1 mM IPTG (c) or without the inducer (a). ZapA levels are 7 fold (500 µM IPTG) and 12 fold higher (1 mM IPTG) than in wt conditions. **D.** Phase-contrast (a, b and c), FtsZ-GFP localization (a', b' and c') and ZapB-mCherry localization (a'', b'' and c'') in living cells of strain DH5α/pEG59 (P_{BAD}*::zapA*) /pEG12 (P_{lac}*::ftsZ::gfp*)/pEG60 (P_{tol}*::zapB::mCherry*) 2 hours after ZapA induction with 0.2% Ara (b and c) or without the inducer (a). ZapA levels are 8 fold higher than in wt conditions. **E.** Localization of YFP-ZapA in living cells of strain MC1000/pNG53 (P_{lac}*::yfp::zapA*) 2 hours after induction with 200 µM IPTG (b), 500 µM IPTG (c), 1 mM IPTG (d) or without the inducer (a). Scale bars = 2 µm.

3.3.7 ZapC is not required for localization of ZapA or ZapB

We investigated FtsZ, ZapA and ZapB localization in cells lacking ZapC. Cells of a *zapC* deletion mutant were slightly elongated but neither FtsZ nor ZapA nor ZapB showed significant localization defects (Fig. 3.10). In the majority of the cells, FtsZ formed a proper band at the division site and only in less than 5% of the cells abnormal structures such as diffuse arcs, spirals or doublets were present (similar Z-ring morphological defects were described in Durandia-Heredia *et al*. (2011)). In Δ*zapC* cells, the localization pattern of ZapA and ZapB resembled that of FtsZ. Therefore, ZapC appeared to be not important for recruitment of ZapA and ZapB to the Z-ring.

3.3.8 ZapA and ZapB interact in the bacterial two-hybrid assay

Using the BTH assay, ZapB was previously reported to interact with itself, with FtsZ and in a lesser extent with FtsA. No positive response could be detected with any other cell division protein (ZipA, FtsK, FtsQ, FtsI, FtsB, FtsL, FtsN, FtsW, FtsX or YmgF) (Ebersbach *et al.*, 2008). We hypothesized that ZapA expressed from the chromosomal *zapA* gene could generate the false positive interaction between FtsZ and ZapB, therefore we repeated the BTH assay both in the wt strain BTH101 and in the mutant strain BTH101Δ*zapA*. We also investigated the pair ZapA-ZapB, not previously tested in the BTH assay.

Indeed, deletion of *zapA* reduced the BTH signal between ZapB–FtsZ and ZapB–FtsA whereas no such reduction was seen for the ZapB–ZapB or ZapB–ZapA pairs (Fig. 3.11).

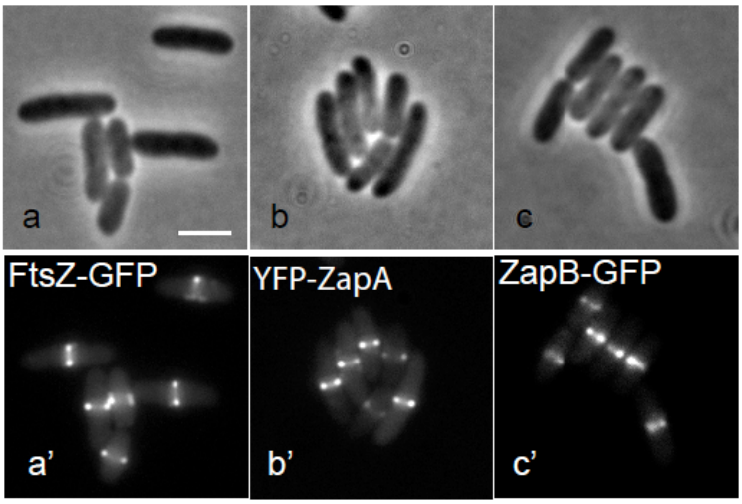

Fig. 3.10 ZapC is not necessary for ZapA, ZapB and FtsZ localization

Phase-contrast (a, b and c) and fluorescence microscopy images showing the localization of FtsZ-GFP (a'), YFP-ZapA (b') and ZapB-GFP (c') in living cells of strain MC1000Δ*zapC*. Cells were grown at 30°C in M9 minimal medium supplemented with glucose and casamino acids. Expression of FtsZ-GFP from plasmid pEG12 (P_{lac}*::ftsZ::gfp*), YFP-ZapA from plasmid pNG53 (P_{lac}*::yfp::zapA*) and ZapB-GFP from plasmid pEG3a (P_{BAD}*::zapB::gfp*) was induced as described in *Materials and Methods*. Scale bar = 2 μm.

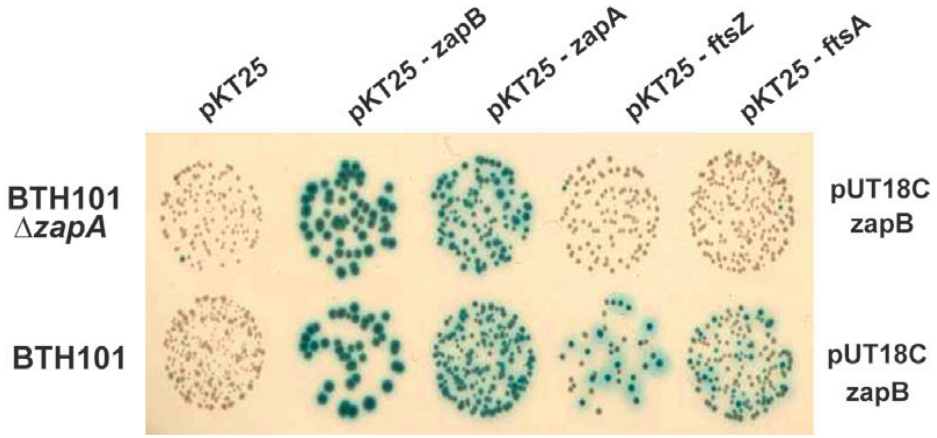

Fig. 3.11 ZapA and ZapB interact in a bacterial two-hybrid assay

Protein interaction detected by bacterial two-hybrid assays (Galli and Gerdes, 2010). *E. coli* wt strain BTH101 and mutant strain BTH101Δ*zapA* were co-transformed with two-hybrid plasmids (pUT18C and pKT25) expressing fusions to various cell division protein genes as indicated. Transformants were spotted onto selective plates containing X-Gal and incubated at 30°C for 48 h. Blue coloration indicates a positive interaction.

3.3.9 ZapA and ZapB interact *in vitro*

To test *in vitro* that ZapB interacts directly with ZapA and through it with FtsZ we used a Sucrose Gradient Sedimentation assay. The purified FtsZ, His-ZapA and ZapB-His were loaded onto a Sucrose Gradient and after ultracentrifugation their sedimentation profile was analysed by SDS-PAGE. FtsZ and ZapA remained at the top of the gradient (Fraction F#1), where the sucrose concentration is lower, whereas ZapB was present in the fractions with a higher sucrose concentration (from F#3 to F#6) (Fig. 3.12A). The formation of ZapB high molecular-weight (HMW) complexes (as indicated by the high sedimentation rate) is consistent with ZapB's propensity to spontaneously form polymers (Ebersbach *et al.*, 2008).

The same experiment was then repeated mixing the three proteins ZapA, ZapB and FtsZ (in a molar ratio of 3:3:1, respectively) in all possible combinations: when ZapA and ZapB were mixed together, 10% of ZapA co-sedimented with ZapB and the two proteins were present at the bottom of the gradient, in the fraction with the highest sucrose concentration (F#6) (Fig. 3.12B). Remarkably, when the three proteins were mixed, they co-sedimented (10% of ZapA and 10% of FtsZ were present in F#6). In contrast, neither ZapA nor ZapB alone had any effect on FtsZ sedimentation in this assay (Fig. 3.12B).

It has to be pointed out that the experiments were performed in the absence of GTP, precluding the formation of HMW FtsZ–ZapA complexes when ZapA and FtsZ were mixed together. The two purified proteins FtsZ and His-ZapA were previously shown to be able to directly interact *in vitro* (Fig. 3.6).

Alongside the *in vivo* data, these results support the direct interaction between ZapA and ZapB and additionally show that ZapB forms an HMW complex with ZapA and FtsZ.

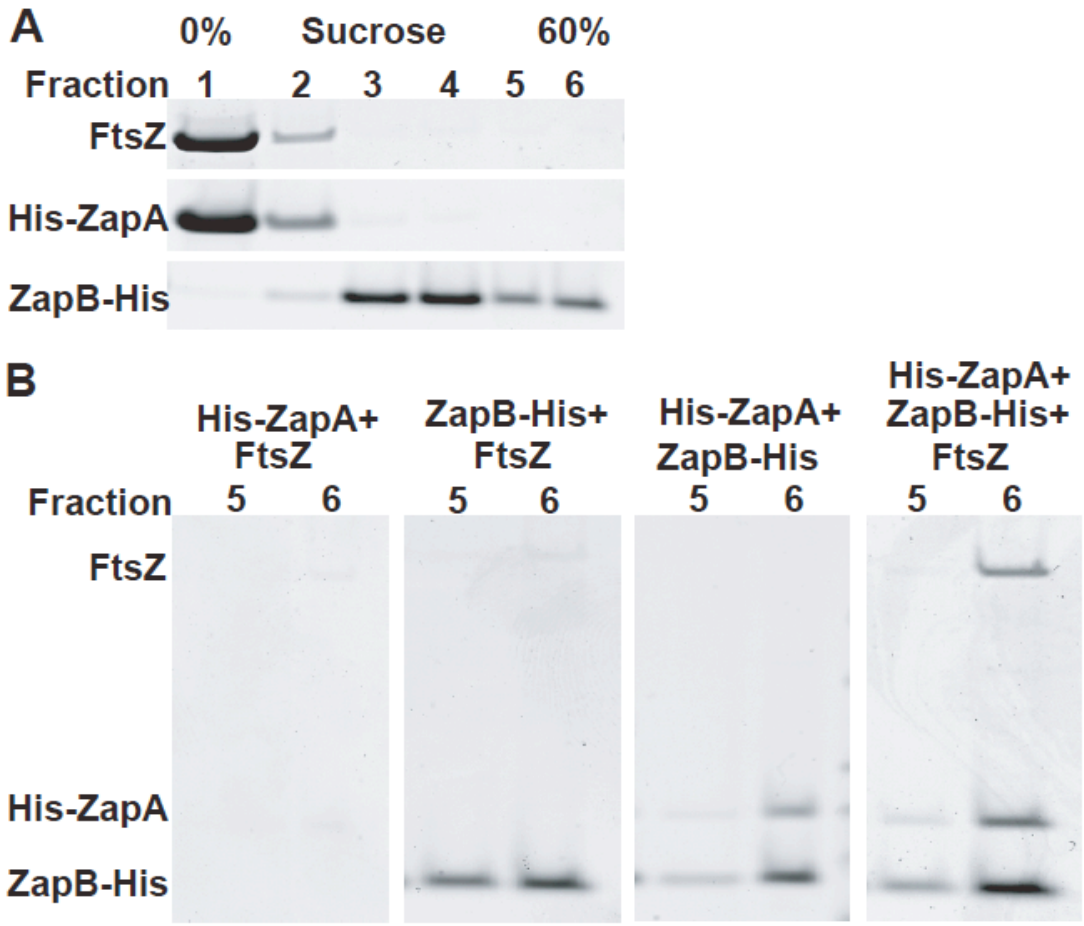

Fig. 3.12 ZapB interacts with ZapA *in vitro*

SDS-PAGE of sucrose gradient fractions after centrifugation (Galli and Gerdes, 2010). Purified proteins were mixed in a 50 mM PIPES pH 6.5 buffer and incubated for 30 minutes at room temperature before loading onto sucrose gradients. **A.** The gradient was divided into six fractions from the lowest (F#1, 0%) to the highest (F#6, 60%) sucrose concentration. FtsZ and His_6-ZapA localized predominantly in F#1, ZapB-His_6 from F#3 to F#6. **B.** The three proteins were mixed together in all possible combinations and the last two fractions of the gradient (F#5 and F#6) are shown. His_6-ZapA in presence of ZapB-His_6 partially precipitated in the last fraction (F#6) and FtsZ sedimented at the bottom of the gradient only when His_6-ZapA and ZapB-His_6 were both present.

3.3.10 The FtsZ-ZapA-ZapB interactome

To further dissect the interaction between ZapA and ZapB, we introduced truncations in both proteins and tested their effect in the bacterial two-hybrid assay (Karimova *et al.*, 1998). The BTH analysis was performed in a BTH101Δ*zapA*Δ*zaB* background, in order to avoid any interference by the endogenously encoded proteins.

ZapB is an 81 aa protein with a 100% coiled-coil structure, without any globular domain (Fig. 3.13A) (Ebersbach *et al.*, 2008). Since there are no specific domains in ZapB structure, we systematically constructed C-terminal and N-terminal deletions differing by 10 aa (a total of 8 truncated ZapB mutants were constructed) (Fig. 3.13B). The N-terminal region of ZapB was essential for the interaction with ZapA: the truncation of the first 10 aa was sufficient to completely abolish the Lac^+ phenotype. Instead, the deletion of up to 41 aa at the ZapB C-terminal end did not affect ZapB-ZapA interaction. To affect ZapB self-interaction it was necessary to truncate larger portions of the protein and neither the N- nor the C-terminal ends were essential.

ZapA is a 108 aa protein characterized by an N-terminal globular domain and a C-terminal coiled-coil domain (Fig. 3.13C) (Low *et al.*, 2004). Mutant ZapA-2 contains the globular domain of ZapA whereas ZapA-4 contains the coiled-coil domain. ZapA interacted through its coiled-coil domain with ZapB and with itself and through its globular domain with FtsZ (Fig. 3.13D). These results support the ZapA-FtsZ interaction model proposed by Low *et al*. (2004).

That ZapB interacts with ZapA via its N-terminal end was confirmed by far-western blot analyses: in this assay purified ZapA was able to interact with purified FtsZ and ZapB but not with Δ10ZapB (ZapB-1) and in the same way ZapB but not Δ10ZapB was able to bind ZapA (Fig. 3.13E).

To pinpoint the amino acids most important for its interaction with ZapA, we constructed *zapB* mutants changing to alanine, two by two, the first 10 amino acids of the protein. As described above, the ZapB variants were tested in a BTH assay for their interaction with ZapA. The aa changes that reduced ZapB's interaction with ZapA were identified (variants $ZapB^{S4L5AA}$, $ZapB^{F8E9AA}$ and $ZapB^{K10L11AA}$) (Fig. 3.14A). By contrast, all these mutants were still able to interact with ZapB seemingly at the same extent as the wt protein did.

Interaction of mutant ZapB-b (henceforth called $ZapB^{S4L5AA}$) with ZapA was assayed *in vitro* by a co-elution experiment using ZapB-His_6 and $ZapB^{S4L5AA}$-His_6 fusion (Fig. 3.14B). ZapB-His_6 bound to a Ni^{2+}-resin was capable of retaining ZapA independently of the presence of FtsZ in the sample. $ZapB^{S4L5AA}$-His_6 instead retained significantly less ZapA than the wild-type protein (Fig. 3.14B, c).

We also analysed if FtsZ was retained in the column by ZapB-His_6 in the presence of ZapA, but the elution profile showed that FtsZ was only slightly more abundant when ZapA was present compared to when it was absent and FtsZ was retained aspecifically in the column (Fig. 3.14B, d). Probably, the complex formed by the three proteins, with ZapA acting as a linker between FtsZ and ZapB, was not strong enough to resist the washing steps performed in the assay and FtsZ was washed away, whereas ZapA, directly interacting with ZapB, was retained in the column.

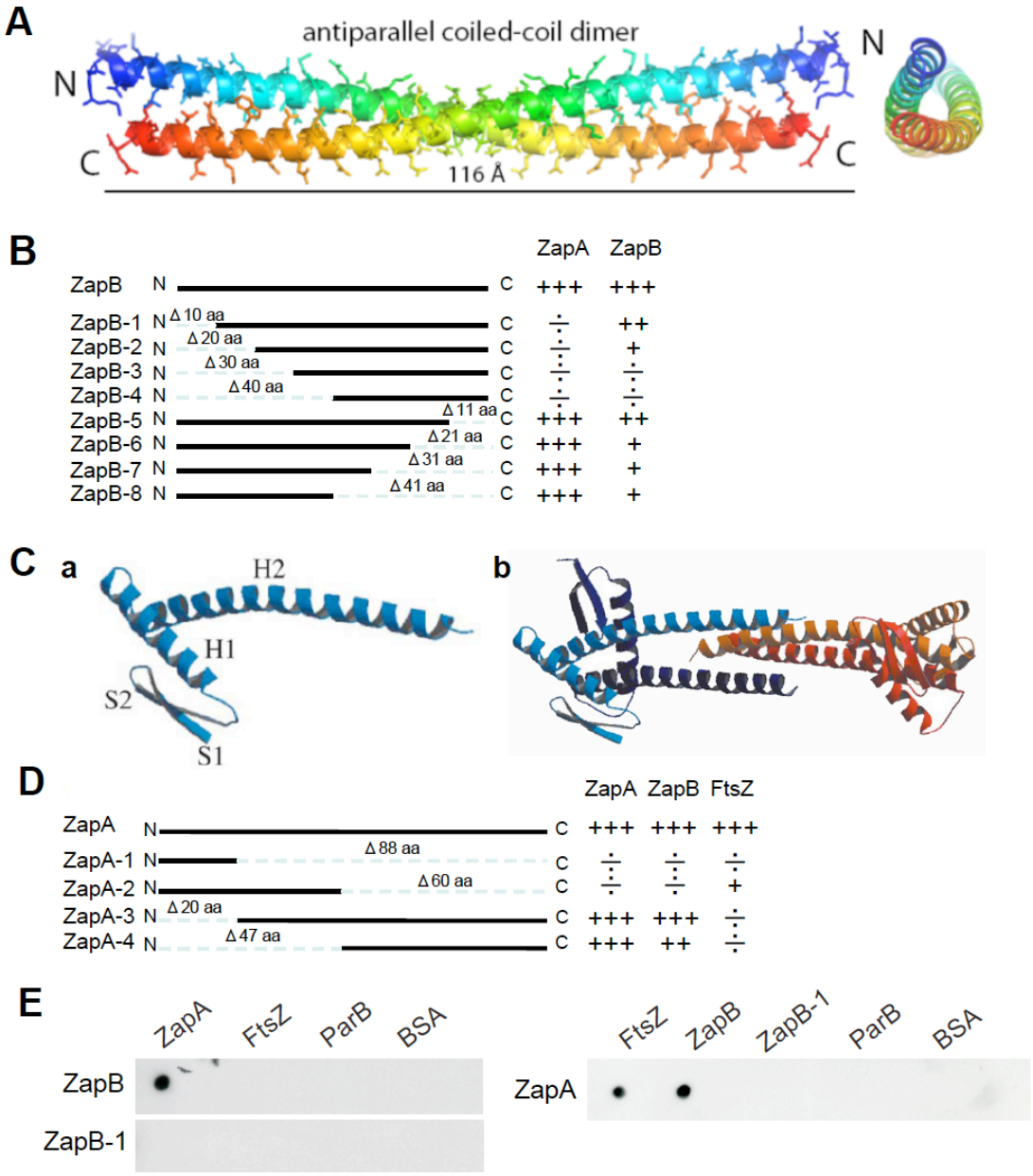

Fig. 3.13 FtsZ-ZapA-ZapB interactome

A. Crystal structure of an *E. coli* ZapB anti-parallel coiled-coil dimer (Ebersbach *et al*., 2008). **B.** Interaction of ZapB mutants fused to T18 fragment and ZapA or ZapB fused to T25 fragment in a BTH assay. **C.** Crystal structure of a *P. aeruginosa* (a) ZapA monomer; (b) ZapA tetramer (Low *et al.*, 2004). **D.** Interaction of ZapA mutants fused to T25 fragment and ZapA or ZapB or FtsZ fused to T18 fragment in a BTH assay. ZapA-1 contains only S1+S2; ZapA-2 contains S1+S2+H1; ZapA-3 contains H1+H2; ZapA-4 contains only H2. **E.** Far-western blot. ZapB-His_6 interacts with ZapA but not FtsZ, ParB or BSA. ZapB-1-His_6 does not interact with any of the proteins tested. ZapA interacts with FtsZ and ZapB but not with ZapB-1, ParB or BSA. In the BTH assay: +, weak interaction; ++, stronger interaction; +++, strong interaction; ÷, no interaction.

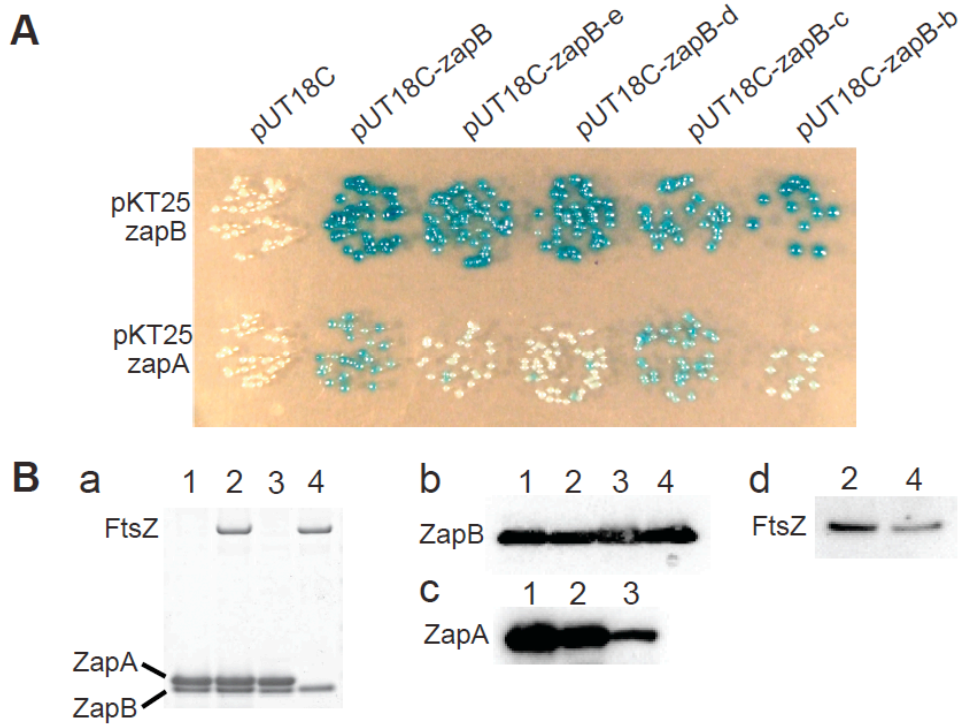

Fig. 3.14 ZapB point mutants and their interaction with ZapA

The mutants constructed are: ZapB-b (S4L5AA), ZapB-c (E6V7AA), ZapB-d (F8E9AA), ZapB-e (K10L11AA). **A.** Protein interaction detected by bacterial two-hybrid assay. *E. coli* mutant strain BTH101Δ*zapA*Δ*zapB* was co-transformed with two-hybrid plasmids (pUT18C and pKT25) expressing fusions to various cell division protein genes as indicated. Transformants were spotted onto selective plates containing X-Gal and incubated at 30°C for 48 h. Blue coloration indicates a positive interaction. **B.** Ni^{2+}–NTA affinity chromatography of ZapA plus or minus FtsZ in the presence of ZapB-His_6 or $ZapB^{S4L5AA}$-His_6. (a) Starting reactions were loaded on a Coomassie stained SDS–PAGE: Lane 1: ZapB-His_6+ZapA; Lane 2: ZapB-His_6+ZapA+FtsZ; Lane 3: $ZapB^{S4L5AA}$-His_6+ZapA; Lane 4: ZapB-His_6+FtsZ. 0.5 mg/ml of BSA was present in each reaction. The elution profiles of the three proteins were inspected separately by Western-Blot analysis: (b) ZapB elution profile; (c) ZapA elution profile; (d) FtsZ elution profile.

3.4 Discussion

We show here that ZapB consistently co-localized with FtsZ (Fig. 3.3 and 3.4) and ZapA (Fig. 3.3) and that ZapB was recruited to the divisome earlier than FtsK (Fig. 3.5). Moreover, ZapB had a dynamic pattern that depended on FtsZ but not on FtsA, ZipA or FtsI (Fig. 3.2). Importantly, ZapB required either functional FtsA or functional ZipA to be recruited to the Z-ring, just like Z-ring assembly itself (Pichoff and Lutkenhaus, 2002).

ZapB recruitment into the Z-ring was indirect, the cell division factor ZapA recruited ZapB to the division site (Fig. 3.7) and consistent with these findings, ZapB interacted with ZapA in a BTH assay (Fig. 3.11). In contrast, ZapA recruitment to the Z-ring did not depend on ZapB (Fig. 3.8).

It is known that a fine balance between the levels of cell division proteins is required for cytokinesis to proceed normally. For example, two to seven fold increases in the level of FtsZ results in induction of the mini-cell phenotype and, at 10 times over its normal level, cell division is inhibited and cells become filamentous (Ward, Jr. and Lutkenhaus, 1985; Dai and Lutkenhaus, 1992). This effect is due to an imbalance of FtsZ:FtsA ratio, which is critical for cell division to occur (Dai and Lutkenhaus, 1992; Dewar *et al.*, 1992). The artificial elevation of ZapB levels has been reported to affect both nucleoid and cell morphology (Ebersbach *et al.*, 2008) (these effects will be addressed in more detail in Chapter 5).

Supporting a key-role of ZapA in recruiting ZapB to the Z-ring, an increased level of ZapA caused the complete delocalization of ZapB in the cytoplasm (Fig. 3.9C). This effect was most readily explained by titration of ZapB away from the Z-ring. Interestingly, ZapA overproduction also resulted in aberrant localization of FtsZ (Fig. 3.9B) that looked very similar to that observed when ZapC was overproduced: two recent papers reported that in the presence of elevated levels of ZapC, the cells formed filaments and FtsZ assembled into spots, spirals, and more linear rod-like structures (Durand-Heredia *et al.*, 2011; Hale *et al.*, 2011). ZapA, as has been proposed for ZapC, is an FtsZ cross-linking and bundling factor (Low *et al.*, 2004; Mohammadi *et al.*, 2009; Dajkovic *et al.*, 2010), so it was not unexpected that increasing its cellular concentration could affect Z-ring morphology. However, ZapC was not important for ZapB and ZapA localization and interaction (Fig. 3.10).

ZapA bridging role was further supported by *in vitro* interaction studies. In a sucrose gradient assay, ZapB spontaneously formed HMW complexes that were able to pull ZapA down to the bottom of the gradients (Fig. 3.12). Moreover, ZapA and ZapB together made a HMW complex with FtsZ whereas neither protein alone was able to pull FtsZ down, even though ZapA was shown to interact with FtsZ *in vitro* (Fig. 3.6) (it should be mentioned that GTP was not present in the reaction, probably precluding the formation of HMW FtsZ–ZapA complexes when ZapA and FtsZ were mixed together).

The N-terminal end of ZapB and the coiled-coil domain of ZapA were identified as the interacting regions of the two proteins in a BTH assay (Fig. 3.13 and 3.14). The importance of the N-terminal end of ZapB for its interaction with ZapA was confirmed *in vitro* in a far-western blot assay (Fig. 3.13) and in a co-elution experiment (Fig. 3.14).

Chapter 4

Spatial resolution of two bacterial cell division proteins

4.1 Introduction

Since the discovery of the green fluorescent protein and the following development of fluorescence microscopy, a great effort has been invested in finding probes with different wavelengths of absorption and emission and in improving their brightness and photostability (Snapp, 2009; Chudakov *et al*., 2010).

Tagging a molecule of interest with fluorescent probes in order to visualize its localization in the cell and investigate its possible dynamics over time is now a well-established technique commonly used both in eukaryotes and in bacterial cell studies (Giepmans *et al*., 2006; Snapp, 2009).

In the last years, besides the research for brighter, more photostable and faster-folding FPs, researchers have developed new imaging techniques able to overcome the spatial resolution limits imposed by the diffraction of light, pushing the lateral and axial resolution limit from the ~250 nm of visible light to ~20-50 nm when using the so-called super-resolution microscopy (Fernandez-Suarez and Ting, 2008). These new techniques include stimulated emission depletion (STED), photoactivated localization microscopy (PALM), fluorescence photoactivation localization microscopy (FPALM) and stochastic optical reconstruction microscopy (STORM) (Fernandez-Suarez and Ting, 2008).

The nanoscale structure of bacterial proteins such as MreB and FtsZ (Biteen *et al.*, 2008; Fu *et al.*, 2010; Jennings *et al.*, 2011) has been investigated and probably in the near future a better insight in the organization and composition of biomolecular complexes will be revealed, thanks to the resolution improvements achieved.

In particular, FtsZ dynamic localization has been carefully scrutinized trying to further advance our understanding of the formation of the Z-ring at mid-cell and the cell division process. Both in *E. coli* and in *B. subtilis*, besides the cytokinetic ring structure at the division site, helical-like intermediates along the entire length of the cell have been described (Thanedar and Margolin, 2004; Peters *et al.*, 2007). It was observed that, after completion of cell division, FtsZ is redistributed in the daughter cells in a highly dynamic helical-like pattern that persists throughout the entire division process (Stricker *et al.*, 2002; Thanedar and Margolin, 2004). Moreover, in *B. subtilis*, aside from the helical permanent cytoskeletal FtsZ also seen in *E. coli*, it was observed that FtsZ localization changes during the cell cycle: in newborn cells FtsZ localized in a helical-pattern along the entire cell, then as the cell became longer the

helical structure became restricted to a central region of the cell and, in the end, the helix collapsed into the well-known ring at mid-cell (Peters *et al.*, 2007).

Following the improvements in the imaging techniques, the next step was to investigate the FtsZ supramolecular structures within the Z-ring that using conventional fluorescence light microscopy appeared like a closed hollow circular structure (Sun and Margolin, 1998).

The first insight into the detailed structure of the Z-ring was captured in *C. crescentus* by electron cryotomography (ECT): it was shown that the Z-ring consisted of short (~100 nm) filaments spaced erratically along the membrane near the constriction site (Li *et al.*, 2007).

In the last year, using high-resolution microscopy techniques, two new studies have described the fine structures of the Z-ring, one in *E. coli* by PALM (Fu *et al.*, 2010) and one in *B. subtilis* by STED (Jennings *et al.*, 2011).

Fu and colleagues (2010) using PALM achieved a spatial resolution of ~35 nm and reported that the *E. coli* Z-ring consists not only of the well-known ring-like structure but also of compressed helical conformations characterized by variable helical lengths and pitches. In their model FtsZ is able to form this newly identified conformation through the weak non-uniform lateral interactions between its protofilaments. They suggest that FtsZ protofilaments could form the Z-ring randomly overlapping with each other in a loosely packed ring-like structure at mid-cell (Fu *et al.*, 2010).

In *B. subtilis*, Jennings *et al*. (2011) analysed by STED the supramolecular structures of FtsZ both in the Z-ring and in what is considered its precursor, the cytoskeletal helix, reaching a lateral resolution of approximately 80 nm. They showed that the FtsZ cytoskeletal helical structure is irregular and discontinuous and they also identified a new FtsZ helix with a smaller pitch compared to the one previously identified with fluorescence light microscopy (Peters *et al.*, 2007). In their model they suggest that this tight helix is the native form of FtsZ in newborn cells, FtsZ is then incorporated in the loose cytoskeletal helix, direct precursor of the Z-ring.

4.2 Aim of this chapter

In the previous chapter we showed that ZapB localizes at the cell division site with FtsZ and ZapA and that its dynamic pattern during a complete cell cycle follows closely that of FtsZ. Exploiting technological and experimental improvements in our microscopy techniques, we then tried to characterize in greater detail the structure of the ZapB-ring and we compared it to that of FtsZ, looking for possible differences between the two. Since the factor recruiting ZapB into the Z-ring is ZapA, we also analysed ZapA's mid-cell ring structure.

4.3 Results

4.3.1 ZapB constricts inside the Z-ring

In the time-lapse experiment described in Chapter 3, ZapB-GFP and FtsZ-mCherry co-localized during the entire cell division process in most of the cells. However, careful scrutiny of the images from the time-lapse series revealed that occasionally the ZapB-GFP ring at mid-cell constricted into a dot just ahead of the FtsZ-mCherry ring (Fig. 3.4, 50′ to 55′). To increase resolution, we analysed the localization of the two proteins in static images, when the exposure times used for both the FPs were much longer and, therefore, the resolution of the images improved. In particular, we paid close attention to pre-divisional cells on the verge of septation. We found that in ~2% of the cells (n = 2000), ZapB-GFP formed one distinct focus that localized between two dots of FtsZ-mCherry (Fig. 4.1A), suggesting that the ZapB signal was ahead of that of FtsZ.

To ensure that this phenomenon was not due to an artefact produced by the fluorescent-tagged proteins, we swapped the fluorophores between the two proteins and repeated the experiment. Using the swapped combination, the ZapB-mCherry signal was now ahead of the FtsZ-GFP signal in ~4% of the cells (n = 2000) (Fig. 4.1A). As FtsZ is the first to assemble and the principal component of the Z-ring, it was unexpected that ZapB was ahead of FtsZ in a significant fraction of the cells. To investigate if this characteristic was specific for ZapB, we analysed ZapA in a similar way using the YFP-ZapA and FtsZ-mCherry fusion protein pair. However, in no case, we observed any significant difference in the patterns of the two fluorescent proteins – that is – the proteins co-localized in all cells that we observed at all stages of the cell cycle (n = 2000) (Fig. 4.1B). Instead, when we inspected in the same way the pair ZapB-mCherry and YFP-ZapA once again ZapB seemed to be ahead of ZapA in ~2% of the cells analysed (n = 2000) (Fig. 4.1D). Furthermore, in almost all pre-divisional cells, in which septum indentations were not yet visible, the FtsZ and ZapA signals were adjacent to the membrane whereas the ZapB signal was slightly shifted towards the internal part of the cell, as if ZapB was forming a ring on the inside of the Z-ring, with a diameter smaller than that of FtsZ or ZapA. This was true for both of the fluorophore combinations that we used when investigating the pair formed by FtsZ

and ZapB (Fig. 4.1C).

Since this is the first time that a cell-division protein is reported to form a ring-structure on the inside of the Z-ring, we decided to analyse in more detail this phenomenon. We improved our time-lapse analysis technique and processed by deconvolution all the fluorescent images, in order to obtain a sharp signal of the fluorescent fusion proteins for as long as possible, through more than one cell division cycle.

The time-lapse series in Fig. 4.2 shows two cells at different stages of the cell cycle, the one on the left had almost completed the division process and deep indentations were visible at the septum whereas the cell on the right was still quite short, at an early stage of the cell cycle, and did not present any septum indentations. After 4' from the beginning of the time-lapse, in the cell on the verge of septation on the left, ZapB-mCherry already formed a single focus enclosed by the FtsZ-GFP signals at mid-cell. The cell division process then proceeded with the formation of two daughter cells that started a new cell division cycle. In both of the daughter cells, at the 48' of the time-lapse, ZapB again was ahead of FtsZ during constriction. The cell on the right in Fig. 4.2 when the time-lapse series started was at the beginning of the cell division process and had visible deep indentations at the septum after 32'. As expected, ZapB was ahead of FtsZ in this cell too. It should also be noted that ZapB-mCherry, as seen in the static pictures in Fig. 4.1C, formed two dots that seemed to be closer to each other than those formed by FtsZ, suggesting that throughout the cell cycle ZapB formed a ring enclosed by the Z-ring at mid-cell.

As a control, the localization of the pair YFP-ZapA / ZapB-mCherry and FtsZ-mCherry / YFP-ZapA were inspected in time-lapse experiments as done for FtsZ-GFP / ZapB-mCherry. ZapB constricted ahead of ZapA in both the cells depicted (Fig. 4.3A, at 20' for the cell on the right and at 24' for the cell on the left). Instead, YFP-ZapA and FtsZ-mCherry always perfectly co-localized at all stages of the cell cycle (Fig. 4.3B).

Therefore, we could conclude that ZapB was able to form a ring located on the inside of the Z-ring, with a smaller diameter and that this was not a peculiar phenomenon true for only a small fraction of the cell population, but that it was maintained in all cells, generation after generation.

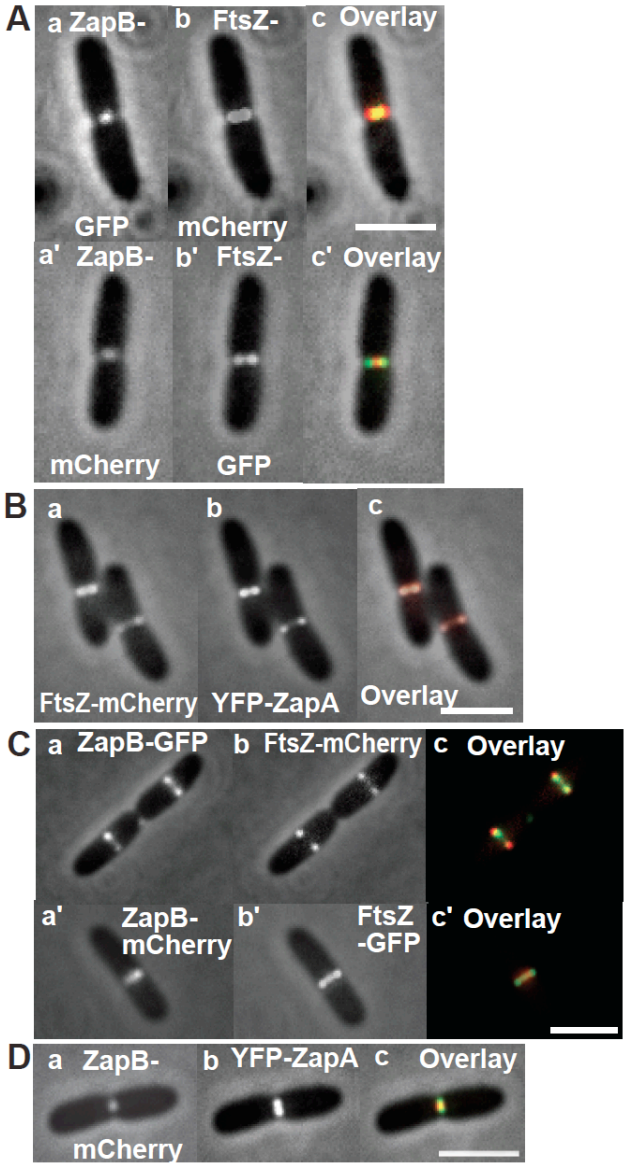

Fig. 4.1 ZapB can constrict ahead of FtsZ

Cells of MC1000 carrying the plasmids listed below were grown in M9 minimal medium supplemented with glucose and casamino acids at 30°C and FPs induced as described in *Materials and Methods* (Galli and Gerdes, 2010). The Figure shows combined phase-contrast and fluorescence microscopy images. **A.** Upper panel: MC1000/pEG3a (P_{BAD}*::zapB::gfp*)/pQW59 (P_{lac}*::ftsZ::mCherry*). Inserts: (a) ZapB-GFP; (b) FtsZ-mCherry; (c) overlay of (a) and (b). Lower panel: MC1000/pEG9 (P_{BAD}*::zapB::mCherry*)/pEG12 (P_{lac}*::ftsZ::gfp*): (a′) ZapB-mCherry; (b′) FtsZ-GFP; (c′) overlay of (a′) and (b′). **B.** MC1000/pEG4 (P_{BAD}*::ftsZ::mCherry*)/pNG53 (P_{lac}*::yfp::zapA*). (a) FtsZ-mCherry; (b) YFP-ZapA; (c) overlay of (a) and (b). **C.** Upper panel: MC1000/pEG3a (P_{BAD}*::zapB::gfp*)/pQW59 (P_{lac}*::ftsZ::mCherry*). Inserts: (a) ZapB-GFP; (b) FtsZ-mCherry; (c) overlay of (a) and (b). Lower panel: MC1000/pEG9 (P_{BAD}*::zapB::mCherry*)/pEG12 (P_{lac}*::ftsZ::gfp*). Inserts: (a′) ZapB-mCherry; (b′) FtsZ-GFP; (c′) overlay of (a′) and (b′). **D.** MC1000/pEG9 (P_{BAD}*::zapB::mCherry*)/pNG53 (P_{lac}*::yfp::zapA*). (a) ZapB-mCherry; (b) YFP-ZapA; (c) overlay of (a) and (b). Scale bars = 2 µm.

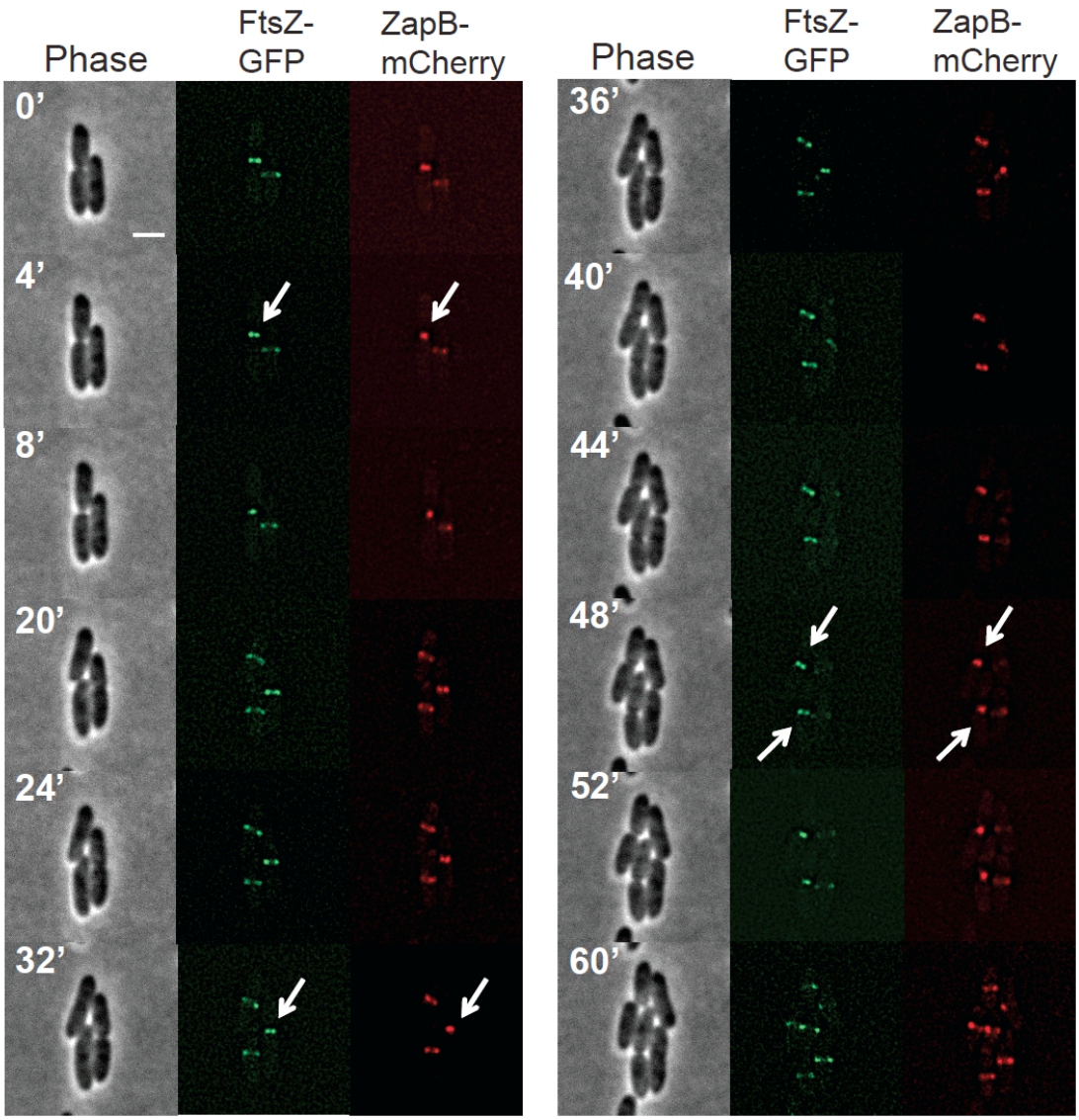

Fig 4.2 Time-lapse: ZapB constricts ahead of FtsZ

Phase-contrast and fluorescence microscopy images showing the localization of FtsZ-GFP and ZapB-mCherry in living cells of strain MC1000/pEG9 (P_{BAD}*::zapB::mCherry*)/pEG12 (P_{lac}*::ftsZ::gfp*). Cells were grown at 37°C in M9 minimal medium supplemented with glucose and casamino acids. Expression of ZapB-mCherry from plasmid pEG9 and FtsZ-GFP from plasmid pEG12 was induced by addition of arabinose and IPTG as described in *Materials and Methods*. Fluorescence images were taken with GFP filter set with 0.5 sec exposure and RFP filter set with 0.6 sec exposure, every 4 minutes. Fluorescence images were deconvolved before analysis. White arrows indicate when ZapB formed a single focus localized between two FtsZ dots. Scale bar = 2 μm.

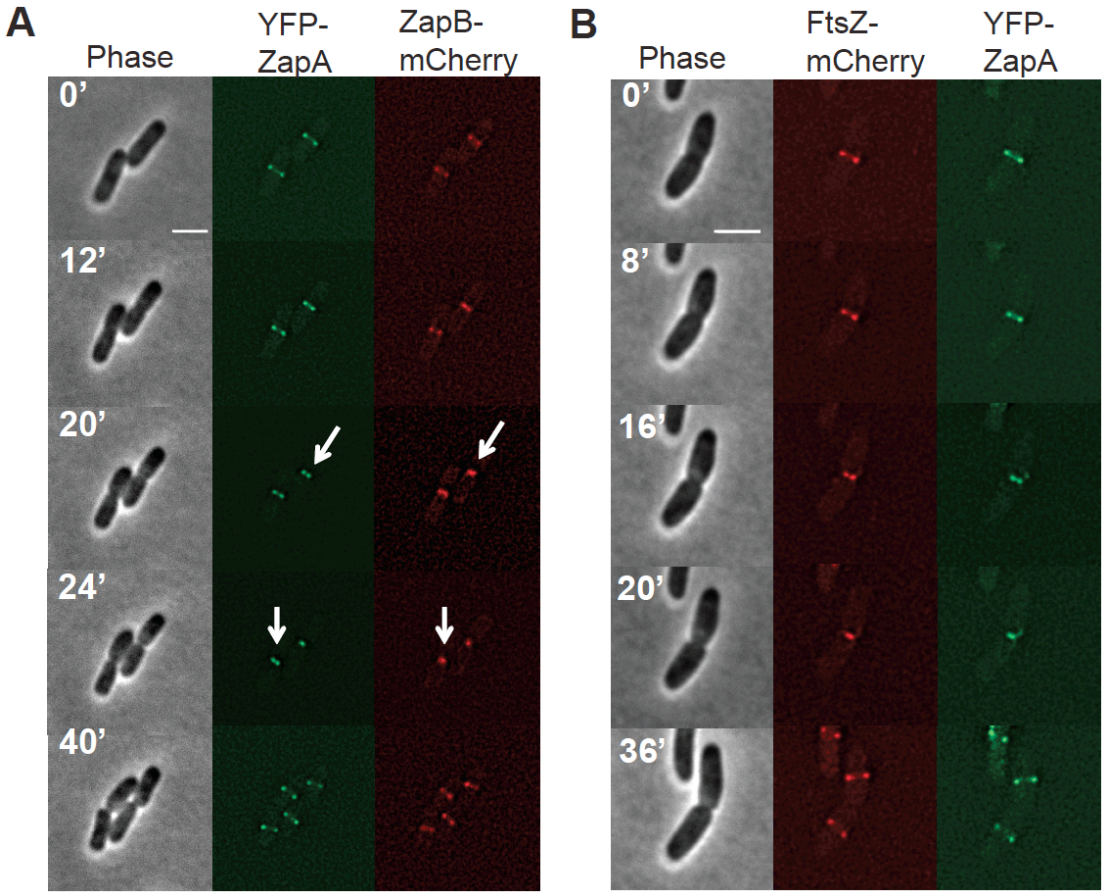

Fig. 4.3 Time-lapse: ZapB constricts ahead of ZapA

Phase-contrast and fluorescence microscopy images showing the localization of (**A**) YFP-ZapA and ZapB-mCherry in living cells of strain MC1000/pNG53 (P_{lac}*::yfp::zapA*)/pEG9 (P_{BAD}*::zapB::mCherry*) and (**B**) YFP-ZapA and FtsZ-mCherry in living cells of strain MC1000/pNG53 (P_{lac}*::yfp::zapA*)/pEG4 (P_{BAD}*::ftsZ::mCherry*). Cells were grown at 37°C in M9 minimal medium supplemented with glucose and casamino acids. Expression of ZapB-mCherry from plasmid pEG9, FtsZ-mCherry from plasmid pEG4 and YFP-ZapA from plasmid pNG53 was induced by addition of arabinose and IPTG as described in *Materials and Methods*. Fluorescence images were taken with YFP filter set with 0.5 sec exposure and with RFP filter set with 0.6 sec exposure, every 4 minutes. Fluorescence images were deconvolved before analysis. White arrows indicate when ZapB formed a single focus localized between two ZapA dots. Scale bars = 2 µm.

4.3.2 Three-dimensional (3D) image reconstruction of FtsZ, ZapA and ZapB ring at mid-cell

3D image reconstructions showing hollow FtsZ-GFP rings at the cell division site were previously described (Ma *et al.*, 1996; Sun and Margolin, 1998). Therefore, to substantiate that ZapB forms a smaller ring enclosed by FtsZ, we processed Z-stacks of FtsZ-GFP and ZapB-mCherry by deconvolution and reconstructed a 3D model of the two proteins in the same cell. Indeed, in all cells processed (n = 27), FtsZ invariably encircled ZapB (Fig. 4.4AB) (the same result was obtained using the pair FtsZ-mCherry/ZapB-GFP (data not shown)). Z-stacks of FtsZ-mCherry and YFP-ZapA were processed in the same way and the two proteins formed rings of identical dimensions in all cells analysed (n = 20) (Fig. 4.5). As a control, ZapB-mCherry and YFP-ZapA were studied in a similar way and now ZapB was encircled by ZapA in all cells processed with the exception of one cell in which the two rings had the same diameter (n = 30): the two structures could be spatially resolved either in cells at a late (Fig. 4.6A) or at an early (Fig. 4.6B) stage of the cell division process.

Fig. 4.7 shows an overview of ZapB-ring localization compared to that of FtsZ or ZapA. In newborn cells ZapB forms a structure enclosed by the ring formed by FtsZ or ZapA and when the diameter of the Z-ring becomes smaller, as it happens in the late stages of division, and the septum indentations become clearly visible, ZapB is seen as a dot in the middle of the contracting ring. Indeed, we could only observe in ~2-4% of the cell population ZapB forming a single focus between the two dots of FtsZ or ZapA, because this phenomenon is only visible in a short frame of time during the division process. After that brief period of time FtsZ and ZapA complete ring contraction too and form a dot as ZapB did ahead of them.

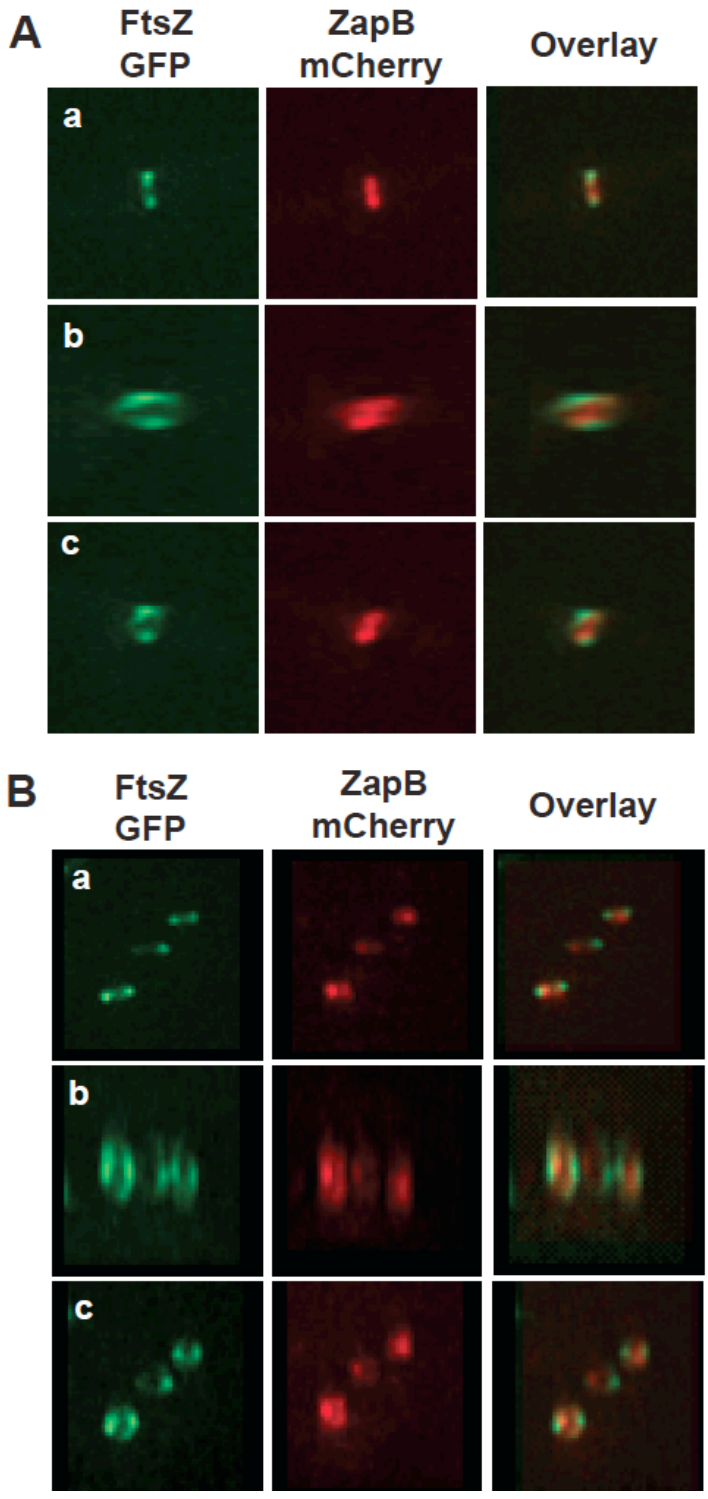

Fig. 4.4 ZapB ring is enclosed by the Z-ring

Cells of MC1000 carrying pEG9 (P_{BAD}*::zapB::mCherry*) and pEG12 (P_{lac}*::ftsZ::gfp*) were grown in M9 minimal medium supplemented with glucose and casamino acids at 30°C and FPs induced as described in *Materials and Methods* (Galli and Gerdes, 2010). All images were processed by deconvolution imaging. The same cell is shown tilted at three different angles (a–c) labelled with FtsZ-GFP or ZapB-mCherry or the overlay of the two.

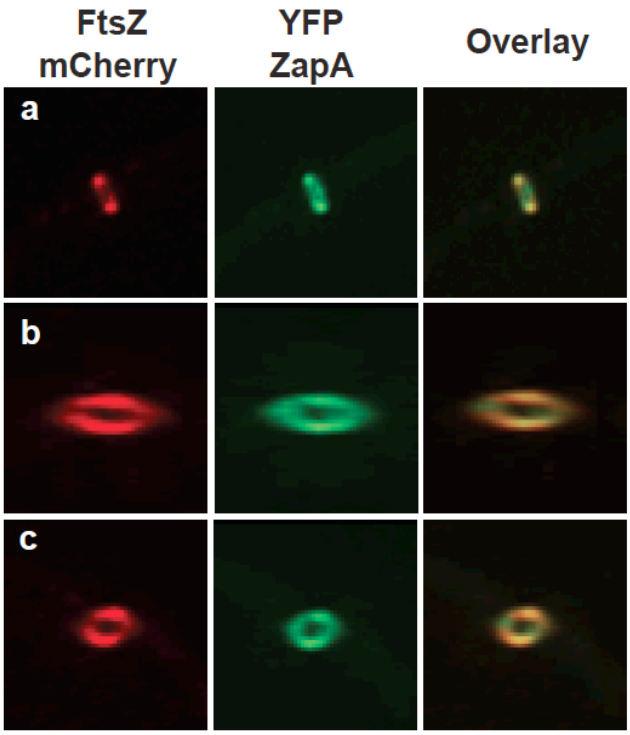

Fig. 4.5 ZapA and FtsZ rings superimpose perfectly

Cells of MC1000 carrying pEG4 (P_{BAD}*::ftsZ::mCherry*) and pNG53 (P_{lac}*::yfp::zapA*) were grown in M9 minimal medium supplemented with glucose and casamino acids at 30°C and FPs induced as described in *Materials and Methods* (Galli and Gerdes, 2010). All images were processed by deconvolution imaging. The same cell is shown tilted at three different angles (a–c) labelled with FtsZ-mCherry or YFP-ZapA or the overlay of the two.

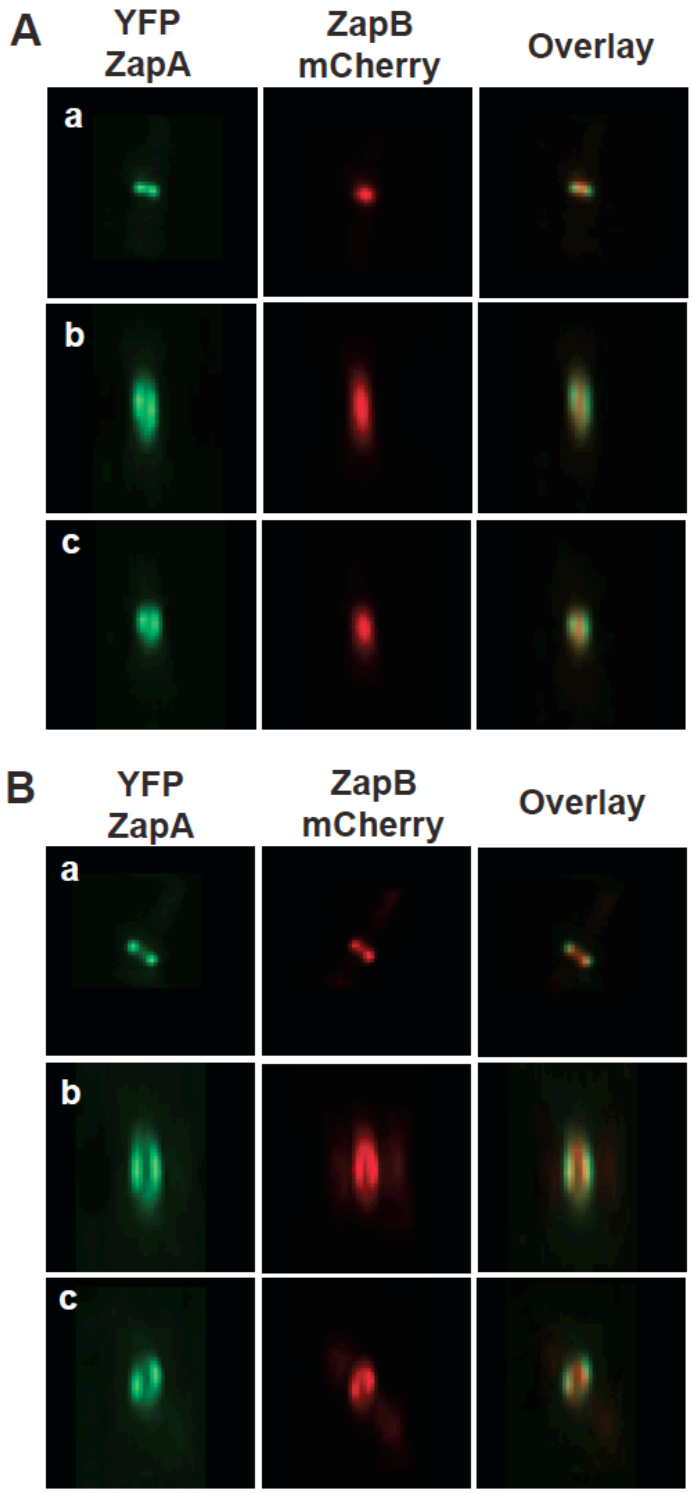

Fig. 4.6 ZapB ring is enclosed by ZapA ring

Cells of MC1000 carrying pEG9 (P_{BAD}*::zapB::mCherry*) and pNG53 (P_{lac}*::yfp::zapA*) were grown in M9 minimal medium supplemented with glucose and casamino acids at 30°C and FPs induced as described in *Materials and Methods* (Galli and Gerdes, 2010). All images were processed by deconvolution imaging. The same cell is shown tilted at three different angles (a–c) labelled with YFP-ZapA or ZapB-mCherry or the overlay of the two. **A.** Cell at an advanced stage of cell division with clear septum indentations. **B.** Pre-divisional cell with a smooth cell wall and no visible septum indentations.

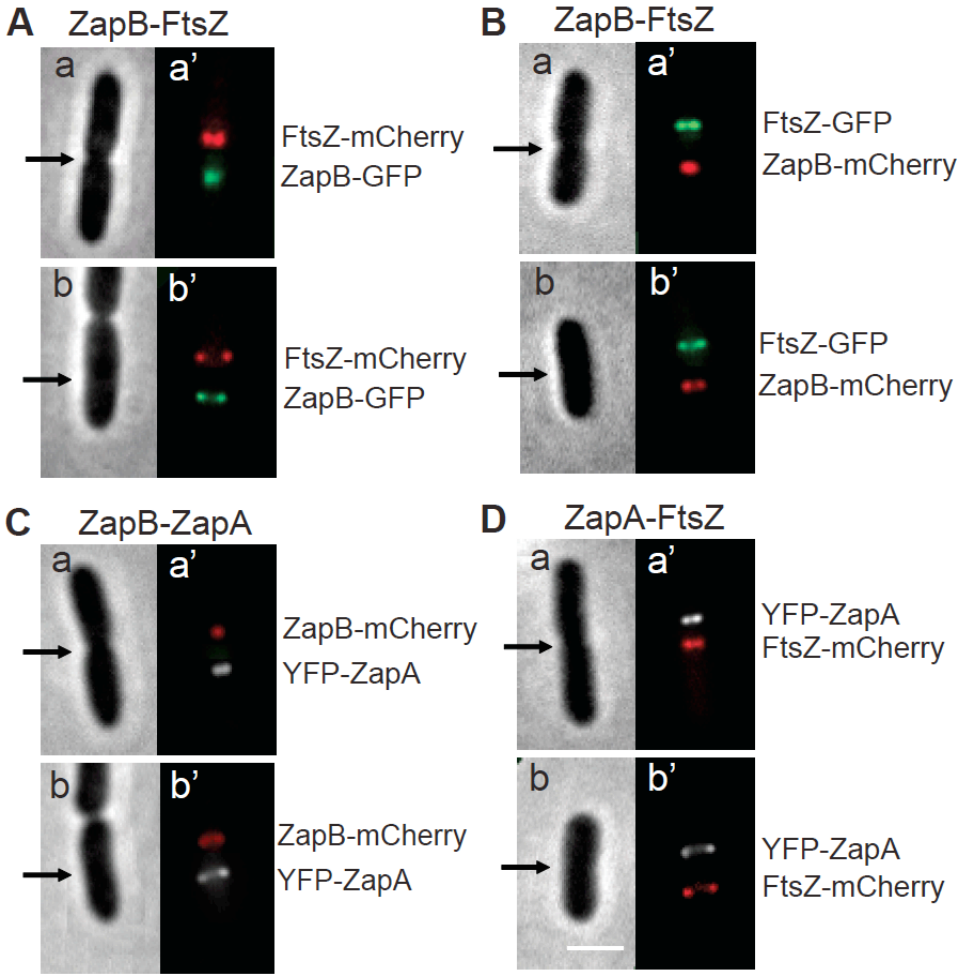

Fig. 4.7 ZapB is enclosed by the Z-ring: overview

ZapB forms a ring enclosed by the Z-ring in newborn cells (b, b') and in cells on the verge of division (a, a'). **A.** ZapB-GFP and FtsZ-mCherry. **B.** ZapB-mCherry and FtsZ-GFP. **C.** ZapB-mCherry and YFP-ZapA. **D.** FtsZ-mCherry and YFP-ZapA. The two FPs localized at mid-cell, black arrows point to the localization site in phase-contrast images (a, b). Fluorescence images shows the FPs pair artificially spaced between each other (a', b'). Scale bar = 2 μm.

4.3.3 Z-ring and B-ring morphology in Δ*mreB** cells

We showed that in wt rod-shaped cells ZapB is able to form a ring encircled by the Z-ring. However, the diameter of an *E. coli* cell is so small (~1 μm) that, to increase the spatial resolution between the two structures, we repeated the same localization analyses in Δ*mreB* cells. Since cells depleted of MreB propagate as small and big spheres (Kruse *et al.*, 2005; Bendezu and de Boer, 2008) and spherical cells have larger diameters than rod-shaped cells. In Δ*mreB* cells FtsZ forms closed or incomplete rings and more-complex structures such as isolated patches and foci (Bendezu and de Boer, 2008). MreB is an essential gene and the strain used in this work, called MC1000Δ*mreB**, contains an unknown suppressor that makes it viable (probably it carries mutations increasing the expression of FtsZ(AQ), a known suppressor of Δ*mreB* lethality) (Kruse *et al.*, 2005).

At first, we inspected FtsZ-GFP localization in MC1000Δ*mreB** and, as reported for cells depleted of MreB, FtsZ formed what appeared to be rings at the division sites (Fig. 4.8A, a) or more undefined, patchy structures (Fig. 4.8A, b). When we processed Z-stacks of FtsZ-GFP and ZapB-mCherry by deconvolution and reconstructed a 3D model of the two proteins in the same cell, we noticed that the large majority of cells did not contain complete Z-rings but helical structures (Fig. 4.8BCF) or open rings (Fig. 4.8E) and only in a few number of cells FtsZ formed a complete hollow ring (Fig. 4.8D).

Even more unexpectedly ZapB always co-localized with the structures formed by FtsZ in all the cells analysed (n = 30), either if they were helical or incomplete open rings or complete rings (Fig. 4.8BCDEF). If in cells with incomplete rings or helical structures we might have expected the loss of spatial resolution between the two proteins, since the Z-ring structures were somehow defective, we could not foresee that also when FtsZ formed what appeared to be complete hollow rings ZapB would have formed a co-localizing structure.

There are a number of explanations for the different ZapB-ring localization, first that MreB is necessary so that ZapB could form a structure discrete from the one of FtsZ and secondly that maintenance of rod shape is essential and consequently loss of resolution between the two proteins was a Δ*mreB* secondary effect.

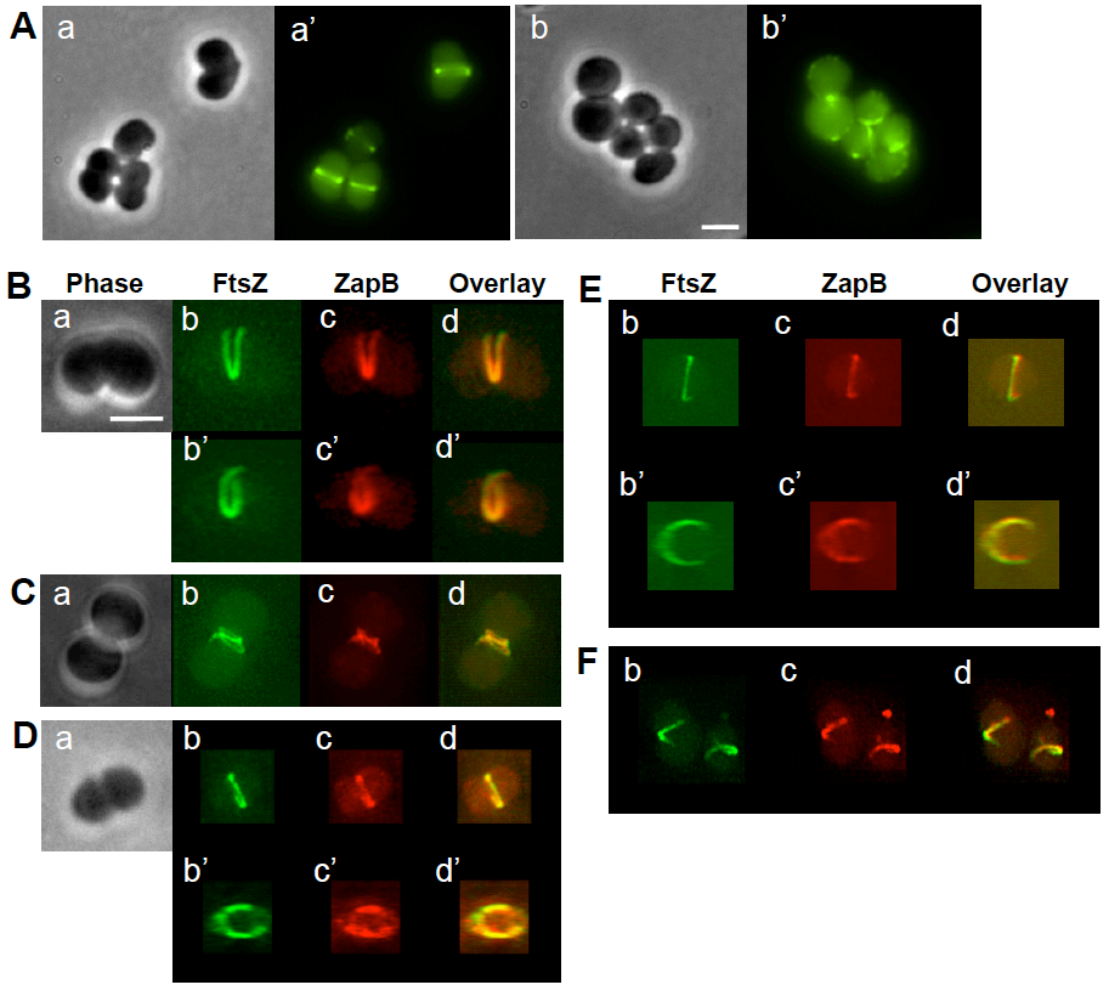

Fig. 4.8 Z-ring and B-ring morphology in Δ*mreB cells**

Cells of MC1000Δ*mreB** carrying pEG9 (P_{BAD}*::zapB::mCherry*) and pEG12 (P_{lac}*::ftsZ::gfp*) were grown in M9 minimal medium supplemented with glucose and casamino acids at 30°C and FPs induced as described in *Materials and Methods*. **A.** Phase-contrast (a, b) and FtsZ-GFP localization (a', b'). **B,C,D,E,F**: examples of different cells. All images were processed by deconvolution imaging. The same cell is shown tilted at two different angles labelled with FtsZ-GFP (b) or ZapB-mCherry (c) or the overlay of the two (d) or the phase-contrast (a). Scale bars = 2 μm.

4.3.4 Z-ring and B-ring morphology in cells treated with A22 or Mecillinam

To assess if the loss of rod-shape had a role in the spatial resolution of ZapB and the Z-ring, we decided to treat wt cells with either A22 or Mecillinam. A22 is an MreB inhibitor that causes depolymerization of MreB (Kim *et al.*, 2006) whereas Mecillinam inhibits PBP2 (Park and Burman, 1973). Treatment with either one of them results in the formation of lemon-shaped or spherical-cells indistinguishable from each other (Karczmarek *et al.*, 2007). Comparing the localization of ZapB and FtsZ in cells with not functional MreB or PBP2 could then allow us to discriminate between the MreB role and the cell-shape role in the formation of a ZapB-ring on the inside of the Z-ring.

At first, we treated MC1000 wild-type cells with different concentrations of A22 and Mecillinam to evaluate their effect on cell morphology and FtsZ localization and to choose a suitable concentration that could be used later on for ZapB and FtsZ co-localization analysis. Cells were treated with 2 μg/ml, 5 μg/ml and 10 μg/ml of A22 and Mecillinam: in all cases cells lost the rod-shaped morphology and became lemon-shaped. FtsZ was still able to form bands at the division sites even if, in some cases, the structures seemed defective (Fig. 4.9BC). We chose to use a concentration of 10 μg/ml of A22 and 2 μg/ml of Mecillinam, because it seemed they had a comparable effect on cells. The concentration used for both of them was well above the minimal inhibitory concentration (Park and Burman, 1973; Iwai *et al.*, 2004).

We analysed FtsZ-GFP and ZapB-mCherry localization in time-lapse experiments during an entire cell-cycle and we processed Z-stacks of FtsZ-GFP and ZapB-mCherry by deconvolution to reconstruct a 3D model of the two proteins.

Fig. 4.10 shows a time-lapse and 3D models of cells treated with A22. In all cells followed in a time-lapse experiment (n = 20) ZapB constricted ahead of FtsZ in the division process (Fig. 4.10A, 15'). However, when we reconstructed the 3D models of FtsZ and ZapB only in half of the cells analysed (14 out of 30) ZapB formed a ring enclosed by the Z-ring (Fig. 4.10B). In the other half of the cells the two rings seemed to co-localize (Fig. 4.10C). Similar results were obtained in cells treated with Mecillinam: in time-lapse experiments ZapB was ahead of FtsZ (Fig. 4.11A, 35') in all the cells analysed (n = 20) and when the 3D models were

reconstructed ZapB formed a ring smaller than the Z-ring (Fig. 4.11B) in only 20 cells out of the 31 analysed, in the remaining cells the two rings were not distinguishable as separated (Fig. 4.11C). It should be noted that for the 3D models only cells in which FtsZ seemed to form a complete hollow ring were considered.

These results excluded the loss of rod shape as the reason why ZapB and FtsZ always co-localized in Δ*mreB** cells. This also showed that in lemon-shaped cells ZapB is able to form rings enclosed by the Z-ring.

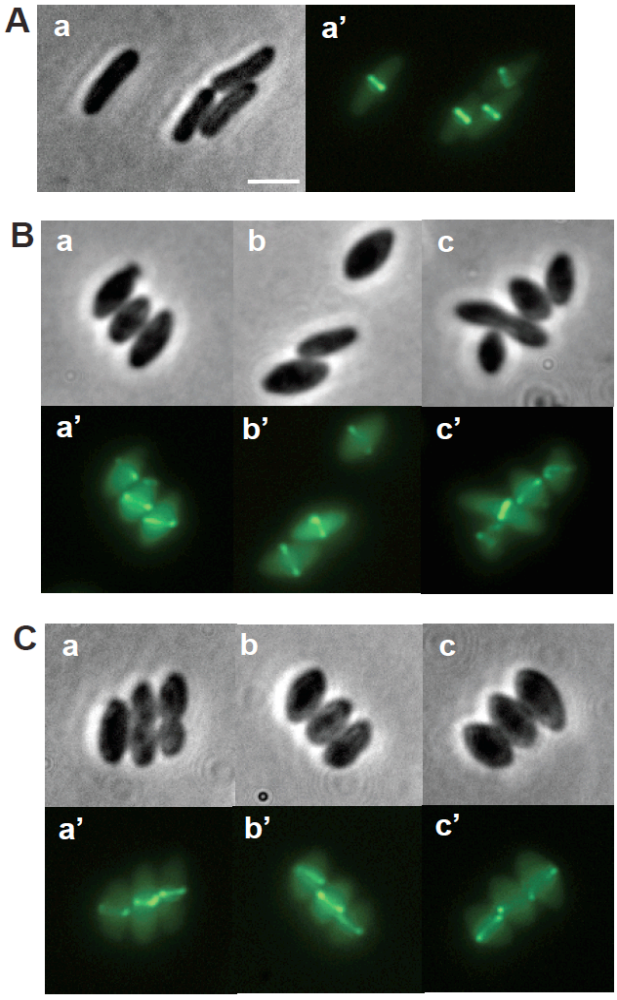

Fig 4.9 A22- and Mecillinam-treated cell morphologies

Phase-contrast and fluorescence microscopy images showing the localization of FtsZ-GFP in living cells of strain MC1000 / pEG12 (P_{lac}*::ftsZ::gfp*). Cells were grown at 37°C in M9 minimal medium supplemented with glucose and casamino acids. Expression of FtsZ-GFP from plasmid pEG12 was induced as described in *Materials and Methods*. **A.** Untreated cells. **B.** Cells treated with A22 for 60 minutes (a, 2 µg/ml; b, 5 µg/ml; c, 10 µg/ml). **C.** Cells treated with Mecillinam for 60 minutes (a, 2 µg/ml; b, 5 µg/ml; c, 10 µg/ml).
Scale bar = 2 µm.

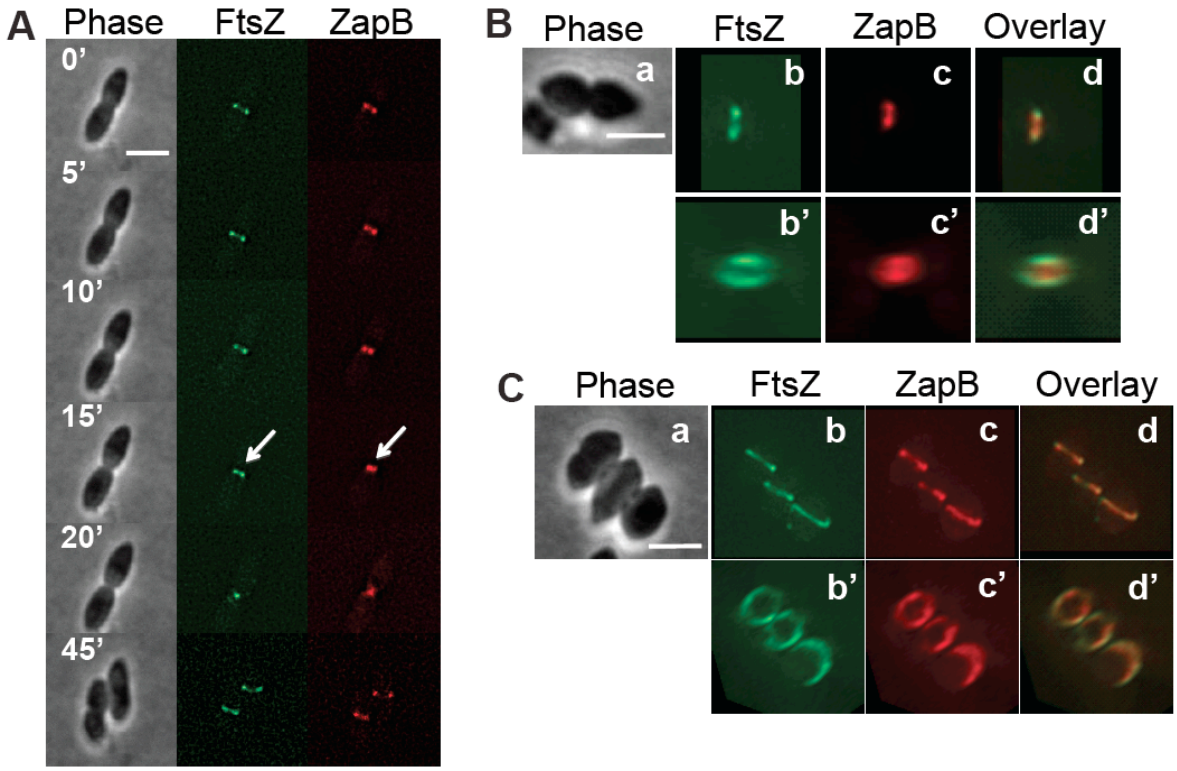

Fig 4.10 Z-ring and B-ring morphologies in A22-treated cells

Phase-contrast and fluorescence microscopy images showing the localization of FtsZ-GFP and ZapB-mCherry in living cells of strain MC1000/pEG12 (P_{lac}*::ftsZ::gfp*)/pEG9 (P_{BAD}*::zapB::mCherry*). Cells were grown at 37°C in M9 minimal medium supplemented with glucose and casamino acids. Expression of ZapB-mCherry from plasmid pEG9 and FtsZ-GFP from plasmid pEG12 as described in *Materials and Methods*. Cells were treated for 60 minutes with 10 µg/ml of A22 before microscopy. Fluorescence images were deconvolved before analysis. **A.** Time-lapse series. Fluorescence images were taken every 5 minutes. White arrows indicate when ZapB formed a single focus localized between two FtsZ dots. **B-C.** A cell is shown tilted at two different angles labelled with FtsZ-GFP (b) or ZapB-mCherry (c) or the overlay of the two (d) or the phase-contrast (a). Scale bars = 2 µm.

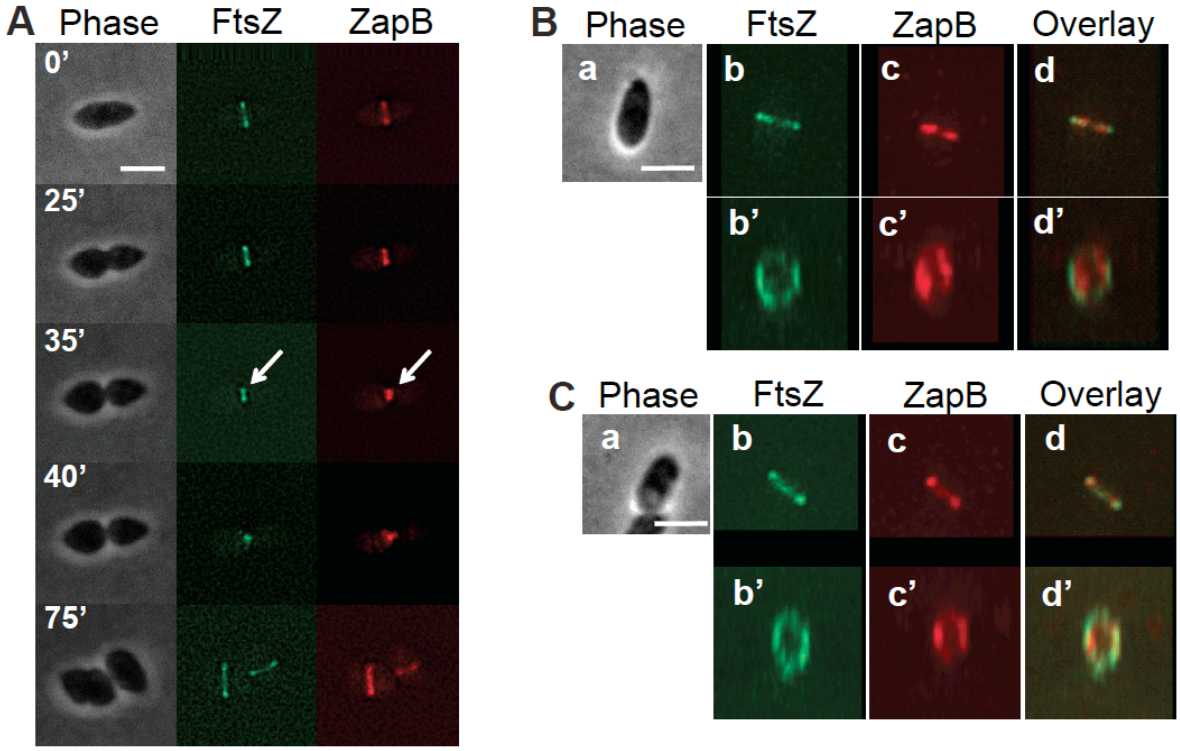

Fig 4.11 Z-ring and B-ring morphologies in Mecillinam-treated cells

Phase-contrast and fluorescence microscopy images showing the localization of FtsZ-GFP and ZapB-mCherry in living cells of strain MC1000/pEG12 (P_{lac}*::ftsZ::gfp*)/pEG9 (P_{BAD}*::zapB::mCherry*). Cells were grown at 37°C in M9 minimal medium supplemented with glucose and casamino acids. Expression of ZapB-mCherry from plasmid pEG9 and FtsZ-GFP from plasmid pEG12 as described in *Materials and Methods*. Cells were treated for 60 minutes with 2 µg/ml of Mecillinam before microscopy. Fluorescence images were deconvolved before analysis. **A.** Time-lapse series. Fluorescence images were taken every 5 minutes. White arrows indicate when ZapB formed a single focus localized between two FtsZ dots. **B-C.** A cell is shown tilted at two different angles labelled with FtsZ-GFP (b) or ZapB-mCherry (c) or the overlay of the two (d) or the phase-contrast (a). Scale bars = 2 µm.

4.4 Discussion

Improved fluorescence microscopic techniques have shown that ZapB was slightly ahead of FtsZ during constriction of the division septum (Fig. 4.1 and 4.2). The careful analysis of the pairs ZapA/FtsZ and ZapA/ZapB using the same microscopic technique showed that ZapB was also ahead of ZapA (Fig. 4.3A), whereas ZapA and FtsZ co-localized in all samples inspected (Fig. 4.3B). ZapB localized to the inner face of the Z-ring forming an open ring with a smaller diameter compared with that of FtsZ (Fig. 4.4) and ZapA (Fig. 4.6).

To our knowledge, this is the first time that a protein recruited to a subcellular structure in bacteria has been discriminated cytologically from the structure itself (i.e. the Z-ring).

Trying to improve the spatial resolution between FtsZ and ZapB rings, we repeated the microscopy analyses in spherical Δ*mreB** cells, but in this background the two proteins co-localized perfectly (Fig. 4.8). Using A22- and Mecillinam-treated cells we excluded that a defective rod shape was causing the loss of spatial resolution (Figs. 4.10 and 4.11). But it is still not clear why in Δ*mreB** cells ZapB did not form a structure encircled by the Z-ring.

Although the biological function behind ZapB constriction ahead of FtsZ and formation of a ZapB structure enclosed by the Z-ring is still unknown, understanding the reason may be important to clarify ZapB role in cell division.

Since the spatial resolution limits imposed by the diffraction of light are around ~250 nm, seeing ZapB forming a structure further inside than the Z-ring makes possible different models of how ZapB and FtsZ structures combine together at the division site. As summarised in Fig. 4.12, ZapA and FtsZ are in close contact in the Z-ring and it was first thought that ZapB formed a ring right underneath it, with ZapA acting as a bridge between FtsZ and ZapB (Fig. 4.12, possibility I). Considering that to be able to visualize the two protein rings spatially resolved they should be at least ~250 nm apart, we then advanced the idea that ZapB (and/or ZapA) may be able to form filament protrusions that connect the two rings and keep them constantly spaced (Fig. 4.12, possibility II). In the third scenario we envisaged (Fig. 4.12, possibility III), the interaction between ZapA and ZapB is only transient and once ZapB has been recruited at mid-cell and the Z-ring is formed, ZapB does form a

completely independent structure that does not maintain any contact with ZapA or FtsZ at this stage of the cell division process. Although there remains the unlikely possibility that an additional unknown factor (not ZapA that in our analyses always co-localizes with FtsZ) is keeping together and connected the two ring structures.

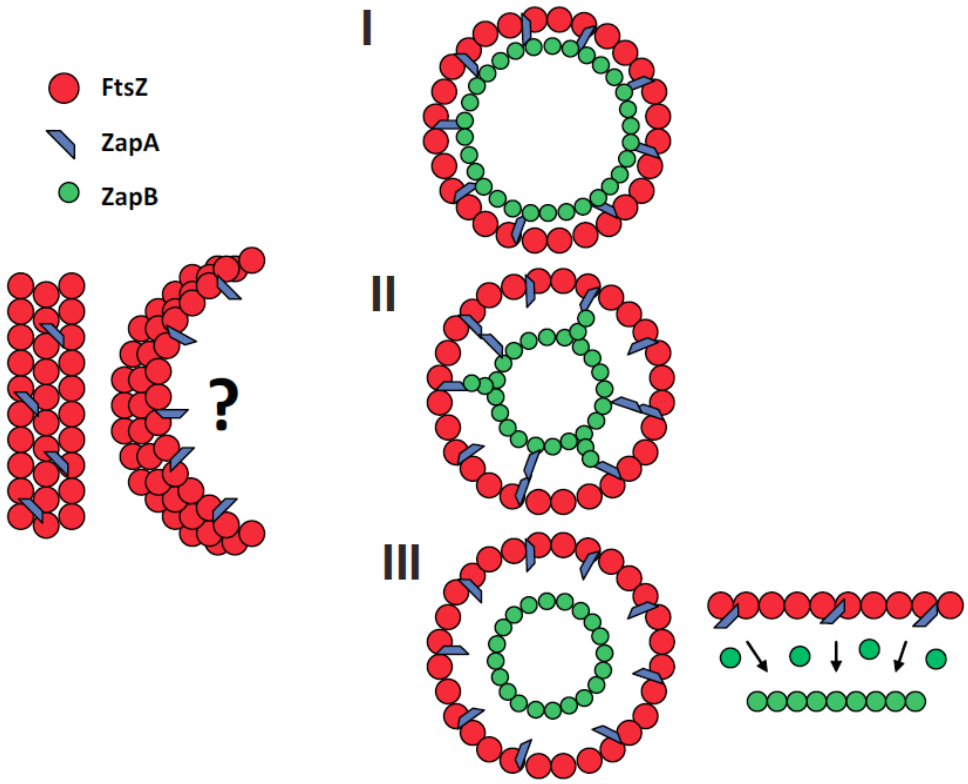

Fig. 4.12 Are ZapB and the Z-ring in contact at the division site?

At mid-cell ZapA and FtsZ are in close contact within the Z-ring. From the data collected we postulated at least three different possibilities for ZapB: **I.** ZapB forms a ring right below the Z-ring with ZapA acting as a bridge between FtsZ and ZapB; **II.** ZapB (or ZapA) may be able to form filament protrusions that connect the two rings and keep them constantly spaced; **III.** The interaction between ZapA and ZapB is only transient and once ZapB has been recruited at mid-cell and the Z-ring is formed, ZapB separates in a completely independent structure (Galli and Gerdes, 2010).

Chapter 5

ZapB stimulates FtsZ protofilament association via ZapA

5.1 Introduction

Over the last decades, various proteins have been identified in *E. coli* that are involved in the selection of the cell division site at mid-cell between the segregated nucleoids (MinCDE and SlmA), in the assembly, anchoring to the membrane and stabilization of the Z-ring (FtsZ, FtsA, ZipA, ZapA, ZapC) and in the synthesis and formation of the cell wall and envelope (PBPs and the so-called late division proteins) (Errington *et al.*, 2003; Adams and Errington, 2009).

To gain further knowledge into the mechanism of the division machinery components, the characterization of cell division mutant morphologies and growth defects have been exploited by *in vivo* studies. To understand how proteins interacting with FtsZ, the main and most important player of the cell division process, affect Z-ring formation, *in vitro* studies have focused on the analysis of FtsZ filament and bundle formation.

In the last few years, in both Gram-negative and Gram-positive bacteria, new cell division factors, often non-essential, have been discovered and reported to have a role in bundling and regulating the superstructures formed by FtsZ filaments: ZapA in 2002 (Gueiros-Filho and Losick, 2002), SepF in 2006 (Hamoen *et al.*, 2006; Ishikawa *et al.*, 2006), FzlA in 2010 (Goley *et al.*, 2010) and ZapC in 2011 (Durand-Heredia *et al.*, 2011; Hale *et al.*, 2011). Therefore, modulating the structures formed by FtsZ within the Z-ring seems to be a conserved and important feature for both Gram-positive and Gram-negative bacteria, even though, with the exception of FzlA in *C. crescentus*, all the proteins involved in regulating FtsZ bundle structure are auxiliary factors in the strains and with conditions used in laboratories.

5.2 Aim of this chapter

In the previous chapters it was shown that ZapB is recruited at the division site in the early stages of Z-ring assembly by ZapA and that through ZapA it interacts with FtsZ. Constructing multiple cell division mutants and characterizing their growth and morphological alterations, we plan to identify in which aspects of cell division ZapB is involved.

Since ZapA is the protein responsible for recruiting ZapB into the Z-ring and it is an auxiliary factor important for FtsZ protofilament bundling and cross-linking (Low *et al.*, 2004; Small *et al.*, 2007; Mohammadi *et al.*, 2009; Dajkovic *et al.*, 2010), we investigated the role ZapB may have on FtsZ bundle formation and stabilization, using *in vitro* biochemical assays such as sedimentation assay, light scattering and TEM analysis of the structures formed by the purified proteins.

5.3 Results

5.3.1 Morphological analysis of cell division mutants

In the attempt to associate ZapB to a specific function in cytokinesis, we combined deletions of *zapB*, *zapA*, *slmA* and *minCD* in all possible permutations and examined the resulting mutant strains for defects in cell growth, morphology and FtsZ localization. The combination Δ*slmA*Δ*minCD* is synthetic lethal (Bernhardt and de Boer, 2005) and was not included in our analyses. These data are summarized in Tables 5.1, 5.2 and Figs. 5.1, 5.2 and 5.3.

The mass-doubling times of all the deletion strains were analysed in both rich and minimal liquid media at 30°C and 37°C and appeared to be indistinguishable from that of the wild-type strain MC1000 (Fig. 5.1A). On solid NA medium cells of the triple Δ*zapA*Δ*zapB*Δ*minCD* mutant grew slower than the other strains forming colonies much smaller than the other deletion mutants (Fig. 5.1B) and displayed a plating defect of one order of magnitude (Fig. 5.1D).

Cell length and morphology and the degree of FtsZ mislocalization were investigated in exponentially growing cells (Tables 5.1, 5.2 and Fig. 5.2A). Deletion of *zapA* or *zapB* resulted in a ~40% increase in cell length in both cases and a significant increase in the fraction of cells with mislocalized Z-rings (25% and 21% respectively). Deletion of *slmA* had a milder effect (30% increase in cell length and 12% cells with mislocalized Z-rings). Deletion of *minCD* resulted in a considerably larger increase in cell length (120%) and more than 50% mislocalized Z-rings. Introduction of the *slmA* deletion into the single Δ*zapA* and Δ*zapB* strains only marginally affected cell length and Z-ring localization. However, unexpectedly, the Δ*zapA*Δ*zapB* double deletion mutant exhibited a 70% increase in cell length and 35% of such cells had mislocalized Z-rings. Cells of the triple Δ*zapA*Δ*zapB*Δ*minCD* mutant produced very long cells (330% increase) and FtsZ was highly mislocalized. In contrast, deleting *slmA* from the Δ*zapA*Δ*zapB* strain did not seriously affect cell growth or division. Again, it is noteworthy that the Δ*zapA*Δ*zapB*Δ*minCD* strain produced cells longer than the Δ*zapA*Δ*minCD* strain (330% vs. 230% increase in cell length).

These results raised the possibility that ZapA and ZapB may have separate

functions in cell division, even though ZapB is recruited to the division site by ZapA (see Chapter 3).

To assess if the phenotypes described above were background-dependent, the Δ*zapA* and Δ*zapB* alleles were transduced into MG1655, a fully sequenced standard *E. coli* K-12 strain. Cell length measurements and growth rate on plate confirmed that the relative increases in cell lengths were very similar in MG1655 and MC1000, showing that the phenotypes were not strain-specific (Table 5.1 and Fig. 5.1C) and supporting the idea that ZapB may have an effect on cell division that is independent of ZapA.

Studying ZapC, Durand-Heredia *et al.* (2011) examined the cell length of Δ*zapA*Δ*zapC* and Δ*zapB*Δ*zapC* double mutants and found it unchanged from those of the single mutants. They also confirmed that a Δ*zapA*Δ*zapB* double mutant forms longer cells than the *zapA* and *zapB* single mutants, independently supporting our results.

Recently, it has been reported that a *zapA* deletion mutant has reduced viability (Dajkovic *et al.*, 2010): in exponentially growing cultures 90% of dead cells are filamentous and these filamentous cells are absent from cultures in stationary phase (Dajkovic *et al.*, 2010). We analysed the viability of a *zapB* mutant and in particular, using a dead/live staining, we inspected if in exponentially growing cultures filamentous cells had an increased death rate compared to cells of normal size. We could not observe any difference between the two cell populations and even the longest filaments were alive (Fig. 5.2B).

We also inspected FtsZ localization in all the mutant strains and classified FtsZ aberrant structures as multiple rings, helices or rings located at the poles (Table 5.2). The combination of *minCD* and *zapA* null mutants produced very long cells in which FtsZ formed multiple aberrant structures and for this reason it was not possible to assign each cell to a single specific category. Fig. 5.3A shows some examples of the high degree of mislocalization that FtsZ had in mutant strains such as Δ*zapA*Δ*minCD* and Δ*zapA*Δ*zapB*Δ*minCD*.

It is interesting that in a Δ*zapB* mutant FtsZ formed a band at the cell pole in 2% of the cells, a double ring at mid-cell in 7% of the cells and a helical structure or multiple bands in 12% of the cells analysed (Fig. 5.3B). It is worth to note that a *zapA* mutant did not present any polar Z-rings or structures as opposed to cells lacking

ZapB, again supporting the hypothesis that ZapB may have an activity not associated to its recruitment into the Z-ring via ZapA.

Immunoblotting of the appropriate strains using α-FtsZ antibodies was used to confirm that FtsZ-GFP was present in equal amounts in all the strains and that FtsZ-GFP mislocalization was not due to differences in the levels of expression (Fig. 5.3C).

5.3.2 Complementation analyses

To further confirm that ZapB has a role in cell division that is independent of ZapA, we repeated cell length analyses of *zapA*, *zapB* and *zapA zapB* deletion strains in the presence of low-copy plasmids that produced ZapA, ZapB or ZapA plus ZapB. Table 5.3 summarizes the results of the complementation analyses. Copies of *zapA* or *zapB* on plasmids fully restored the wild-type cell length phenotype. Strikingly, however, ZapB and the mutant Δ10ZapB were able to significantly mitigate the cell length defect of the *zapA zapB* double mutant – that is – ZapB remains seemingly functional even in the absence of ZapA.

The same low-copy plasmid was used to investigate the ability of the tagged proteins used in this study (ZapB-GFP, ZapB-mCherry, ZapB-His_6, His_6-ZapA and YFP-ZapA) to complement the cell length defects of the corresponding deletion mutants (Table 5.3). The ZapB-GFP and the ZapB-His_6 fusions were able to complement the cell length defect of a *zapB* deletion mutant and cells carrying ZapB-mCherry were only slightly longer (~10% longer) than the wt. The His_6-ZapA fusion complemented only partially the cell length defect of a *zapA* mutant and for this reason we developed a protocol for the purification of native ZapA to be used in our *in vitro* assays. Instead, Δ*zapA* cells carrying YFP-ZapA were only slightly longer (~10% longer) than the wt strain.

The R1 low-copy plasmids used in the complementation analyses were also employed to verify that the mutant deletion strains we constructed were viable and not the results of suppressors arisen during the deletion process. The R1 low-copy plasmids are highly unstable and easily lost in the absence of a selective antibiotic (Nordstrom, 2006). The pOU82-derived plasmids we used in this study are lac^+ and this makes possible to investigate if cells of a lac^- strain (such as TB28) retain or lose the plasmid when streaked out on X-Gal plates in the absence of the selective

antibiotic. Indeed, only cells keeping the plasmid would appear blue whereas cells that have lost the plasmid would appear white: the unstable plasmids would be retained only if they carry a gene essential to cell viability.

We created deletion mutants in TB28 cells carrying the complementing plasmids and then streaked the new deletion strains on X-Gal plates in the absence of antibiotic selection. In both TB28Δ*zapA*Δ*minCD* and TB28Δ*zapA*Δ*zapB*Δ*minCD* the plasmid carrying ZapA or ZapA plus ZapB was lost and white colonies appeared (Fig. 5.4), meaning that the double and triple mutant are viable and not the result of the presence of a suppressor.

Using qPCR we also inspected if the absence of *zapA* had an effect on the transcriptional levels of *zapB* and vice versa if *zapB* deletion had an effect on *zapA*: the mRNA levels of the two proteins were unchanged between the wt and the mutant strains (data not shown).

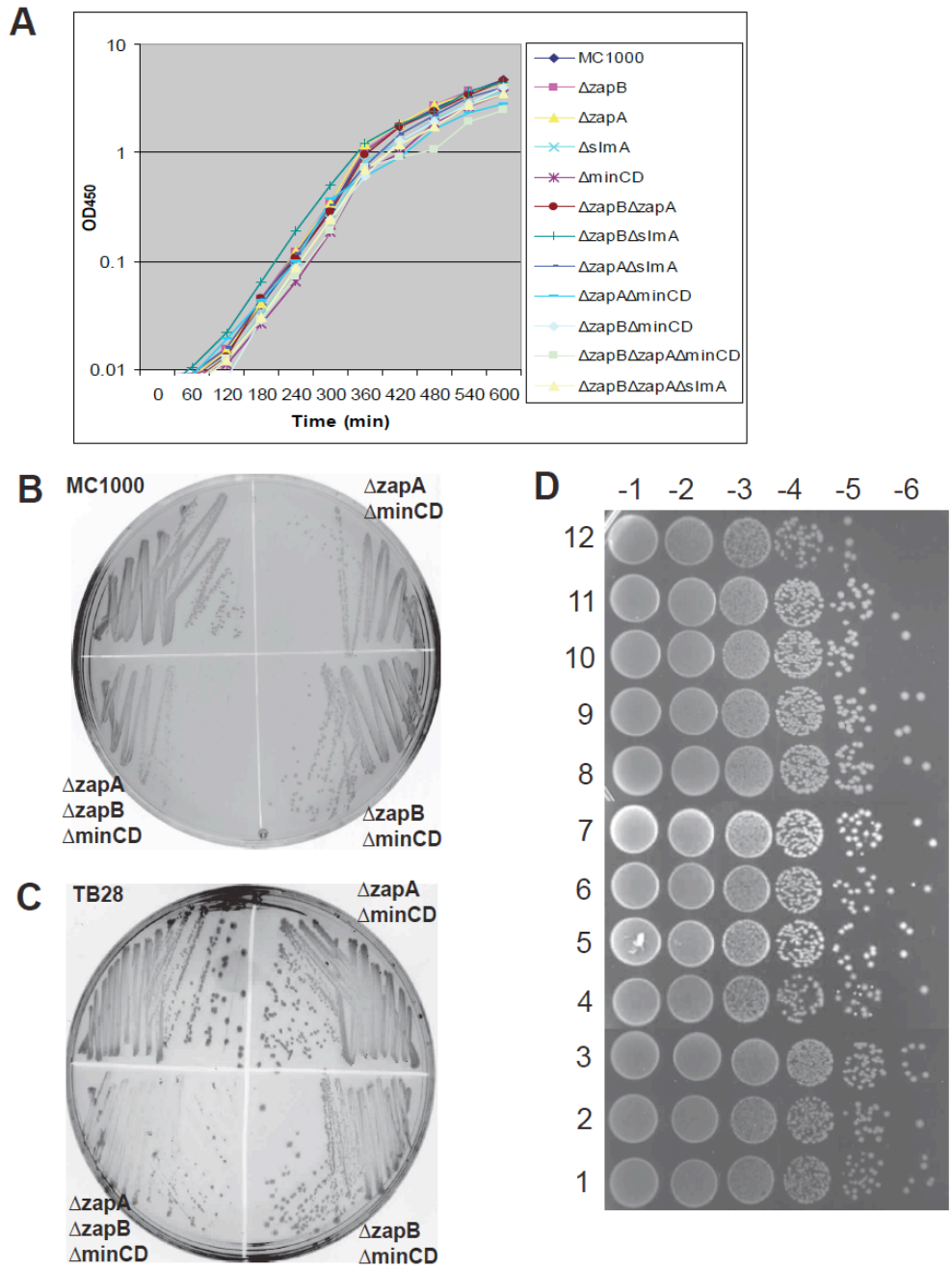

Fig. 5.1 Growth analysis of cell division mutants

A. Growth curves of the deletion strains in LB medium at 30°C (Galli and Gerdes, 2010). Similar growth curves were obtained in LB and M9 minimal medium at 37°C (data not shown). **B.** Growth of MC1000 and MC1000 derived mutants Δ*zapA*Δ*minCD*, Δ*zapB*Δ*minCD* and Δ*zapA*Δ*zapB*Δ*minCD* was assayed on NA plates after over-night incubation at 30°C. The triple mutant Δ*zapA*Δ*zapB*Δ*minCD* grew slower than all the other deletion mutants. **C.** Growth of TB28 and TB28 derived mutants Δ*zapA*Δ*minCD*, Δ*zapB*Δ*minCD* and Δ*zapA*Δ*zapB*Δ*minCD* was assayed on NA plates after over-night incubation at 30°C. The triple mutant Δ*zapA*Δ*zapB*Δ*minCD* grew slower than all the other deletion mutants. **D.** Over-night cultures of MC1000 (1), Δ*zapA* (2), Δ*zapB* (3), Δ*slmA* (4), Δ*minCD* (5), Δ*zapA*Δ*slmA* (6), Δ*zapB*Δ*slmA* (7), Δ*zapA*Δ*zapB* (8), Δ*zapA*Δ*minCD* (9), Δ*zapB*Δ*minCD* (10), Δ*zapA*Δ*zapB*Δ*slmA* (11), Δ*zapA*Δ*zapB*Δ*minCD* (12) were grown to equal density and serially diluted (10^{-1}–10^{-6}) in LB. Aliquots (10 µl) were spotted on NA plates. The Δ*zapA*Δ*zapB*Δ*minCD* (12) strain displayed a plating defect of one order of magnitude.

Table 5.1: Morphological analysis of cell division mutants

Strain	Cell length (µm)[1]	mutant/wt ratio	FtsZ-GFP mislocalized[2]
MC1000	2.80 ± 0.04	1	2%
Δ*zapA*	3.89 ± 0.07	1.4	25%
Δ*zapB*	3.93 ± 0.07	1.4	21%
Δ*slmA*	3.61 ± 0.05	1.3	12%
Δ*minCD*	6.13 ± 0.18	2.2	53%
Δ*zapA*Δ*slmA*	4.06 ± 0.06	1.5	25%
Δ*zapB*Δ*slmA*	4.27 ± 0.07	1.5	27%
Δ*zapA*Δ*zapB*	4.70 ± 0.11	1.7	35%
Δ*zapB*Δ*minCD*	6.89 ± 0.24	2.5	61%
Δ*zapA*Δ*minCD*	9.34 ± 0.36	3.3	94%
Δ*zapA*Δ*zapB*Δ*minCD*	11.92 ± 0.64	4.3	95%
Δ*zapA*Δ*zapB*Δ*slmA*	4.52 ± 0.09	1.6	35%
MG1655 (=TB28)	3.15 ± 0.05	1	ND
Δ*zapA*	4.52 ± 0.05	1.4	ND
Δ*zapB*	4.32 ± 0.10	1.4	ND
Δ*zapA*Δ*zapB*	5.69 ± 0.07	1.8	ND

All the strains were grown in LB at 37°C; at an OD_{450} value of about 0.4 samples were collected and cell lengths measured (Galli and Gerdes, 2010). FtsZ-GFP was expressed from plasmid pEG12 as described in *Materials and Methods* and samples analysed 1 hour after induction. For all entries except the last 4, 250 cells were measured for every strain. For the last 4 entries, 100 cells were measured for every strain. FtsZ-GFP localization was analysed in about 1000 cells for each strain.
ND = no data.
1) Standard error is indicated.
2) Immunoblotting on the appropriate strains using FtsZ antibodies was used to assess that FtsZ-GFP was present in equal amounts in all the strains and that FtsZ-GFP mislocalization was not due to a different level of expression (Fig. 5.3C).

Table 5.2: Classification of FtsZ-GFP mislocalization in the deletion strains

Strain	Cell Pole	Double rings	Helices
MC1000	0%	1%	1%
Δ*zapA*	0%	8%	17%
Δ*zapB*	2%	7%	12%
Δ*slmA*	0%	5%	7%
Δ*minCD*	6%	25%	22%
Δ*zapA*Δ*slmA*	0%	11%	14%
Δ*zapB*Δ*slmA*	0%	13%	14%
Δ*zapA*Δ*zapB*	0%	12%	23%
Δ*zapB*Δ*minCD*	16%	15%	30%
Δ*zapA*Δ*minCD*	NA	NA	NA
Δ*zapA*Δ*zapB*Δ*minCD*	NA	NA	NA
Δ*zapA*Δ*zapB*Δ*slmA*	0%	13%	22%

All the strains were grown in LB at 37°C; at an OD_{450} value of about 0.4 samples were collected and cell lengths measured (Galli and Gerdes, 2010). FtsZ-GFP was expressed from plasmid pEG12 as described in *Materials and Methods* and samples analysed 1 hour after induction. For all entries at least 1000 cells were analysed for every strain.
NA = not available.

Table 5.3: Complementation analysis of cell division mutants

Strain	Cell length (µm)[1]	mutant/wt ratio
MC1000 / pOU82 (vector)	3.70 ± 0.06	1
Δ*zapA* / pOU82 (vector)	4.80 ± 0.30	1.3
Δ*zapA* / pEG83 (P_{zapA}*::zapA*)	3.80 ± 0.07	1
Δ*zapA* / pNG53 (P_{lac}*::yfp::zapA*)	4.03 ± 0.12	1.1
Δ*zapA* / pEG89 (P_{zapA}*::his$_6$::zapA*)	4.44 ± 0.12	1.2
Δ*zapB* / pOU82 (vector)	4.80 ± 0.13	1.3
Δ*zapB* / pEG82b (P_{zapB}*::zapB*)	3.80 ± 0.08	1
Δ*zapB* / pEG84 (P_{zapB}*::Δ10zapB*)	4.20 ± 0.11	1.1
Δ*zapB* / pEG86 (P_{zapB}*::zapB::gfp)*	3.85 ± 0.08	1
Δ*zapB* / pEG90 (P_{zapB}*::zapB::mCherry*)	3.96 ± 0.15	1.1
Δ*zapB* / pEG88 (P_{zapB}*::zapB::his$_6$*)	3.88 ± 0.07	1
Δ*zapA*Δ*zapB* / pOU82 (vector)	5.90 ± 0.03	1.6
Δ*zapA*Δ*zapB* / pEG83 (P_{zapA}*::zapA)*	5.30 ± 0.20	1.4
Δ*zapA*Δ*zapB* / pEG82b (P_{zapB}*::zapB*)	5.10 ± 0.20	1.4
Δ*zapA*Δ*zapB* / pEG84 (P_{zapB}*::Δ10zapB*)	5.00 ± 0.21	1.4
Δ*zapA*Δ*zapB* / pEG82 (P_{zapB}*::zapB zapA*)	4.00 ± 0.06	1.1

All the strains were grown in LB at 37°C; at an OD_{450} value of about 0.4 samples were collected and cell lengths measured (Galli and Gerdes, 2010). For all entries, 100 cells were measured for every strain (2 replicates each). 1) Standard error is indicated.

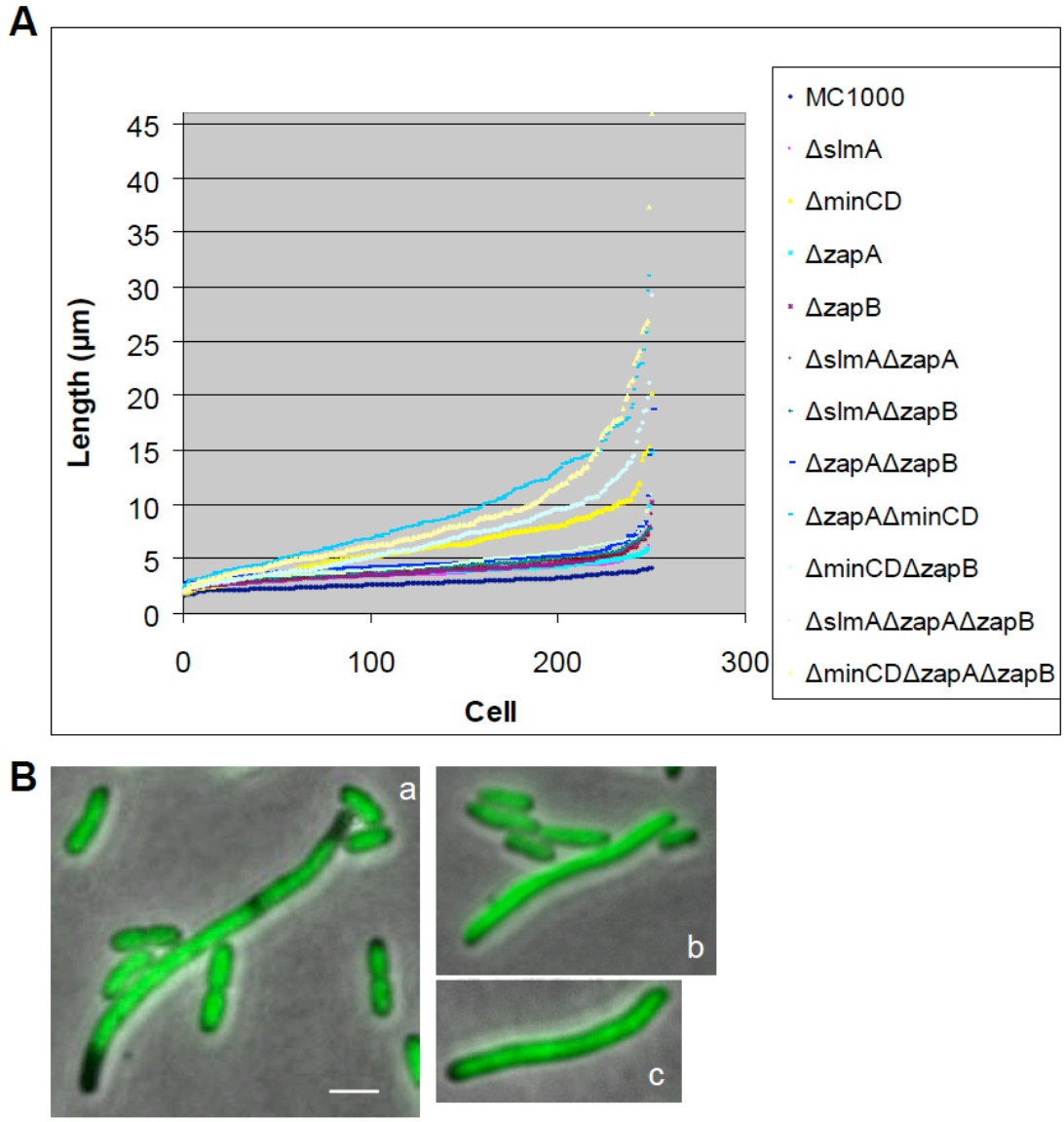

Fig. 5.2 Cell length analysis of the deletion mutants

A. Diagram showing the cell length distribution of MC1000 deletion strains grown in LB at 37°C. A total of 250 cells of each strain were measured. ◆MC1000, ◆Δ*slmA*, ◆ Δ*minCD*, ×Δ*zapA*, ◆Δ*zapB*, ◆Δ*slmA*Δ*zapA*, ◆Δ*slmA*Δ*zapB*, ◆Δ*zapA*Δ*zapB*, ◆Δ*zapA*Δ*minCD*, ◆Δ*minCD*Δ*zapB*, ◆Δ*slmA*Δ*zapA*Δ*zapB*, ◆Δ*minCD*Δ*zapA*Δ*zapB*. **B.** Combined phase-contrast and fluorescence (GFP) microscopy images showing that filamentous cells in MC1000Δ*zapB* strain are alive since they are stained in green using the LIVE/DEAD BacLight Bacterial Viability Assay (Invitrogen) (Galli and Gerdes, 2010). Scale bar = 2 µm.

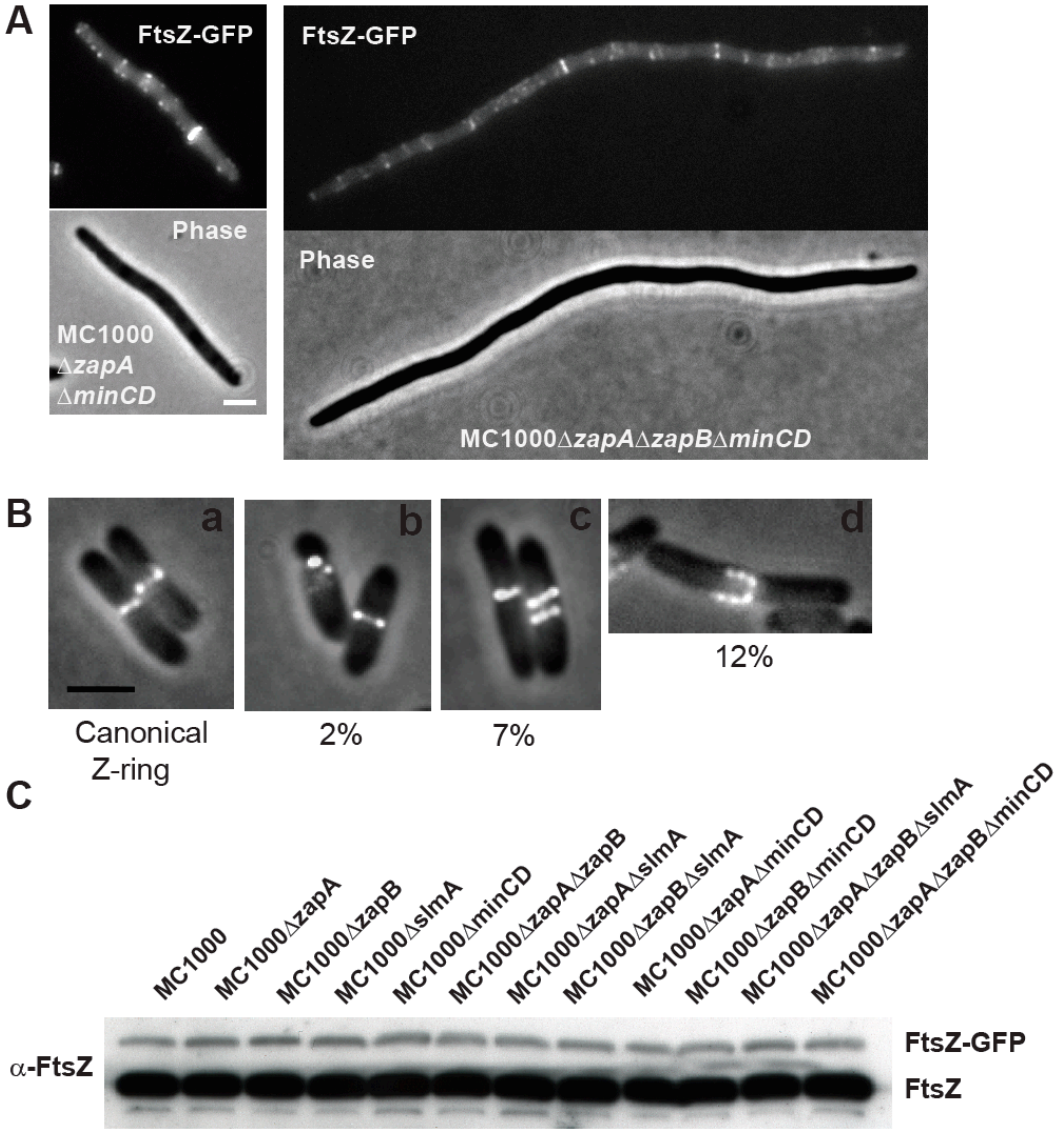

Fig. 5.3 FtsZ mislocalization analysis

Cells were grown at 30°C in M9 minimal medium supplemented with glucose and casamino acids (Galli and Gerdes, 2010). Expression of FtsZ-GFP from plasmid pEG12 was induced as described in *Materials and Methods*. **A.** Fluorescence microscopy images showing FtsZ-GFP localization in MC1000Δ*zapA*Δ*minCD* and MC1000Δ*zapA*Δ*zapB*Δ*minCD*. **B.** Combined phase-contrast and fluorescence microscopy images showing the localization of FtsZ-GFP in MC1000Δ*zapB* strain. FtsZ-GFP forms a canonical Z-ring (a); a band at the cell pole (b); double bands around mid-cell (c); helices or multiple bands (d). **C.** Immunoblotting analysis of FtsZ and FtsZ-GFP expression. Immediately before microscopy examination, samples were collected and a Western-blot performed using α-FtsZ antibodies. Scale bars = 2 μm.

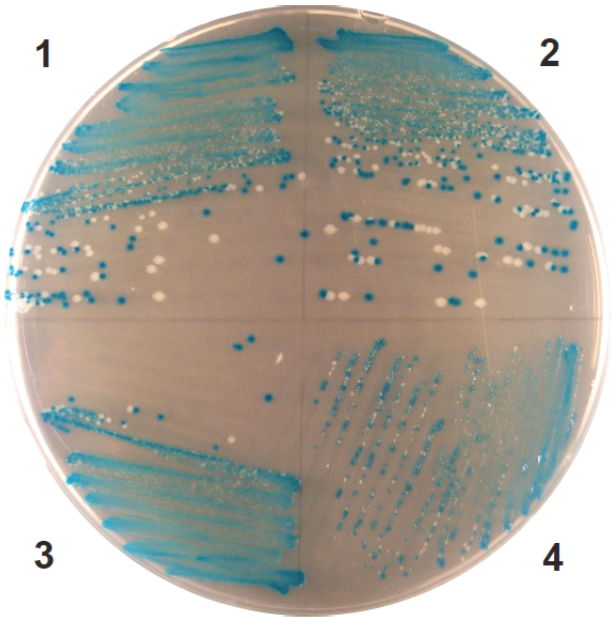

Fig. 5.4 Δ*zapA*Δ*minCD* and Δ*zapA*Δ*zapB*Δ*minCD* strains are viable

The deletion mutants were assayed on NA plates supplemented with 0.004% X-Gal after over-night incubation at 30°C. White colonies have lost the pOU82 derived plasmid. **1.** TB28Δ*zapA* / pEG83 (P_{zapA}::*zapA*); **2.** TB28Δ*zapA*Δ*zapB* / pEG82 (P_{zapB}::*zapB zapA*); **3.** TB28Δ*zapA*Δ*minCD* / pEG83 (P_{zapA}::*zapA*); **4.** TB28Δ*zapA*Δ*zapB*Δ*minCD* / pEG82 (P_{zapB}::*zapB zapA*).

5.3.3 Synthetic detrimental phenotype of Δ*zapB* and *ftsZ84*

ZapA is recruited early to the Z-ring (Goehring *et al.*, 2005) and Dajkovic *et al*. (2010) showed that it acts synergistically with early cell division proteins (FtsZ, FtsA, ZipA). We described that ZapB is recruited early to the Z-ring by ZapA (see Chapter 3) and to inspect if it has a biological function in the early and/or late stages of the division process, we combined a *zapB* deletion with strains carrying temperature sensitive (*ts*) mutations in FtsZ, FtsA, ZipA and FtsI, the latter encoding a late recruit.

The combination of Δ*zapB* and *ftsZ84* was previously characterized and described to produce a synthetic detrimental phenotype: over-night colonies of the double mutant strain were tiny and grew slower than both wt and single mutant cells. In liquid medium the strain generated cells with highly abnormal morphologies such as DNA-free mini cells, blebs and branches (Ebersbach *et al.*, 2008). When isolated on plates the KG22Z84Δ*zapB* strain produced very small colonies but also few big ones that when isolated retained the *ts* phenotype of *ftsZ84* and in which the *zapB* gene was confirmed to be deleted. The big colonies supposedly originated from cells carrying mutations that suppressed the detrimental phenotype. To further characterize the phenomenon, we re-constructed a KG22Z84Δ*zapB* strain. The latter formed tiny colonies on solid medium and again a few bigger colonies appeared, probably containing unknown suppressors of the very sick double mutant.

We were able to isolate at least 2 different suppressors (called *sup77* and *sup78*). The single mutant strains, the double mutant strain and the two suppressors were analysed and compared for defects in cell growth and morphology in liquid (LB) or on solid medium (NA). On solid medium KG22Z84Δ*zapB* formed tiny colonies, visible only after at least 20 hours of growth at 30°C, *sup77* formed small colonies but clearly bigger than the double mutant and *sup78* formed colonies with a mucoid phenotype, very similar to the appearance of cells with increased levels of capsule synthesis typical of a *lon* mutant (Van Melderen and Aertsen, 2009) (Fig. 5.5A). The growth rates of the strains in liquid medium showed that the single mutants *Z84* and *zapB* did not highlight any particular difference compared to the parental strain KG22 while the double mutant KG22Z84Δ*zapB* grew very slowly. The two suppressors still showed a growth defect but slightly less severe than that of the double mutant (Fig. 5.5B). Spots of serial dilutions of the four *ftsZ84 ts* strains were incubated at

increasing temperatures and already at 30°C the double mutant displayed a plating defect of several orders of magnitude while the two suppressors were able to mitigate the defect (Fig. 5.5C). Cell samples taken from plates or from exponentially growing cultures were compared for morphological defects and phenotypes: as described above the double mutant showed highly abnormal morphology defects that were alleviated in cells carrying the suppressors (Fig, 5.5E). Grown over-night on plates, the Z84Δ*zapB* mutant formed very long filaments whereas the two suppressors formed cells of normal size and only few filaments (Fig. 5.5D).

To assess if the phenotypes described above were background-dependent, the combination Δ*zapB ftsZ84* was recreated in MC1000, the strain we routinely used for our studies. In this background the Z84Δ*zapB* mutant did not show growth defects as severe as in KG22. On plate colonies were slightly smaller than wt or single mutants and the phenotype was not as detrimental as previously described in KG22 (Fig. 5.5A). In MC1000, we also constructed the double mutant Z84Δ*zapA* and this strain showed more aggravated growth defects, forming quite small colonies after over-night incubation. The repeated attempts to construct the double mutant Z84Δ*zapA* in KG22 were unsuccessful, suggesting that this combination is not viable or very detrimental. Taken together, these results showed that ZapB acts through ZapA in the first stages of Z-ring assembly. We do not know why strain KG22 is more seriously affected than MC1000 by the absence of ZapA or ZapB when carrying a Z84 mutation.

We also inspected the morphology and growth defects of strains carrying a *zapB* mutant combined with *ts* mutants of *ftsA*, *zipA* and *ftsI*. The mass-doubling times of all the single *ts* strains appeared to be indistinguishable from that of the corresponding *ts* strains carrying the *zapB* deletion (Fig. 5.6A). Spots of serial dilutions of the three pairs of *ts* strains were incubated at increasing temperatures (30°C, 37°C and 42°C) and the presence of a *zapB* deletion did not show an increased temperature sensitivity (Fig. 5.6B). Morphology of cells from exponentially growing cultures was also inspected: cells carrying the *zapB* deletion were more elongated and had a higher degree of morphological defects (blebs and branches) compared to the parental *ts* strains (Fig. 5.6C), but not to such a high level as seen for the mutant KG22Z84Δ*zapB*.

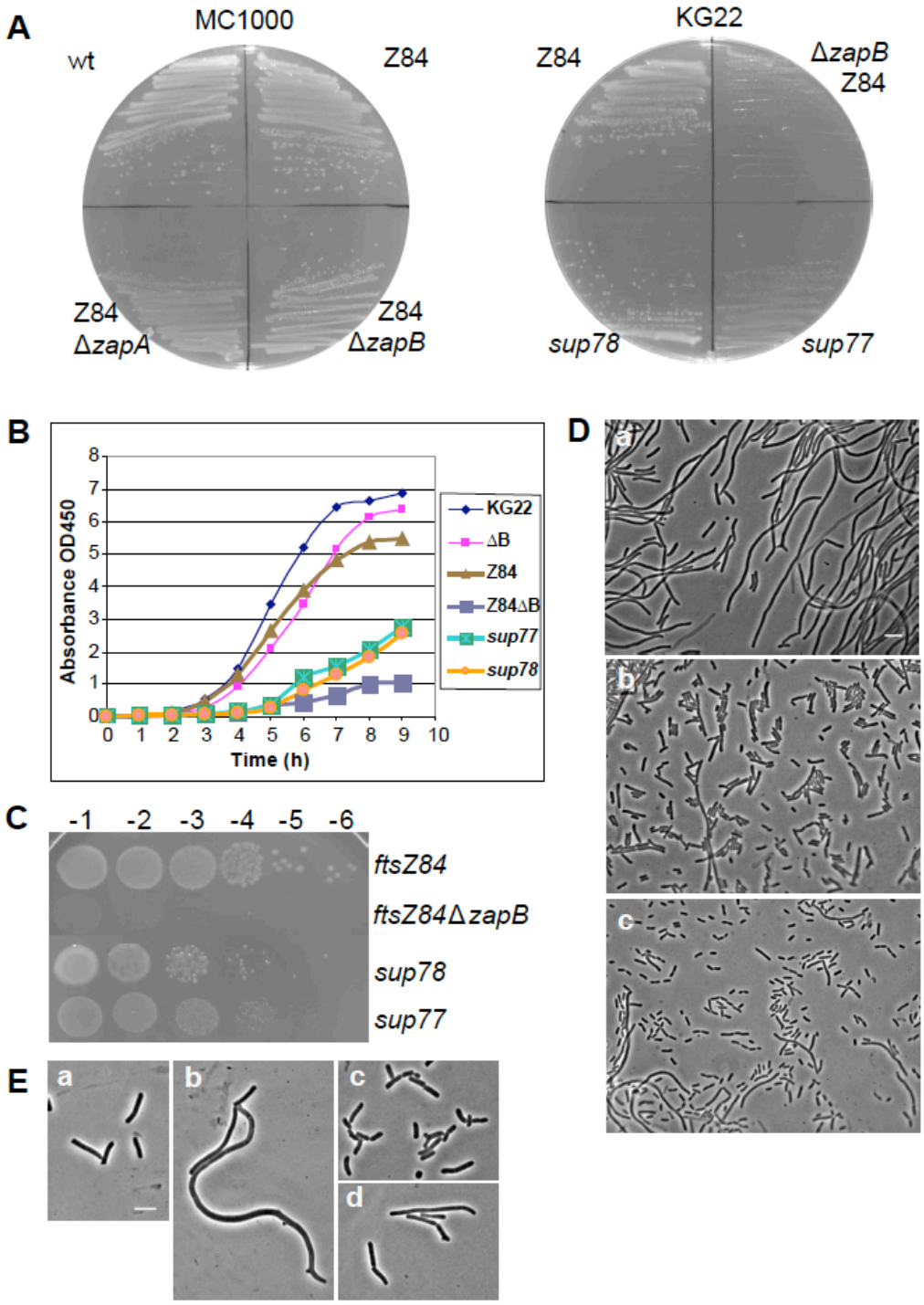

Fig. 5.5 The Z84Δ*zapB* double mutant accumulates suppressors

A. Growth of MC1000 and KG22 derived Z84Δ*zapB* mutants assayed on NA plates after over-night incubation at 30°C. **B.** Growth curves of KG22 derived mutants in LB medium at 30°C (◆KG22; ■KG22Δ*zapB*; ▲KG22Z84; ■KG22Z84Δ*zapB*; ☒*sup77*; ● *sup78*). **C.** Over-night cultures of KG22 mutant strains were grown at 30°C to equal density in LB and serially diluted (10^{-1}–10^{-6}) in LB. Aliquots (10 µl) were spotted on NA plates incubated at 30°C over-night. **D.** Phase-contrast images showing KG22Z84Δ*zapB* (a), *sup77* (b) and *sup78* (c) cell morphology after over-night incubation at 30°C on a NA plate. **E.** Phase-contrast images showing KG22Z84 (a), KG22Z84Δ*zapB* (b), *sup77* (c) and *sup78* (d) cells grown at 30°C in LB liquid medium. Scale bars = 5 µm.

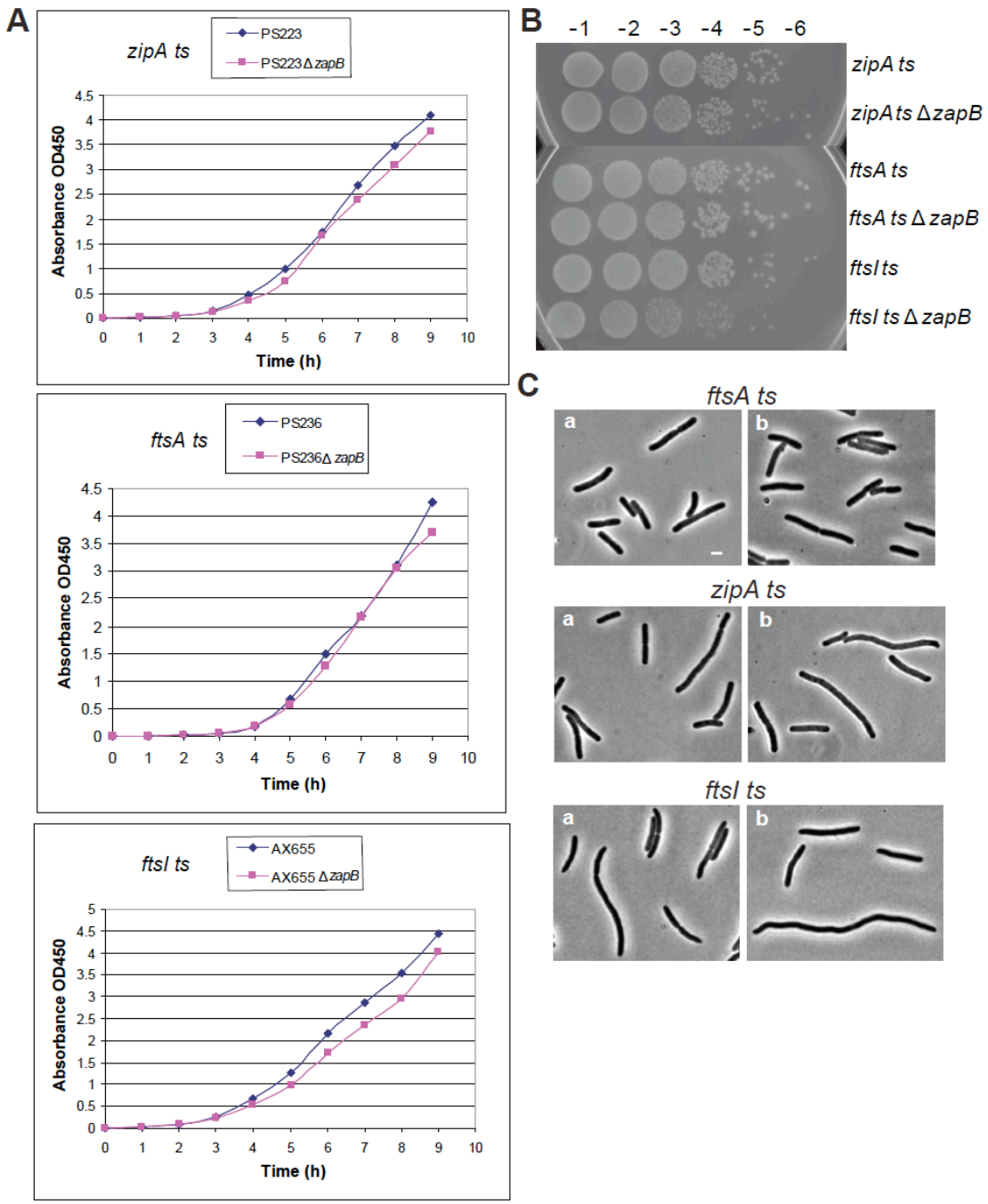

Fig. 5.6 Characterization of Δ*zapB* combined with *ftsA*, *zipA*, *ftsI ts* mutants

A. Growth curves of *ts* mutants grown in LB medium at 30°C. **B.** Over-night cultures of *ts* mutant strains were grown to equal density in LB at 30°C and serially diluted (10^{-1}–10^{-6}) in LB. Aliquots (10 µl) were spotted on NA plates incubated at 30°C over-night (at 37°C and 42°C no differences were visible between each pair of strains (data not shown)). **C.** Phase-contrast images showing cells of *ftsA ts*, *zipA ts*, *ftsI ts* (a) and Δ*zapB ftsA ts*, Δ*zapB zipA ts*, Δ*zapB ftsI ts* (b) from cultures growing exponentially at 30°C in LB liquid medium.
Scale bar = 1 µm.

5.3.4 ZapB does not affect FtsZ GTPase activity

Proteins promoting FtsZ protofilament lateral association or bundling increase FtsZ filament stability and, therefore, they likely cause a reduction in the GTPase activity of FtsZ (Mukherjee and Lutkenhaus, 1999; Small *et al.*, 2007; Hale *et al.*, 2011).

Small *et al*. (2007) described that ZapA strongly inhibits FtsZ GTPase activity whereas Mohammadi *et al*. (2009) reported a milder effect and the latter group suggested that the modest decrease they observed was a consequence of the lateral association of FtsZ protofilaments, known to decrease the GTPase activity of FtsZ (Mukherjee and Lutkenhaus, 1999), and not an effect directly induced by ZapA.

Here, we analysed the results that the addition of ZapB had on the GTPase activity of FtsZ when present in equimolar concentration with ZapA and FtsZ, both at pH 6.5 and 7.5. We first measured the amount of P_i released after 30 minutes in reactions containing FtsZ, FtsZ plus ZapA, FtsZ plus ZapB and FtsZ plus ZapA and ZapB. Interestingly, at pH 6.5, in samples containing ZapA, there was a ~50% reduction in the GTPase activity whereas at pH 7.5 the P_i released in all the four cases was unaltered (Fig. 5.7A). The difference with the results published by Mohammadi *et al*. (2009) might be explained by the fact that we used a buffer containing 10 mM $MgCl_2$ instead of 5 mM $MgCl_2$, this may affect FtsZ bundling and therefore FtsZ GTPase activity in the presence of ZapA. ZapB alone had no effect on FtsZ GTPase activity. Next, we followed the P_i released over a 30 minutes time course, taking samples at minute 0 (immediately after the addition of GTP) and after 5, 10, 20 and 30 minutes from the beginning of the reaction. Both at pH 6.5 (Fig. 5.7B) and at pH 7.5 (Fig. 5.7C), in the absence of ZapA, FtsZ GTPase activity was able to reach only after ~10 minutes a plateau in the level of P_i released, instead when ZapA was added to the reaction the rate at which P_i was released was strongly reduced. Indeed, at pH 6.5 after 30 minutes the GTPase activity had a ~50% reduction and at pH 7.5 the P_i release rate was slower than when only FtsZ was present and it reached the plateau only after 30 minutes. Interestingly, if at pH 6.5 there was no difference in the FtsZ GTPase activity of samples containing only ZapA or both ZapA and ZapB, at pH 7.5 the presence of ZapB partially relieved the inhibitory effect of ZapA.

Reactions containing only ZapA or ZapB did not show any measurable GTPase activity (data not shown).

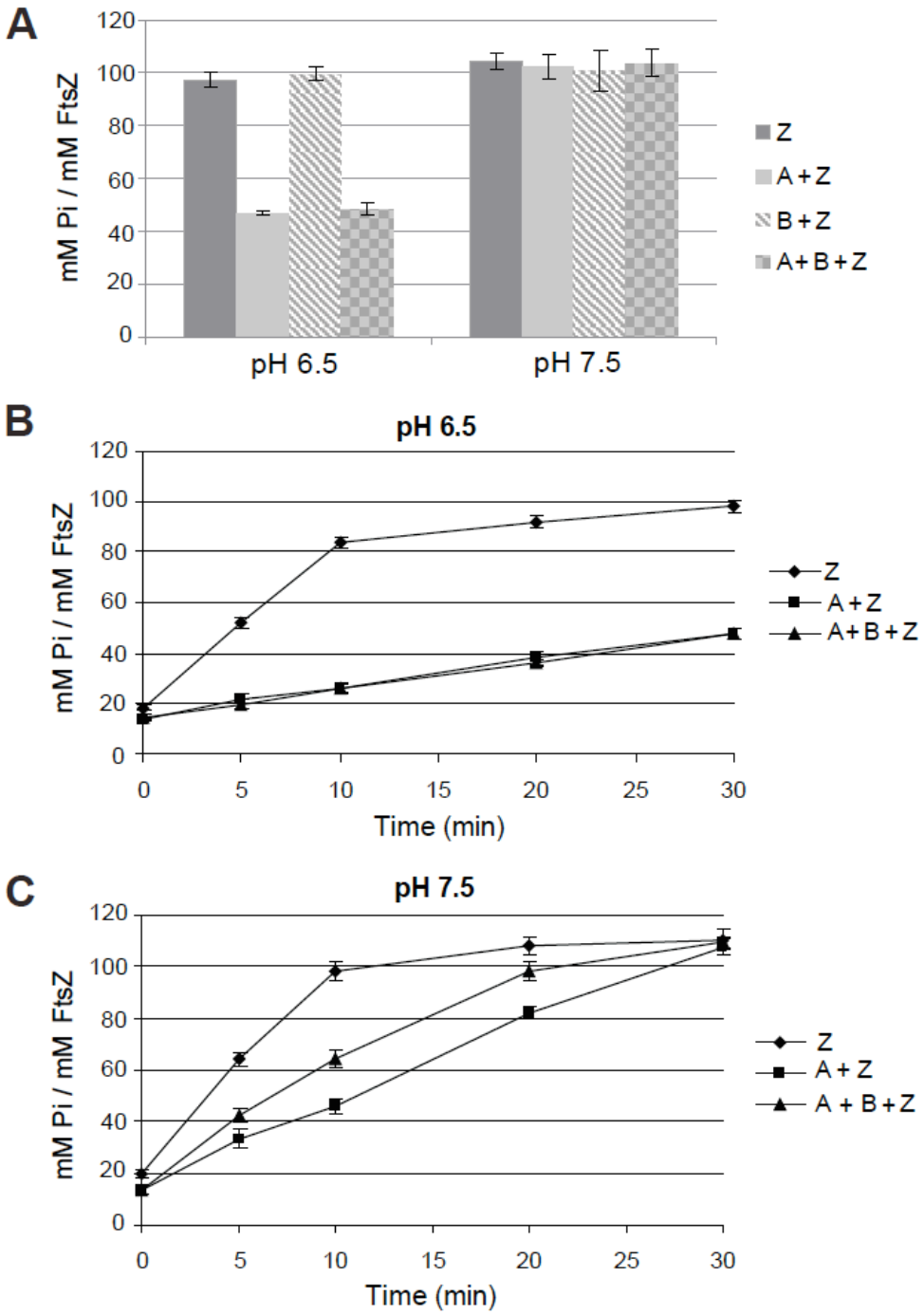

Fig. 5.7 Analysis of FtsZ GTPase activity

In all experiments 1 mM GTP, 5 µM FtsZ, 5 µM ZapA and 5 µM ZapB were used. **A.** FtsZ GTP hydrolysis after 30 minutes. **B.** GTP hydrolysis during FtsZ polymerization in a 30 minute time-course at pH 6.5. **C.** GTP hydrolysis during FtsZ polymerization in a 30 minute time-course at pH 7.5. The graphs report the average of three independent experiments, error bars are the standard deviation of the mean.

5.3.5 ZapB effects on FtsZ bundling

First, we inspected FtsZ polymerization using sedimentation assays and light scattering: FtsZ was found to polymerize and pellet in the presence of GTP (Fig. 5.8AB), as expected (Bramhill and Thompson, 1994; Mukherjee and Lutkenhaus, 1994). ZapB, which does not interact directly with FtsZ, did not have any significant effect on FtsZ bundling (Fig. 5.8AB). We also confirmed that ZapB polymerizes and bundles in presence of divalent cations such as Ca^{2+} (Fig. 5.8BE) (Ebersbach *et al.*, 2008) and that ZapA increases ZapB sedimentation (Fig. 5.8E). ZapA was in the pellet fractions only when FtsZ or ZapB were present (Fig. 5.8F). We then inspected in sedimentation assays FtsZ polymerization and filament bundling induced by ZapA. Increasing amounts of ZapA enhanced FtsZ sedimentation and decreased FtsZ levels in the soluble fraction after ultracentrifugation. The highest amount of FtsZ in the pellet fraction was found when ZapA was at a concentration of 4.8 μM and further increasing ZapA concentration did not enhance FtsZ sedimentation (Fig. 5.8C). Using light scattering we confirmed that increasing ZapA concentration in the polymerization reaction enhanced FtsZ bundle formation (Fig. 5.8D).

We then tested the effect of ZapB plus ZapA on FtsZ polymerization: in sedimentation assays when ZapB was present at low concentrations (1-2 μM) there was a visible decrease of FtsZ and ZapA in the soluble fractions whereas increasing ZapB concentration (above 8 μM) had an evident depolymerizing effect on FtsZ that was now present together with ZapA almost completely in the soluble fractions (Fig. 5.9A). Increasing amounts of ZapB did not change the sedimentation pattern of ZapA, in the absence of FtsZ (Fig. 5.9C). In the same assay, a ZapB mutant unable to interact with ZapA or a small MW unrelated protein such as ParB did not have any effect on FtsZ sedimentation (Fig. 5.9B).

Light scattering experiments supported the results obtained in the sedimentation assays (Fig. 5.9D): low amounts of ZapB increased FtsZ bundling, whereas high amounts decreased or even abolished FtsZ bundling. This latter effect may be due to titration of ZapA by ZapB. We previously showed (Fig. 3.14B) that ZapB strongly interacts with ZapA but that the complex formed by ZapB, ZapA and FtsZ is not as stable as the one formed by solely ZapB and ZapA.

All the sedimentation and light scattering assays were performed in a buffer at pH 6.5 and not at the physiological pH of 7.5 because polymerization assays carried

out with the three proteins ZapA-FtsZ-ZapB did not give reproducible results at the higher pH. In Fig. 5.9E three replicates of the same light scattering experiment performed at pH 7.5 are represented.

It is known that in studying FtsZ polymers and bundles formation the light scattering signal is proportional to polymer mass (Gaskin *et al.*, 1974; Mukherjee and Lutkenhaus, 1999), but ZapB itself is able to form polymers and bundles in the conditions used for the assay (TEM data in the next paragraph will confirm it). In order to subtract ZapB own contribution to the light scattering signal, we measured a baseline for 5 minutes before the addition of GTP and we then reported in the graph the ΔAU (Δ is defined in Materials and Methods) vs. time.

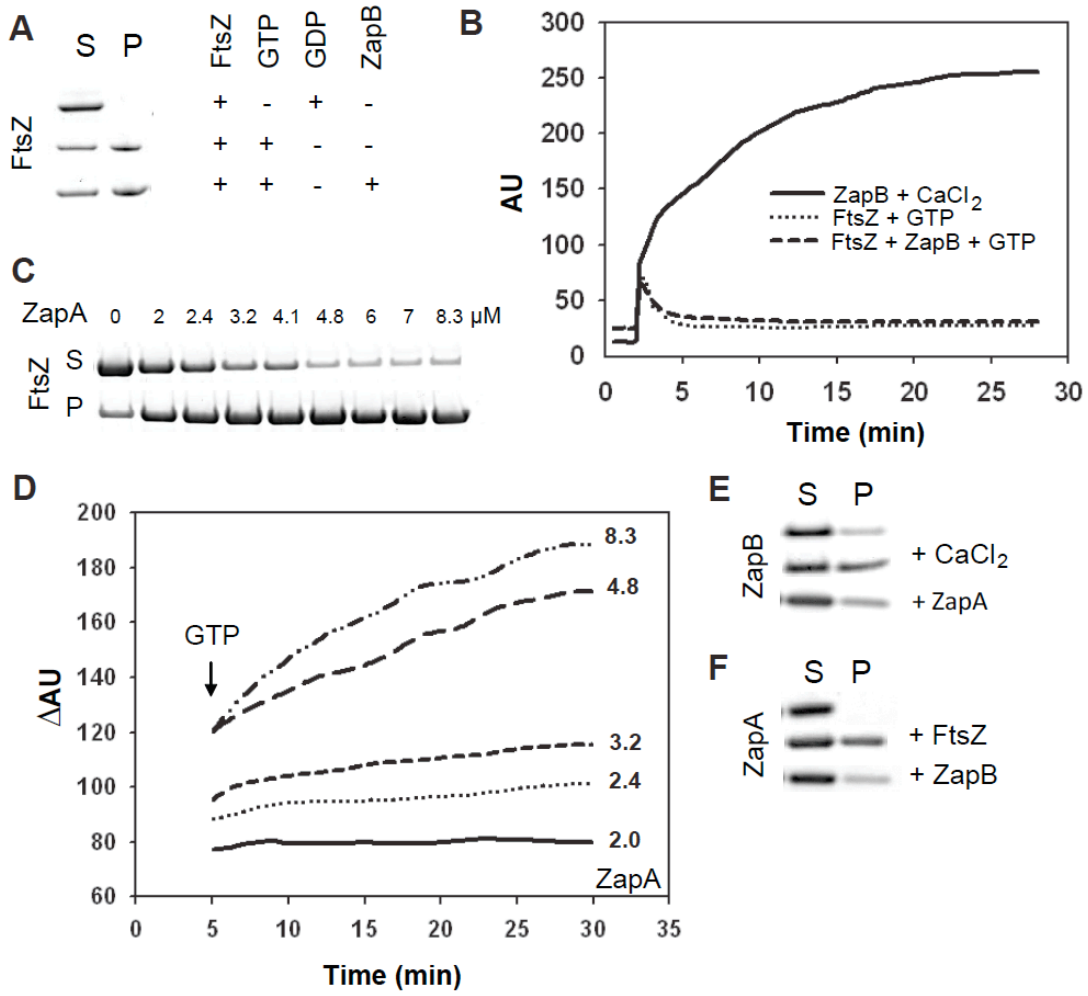

Fig. 5.8 FtsZ polymerization and bundling

Sedimentation and light scattering assays were performed as described in *Materials and Methods* in a polymerization buffer at pH 6.5. **A.** Sedimentation assay of FtsZ. FtsZ (8.3 µM) was incubated with 1 mM nucleotide and ZapB (8.3 µM). **B.** Light scattering. FtsZ (8.3 µM) polymerization reaction with and without ZapB (8.3 µM) was started by the addition of 1 mM nucleotide after recording a baseline for 2.5 minutes. ZapB (8.3 µM) filament bundling was started by the addition of 20 mM $CaCl_2$. **C.** Sedimentation assay of FtsZ. Titration of ZapA against FtsZ. FtsZ (8.3 µM) was incubated with 0.5 mM GTP and ZapA (from 0 to 8.3 µM). **D.** Light scattering. Titration of ZapA against FtsZ. FtsZ (8.3 µM) and ZapA (from 2 to 8.3 µM). Polymerization reaction was started by the addition of 0.5 mM GTP after recording a baseline for 5 minutes. **E.** Sedimentation assay of ZapB. ZapB (8.3 µM) with addition of 20 mM $CaCl_2$ or ZapA (8.3 µM). **F.** Sedimentation assay of ZapA. ZapA (8.3 µM) with addition of FtsZ (8.3 µM) and GTP (1 mM) or ZapB (8.3 µM). S = surnatant, P = pellet. AU = arbitrary unit.

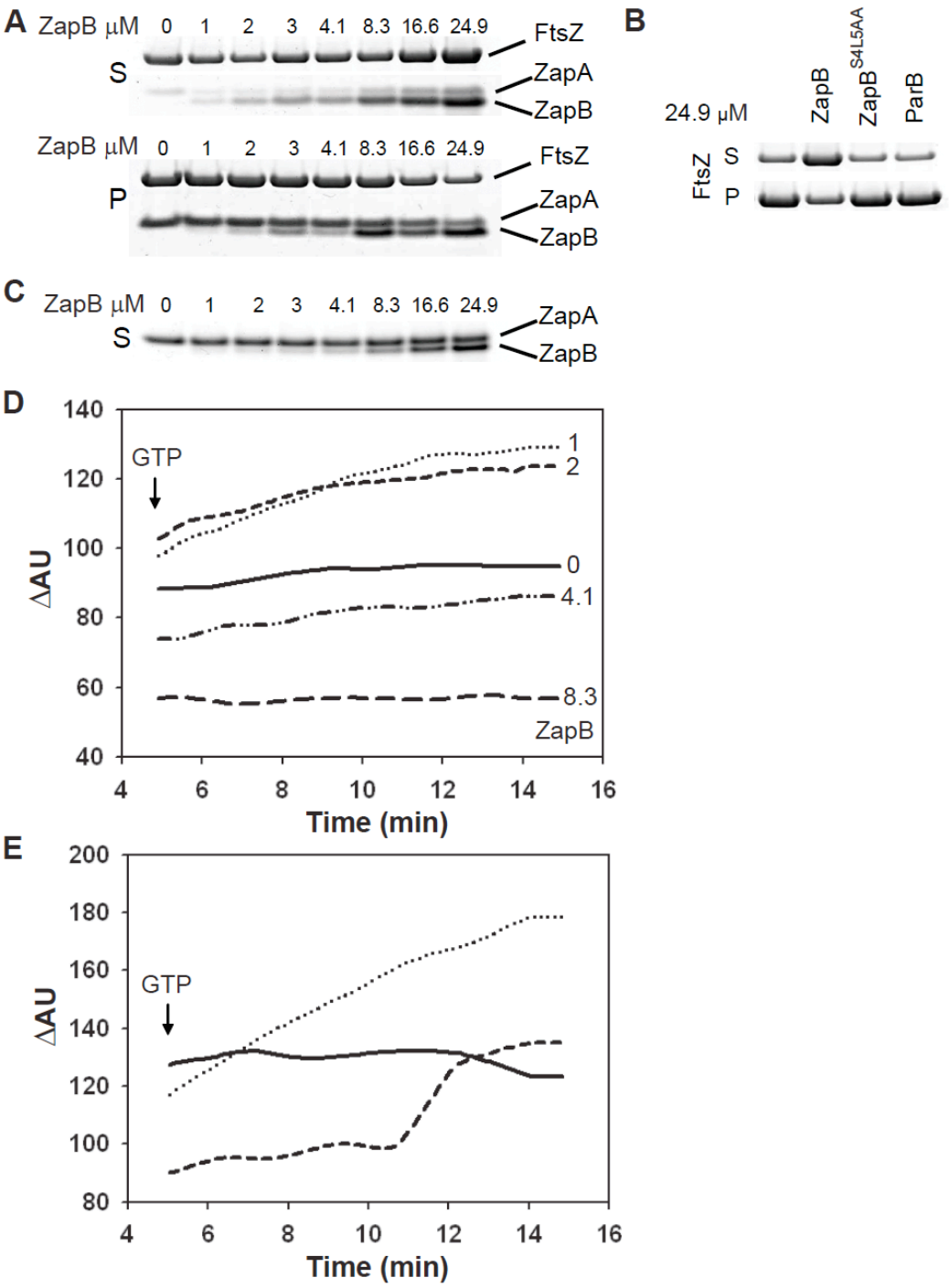

Fig. 5.9 FtsZ polymerization and bundling

The sedimentation and the light scattering assays were performed as described in *Materials and Methods* in a polymerization buffer at pH 6.5 (A, B, C, D) or pH 7.5 (E). Polymerization reactions were started by addition of 0.5 mM GTP. **A.** Sedimentation assay. Titration of ZapB against FtsZ (8.3 µM) and ZapA (3.2 µM). **B.** Sedimentation assay. FtsZ (8.3 µM) and ZapA (3.2 µM) incubated with ZapB, ZapB^{S4L5AA}, ParB (24.9 µM). **C.** Sedimentation assay. Titration of ZapB against ZapA (3.2 µM). **D.** Light scattering. Titration of ZapB against FtsZ (8.3 µM) and ZapA (3.2 µM). **E.** Light scattering. Polymerization of FtsZ (8.3 µM) in the presence of ZapA (3.2 µM) and ZapB (2 µM). Graphs shown are representative of three replicates. S = surnatant, P = pellet. AU = arbitrary unit.

5.3.6 Morphology of FtsZ-ZapA-ZapB structures

The morphology of the structures formed by FtsZ, ZapA and ZapB was inspected by TEM. ZapB, as we previously described (Ebersbach *et al.*, 2008), assembled into cables and bundles with a characteristic regularly striated pattern in the negative stain both in a buffer at pH 6.5 (Fig. 5.10A) and at pH 7.5 (Fig. 5.11A). The ZapB mutant unable to interact with ZapA, $ZapB^{S4L5AA}$, formed structures indistinguishable from those of the wild-type protein (data not shown). Besides thick cables and bundles, long filaments with a less ordered and organized structure were also present (black arrows, Fig. 5.10A). We then studied by EM, using a polymerization buffer at pH 6.5, the structures formed by FtsZ, ZapA and ZapB when two of the three proteins were combined together in all the possible combinations. As previously reported (Low *et al.*, 2004; Small *et al.*, 2007; Mohammadi *et al.*, 2009), FtsZ in the presence of ZapA formed arrays of parallel filaments (Fig. 5.10B). Mohammadi *et al*. (2009) suggested that each filament is formed by two FtsZ single protofilaments and that ZapA tetramers would bind in between and on top of the double FtsZ filaments, favouring their association. The cables that ZapB formed in the presence of ZapA were different from those formed by ZapB alone: they assembled into thicker bundles and the filaments with a disorganized structure disappeared (Fig. 5.10C). ZapB and FtsZ together in the polymerization reaction formed two distinct structures, similar to the ones formed by the two proteins alone (Fig. 5.10D). Next, we examined the structures formed by the three proteins combined. The mutant $ZapB^{S4L5AA}$ was included in the reactions as a negative control. In the presence of $ZapB^{S4L5AA}$ there were visible disordered long filaments apparently formed by $ZapB^{S4L5AA}$ and arrays of parallel FtsZ filaments very similar to the ones formed by FtsZ in the presence of ZapA (black arrow, Fig. 5.10E). Instead, when the wt ZapB protein was used in the polymerization reactions (using high (8.3 μM) or low (2 μM) concentrations of ZapB did not change the morphology of the structures formed) the thick cables formed by ZapB disappeared and the only structures visible were long cable-like filaments, much smaller in diameter than the structures formed by ZapB alone, running parallel to each other or bundling together in bigger complexes (Fig. 5.10F). The bundles had a characteristic striation, with bands parallel to each other and perpendicular to the tube long axis. The structures formed by the three proteins at

pH 7.5 (Fig. 5.11B) were indistinguishable from the ones formed at pH 6.5 (Fig. 5.10F).

The structures with a striated pattern resembled the ones formed by FtsZ in the presence of DEAE-dextran or Ca^{2+} (Lu *et al.*, 2000). Lu *et al*. (2000) reported that FtsZ in presence of DEAE-dextran or $CaCl_2$ forms tubular polymers with an oblique striation pattern and they hypothesized that this striation is indicative of the presence of helical protofilaments in the tubes: FtsZ initially present in pairs of straight protofilaments then transformed into a curved helical conformation after GTP hydrolysis. The structural change would be due to the different conformation that FtsZ polymers adopt in the presence of GTP or GDP: it forms straight protofilaments in the presence of GTP and bent protofilaments in the presence of GDP (Lu *et al.*, 2000).

$CaCl_2$ has been reported to promote lateral association and bundling of FtsZ protofilaments, reducing the dynamic behaviour of FtsZ assembly and stabilizing the Z-polymers (Yu and Margolin, 1997; Lowe and Amos, 1999; Mukherjee and Lutkenhaus, 1999; Lu *et al.*, 2000; Esue *et al.*, 2005b; Jaiswal and Panda, 2009; Kuchibhatla *et al.*, 2009). In the presence of $CaCl_2$ FtsZ formed single cable-like filaments (Fig. 5.12A), but the striation patterns seemed to be perpendicular to the longitudinal axis of the tube and not oblique as described by Lu *et al*. (2000) with DEAE-dextran and Ca^{2+}. When ZapA and $CaCl_2$ were both added to an FtsZ polymerization reaction, the tubular filaments aligned along the long axes, forming bundles with two to five FtsZ cables (Fig. 5.12B) almost indistinguishable from the structures seen when ZapB was added to a reaction containing ZapA and FtsZ (Fig. 5.10F and Fig. 5.11B). The striated pattern of the cross-linked tubules in samples containing FtsZ, ZapA and Ca^{2+} or ZapB differed from the striation of the ZapB-cables in the width of the stripes that was much wider in the cables formed by ZapB alone. Also the size of the cable-like structures was different, ZapB-cables often merged together when running parallel to each other forming structures with bigger diameters (especially in the presence of ZapA) (Fig. 5.10C, c'), whereas the cables formed by FtsZ-ZapA-ZapB remained independent producing arrays of parallel tubules.

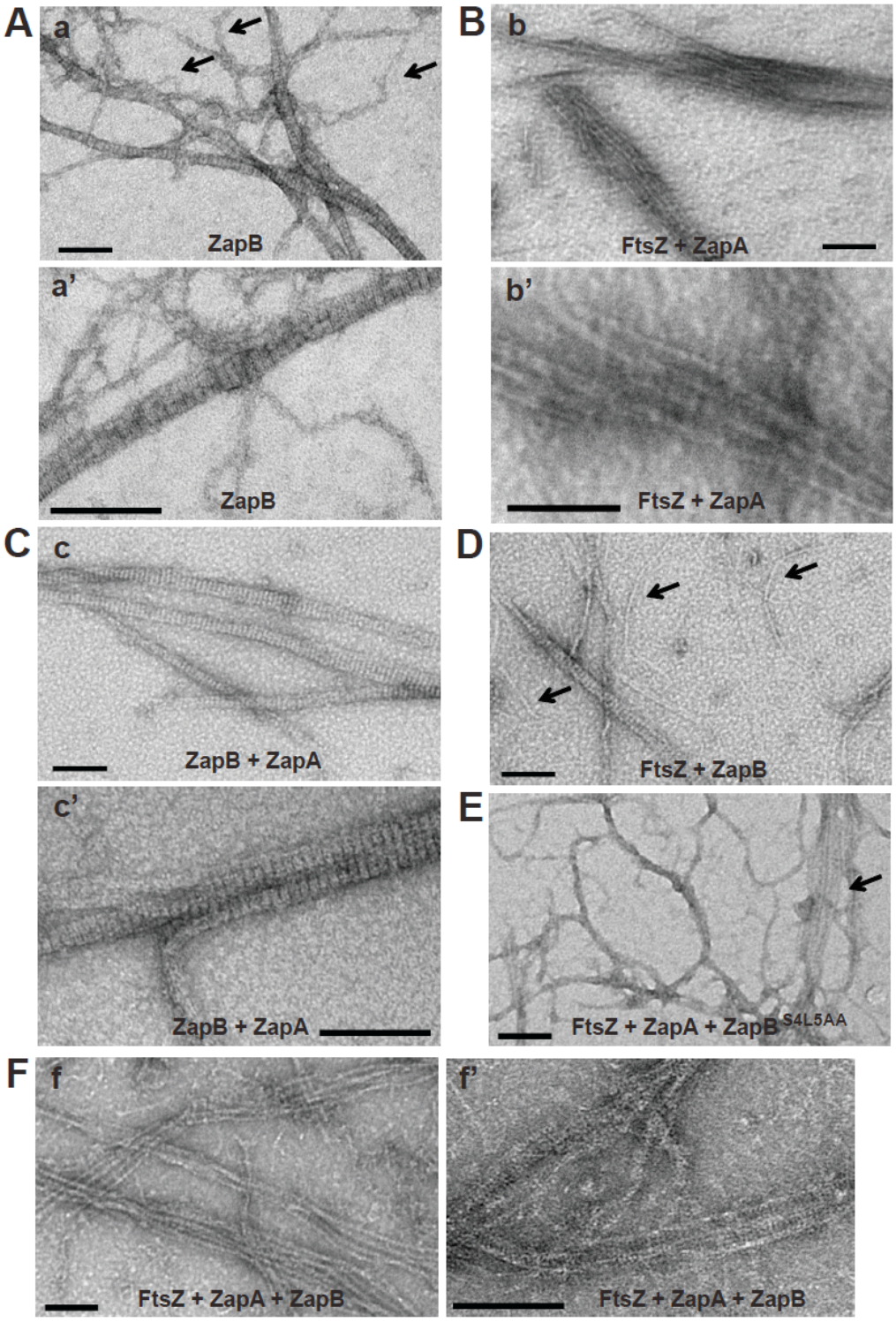

Fig. 5.10 Morphology of FtsZ-ZapA-ZapB structures

Electron microscopy images of uranyl acetate stained filaments and bundles. Polymerization reactions were performed at pH 6.5 as described in *Materials and Methods*. **A. a,a':** ZapB (4.1 µM). Black arrows: unstructured ZapB filaments. **B. b,b':** FtsZ (8.3 µM) and ZapA (3.2 µM). **C. c,c':** ZapB (2 µM) and ZapA (3.2 µM). **D.** FtsZ (8.3 µM) and ZapB (2 µM). Black arrows: FtsZ protofilaments. **E.** FtsZ (8.3 µM), ZapA (3.2 µM) and ZapB^{S4L5AA} (2 µM). Black arrow: array of parallel filaments. **F. f,f':** FtsZ (8.3 µM), ZapA (3.2 µM) and ZapB (2 µM). Scale bars = 100 nm.

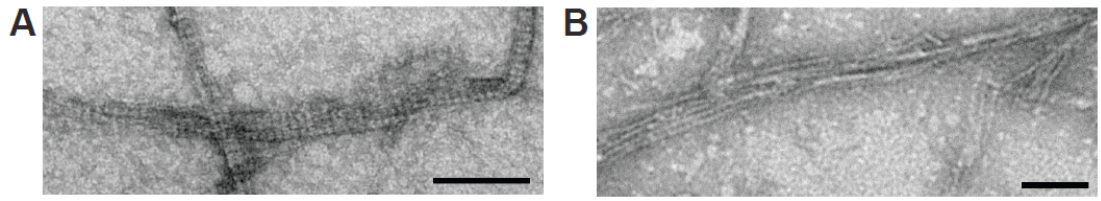

Fig. 5.11 Electron Microscopy analysis at pH 7.5

Electron microscopy images of uranyl acetate stained filaments and bundles. Polymerization reactions were performed at pH 7.5 as described in *Materials and Methods*. **A.** ZapB (4.1 µM). **B.** FtsZ (8.3 µM), ZapA (3.2 µM) and ZapB (2 µM). Scale bars = 100 nm.

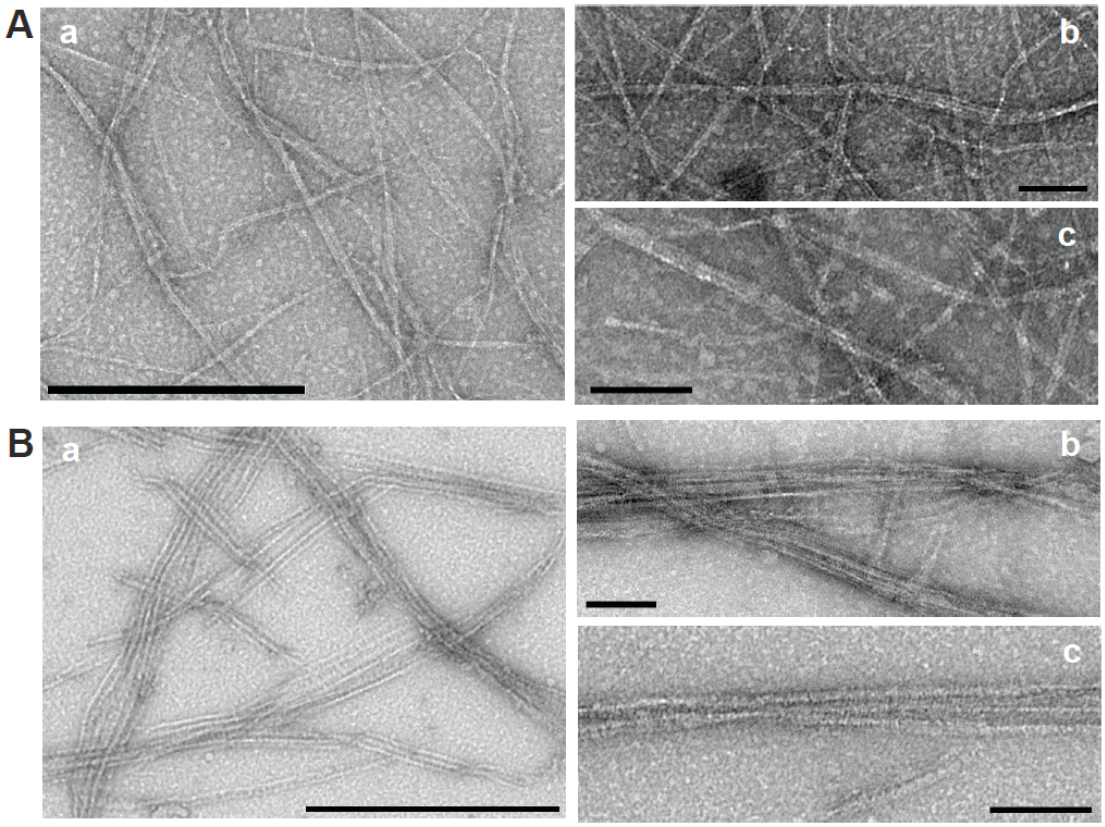

Fig. 5.12 Assembly of FtsZ in calcium

Electron microscopy images of uranyl acetate stained filaments and bundles. Polymerization reactions were performed at pH 6.5 as described in *Materials and Methods*. **A.** FtsZ (8.3 µM) in the presence of 20 mM $CaCl_2$. **B.** FtsZ (8.3 µM) and ZapA (3.2 µM) in the presence of 20 mM $CaCl_2$. Scale bars = 100 nm (Ab-c, Bb-c); scale bars = 500 nm (Aa, Ba).

5.3.7 Investigating ZapA-independent function of ZapB

The morphological analysis of cell division mutants hinted to a possible role of ZapB in cell division that is independent of ZapA and of ZapB recruitment at the division site.

Since it has been reported that the overproduction of ZapB leads to highly compaction and mislocalization of nucleoids (Ebersbach *et al.*, 2008), we analysed nucleoid sizes in *zapB* mutant cells. We first inspected the chromosome morphology of KG22 and KG22Δ*zapB* cells treated with cephalexin: the filamentous cells of both strains harboured multiple nucleoids, but we could not detect any significant difference between them and the nucleoids in the *zapB* deletion strain did not appear decondensed (Fig. 5.13A), as it might have been expected if ZapB had an active role in nucleoid compaction.

We further inspected the effects of ZapB overproduction examining cell viability and FtsZ localization in cells overproducing ZapB. The graphs in Fig. 5.13B show that ZapB overproduction severely reduced the increase in viable counts, even though the growth curve of a strain overproducing ZapB did not highlight a growth defect.

Next, we simultaneously analysed nucleoid morphology and FtsZ localization in cells with enhanced levels of ZapB. As previously described (Ebersbach *et al.*, 2008), overproduction of ZapB led to highly compaction of the nucleoids and FtsZ-GFP had an aberrant localization in more than the half of the cell population. We could classify FtsZ localization into different categories (Fig. 5.13C): as a band at mid-cell between the segregated nucleoids (40% of the cells), as a band or two dots at the cell pole (40%) (in few cells FtsZ localized even at both of the cell poles), as a double band at mid-cell (10%) and there was also a small percentage of cells (2%) forming short filaments with multiple nucleoids and only a single FtsZ band at mid-cell. In the remaining 8% of cells a distinct FtsZ structure was not identifiable.

We envisaged the possibility that ZapB overproduction mediated nucleoid condensation by physically pushing them toward the ZapB-free regions and that the phenotype we saw was not related to a ZapB biological function. To assess this hypothesis, we overproduced a ZapB-mCherry fusion protein and stained the nucleoids with DAPI. Fig. 5.13D shows that the compacted nucleoids and ZapB-mCherry signals were juxtaposed but in separate regions of the cells, thus supporting

the hypothesis that ZapB overproduction leads to physical condensation or compaction of the nucleoids.

We also analysed the possible involvement of *zapB* with the SOS response combining a *sulA* deletion with a *zapB* deletion. We measured the cell length distributions of the single and the double deletion strains: the combination of *sulA* and *zapB* mutants did not seriously affect the cell length distribution (Fig. 5.14). Therefore, we do not believe that ZapB is involved in the SOS response.

Finally, we thought possible that the slight elongation defect seen in the *zapB* deletion mutant could be due to impairment in septum formation. In *B. subtilis*, the lack of the early cell division protein SepF resulted in septa with an abnormal and incomplete morphology (Hamoen *et al.*, 2006; Ishikawa *et al.*, 2006). Therefore, the ultrastructure of division septa was analysed using electron microscopy (TEM). However, septum formation was not impaired. We could only confirm the presence of short filaments with no constriction at mid-cell or cell with a double invagination of the cell wall around mid-cell or septum formation at the cell pole (Fig. 5.15), as we expected since FtsZ in a *zapB* mutant was shown to localize at the cell-pole or as a double-band around mid-cell (Fig. 5.3B).

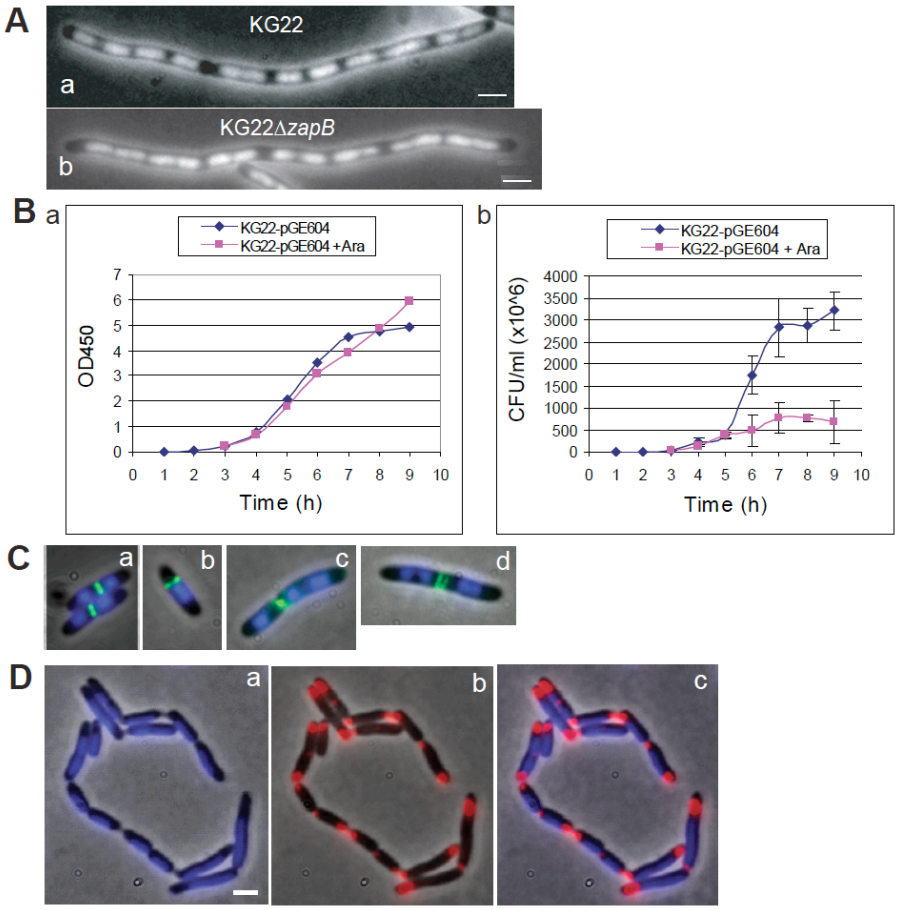

Fig. 5.13 ZapB is not involved in chromosome condensation

(Galli and Gerdes, 2010). **A.** Deletion of *zapB* does not affect the nucleoid morphology. Combined phase-contrast and fluorescence (DAPI) microscopy images showing the localization of the nucleoids in living cells of strain KG22 (a) and KG22Δ*zapB* (b). Cells were grown at 30°C in LB medium and exponentially growing cultures were treated with 10 µg/ml of cephalexin 60 minutes before samples were collected for microscopy. **B.** Cells of strain KG22 carrying the plasmid pGE604 (P_{BAD}*::zapB*) were grown in LB at 37°C. At an OD_{450} value of about 0.2, the culture was split in two and 0.2% arabinose added to one half. Samples were collected every hour for a total of 9 hours and plated on NA + 30 µg/ml Cml plates. After incubation at 37°C over-night colonies were counted and the CFU calculated. The graph on the left (a) shows the growth curves and the one on the right (b) the viable count curves. The viable count curves report the average of two independent experiments, error bars are the standard deviation of the mean. **C**. ZapB overproduction and FtsZ-GFP localization. Cells of strain KG22 / pEG12 (P_{lac}*::ftsZ::gfp*) / pGE604 (P_{BAD}*::zapB*) were grown at 30°C in LB. Expression of ZapB from plasmid pGE604 and FtsZ-GFP from pEG12 was induced as described in *Materials and Methods*. Combined phase-contrast and fluorescence microscopy images showing the localization of nucleoids stained with DAPI (blue) and FtsZ-GFP (green). FtsZ-GFP localizes at mid-cell in 40% of cells (a); at the cell pole or even at both of the cell poles in 40% of the cells (b); 2% of cells are short filaments with multiple nucleoids and a single FtsZ band at mid-cell (c); FtsZ-GFP forms helices or double bands in 10% of the cells (d). **D.** Overproduced ZapB-mCherry and nucleoid localization. KG22 / pEG6 (P_{lac}*::zapB::mCherry*) cells were grown in LB at 37°C. Combined phase-contrast and fluorescence microscopy images showing the localization of the nucleoid stained with DAPI (a), ZapB-mCherry (b) and the overlay of ZapB-mCherry and DAPI (c) in living cells of strain KG22. Scale bars = 2 µm.

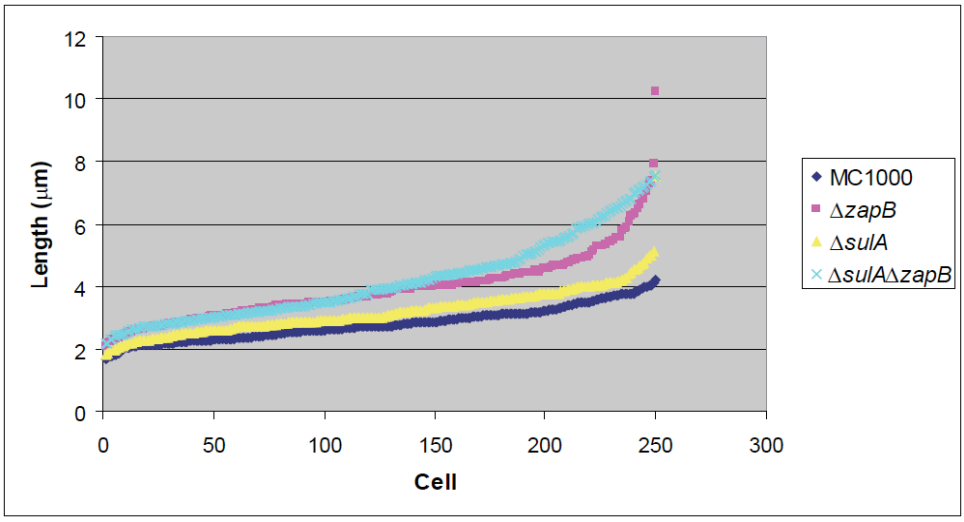

Fig. 5.14 ZapB is not involved in the SOS response

Diagram showing the cell length distribution of MC1000 and the deletion strains Δ*zapB* (Galli and Gerdes, 2010). Δ*sulA* and Δ*sulA*Δ*zapB* grown in LB at 37°C. A total of 250 cells of each strain were measured.

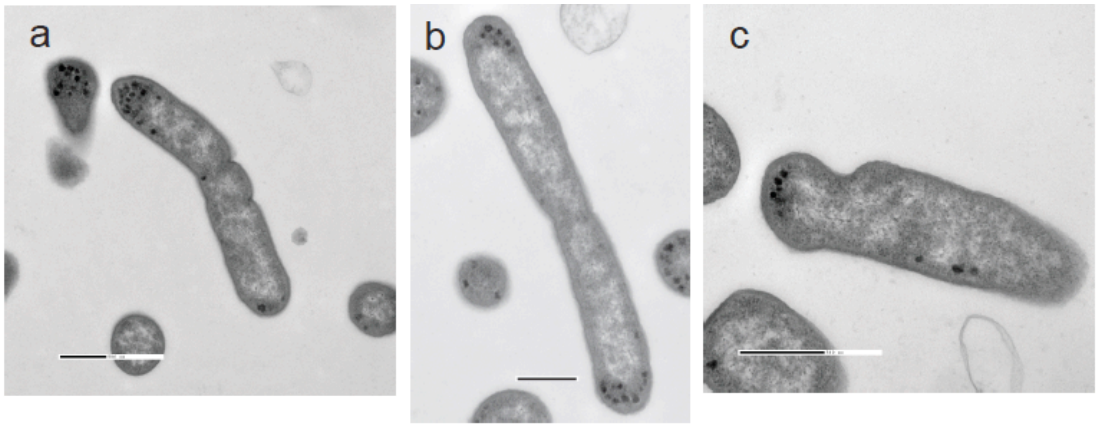

Fig. 5.15 Δ*zapB* cell morphology

Transmission electron microscopy (TEM) of ultrathin sections of Δ*zapB* cells grown in LB at 37°C (Galli and Gerdes, 2010). Scale bars = 500 nm.

5.4 Discussion

FtsZ84 has been described to have a reduced GTPase activity and to polymerize inefficiently (Bramhill and Thompson, 1994; Addinall *et al.*, 2005). In a strain carrying the *ftsZ84* allele, deletion of *zapB* resulted in very sick cells that rapidly accumulated suppressors (Fig. 5.5). This phenotype raised the possibility that ZapB stabilizes or bundles FtsZ polymers. The suppressors in the double mutant probably mitigated the defects of the *ftsZ84* allele. Phoenix and Drapeau (1988) showed that normal cell division activity in a strain carrying the *ftsZ84* mutation could be restored by a modest increase in the expression of the *ts* mutant *ftsZ84* or by acquiring a *lon* mutation. Indeed, at least one of the KG22Z84Δ*zapB* suppressors we isolated (*sup78*) has the mucoid colony phenotype typical of *lon* mutants. Phoenix and Drapeau (1988) suggested that *lon* mutations could rescue the Z84 phenotype by reducing the degradation of the temperature-sensitive protein. A *zapA* deletion exhibited an even more severe effect when combined with the *ftsZ84* allele. This observation agreed with the hypothesis that ZapB acts via ZapA on FtsZ bundling. In contrast, the combination of the *zapB* deletion with *ts* mutations in *ftsA*, *zipA* or *ftsI*, did not result in synthetic defects (Fig. 5.6), in keeping with a role for ZapB in FtsZ polymerization or early Z-ring assembly.

The not essential Z-ring associated protein ZapA associates with early FtsZ assemblies and promotes stabilization, cross-linking and bundling of FtsZ protofilaments in the Z-ring (Low *et al.*, 2004; Small *et al.*, 2007; Mohammadi *et al.*, 2009; Dajkovic *et al.*, 2010). Mohammadi *et al*. (2009) carefully analysed the ZapA-FtsZ interaction using buffers with different compositions and pH and proposed that ZapA is involved in FtsZ filament association during the transition from helical filament to mid-cell ring.

To study the effect of ZapB on FtsZ dynamics, we used the buffers suggested to stimulate FtsZ protofilament association via ZapA. Both at the physiological pH of 7.5 and at the optimal pH for FtsZ polymerization of 6.5, ZapA reduced FtsZ GTPase activity (Fig. 5.7). The same strong inhibition was previously reported by Small *et al*. (2007) even though Mohammadi *et al*. (2009) only detected a minor reduction probably originated by lateral association of FtsZ protofilaments. ZapB at pH 6.5 did not have any effect on FtsZ GTPase activity but at pH 7.5, where ZapA inhibition was less effective, ZapB partially relieved the inhibition. This effect is most easily

explained by titration of ZapA by ZapB, consistent with the effect observed in the sedimentation and light scattering assays (Fig. 5.9). In these two assays, low amounts of ZapB had a positive effect on FtsZ bundling whereas higher concentrations caused a dramatic depolymerization. This effect was specifically induced by ZapB via ZapA, since a ZapB mutant with a reduced ability to bind ZapA did not have any consequence on FtsZ polymerization.

TEM analysis (Fig. 5.10) showed that, in the presence of ZapA, FtsZ formed arrays of parallel protofilaments. ZapB and FtsZ formed two independent structures. ZapB cables in the presence of ZapA often merged, forming very large and long cable-like structures. FtsZ, ZapA and ZapB (present at concentrations that did not induce FtsZ depolymerization) formed aligned filaments (from two to five filaments in each array) with a regularly striated pattern. These bundles were reminiscent of the cable-like filaments formed by FtsZ in the presence of DEAE-dextran and calcium (Lu *et al.*, 2000). Indeed, in the presence of Ca^{2+}, FtsZ formed single tubular polymers that by addition of ZapA aligned laterally forming assemblies indistinguishable from the ones formed by FtsZ, ZapA and ZapB (Fig. 5.12). Small *et al*. (2007) previously reported that ZapA and calcium effects on FtsZ filaments lateral association were not additive and that the two reagents likely competed for binding to FtsZ polymers. The discrepancy between these results and the ones presented here on the effect of ZapA and Ca^{2+} may be due to the fact the we used native ZapA and they used a His-tagged version of the protein, since it has been shown that the His-tag is a steric hindrance for ZapA interaction with FtsZ (Mohammadi *et al.*, 2009) and therefore the filament lateral association induced by His-ZapA could be defective.

Overall, ZapB induced a conformational change in the structures formed by FtsZ and ZapA that was very similar to the effect induced by Ca^{2+} on *E. coli* FtsZ. This morphological change could have an effect on the ability of FtsZ to modulate Z-ring structure and assembly/disassembly dynamics.

Unexpectedly, our genetic analysis showed that ZapB could stimulate Z-ring assembly independently of ZapA. Thus, the deletion of *zapB* increased cell length and Z-ring mislocalization, irrespective of the presence or absence of *zapA* (Tables 5.1 and 5.2). Furthermore, expression of ZapB in a Δ*zapA* Δ*zapB* double deletion strain mitigated the cell length defect (Table 5.3). To reconcile these observations with the recruitment of ZapB-GFP to the Z-ring via ZapA, we note the possibility that ZapB

may be able to affect Z-ring formation by two different mechanisms: directly via ZapA and indirectly by an as yet unknown mechanism.

Previously, we showed that overproduction of ZapB leads to highly compacted and mislocalized nucleoids (Ebersbach *et al.*, 2008). In an attempt to understand the ZapA-independent effect of ZapB, we further characterized the effects of ZapB overproduction. But the results, most likely, suggest that nucleoid condensation induced by ZapB overproduction is an artificial effect (Fig. 5.13). In *B. subtilis*, deletion of *zapA* caused no recognizable phenotype (Gueiros-Filho and Losick, 2002). However, we show here that the deletion of *zapA* in *E. coli* increased cell length reproducibly (Tables 5.1 and 5.3) and is consistent with data presented recently (Mohammadi *et al.*, 2009). In *B. subtilis*, the combination of a *zapA* deletion and a mutation in *divIVA*, responsible for the polar localization of MinCD, had a synergistic effect and resulted in highly filamentous cells (Gueiros-Filho and Losick, 2002). This effect is reminiscent of that seen with *E. coli* cells lacking ZapA and MinCD (Table 5.1 and 5.2). In *E. coli*, the Δ*zapB* and Δ*zapA* phenotypes are very similar: the deletions resulted in similar increases in cell length, FtsZ double bands and helix-formation at mid-cell. These phenotypes are consistent with a less stable or incorrectly organized Z-ring. The main difference however was that ~2% of Δ*zapB* cells had polar Z-rings, which were not seen with Δ*zapA* cells (Fig. 5.3). In *B. subtilis*, deletion of the early cell division protein SepF resulted in septa with an abnormal and incomplete morphology (Hamoen *et al.*, 2006; Ishikawa *et al.*, 2006). To see if this was also the case with ZapB of *E. coli*, we investigated septum morphology by EM. However, EM analysis did not show any altered morphology of the division septum, consistently with an early recruitment of ZapB to the divisome (Fig. 5.15).

We also analysed the effect of *zapB* on the SOS response, combining a Δ*sulA* with a Δ*zapB* mutant and we measured the cell length of the single and the double deletion strains. The deletion of *sulA* did not affect the effect of Δ*zapB* on the cell length making unlikely an involvement of ZapB in the SOS response (Fig. 5.14).

Chapter 6

Summary and General discussion

Cytokinesis in bacteria has been extensively studied and more than two dozen different proteins have been reported to be part of the so-called divisome, although only ten of these factors have been shown to be essential for cell survival (Adams and Errington, 2009; de Boer, 2010).

Here, we have described the characterization of a novel auxiliary cell division factor, ZapB, discovered in a screening for host factors specific for plasmid-partitioning mechanisms (Ebersbach *et al.*, 2008).

We showed (Chapter 3) that ZapB is recruited by ZapA into the divisome in the early stages of the division process and that other early (FtsA, ZipA) or late cell division proteins (FtsI) are not necessary for its localization at the division site. ZapB dynamic localization pattern depended solely on FtsZ and ZapA, the inactivation (FtsZ) or absence (and overproduction for ZapA) of one of these two components caused ZapB diffusion in the cytoplasm and the complete loss of septal localization. ZapA on the other hand was not affected by the absence of ZapB. We also inspected the effects that inactivation of the newly Z-ring associated protein ZapC (Durand-Heredia *et al.*, 2011; Hale *et al.*, 2011) had on ZapA and ZapB recruitment into the divisome: neither of the two proteins seemed to be affected by ZapC absence.

Using *in vivo* and *in vitro* assays, we showed that ZapA, interacting directly with both FtsZ and ZapB, acts as a bridge between the two division factors and that ZapB does not interact directly with FtsZ. It was previously reported that in a BTH assay ZapB interacted with FtsZ and FtsA (Ebersbach *et al.*, 2008), but here we have shown that the described BTH positive interactions were artifacts produced by the chromosomal copy of *zapA* and that when we repeated the same assay in an *E. coli* BTH strain lacking *zapA* we could not detect the interactions previously reported. We also identified the domain with which ZapB binds ZapA: ZapB N-terminal end, in a BTH assay and using purified proteins *in vitro*, was shown to be essential and we were also able to identify ZapB point-mutants close to the N-terminus with a reduced ability to associate with ZapA.

We then carefully analysed ZapB dynamic localization pattern and compared it to that of FtsZ and ZapA (Chapter 4). ZapB closely followed FtsZ along the entire division process, from the formation of the nascent Z-ring to its dissociation, but strikingly and unexpectedly it formed a ring with a slightly smaller diameter compared to those of FtsZ and ZapA. Especially in the last stages of division, using fluorescence light microscopy, ZapB was clearly ahead of the Z-ring during

constriction. This peculiar characteristic was not a phenomenon present only in a subset of the cell population, but it was common in all the cells and maintained throughtout the cell cycle, generation after generation. In cells that have lost the characteristic rod shape, after treatment with A22 (MreB inhibitor) or Mecillinam (PBP2 inhibitor), ZapB was still able to form a structure decorating the inside of the Z-ring. However, in cells lacking MreB this ability was lost and ZapB structures seemed to superimpose perfectly with the ones formed by FtsZ. In the Δ*mreB** strain we used, the structures FtsZ and ZapB formed were often incomplete rings or helices and maybe these structures were somehow defective, missing the unknown property that renders ZapB spatially resolved from the Z-ring.

To be able to understand how ZapB can form a ring located on the inner side of the ring formed by FtsZ and the other Z-ring associated proteins and to be able to detect possible ZapB or ZapA structures connecting the two rings, the light microscopy techniques we used in this study are not sensitive enough, having a spatial resolution limit of ~250 nm. The only possibility, to further improve our knowledge of ZapB localization in the cells, would be to employ one of the new super resolution microscopy techniques, such as STORM, STED or PALM, which could reduce the resolution limits and gain detailed and informative images of the structures formed by FtsZ and ZapB within the cells.

Investigating ZapB role in the divisome (Chapter 5), we discovered that ZapB might be involved in two different aspects of cell division, the first is Z-ring stabilization through ZapA and the second, ZapA-independent, is as yet unknown. Preliminary data would exclude an involvment of ZapB in the SOS response or in septum formation and the late stages of cytokinesis. We have shown that ZapB induces a conformational change in the cross-linked filament assemblies formed by FtsZ and ZapA, these new structures might improve Z-ring stabilization or dynamics and this could be beneficial for the cells. The presence, in *E. coli*, of at least other two proteins (ZapA and ZapC) modulating Z-ring assembly might explain the modest division defects of a *zapB* mutant, caused by the redundancy and the partially overlapping roles of these factors.

All data, *in vivo* and *in vitro*, support the formation of a stable complex between ZapA and ZapB and ZapA seems to associate more strongly to ZapB than to FtsZ. It is possible that the complex formed by FtsZ, ZapA and ZapB together is only transient and that ZapB strongly interacting with ZapA might regulate how and when

during a cell division cycle ZapA interacts and induces FtsZ cross-linking and bundling. It could be possible that ZapB sequestering ZapA hampers the ZapA-FtsZ interaction away from mid-cell, for example at the cell poles, soon after Z-ring constriction and before migration of FtsZ to the new cell division site in the two daughter cells. This could explain why in a *zapB* mutant there is a fraction of the cell population with polar Z-ring and mini-cells are produced.

It is also interesting that a ZapA tetramer and a ZapB molecule have very similar lengths (between ~10 nm and ~12 nm) and that when forming a dimer the aa S4L5 (important for ZapB interaction with ZapA) of each molecule are on the same side, probably stabilizing the ZapA-ZapB complex (Fig. 6.1).

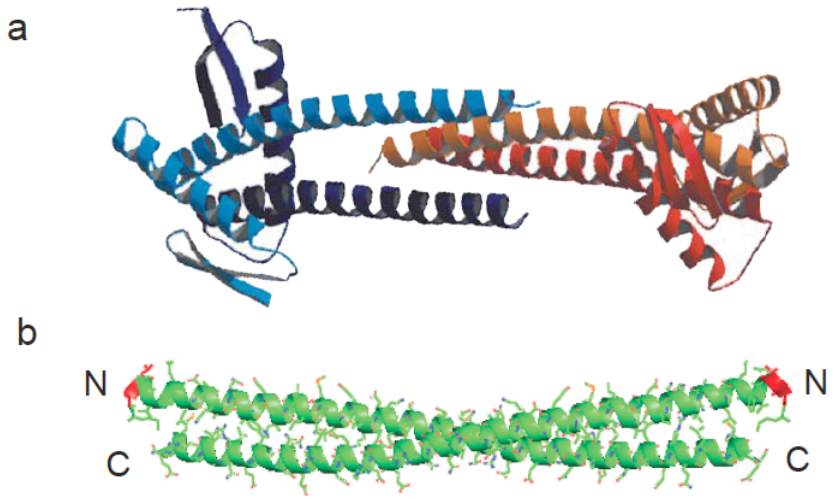

Fig. 6.1 ZapA-ZapB interaction

a. Crystal structure of two ZapA dimer (formed by two parallel coiled-coil ZapA monomer) forming an anti-parallel tetramer, ~10 nm long (Low *et al.*, 2004). **b.** Predicted crystal structure of the ZapB^{S4L5AA} dimer, ~11.6 nm long, in red S4L5 aa.

Improving our knowledge of ZapB structures in living cells by super-resolution microscopy and more detailed structural informations on the complex formed by the purified proteins *in vitro* will be fundamental to fully elucidate the biological role ZapB has in cell division.

References

Aarsman, M.E., Piette, A., Fraipont, C., Vinkenvleugel, T.M., Nguyen-Disteche, M., and den Blaauwen, T. (2005) Maturation of the *Escherichia coli* divisome occurs in two steps. *Mol Microbiol* **55**: 1631-1645.

Adam, M., Fraipont, C., Rhazi, N., Nguyen-Disteche, M., Lakaye, B., Frere, J.M., Devreese, B., Van Beeumen, J., van Heijenoort, Y., van Heijenoort, J., and Ghuysen, J.M. (1997) The bimodular G57-V577 polypeptide chain of the class B penicillin-binding protein 3 of *Escherichia coli* catalyzes peptide bond formation from thiolesters and does not catalyze glycan chain polymerization from the lipid II intermediate. *J Bacteriol* **179**: 6005-6009.

Adams, D.W., and Errington, J. (2009) Bacterial cell division: assembly, maintenance and disassembly of the Z-ring. *Nat Rev Microbiol* **7**: 642-653.

Addinall, S.G., and Lutkenhaus, J. (1996) FtsZ-spirals and -arcs determine the shape of the invaginating septa in some mutants of *Escherichia coli*. *Mol. Microbiol.* **22**: 231-237.

Addinall, S.G., Bi, E., and Lutkenhaus, J. (1996) FtsZ ring formation in *fts* mutants. *J Bacteriol* **178**: 3877-3884.

Addinall, S.G., Cao, C., and Lutkenhaus, J. (1997) Temperature shift experiments with an *ftsZ84*(Ts) strain reveal rapid dynamics of FtsZ localization and indicate that the Z-ring is required throughout septation and cannot reoccupy division sites once constriction has initiated. *J Bacteriol* **179**: 4277-4284.

Addinall, S.G., Small, E., Whitaker, D., Sturrock, S., Donachie, W.D., and Khattar, M.M. (2005) New temperature-sensitive alleles of *ftsZ* in *Escherichia coli*. *J Bacteriol* **187**: 358-365.

Allard, J.F., and Cytrynbaum, E.N. (2009) Force generation by a dynamic Z-ring in *Escherichia coli* cell division. *Proc Natl Acad Sci U S A* **106**: 145-150.

Alyahya, S.A., Alexander, R., Costa, T., Henriques, A.O., Emonet, T., and Jacobs-Wagner, C. (2009) RodZ, a component of the bacterial core morphogenic apparatus. *Proc Natl Acad Sci U S A* **106**: 1239-1244.

Anderson, D.E., Gueiros-Filho, F.J., and Erickson, H.P. (2004) Assembly dynamics of FtsZ rings in *Bacillus subtilis* and *Escherichia coli* and effects of FtsZ-regulating proteins. *J Bacteriol* **186**: 5775-5781.

Arends, S.J., Kustusch, R.J., and Weiss, D.S. (2009) ATP-binding site lesions in FtsE impair cell division. *J Bacteriol* **191**: 3772-3784.

Bachmann, B.J. (1972) Pedigrees of some mutant strains of *Escherichia coli* K-12. *Bacteriol Rev* **36**: 525–557.

Barak, I., and Wilkinson, A.J. (2007) Division site recognition in *Escherichia coli* and *Bacillus subtilis*. *FEMS Microbiol Rev* **31**: 311-326.

Beall, B., and Lutkenhaus, J. (1989) Nucleotide sequence and insertional inactivation of a *Bacillus subtilis* gene that affects cell division, sporulation, and temperature sensitivity. *J Bacteriol* **171**: 6821-6834.

Beall, B., and Lutkenhaus, J. (1992) Impaired cell division and sporulation of a *Bacillus subtilis* strain with the *ftsA* gene deleted. *J Bacteriol* **174**: 2398-2403.

Bendezu, F.O., and de Boer, P.A. (2008) Conditional lethality, division defects, membrane involution, and endocytosis in *mre* and *mrd* shape mutants of *Escherichia coli*. *J Bacteriol* **190**: 1792-1811.

Bendezu, F.O., Hale, C.A., Bernhardt, T.G., and de Boer, P.A. (2009) RodZ (YfgA) is required for proper assembly of the MreB actin cytoskeleton and cell shape in *E. coli*. *EMBO J* **28**: 193-204.

Bernard, C.S., Sadasivam, M., Shiomi, D., and Margolin, W. (2007) An altered FtsA can compensate for the loss of essential cell division protein FtsN in *Escherichia coli*. *Mol Microbiol* **64**: 1289-1305.

Bernhardt, T.G., and de Boer, P.A. (2003) The *Escherichia coli* amidase AmiC is a periplasmic septal ring component exported via the twin-arginine transport pathway. *Mol Microbiol* **48**: 1171-1182.

Bernhardt, T.G., and de Boer, P.A. (2004) Screening for synthetic lethal mutants in *Escherichia coli* and identification of EnvC (YibP) as a periplasmic septal ring factor with murein hydrolase activity. *Mol Microbiol* **52**: 1255-1269.

Bernhardt, T.G., and de Boer, P.A. (2005) SlmA, a nucleoid-associated, FtsZ binding protein required for blocking septal ring assembly over chromosomes in *E. coli*. *Mol Cell* **18**: 555-564.

Bi, E.F., and Lutkenhaus, J. (1991) FtsZ ring structure associated with division in *Escherichia coli*. *Nature* **354**: 161-164.

Bigot, S., Sivanathan, V., Possoz, C., Barre, F.X., and Cornet, F. (2007) FtsK, a literate chromosome segregation machine. *Mol Microbiol* **64**: 1434-1441.

Biteen, J.S., Thompson, M.A., Tselentis, N.K., Bowman, G.R., Shapiro, L., and Moerner, W.E. (2008) Super-resolution imaging in live *Caulobacter crescentus* cells using photoswitchable EYFP. *Nat Methods* **5**: 947-949.

Blatny, J.M., Brautaset, T., Winther-Larsen, H.C., Haugan, K., and Valla, S. (1997) Construction and use of a versatile set of broad-host-range cloning and expression vectors based on the RK2 replicon. *Appl Environ Microbiol* **63**: 370-379.

Bork, P., Sander, C., and Valencia, A. (1992) An ATPase domain common to prokaryotic cell cycle proteins, sugar kinases, actin, and hsp70 heat shock proteins. *Proc Natl Acad Sci U S A* **89**: 7290-7294.

Born, P., Breukink, E., and Vollmer, W. (2006) *In vitro* synthesis of cross-linked murein and its attachment to sacculi by PBP1A from *Escherichia coli*. *J Biol Chem* **281**: 26985-26993.

Botta, G.A., and Park, J.T. (1981) Evidence for involvement of penicillin-binding protein 3 in murein synthesis during septation but not during cell elongation. *J Bacteriol* **145**: 333-340.

Bradford, M.M. (1976) A rapid and sensitive method for the quantitation of microgram quantities of protein utilizing the principle of protein-dye binding. *Anal Biochem* **72**: 248-254.

Bramhill, D., and Thompson, C.M. (1994) GTP-dependent polymerization of *Escherichia coli* FtsZ protein to form tubules. *Proc Natl Acad Sci U S A* **91**: 5813-5817.

Bramkamp, M., Emmins, R., Weston, L., Donovan, C., Daniel, R.A., and Errington, J. (2008) A novel component of the division-site selection system of *Bacillus subtilis* and a new mode of action for the division inhibitor MinCD. *Mol Microbiol* **70**: 1556-1569.

Bramkamp, M., and van Baarle, S. (2009) Division site selection in rod-shaped bacteria. *Curr Opin Microbiol* **12**: 683-688.

Bramkamp, M., Weston, L., Daniel, R.A., and Errington, J. (2006) Regulated intramembrane proteolysis of FtsL protein and the control of cell division in *Bacillus subtilis*. *Mol Microbiol* **62**: 580-591.

Buddelmeijer, N., Aarsman, M.E., Kolk, A.H., Vicente, M., and Nanninga, N. (1998) Localization of cell division protein FtsQ by immunofluorescence microscopy in dividing and nondividing cells of *Escherichia coli*. *J Bacteriol* **180**: 6107-6116.

Buddelmeijer, N., and Beckwith, J. (2004) A complex of the *Escherichia coli* cell division proteins FtsL, FtsB and FtsQ forms independently of its localization to the septal region. *Mol Microbiol* **52**: 1315-1327.

Buddelmeijer, N., Judson, N., Boyd, D., Mekalanos, J.J., and Beckwith, J. (2002) YgbQ, a cell division protein in *Escherichia coli* and *Vibrio cholerae*, localizes in codependent fashion with FtsL to the division site. *Proc Natl Acad Sci U S A* **99**: 6316-6321.

Cabeen, M.T., and Jacobs-Wagner, C. (2010) The bacterial cytoskeleton. *Annu Rev Genet* **44**: 365-392.

Camberg, J.L., Hoskins, J.R., and Wickner, S. (2009) ClpXP protease degrades the cytoskeletal protein, FtsZ, and modulates FtsZ polymer dynamics. *Proc Natl Acad Sci U S A* **106**: 10614-10619.

Camberg, J.L., Hoskins, J.R., and Wickner, S. (2011) The interplay of ClpXP with the cell division machinery in *Escherichia coli*. *J Bacteriol* **193**: 1911-1918.

Caplan, M.R., and Erickson, H.P. (2003) Apparent cooperative assembly of the bacterial cell division protein FtsZ demonstrated by isothermal titration calorimetry. *J Biol Chem* **278**: 13784-13788.

Carballido-Lopez, R., and Errington, J. (2003) The bacterial cytoskeleton: *in vivo* dynamics of the actin-like protein Mbl of *Bacillus subtilis*. *Dev Cell* **4**: 19-28.

Carson, M.J., Barondess, J., and Beckwith, J. (1991) The FtsQ protein of *Escherichia coli*: membrane topology, abundance, and cell division phenotypes due to overproduction and insertion mutations. *J Bacteriol* **173**: 2187-2195.

Casadaban, M.J., and Cohen, S.N. (1980) Analysis of gene control signals by DNA fusion and cloning in *Escherichia coli*. *J Mol Biol* **138**: 179-207.

Chen, J.C., and Beckwith, J. (2001) FtsQ, FtsL and FtsI require FtsK, but not FtsN, for co-localization with FtsZ during *Escherichia coli* cell division. *Mol Microbiol* **42**: 395-413.

Chen, J.C., Weiss, D.S., Ghigo, J.M., and Beckwith, J. (1999) Septal localization of FtsQ, an essential cell division protein in *Escherichia coli*. *J Bacteriol* **181**: 521-530.

Chen, Y., and Erickson, H.P. (2005) Rapid *in vitro* assembly dynamics and subunit turnover of FtsZ demonstrated by fluorescence resonance energy transfer. *J Biol Chem* **280**: 22549-22554.

Chen, Y., and Erickson, H.P. (2009) FtsZ filament dynamics at steady state: subunit exchange with and without nucleotide hydrolysis. *Biochemistry* **48**: 6664-6673.

Chien, P., Perchuk, B.S., Laub, M.T., Sauer, R.T., and Baker, T.A. (2007) Direct and adaptor-mediated substrate recognition by an essential AAA+ protease. *Proc Natl Acad Sci U S A* **104**: 6590-6595.

Cho, H., McManus, H.R., Dove, S.L., and Bernhardt, T.G. (2011) Nucleoid occlusion factor SlmA is a DNA-activated FtsZ polymerization antagonist. *Proc Natl Acad Sci U S A* **108**: 3773-3778.

Chudakov, D.M., Matz, M.V., Lukyanov, S., and Lukyanov, K.A. (2010) Fluorescent proteins and their applications in imaging living cells and tissues. *Physiol Rev* **90**: 1103-1163.

Chung, K.M., Hsu, H.H., Yeh, H.Y., and Chang, B.Y. (2007) Mechanism of regulation of prokaryotic tubulin-like GTPase FtsZ by membrane protein EzrA. *J Biol Chem* **282**: 14891-14897.

Claessen, D., Emmins, R., Hamoen, L.W., Daniel, R.A., Errington, J., and Edwards, D.H. (2008) Control of the cell elongation-division cycle by shuttling of PBP1 protein in *Bacillus subtilis*. *Mol Microbiol* **68**: 1029-1046.

Corbin, B.D., Geissler, B., Sadasivam, M., and Margolin, W. (2004) Z-ring-independent interaction between a subdomain of FtsA and late septation proteins as revealed by a polar recruitment assay. *J Bacteriol* **186**: 7736-7744.

Cordell, S.C., Robinson, E.J., and Lowe, J. (2003) Crystal structure of the SOS cell division inhibitor SulA and in complex with FtsZ. *Proc Natl Acad Sci U S A* **100**: 7889-7894.

Crozat, E., and Grainge, I. (2010) FtsK DNA translocase: the fast motor that knows where it's going. *Chembiochem* **11**: 2232-2243.

D'Ulisse, V., Fagioli, M., Ghelardini, P., and Paolozzi, L. (2007) Three functional subdomains of the *Escherichia coli* FtsQ protein are involved in its interaction with the other division proteins. *Microbiology* **153**: 124-138.

Dai, K., and Lutkenhaus, J. (1992) The proper ratio of FtsZ to FtsA is required for cell division to occur in *Escherichia coli*. *J Bacteriol* **174**: 6145-6151.

Dai, K., Xu, Y., and Lutkenhaus, J. (1993) Cloning and characterization of *ftsN*, an essential cell division gene in *Escherichia coli* isolated as a multicopy suppressor of *ftsA12*(Ts). *J Bacteriol* **175**: 3790-3797.

Dai, K., Xu, Y., and Lutkenhaus, J. (1996) Topological characterization of the essential *Escherichia coli* cell division protein FtsN. *J Bacteriol* **178**: 1328-1334.

Dajkovic, A., Lan, G., Sun, S.X., Wirtz, D., and Lutkenhaus, J. (2008a) MinC spatially controls bacterial cytokinesis by antagonizing the scaffolding function of FtsZ. *Curr Biol* **18**: 235-244.

Dajkovic, A., Mukherjee, A., and Lutkenhaus, J. (2008b) Investigation of regulation of FtsZ assembly by SulA and development of a model for FtsZ polymerization. *J Bacteriol* **190**: 2513-2526.

Dajkovic, A., Pichoff, S., Lutkenhaus, J., and Wirtz, D. (2010) Cross-linking FtsZ polymers into coherent Z-rings. *Mol Microbiol* **78**: 651-668.

Daniel, R.A., and Errington, J. (2000) Intrinsic instability of the essential cell division protein FtsL of *Bacillus subtilis* and a role for DivIB protein in FtsL turnover. *Mol Microbiol* **36**: 278-289.

Daniel, R.A., and Errington, J. (2003) Control of cell morphogenesis in bacteria: two distinct ways to make a rod-shaped cell. *Cell* **113**: 767-776.

Daniel, R.A., Noirot-Gros, M.F., Noirot, P., and Errington, J. (2006) Multiple interactions between the transmembrane division proteins of *Bacillus subtilis* and the role of FtsL instability in divisome assembly. *J Bacteriol* **188**: 7396-7404.

Datsenko, K.A., and Wanner, B.L. (2000) One-step inactivation of chromosomal genes in *Escherichia coli* K-12 using PCR products. *Proc Natl Acad Sci U S A* **97**: 6640-6645.

Datta, P., Dasgupta, A., Singh, A.K., Mukherjee, P., Kundu, M., and Basu, J. (2006) Interaction between FtsW and penicillin-binding protein 3 (PBP3) directs PBP3 to mid-cell, controls cell septation and mediates the formation of a trimeric complex involving FtsZ, FtsW and PBP3 in mycobacteria. *Mol Microbiol* **62**: 1655-1673.

de Boer, P.A. (2010) Advances in understanding *E. coli* cell fission. *Curr Opin Microbiol* **13**: 730-737.

de Boer, P.A., Crossley, R.E., and Rothfield, L.I. (1989) A division inhibitor and a topological specificity factor coded for by the minicell locus determine proper placement of the division septum in *E. coli*. *Cell* **56**: 641-649.

de Boer, P., Crossley, R., and Rothfield, L. (1992) The essential bacterial cell-division protein FtsZ is a GTPase. *Nature* **359**: 254-256.

de Leeuw, E., Graham, B., Phillips, G.J., ten Hagen-Jongman, C.M., Oudega, B., and Luirink, J. (1999) Molecular characterization of *Escherichia coli* FtsE and FtsX. *Mol Microbiol* **31**: 983-993.

den Blaauwen, T., Aarsman, M.E., Vischer, N.O., and Nanninga, N. (2003) Penicillin-binding protein PBP2 of *Escherichia coli* localizes preferentially in the lateral wall and at mid-cell in comparison with the old cell pole. *Mol Microbiol* **47**: 539-547.

de Pedro, M., Donachie, W.D., Holtje, J., and Schwarz, H. (2001) Constitutive septal murein synthesis in *Escherichia coli* with impaired activity of the morphogenetic proteins RodA and penicillin-binding protein 2. *J Bacteriol* **183**: 4115-4126.

Denome, S.A., Elf, P.K., Henderson, T.A., Nelson, D.E., and Young, K.D. (1999) *Escherichia coli* mutants lacking all possible combinations of eight penicillin binding proteins: viability, characteristics, and implications for peptidoglycan synthesis. *J Bacteriol* **181**: 3981-3993.

Dewar, S.J., Begg, K.J., and Donachie, W.D. (1992) Inhibition of cell division initiation by an imbalance in the ratio of FtsA to FtsZ. *J Bacteriol* **174**: 6314-6316.

Di Lallo, G., Fagioli, M., Barionovi, D., Ghelardini, P., and Paolozzi, L. (2003) Use of a two-hybrid assay to study the assembly of a complex multicomponent protein machinery: bacterial septosome differentiation. *Microbiology* **149**: 3353-3359.

Divakaruni, A.V., Baida, C., White, C.L., and Gober, J.W. (2007) The cell shape proteins MreB and MreC control cell morphogenesis by positioning cell wall synthetic complexes. *Mol Microbiol* **66**: 174-188.

Divakaruni, A.V., Loo, R.R., Xie, Y., Loo, J.A., and Gober, J.W. (2005) The cell-shape protein MreC interacts with extracytoplasmic proteins including cell wall assembly complexes in *Caulobacter crescentus*. *Proc Natl Acad Sci U S A* **102**: 18602-18607.

Dominguez-Escobar, J., Chastanet, A., Crevenna, A.H., Fromion, V., Wedlich-Soldner, R., and Carballido-Lopez, R. (2011) Processive movement of MreB-associated cell wall biosynthetic complexes in bacteria. *Science* **333**: 225-228.

Draper, G.C., McLennan, N., Begg, K., Masters, M., and Donachie, W.D. (1998) Only the N-terminal domain of FtsK functions in cell division. *J Bacteriol* **180**: 4621-4627.

Dubarry, N., and Barre, F.X. (2010) Fully efficient chromosome dimer resolution in *Escherichia coli* cells lacking the integral membrane domain of FtsK. *EMBO J* **29**: 597-605.

Durand-Heredia, J.M., Yu, H.H., De Carlo, S., Lesser, C.F., and Janakiraman, A. (2011) Identification and characterization of ZapC, a stabilizer of the FtsZ ring in *Escherichia coli*. *J Bacteriol* **193**: 1405-1413.

Dye, N.A., Pincus, Z., Theriot, J.A., Shapiro, L., and Gitai, Z. (2005) Two independent spiral structures control cell shape in *Caulobacter*. *Proc Natl Acad Sci U S A* **102**: 18608-18613.

Dziedzic, R., Kiran, M., Plocinski, P., Ziolkiewicz, M., Brzostek, A., Moomey, M., Vadrevu, I.S., Dziadek, J., Madiraju, M., and Rajagopalan, M. (2010) *Mycobacterium tuberculosis* ClpX interacts with FtsZ and interferes with FtsZ assembly. *PLoS One* **5**: e11058.

Ebersbach, G., Galli, E., Moller-Jensen, J., Lowe, J., and Gerdes, K. (2008) Novel coiled-coil cell division factor ZapB stimulates Z-ring assembly and cell division. *Mol Microbiol* **68**: 720-735.

Ebersbach, G., and Gerdes, K. (2001) The double *par* locus of virulence factor pB171: DNA segregation is correlated with oscillation of ParA. *Proc Natl Acad Sci U S A* **98**: 15078-15083.

Erickson, H.P. (2009) Modeling the physics of FtsZ assembly and force generation. *Proc Natl Acad Sci U S A* **106**: 9238-9243.

Erickson, H.P., Anderson, D.E., and Osawa, M. (2010) FtsZ in bacterial cytokinesis: cytoskeleton and force generator all in one. *Microbiol Mol Biol Rev* **74**: 504-528.

Erickson, H.P., and Stoffler, D. (1996) Protofilaments and rings, two conformations of the tubulin family conserved from bacterial FtsZ to alpha/beta and gamma tubulin. *J Cell Biol* **135**: 5-8.

Errington, J., Daniel, R.A., and Scheffers, D.J. (2003) Cytokinesis in bacteria. *Microbiol Mol Biol Rev* **67**: 52-65, table.

Esue, O., Cordero, M., Wirtz, D., and Tseng, Y. (2005a) The assembly of MreB, a prokaryotic homolog of actin. *J Biol Chem* **280**: 2628-2635.

Esue, O., Tseng, Y., and Wirtz, D. (2005b) The rapid onset of elasticity during the assembly of the bacterial cell-division protein FtsZ. *Biochem Biophys Res Commun* **333**: 508-516.

Fadda, D., Pischedda, C., Caldara, F., Whalen, M.B., Anderluzzi, D., Domenici, E., and Massidda, O. (2003) Characterization of *divIVA* and other genes located in the chromosomal region downstream of the *dcw* cluster in *Streptococcus pneumoniae*. *J Bacteriol* **185**: 6209-6214.

Fernandez-Suarez, M., and Ting, A.Y. (2008) Fluorescent probes for super-resolution imaging in living cells. *Nat Rev Mol Cell Biol* **9**: 929-943.

Feucht, A., Lucet, I., Yudkin, M.D., and Errington, J. (2001) Cytological and biochemical characterization of the FtsA cell division protein of *Bacillus subtilis*. *Mol Microbiol* **40**: 115-125.

Figge, R.M., Divakaruni, A.V., and Gober, J.W. (2004) MreB, the cell shape-determining bacterial actin homologue, co-ordinates cell wall morphogenesis in *Caulobacter crescentus*. *Mol Microbiol* **51**: 1321-1332.

Flynn, J.M., Neher, S.B., Kim, Y.I., Sauer, R.T., and Baker, T.A. (2003) Proteomic discovery of cellular substrates of the ClpXP protease reveals five classes of ClpX-recognition signals. *Mol Cell* **11**: 671-683.

Formstone, A., and Errington, J. (2005) A magnesium-dependent *mreB* null mutant: implications for the role of *mreB* in *Bacillus subtilis*. *Mol Microbiol* **55**: 1646-1657.

Fraipont, C., Alexeeva, S., Wolf, B., van der Ploeg, R., Schloesser, M., den Blaauwen, T., and Nguyen-Disteche, M. (2011) The integral membrane FtsW protein and peptidoglycan synthase PBP3 form a subcomplex in *Escherichia coli*. *Microbiology* **157**: 251-259.

Fu, G., Huang, T., Buss, J., Coltharp, C., Hensel, Z., and Xiao, J. (2010) *In vivo* structure of the *E. coli* FtsZ-ring revealed by photoactivated localization microscopy (PALM). *PLoS One* **5**: e12682.

Fu, X., Shih, Y.L., Zhang, Y., and Rothfield, L.I. (2001) The MinE ring required for proper placement of the division site is a mobile structure that changes its cellular location during the *Escherichia coli* division cycle. *Proc Natl Acad Sci U S A* **98**: 980-985.

Garner, E.C., Bernard, R., Wang, W., Zhuang, X., Rudner, D.Z., and Mitchison, T. (2011) Coupled, circumferential motions of the cell wall synthesis machinery and MreB filaments in *B. subtilis*. *Science* **333**: 222-225.

Garti-Levi, S., Hazan, R., Kain, J., Fujita, M., and Ben-Yehuda, S. (2008) The FtsEX ABC transporter directs cellular differentiation in *Bacillus subtilis*. *Mol Microbiol* **69**: 1018-1028.

Gaskin, F., Cantor, C.R., and Shelanski, M.L. (1974) Turbidimetric studies of the *in vitro* assembly and disassembly of porcine neurotubules. *J Mol Biol* **89**: 737-755.

Geissler, B., Elraheb, D., and Margolin, W. (2003) A gain-of-function mutation in *ftsA* bypasses the requirement for the essential cell division gene *zipA* in *Escherichia coli*. *Proc Natl Acad Sci U S A* **100**: 4197-4202.

Gerdes, K. (2009) RodZ, a new player in bacterial cell morphogenesis. *EMBO J* **28**: 171-172.

Gerdes, K., Moller-Jensen, J., and Bugge, J.R. (2000) Plasmid and chromosome partitioning: surprises from phylogeny. *Mol Microbiol* **37**: 455-466.

Gerding, M.A., Liu, B., Bendezu, F.O., Hale, C.A., Bernhardt, T.G., and de Boer, P.A. (2009) Self-enhanced accumulation of FtsN at division sites and roles for other

proteins with a SPOR domain (DamX, DedD, and RlpA) in *Escherichia coli* cell constriction. *J Bacteriol* **191**: 7383-7401.

Gerding, M.A., Ogata, Y., Pecora, N.D., Niki, H., and de Boer, P.A. (2007) The trans-envelope Tol-Pal complex is part of the cell division machinery and required for proper outer-membrane invagination during cell constriction in *E. coli*. *Mol Microbiol* **63**: 1008-1025.

Ghigo, J.M., Weiss, D.S., Chen, J.C., Yarrow, J.C., and Beckwith, J. (1999) Localization of FtsL to the *Escherichia coli* septal ring. *Mol Microbiol* **31**: 725-737.

Ghuysen, J.M. (1968) Use of bacteriolytic enzymes in determination of wall structure and their role in cell metabolism. *Bacteriol Rev* **32**: 425-464.

Giepmans, B.N., Adams, S.R., Ellisman, M.H., and Tsien, R.Y. (2006) The fluorescent toolbox for assessing protein location and function. *Science* **312**: 217-224.

Gill, D.R., Hatfull, G.F., and Salmond, G.P. (1986) A new cell division operon in *Escherichia coli*. *Mol Gen Genet* **205**: 134-145.

Gill, D.R., and Salmond, G.P. (1987) The *Escherichia coli* cell division proteins FtsY, FtsE and FtsX are inner membrane-associated. *Mol Gen Genet* **210**: 504-508.

Gitai, Z., Dye, N., and Shapiro, L. (2004) An actin-like gene can determine cell polarity in bacteria. *Proc Natl Acad Sci U S A* **101**: 8643-8648.

Glauner, B., and Holtje, J.V. (1990) Growth pattern of the murein sacculus of *Escherichia coli*. *J Biol Chem* **265**: 18988-18996.

Goehring, N.W., and Beckwith, J. (2005) Diverse paths to midcell: assembly of the bacterial cell division machinery. *Curr Biol* **15**: R514-R526.

Goehring, N.W., Gonzalez, M.D., and Beckwith, J. (2006) Premature targeting of cell division proteins to midcell reveals hierarchies of protein interactions involved in divisome assembly. *Mol Microbiol* **61**: 33-45.

Goehring, N.W., Gueiros-Filho, F., and Beckwith, J. (2005) Premature targeting of a cell division protein to midcell allows dissection of divisome assembly in *Escherichia coli*. *Genes Dev* **19**: 127-137.

Goehring, N.W., Robichon, C., and Beckwith, J. (2007) Role for the nonessential N-terminus of FtsN in divisome assembly. *J Bacteriol* **189**: 646-649.

Goffin, C., and Ghuysen, J.M. (1998) Multimodular penicillin-binding proteins: an enigmatic family of orthologs and paralogs. *Microbiol Mol Biol Rev* **62**: 1079-1093.

Goley, E.D., Dye, N.A., Werner, J.N., Gitai, Z., and Shapiro, L. (2010) Imaging-based identification of a critical regulator of FtsZ protofilament curvature in *Caulobacter*. *Mol Cell* **39**: 975-987.

Gonzalez, J.M., Jimenez, M., Velez, M., Mingorance, J., Andreu, J.M., Vicente, M., and Rivas, G. (2003) Essential cell division protein FtsZ assembles into one

monomer-thick ribbons under conditions resembling the crowded intracellular environment. *J Biol Chem* **278**: 37664-37671.

Gonzalez, M.D., Akbay, E.A., Boyd, D., and Beckwith, J. (2010) Multiple interaction domains in FtsL, a protein component of the widely conserved bacterial FtsLBQ cell division complex. *J Bacteriol* **192**: 2757-2768.

Gonzalez, M.D., and Beckwith, J. (2009) Divisome under construction: distinct domains of the small membrane protein FtsB are necessary for interaction with multiple cell division proteins. *J Bacteriol* **191**: 2815-2825.

Gonzalez-Leiza, S.M., de Pedro, M.A., and Ayala, J.A. (2011) AmpH, a bifunctional DD-endopeptidase and DD-carboxypeptidase of *Escherichia coli*. J Bacteriol PMID: 22001512.

Gotfredsen, M., and Gerdes, K. (1998) The *Escherichia coli relBE* genes belong to a new toxin-antitoxin gene family. *Mol Microbiol* **29**: 1065-1076.

Gottesman, S. (1981) Genetic control of the SOS system in E. coli. *Cell* **23**: 1-2.

Gregory, J.A., Becker, E.C., and Pogliano, K. (2008) *Bacillus subtilis* MinC destabilizes FtsZ-rings at new cell poles and contributes to the timing of cell division. *Genes Dev* **22**: 3475-3488.

Gueiros-Filho, F.J., and Losick, R. (2002) A widely conserved bacterial cell division protein that promotes assembly of the tubulin-like protein FtsZ. *Genes Dev* **16**: 2544-2556.

Gundogdu, M.E., Kawai, Y., Pavlendova, N., Ogasawara, N., Errington, J., Scheffers, D.J., and Hamoen, L.W. (2011) Large ring polymers align FtsZ polymers for normal septum formation. *EMBO J* **30**: 617-626.

Guzman, L.M., Barondess, J.J., and Beckwith, J. (1992) FtsL, an essential cytoplasmic membrane protein involved in cell division in *Escherichia coli*. *J Bacteriol* **174**: 7716-7728.

Guzman, L.M., Belin, D., Carson, M.J., and Beckwith, J. (1995) Tight regulation, modulation, and high-level expression by vectors containing the arabinose P_{BAD} promoter. *J Bacteriol* **177**: 4121-4130.

Haeusser, D.P., Garza, A.C., Buscher, A.Z., and Levin, P.A. (2007) The division inhibitor EzrA contains a seven-residue patch required for maintaining the dynamic nature of the medial FtsZ ring. *J Bacteriol* **189**: 9001-9010.

Haeusser, D.P., Lee, A.H., Weart, R.B., and Levin, P.A. (2009) ClpX inhibits FtsZ assembly in a manner that does not require its ATP hydrolysis-dependent chaperone activity. *J Bacteriol* **191**: 1986-1991.

Haeusser, D.P., Schwartz, R.L., Smith, A.M., Oates, M.E., and Levin, P.A. (2004) EzrA prevents aberrant cell division by modulating assembly of the cytoskeletal protein FtsZ. *Mol Microbiol* **52**: 801-814.

Hale, C.A., and de Boer, P.A. (1997) Direct binding of FtsZ to ZipA, an essential component of the septal ring structure that mediates cell division in *E. coli*. *Cell* **88**: 175-185.

Hale, C.A., and de Boer, P.A. (1999) Recruitment of ZipA to the septal ring of *Escherichia coli* is dependent on FtsZ and independent of FtsA. *J Bacteriol* **181**: 167-176.

Hale, C.A., and de Boer, P.A. (2002) ZipA is required for recruitment of FtsK, FtsQ, FtsL, and FtsN to the septal ring in *Escherichia coli*. *J Bacteriol* **184**: 2552-2556.

Hale, C.A., Rhee, A.C., and de Boer, P.A. (2000) ZipA-induced bundling of FtsZ polymers mediated by an interaction between C-terminal domains. *J Bacteriol* **182**: 5153-5166.

Hale, C.A., Shiomi, D., Liu, B., Bernhardt, T.G., Margolin, W., Niki, H., and de Boer, P.A. (2011) Identification of *Escherichia coli* ZapC (YcbW) as a component of the division apparatus that binds and bundles FtsZ polymers. *J Bacteriol* **193**: 1393-1404.

Hamoen, L.W., Meile, J.C., de Jong, W., Noirot, P., and Errington, J. (2006) SepF, a novel FtsZ-interacting protein required for a late step in cell division. *Mol Microbiol* **59**: 989-999.

Hara, H., Narita, S., Karibian, D., Park, J.T., Yamamoto, Y., and Nishimura, Y. (2002) Identification and characterization of the *Escherichia coli envC* gene encoding a periplasmic coiled-coil protein with putative peptidase activity. *FEMS Microbiol Lett* **212**: 229-236.

Harz, H., Burgdorf, K., and Holtje, J.V. (1990) Isolation and separation of the glycan strands from murein of *Escherichia coli* by reversed-phase high-performance liquid chromatography. *Anal Biochem* **190**: 120-128.

Hedge, P.J., and Spratt, B.G. (1985) Amino acid substitutions that reduce the affinity of penicillin-binding protein 3 of *Escherichia coli* for cephalexin. *Eur J Biochem* **151**: 111-121.

Heidrich, C., Ursinus, A., Berger, J., Schwarz, H., and Holtje, J.V. (2002) Effects of multiple deletions of murein hydrolases on viability, septum cleavage, and sensitivity to large toxic molecules in *Escherichia coli*. *J Bacteriol* **184**: 6093–6099.

Heidrich, C., Templin, M.F., Ursinus, A., Merdanovic, M., Berger, J., Schwarz, H., de Pedro, M.A., and Holtje, J.V. (2001) Involvement of N-acetylmuramyl-L-alanine amidases in cell separation and antibiotic-induced autolysis of *Escherichia coli*. *Mol Microbiol* **41**: 167-178.

Hellemans, J., Mortier, G., De Paepe, A., Speleman, F., and Vandesompele, J. (2007) qBase relative quantification framework and software for management and automated analysis of real-time quantitative PCR data. *Genome Biol* **8**: R19.

Henriques, A.O., Glaser, P., Piggot, P.J., and Moran, C.P., Jr. (1998) Control of cell shape and elongation by the *rodA* gene in *Bacillus subtilis*. *Mol Microbiol* **28**: 235-247.

Hirota, Y., Ryter, A., and Jacob, F. (1968) Thermosensitive mutants of *E. coli* affected in the processes of DNA synthesis and cellular division. *Cold Spring Harb Symp Quant Biol* **33**: 677-693.

Holtje, J.V. (1998) Growth of the stress-bearing and shape-maintaining murein sacculus of *Escherichia coli*. *Microbiol Mol Biol Rev* **62**: 181-203.

Horger, I., Velasco, E., Mingorance, J., Rivas, G., Tarazona, P., and Velez, M. (2008) Langevin computer simulations of bacterial protein filaments and the force-generating mechanism during cell division. *Phys Rev E Stat Nonlin Soft Matter Phys* **77**: 011902.

Hu, Z., and Lutkenhaus, J. (2001) Topological regulation of cell division in *E. coli*: spatiotemporal oscillation of MinD requires stimulation of its ATPase by MinE and phospholipid. *Mol Cell* **7**: 1337-1343.

Huecas, S., and Andreu, J.M. (2003) Energetics of the cooperative assembly of cell division protein FtsZ and the nucleotide hydrolysis switch. *J Biol Chem* **278**: 46146-46154.

Huecas, S., Llorca, O., Boskovic, J., Martin-Benito, J., Valpuesta, J.M., and Andreu, J.M. (2008) Energetics and geometry of FtsZ polymers: nucleated self-assembly of single protofilaments. *Biophys J* **94**: 1796-1806.

Huisman, O., D'Ari, R., and Gottesman, S. (1984) Cell-division control in *Escherichia coli*: specific induction of the SOS function SfiA protein is sufficient to block septation. *Proc Natl Acad Sci U S A* **81**: 4490-4494.

Ikeda, M., Sato, T., Wachi, M., Jung, H.K., Ishino, F., Kobayashi, Y., and Matsuhashi, M. (1989) Structural similarity among *Escherichia coli* FtsW and RodA proteins and *Bacillus subtilis* SpoVE protein, which function in cell division, cell elongation, and spore formation, respectively. *J Bacteriol* **171**: 6375-6378.

Ishikawa, S., Kawai, Y., Hiramatsu, K., Kuwano, M., and Ogasawara, N. (2006) A new FtsZ-interacting protein, YlmF, complements the activity of FtsA during progression of cell division in *Bacillus subtilis*. *Mol Microbiol* **60**: 1364-1380.

Iwai, N., Ebata, T., Nagura, H., Kitazume, T., Nagai, K., and Wachi, M. (2004) Structure-activity relationship of S-benzylisothiourea derivatives to induce spherical cells in *Escherichia coli*. *Biosci Biotechnol Biochem* **68**: 2265-2269.

Iwai, N., Nagai, K., and Wachi, M. (2002) Novel nemzylisothiourea compound that induces spherical cells in *Echerichia coli* probably by acting on a rod-shape-determining protein(s) other than penicillin-binding protein 2. *Biosci Biotechnol Biochem* **66**: 2658-2662.

Jaiswal, R., and Panda, D. (2009) Differential assembly properties of *Escherichia coli* FtsZ and *Mycobacterium tuberculosis* FtsZ: an analysis using divalent calcium. *J Biochem* **146**: 733-742.

Jenal, U., and Fuchs, T. (1998) An essential protease involved in bacterial cell-cycle control. *EMBO J* **17**: 5658-5669.

Jennings, P.C., Cox, G.C., Monahan, L.G., and Harry, E.J. (2011) Super-resolution imaging of the bacterial cytokinetic protein FtsZ. *Micron* **42**: 336-341.

Jensen, S.O., Thompson, L.S., and Harry, E.J. (2005) Cell division in *Bacillus subtilis*: FtsZ and FtsA association is Z-ring independent, and FtsA is required for efficient midcell Z-Ring assembly. *J Bacteriol* **187**: 6536-6544.

Joris, B., Dive, G., Henriques, A., Piggot, P.J., and Ghuysen, J.M. (1990) The life-cycle proteins RodA of *Escherichia coli* and SpoVE of *Bacillus subtilis* have very similar primary structures. *Mol Microbiol* **4**: 513-517.

Kang, M.S., Kim, S.R., Kwack, P., Lim, B.K., Ahn, S.W., Rho, Y.M., Seong, I.S., Park, S.C., Eom, S.H., Cheong, G.W., and Chung, C.H. (2003) Molecular architecture of the ATP-dependent CodWX protease having an N-terminal serine active site. *EMBO J* **22**: 2893-2902.

Karczmarek, A., Martinez-Arteaga, R., Alexeeva, S., Hansen, F.G., Vicente, M., Nanninga, N., and den Blaauwen, T. (2007) DNA and origin region segregation are not affected by the transition from rod to sphere after inhibition of *Escherichia coli* MreB by A22. *Mol Microbiol* **65**: 51-63.

Karimova, G., Dautin, N., and Ladant, D. (2005) Interaction network among *Escherichia coli* membrane proteins involved in cell division as revealed by bacterial two-hybrid analysis. *J Bacteriol* **187**: 2233-2243.

Karimova, G., Pidoux, J., Ullmann, A., and Ladant, D. (1998) A bacterial two-hybrid system based on a reconstituted signal transduction pathway. *Proc Natl Acad Sci U S A* **95**: 5752-5756.

Karimova, G., Robichon, C., and Ladant, D. (2009) Characterization of YmgF, a 72-residue inner membrane protein that associates with the *Escherichia coli* cell division machinery. *J Bacteriol* **191**: 333-346.

Katis, V.L., Harry, E.J., and Wake, R.G. (1997) The *Bacillus subtilis* division protein DivIC is a highly abundant membrane-bound protein that localizes to the division site. *Mol Microbiol* **26**: 1047-1055.

Kawai, Y., Moriya, S., and Ogasawara, N. (2003) Identification of a protein, YneA, responsible for cell division suppression during the SOS response in *Bacillus subtilis*. *Mol Microbiol* **47**: 1113-1122.

Kawai, Y., and Ogasawara, N. (2006) *Bacillus subtilis* EzrA and FtsL synergistically regulate FtsZ ring dynamics during cell division. *Microbiology* **152**: 1129-1141.

Kennedy, S.P., Chevalier, F., Barre, F.X. (2008) Delayed activation of Xer recombination at *dif* by FtsK during septum assembly in *Escherichia coli*. *Mol Microbiol* **68**: 1018-1028.

Khattar, M.M., Begg, K.J., and Donachie, W.D. (1994) Identification of FtsW and characterization of a new *ftsW* division mutant of *Escherichia coli*. *J Bacteriol* **176**: 7140-7147.

Kim, S.Y., Gitai, Z., Kinkhabwala, A., Shapiro, L., and Moerner, W.E. (2006) Single molecules of the bacterial actin MreB undergo directed treadmilling motion in *Caulobacter crescentus*. *Proc Natl Acad Sci U S A* **103**: 10929-10934.

Kitagawa, M., Ara, T., Arifuzzaman, M., Ioka-Nakamichi, T., Inamoto, E., Toyonaga, H., and Mori, H. (2005) Complete set of ORF clones of *Escherichia coli* ASKA library (a complete set of *E. coli* K-12 ORF archive): unique resources for biological research. *DNA Res* **12**: 291-299.

Kruse, T., Blagoev, B., Lobner-Olesen, A., Wachi, M., Sasaki, K., Iwai, N., Mann, M., and Gerdes, K. (2006) Actin homolog MreB and RNA polymerase interact and are both required for chromosome segregation in *Escherichia coli*. *Genes Dev* **20**: 113-124.

Kruse, T., Bork-Jensen, J., and Gerdes, K. (2005) The morphogenetic MreBCD proteins of *Escherichia coli* form an essential membrane-bound complex. *Mol Microbiol* **55**: 78-89.

Kruse, T., Moller-Jensen, J., Lobner-Olesen, A., and Gerdes, K. (2003) Dysfunctional MreB inhibits chromosome segregation in *Escherichia coli*. *EMBO J* **22**: 5283-5292.

Kuchibhatla, A., Rasheed, A.S., Narayanan, J., Bellare, J., and Panda, D. (2009) An analysis of FtsZ assembly using small angle X-ray scattering and electron microscopy. *Langmuir* **25**: 3775-3785.

Lan, G., Daniels, B.R., Dobrowsky, T.M., Wirtz, D., and Sun, S.X. (2009) Condensation of FtsZ filaments can drive bacterial cell division. *Proc Natl Acad Sci U S A* **106**: 121-126.

Lanzetta, P.A., Alvarez, L.J., Reinach, P.S., and Candia, O.A. (1979) An improved assay for nanomole amounts of inorganic phosphate. *Anal Biochem* **100**: 95-97.

Lara, B., and Ayala, J.A. (2002) Topological characterization of the essential *Escherichia coli* cell division protein FtsW. *FEMS Microbiol Lett* **216**: 23-32.

Lara, B., Rico, A.I., Petruzzelli, S., Santona, A., Dumas, J., Biton, J., Vicente, M., Mingorance, J., and Massidda, O. (2005) Cell division in cocci: localization and properties of the *Streptococcus pneumoniae* FtsA protein. *Mol Microbiol* **55**: 699-711.

Leaver, M., Dominguez-Cuevas, P., Coxhead, J.M., Daniel, R.A., and Errington, J. (2009) Life without a wall or division machine in *Bacillus subtilis*. *Nature* **457**: 849-853.

Leaver, M., and Errington, J. (2005) Roles for MreC and MreD proteins in helical growth of the cylindrical cell wall in *Bacillus subtilis*. *Mol Microbiol* **57**: 1196-1209.

Levin, P.A., Kurtser, I.G., and Grossman, A.D. (1999) Identification and characterization of a negative regulator of FtsZ ring formation in *Bacillus subtilis*. *Proc Natl Acad Sci U S A* **96**: 9642-9647.

Levin, P.A., Schwartz, R.L., and Grossman, A.D. (2001) Polymer stability plays an important role in the positional regulation of FtsZ. *J Bacteriol* **183**: 5449-5452.

Li, Z., Trimble, M.J., Brun, Y.V., and Jensen, G.J. (2007) The structure of FtsZ filaments *in vivo* suggests a force-generating role in cell division. *EMBO J* **26**: 4694-4708.

Loose, M., Kruse, K., and Schwille, P. (2011) Protein self-organization: lessons from the Min system. *Annu Rev Biophys* **40**: 315-336.

Low, H.H., Moncrieffe, M.C., and Lowe, J. (2004) The crystal structure of ZapA and its modulation of FtsZ polymerisation. *J Mol Biol* **341**: 839-852.

Lowe, J., and Amos, L.A. (1998) Crystal structure of the bacterial cell-division protein FtsZ. *Nature* **391**: 203-206.

Lowe, J., and Amos, L.A. (1999) Tubulin-like protofilaments in Ca^{2+}-induced FtsZ sheets. *EMBO J* **18**: 2364-2371.

Lu, C., Reedy, M., and Erickson, H.P. (2000) Straight and curved conformations of FtsZ are regulated by GTP hydrolysis. *J Bacteriol* **182**: 164-170.

Lu, C., Stricker, J., and Erickson, H.P. (1998) FtsZ from *Escherichia coli*, *Azotobacter vinelandii*, and *Thermotoga maritima* - quantitation, GTP hydrolysis, and assembly. *Cell Motil Cytoskeleton* **40**: 71-86.

Lutkenhaus, J. (2007) Assembly dynamics of the bacterial MinCDE system and spatial regulation of the Z-ring. *Annu Rev Biochem* **76**: 539-562.

Lutkenhaus, J. (2009) FtsN - trigger for septation. *J Bacteriol* **191**: 7381-7382.

Ma, X., Ehrhardt, D.W., and Margolin, W. (1996) Colocalization of cell division proteins FtsZ and FtsA to cytoskeletal structures in living *Escherichia coli* cells by using green fluorescent protein. *Proc Natl Acad Sci U S A* **93**: 12998-13003.

Madabhushi, R., and Marians, K.J (2009) Actin homolog MreB affects chromosome segregation by regulating topoisomerase IV in *Escherichia coli*. *Mol Cell* **33**: 171-180.

Marbouty, M., Saguez, C., Cassier-Chauvat, C., and Chauvat, F. (2009) ZipN, an FtsA-like orchestrator of divisome assembly in the model cyanobacterium *Synechocystis* PCC6803. *Mol Microbiol* **74**: 409-420.

Margolin, W. (2000) Themes and variations in prokaryotic cell division. *FEMS Microbiol Rev* **24**: 531-548.

Margolin, W. (2005) FtsZ and the division of prokaryotic cells and organelles. *Nat Rev Mol Cell Biol* **6**: 862-871.

Matsuhashi, M., Wachi, M., and Ishino, F. (1990) Machinery for cell growth and division: penicillin-binding proteins and other proteins. *Res Microbiol* **141**: 89-103.

Mazouni, K., Domain, F., Cassier-Chauvat, C., and Chauvat, F. (2004) Molecular analysis of the key cytokinetic components of cyanobacteria: FtsZ, ZipN and MinCDE. *Mol Microbiol* **52**: 1145-1158.

Mercer, K.L., and Weiss, D.S. (2002) The *Escherichia coli* cell division protein FtsW is required to recruit its cognate transpeptidase, FtsI (PBP3), to the division site. *J Bacteriol* **184**: 904-912.

Miraldi, E.R., Thomas, P.J., and Romberg, L. (2008) Allosteric models for cooperative polymerization of linear polymers. *Biophys J* **95**: 2470-2486.

Miyagishima, S.Y., Wolk, C.P., and Osteryoung, K.W. (2005) Identification of cyanobacterial cell division genes by comparative and mutational analyses. *Mol Microbiol* **56**: 126-143.

Mizusawa, S., and Gottesman, S. (1983) Protein degradation in *Escherichia coli*: the *lon* gene controls the stability of *sulA* protein. *Proc Natl Acad Sci U S A* **80**: 358-362.

Mo, A.H., and Burkholder, W.F. (2010) YneA, an SOS-induced inhibitor of cell division in *Bacillus subtilis*, is regulated posttranslationally and requires the transmembrane region for activity. *J Bacteriol* **192**: 3159-3173.

Mohammadi, T., Ploeger, G.E., Verheul, J., Comvalius, A.D., Martos, A., Alfonso, C., van Marle, J., Rivas, G., and den Blaauwen, T. (2009) The GTPase activity of *Escherichia coli* FtsZ determines the magnitude of the FtsZ polymer bundling by ZapA *in vitro*. *Biochemistry* **48**: 11056-11066.

Mohammadi, T., van Dam, V., Sijbrandi, R., Vernet, T., Zapun, A., Bouhss, A., Diepeveen-de Bruin, M., Nguyen-Disteche, M., de Kruijff, B., and Breukink, E. (2011) Identification of FtsW as a transporter of lipid-linked cell wall precursors across the membrane. *EMBO J* **30**: 1425-1432.

Moll, A., and Thanbichler, M. (2009) FtsN-like proteins are conserved components of the cell division machinery in proteobacteria. *Mol Microbiol* **72**: 1037-1053.

Mosyak, L., Zhang, Y., Glasfeld, E., Haney, S., Stahl, M., Seehra, J., and Somers, W.S. (2000) The bacterial cell-division protein ZipA and its interaction with an FtsZ fragment revealed by X-ray crystallography. *EMBO J* **19**: 3179-3191.

Moy, F.J., Glasfeld, E., Mosyak, L., and Powers, R. (2000) Solution structure of ZipA, a crucial component of *Escherichia coli* cell division. *Biochemistry* **39**: 9146-9156.

Mukherjee, A., Cao, C., and Lutkenhaus, J. (1998) Inhibition of FtsZ polymerization by SulA, an inhibitor of septation in *Escherichia coli*. *Proc Natl Acad Sci U S A* **95**: 2885-2890.

Mukherjee, A., Dai, K., and Lutkenhaus, J. (1993) *Escherichia coli* cell division protein FtsZ is a guanine nucleotide binding protein. *Proc Natl Acad Sci U S A* **90**: 1053-1057.

Mukherjee, A., and Lutkenhaus, J. (1994) Guanine nucleotide-dependent assembly of FtsZ into filaments. *J Bacteriol* **176**: 2754-2758.

Mukherjee, A., and Lutkenhaus, J. (1998) Dynamic assembly of FtsZ regulated by GTP hydrolysis. *EMBO J* **17**: 462-469.

Mukherjee, A., and Lutkenhaus, J. (1999) Analysis of FtsZ assembly by light scattering and determination of the role of divalent metal cations. *J Bacteriol* **181**: 823-832.

Muller, P., Ewers, C., Bertsche, U., Anstett, M., Kallis, T., Breukink, E., Fraipont, C., Terrak, M., Nguyen-Disteche, M., and Vollmer, W. (2007) The essential cell division protein FtsN interacts with the murein (peptidoglycan) synthase PBP1B in *Escherichia coli*. *J Biol Chem* **282**: 36394-36402.

Nanninga, N. (1998) Morphogenesis of *Escherichia coli*. *Microbiol Mol Biol Rev* **62**: 110–129.

Nguyen-Disteche, M., Fraipont, C., Buddelmeijer, N., and Nanninga, N. (1998) The structure and function of *Escherichia coli* penicillin-binding protein 3. *Cell Mol Life Sci* **54**: 309-316.

Nordstrom, K. (2006) Plasmid R1-replication and its control. *Plasmid* **55**: 1-26.

Oliva, M.A., Cordell, S.C., and Lowe, J. (2004) Structural insights into FtsZ protofilament formation. *Nat Struct Mol Biol* **11**: 1243-1250.

Osawa, M., and Erickson, H.P. (2006) FtsZ from divergent foreign bacteria can function for cell division in *Escherichia coli*. *J Bacteriol* **188**: 7132–7140.

Osawa, M., Anderson, D.E., and Erickson, H.P. (2008) Reconstitution of contractile FtsZ rings in liposomes. *Science* **320**: 792-794.

Osawa, M., Anderson, D.E., and Erickson, H.P. (2009) Curved FtsZ protofilaments generate bending forces on liposome membranes. *EMBO J* **28**: 3476-3484.

Osawa, M., and Erickson, H.P. (2011) Inside-out Z rings - constriction with and without GTP hydrolysis. *Mol Microbiol*.

Osborn, M.J., and Rothfield, L. (2007) Cell shape determination in *Escherichia coli*. *Curr Opin Microbiol* **10**: 606-610.

Park, J.T., and Burman, L. (1973) FL-1060: a new penicillin with a unique mode of action. *Biochem Biophys Res Commun* **51**: 863-868.

Patrick, J.E., and Kearns, D.B. (2008) MinJ (YvjD) is a topological determinant of cell division in *Bacillus subtilis*. *Mol Microbiol* **70**: 1166-1179.

Peters, P.C., Migocki, M.D., Thoni, C., and Harry, E.J. (2007) A new assembly pathway for the cytokinetic Z-ring from a dynamic helical structure in vegetatively growing cells of *Bacillus subtilis*. *Mol Microbiol* **64**: 487-499.

Pichoff, S., and Lutkenhaus, J. (2002) Unique and overlapping roles for ZipA and FtsA in septal ring assembly in *Escherichia coli*. *EMBO J* **21**: 685-693.

Pichoff, S., and Lutkenhaus, J. (2005) Tethering the Z-ring to the membrane through a conserved membrane targeting sequence in FtsA. *Mol Microbiol* **55**: 1722-1734.

Pichoff, S., and Lutkenhaus, J. (2007a) Identification of a region of FtsA required for interaction with FtsZ. *Mol Microbiol* **64**: 1129-1138.

Pichoff, S., and Lutkenhaus, J. (2007b) Overview of cell shape: cytoskeletons shape bacterial cells. *Curr Opin Microbiol* **10**: 601-605.

Piette, A., Fraipont, C., den Blaauwen, T., Aarsman, M.E., Pastoret, S., and Nguyen-Disteche, M. (2004) Structural determinants required to target penicillin-binding protein 3 to the septum of *Escherichia coli*. *J Bacteriol* **186**: 6110-6117.

Phoenix, P., and Drapeau, G.R. (1988) Cell division control in *Escherichia coli* K-12: some properties of the *ftsZ84* mutation and suppression of this mutation by the product of a newly identified gene. *J Bacteriol* **170**:4338-4342.

Pogliano, J., Pogliano, K., Weiss, D.S., Losick, R., and Beckwith, J. (1997) Inactivation of FtsI inhibits constriction of the FtsZ cytokinetic ring and delays the assembly of FtsZ rings at potential division sites. *Proc Natl Acad Sci U S A* **94**: 559-564.

Popp, D., Iwasa, M., Narita, A., Erickson, H.P., and Maeda, Y. (2009) FtsZ condensates: an *in vitro* electron microscopy study. *Biopolymers* **91**: 340-350.

Radhakrishnan, S.K., Pritchard, S., and Viollier, P.H. (2010) Coupling prokaryotic cell fate and division control with a bifunctional and oscillating oxidoreductase homolog. *Dev Cell* **18**: 90-101.

Raskin, D.M., and de Boer, P.A. (1999) Rapid pole-to-pole oscillation of a protein required for directing division to the middle of *Escherichia coli*. *Proc Natl Acad Sci U S A* **96**: 4971-4976.

RayChaudhuri, D. (1999) ZipA is a MAP-Tau homolog and is essential for structural integrity of the cytokinetic FtsZ ring during bacterial cell division. *EMBO J* **18**: 2372-2383.

RayChaudhuri, D., and Park, J.T. (1992) *Escherichia coli* cell-division gene *ftsZ* encodes a novel GTP-binding protein. *Nature* **359**: 251-254.

Reddy, M. (2007) Role of FtsEX in cell division of *Escherichia coli*: viability of *ftsEX* mutants is dependent on functional SufI or high osmotic strength. *J Bacteriol* **189**: 98-108.

Rico, A.I., Garcia-Ovalle, M., Mingorance, J., and Vicente, M. (2004) Role of two essential domains of *Escherichia coli* FtsA in localization and progression of the division ring. *Mol Microbiol* **53**: 1359-1371.

Rico, A.I., Garcia-Ovalle, M., Palacios, P., Casanova, M., and Vicente, M. (2010) Role of *Escherichia coli* FtsN protein in the assembly and stability of the cell division ring. *Mol Microbiol* **76**: 760-771.

Rivas, G., Lopez, A., Mingorance, J., Ferrandiz, M.J., Zorrilla, S., Minton, A.P., Vicente, M., and Andreu, J.M. (2000) Magnesium-induced linear self-association of

the FtsZ bacterial cell division protein monomer. The primary steps for FtsZ assembly. *J Biol Chem* **275**: 11740-11749.

Romberg, L., and Mitchison, T.J. (2004) Rate-limiting guanosine 5'-triphosphate hydrolysis during nucleotide turnover by FtsZ, a prokaryotic tubulin homologue involved in bacterial cell division. *Biochemistry* **43**: 282-288.

Romberg, L., Simon, M., and Erickson, H.P. (2001) Polymerization of FtsZ, a bacterial homolog of tubulin, is assembly cooperative? *J Biol Chem* **276**: 11743-11753.

Rowland, S.L., Katis, V.L., Partridge, S.R., and Wake, R.G. (1997) DivIB, FtsZ and cell division in *Bacillus subtilis*. *Mol Microbiol* **23**: 295-302.

Rueda, S., Vicente, M., and Mingorance, J. (2003) Concentration and assembly of the division ring proteins FtsZ, FtsA, and ZipA during the *Escherichia coli* cell cycle. *J Bacteriol* **185**: 3344-3351.

Samaluru, H., SaiSree, L., and Reddy, M. (2007) Role of SufI (FtsP) in cell division of *Escherichia coli*: evidence for its involvement in stabilizing the assembly of the divisome. *J Bacteriol* **189**: 8044-8052.

Sauer, R.T., Bolon, D.N., Burton, B.M., Burton, R.E., Flynn, J.M., Grant, R.A., Hersch, G.L., Joshi, S.A., Kenniston, J.A., Levchenko, I., Neher, S.B., Oakes, E.S., Siddiqui, S.M., Wah, D.A., and Baker, T.A. (2004) Sculpting the proteome with AAA(+) proteases and disassembly machines. *Cell* **119**: 9-18.

Sauvage, E., Kerff, F., Terrak, M., Ayala, J.A., and Charlier, P. (2008) The penicillin-binding proteins: structure and role in peptidoglycan biosynthesis. *FEMS Microbiol Rev* **32**: 234-258.

Scheffers, D.J. (2008) The effect of MinC on FtsZ polymerization is pH dependent and can be counteracted by ZapA. *FEBS Lett* **582**: 2601-2608.

Scheffers, D.J., de Wit, J.G., den Blaauwen, T., and Driessen, A.J. (2002) GTP hydrolysis of cell division protein FtsZ: evidence that the active site is formed by the association of monomers. *Biochemistry* **41**: 521-529.

Schiffer, G., and Holtje, J.V. (1999) Cloning and characterization of PBP 1C, a third member of the multimodular class A penicillin-binding proteins of *Escherichia coli*. *J Biol Chem* **274**: 32031-32039.

Schleifer, K.H., and Kandler, O. (1972) Peptidoglycan types of bacterial cell walls and their taxonomic implications. *Bacterial Rev* **36**: 407-477.

Schmidt, K.L., Peterson, N.D., Kustusch, R.J., Wissel, M.C., Graham, B., Phillips, G.J., and Weiss, D.S. (2004) A predicted ABC transporter, FtsEX, is needed for cell division in *Escherichia coli*. *J Bacteriol* **186**: 785-793.

Schwarz, U., and Leutgeb, W. (1971) Morphogenetic aspects of murein structure and biosynthesis. *J Bacteriol* **106**: 588-595.

Shiomi, D., and Margolin, W. (2007) Dimerization or oligomerization of the actin-like FtsA protein enhances the integrity of the cytokinetic Z-ring. *Mol Microbiol* **66**: 1396-1415.

Shiomi, D., Sakai, M., and Niki, H. (2008) Determination of bacterial rod shape by a novel cytoskeletal membrane protein. *EMBO J* **27**: 3081-3091.

Singh, J.K., Makde, R.D., Kumar, V., and Panda, D. (2007) A membrane protein, EzrA, regulates assembly dynamics of FtsZ by interacting with the C-terminal tail of FtsZ. *Biochemistry* **46**: 11013-11022.

Singh, J.K., Makde, R.D., Kumar, V., and Panda, D. (2008) SepF increases the assembly and bundling of FtsZ polymers and stabilizes FtsZ protofilaments by binding along its length. *J Biol Chem* **283**: 31116-31124.

Skerra, A. (1994) Use of the tetracycline promoter for the tightly regulated production of a murine antibody fragment in *Escherichia coli*. *Gene* **151**: 131-135.

Small, E., Marrington, R., Rodger, A., Scott, D.J., Sloan, K., Roper, D., Dafforn, T.R., and Addinall, S.G. (2007) FtsZ polymer-bundling by the *Escherichia coli* ZapA orthologue, YgfE, involves a conformational change in bound GTP. *J Mol Biol* **369**: 210-221.

Snapp, E.L. (2009) Fluorescent proteins: a cell biologist's user guide. *Trends Cell Biol* **19**: 649-655.

Spratt, B.G. (1977) Temperature-sensitive cell division mutants of *Escherichia coli* with thermolabile penicillin-binding proteins. *J Bacteriol* **131**: 293-305.

Steele, V.R., Bottomley, A.L., Garcia-Lara, J., Kasturiarachchi, J., and Foster, S.J. (2011) Multiple essential roles for EzrA in cell division of *Staphylococcus aureus*. *Mol Microbiol* **80**: 542-555.

Stricker, J., Maddox, P., Salmon, E.D., and Erickson, H.P. (2002) Rapid assembly dynamics of the *Escherichia coli* FtsZ-ring demonstrated by fluorescence recovery after photobleaching. *Proc Natl Acad Sci U S A* **99**: 3171-3175.

Sturgis, J.N. (2001) Organisation and evolution of the *tol-pal* gene cluster. *J Mol Microbiol Biotechnol* **3**: 113-122.

Sugimoto, S., Yamanaka, K., Nishikori, S., Miyagi, A., Ando, T., and Ogura, T. (2010) AAA+ chaperone ClpX regulates dynamics of prokaryotic cytoskeletal protein FtsZ. *J Biol Chem* **285**: 6648-6657.

Sun, Q., and Margolin, W. (1998) FtsZ dynamics during the division cycle of live *Escherichia coli* cells. *J Bacteriol* **180**: 2050-2056.

Sureka, K., Hossain, T., Mukherjee, P., Chatterjee, P., Datta, P., Kundu, M., and Basu, J. (2010) Novel role of phosphorylation-dependent interaction between FtsZ and FipA in mycobacterial cell division. *PLoS One* **5**: e8590.

Tarry, M., Arends, S.J., Roversi, P., Piette, E., Sargent, F., Berks, B.C., Weiss, D.S., and Lea, S.M. (2009) The *Escherichia coli* cell division protein and model Tat substrate SufI (FtsP) localizes to the septal ring and has a multicopper oxidase-like structure. *J Mol Biol* **386**: 504-519.

Thanbichler, M., and Shapiro, L. (2006) MipZ, a spatial regulator coordinating chromosome segregation with cell division in *Caulobacter*. *Cell* **126**: 147-162.

Thanedar, S., and Margolin, W. (2004) FtsZ exhibits rapid movement and oscillation waves in helix-like patterns in *Escherichia coli*. *Curr Biol* **14**: 1167-1173.

Thompson, L.S., Beech, P.L., Real, G., Henriques, A.O., and Harry, E.J. (2006) Requirement for the cell division protein DivIB in polar cell division and engulfment during sporulation in *Bacillus subtilis*. *J Bacteriol* **188**: 7677-7685.

Tiyanont, K., Doan, T., Lazarus, M.B., Fang, X., Rudner, D.Z., and Walker, S. (2006) Imaging peptidoglycan biosynthesis in *Bacillus subtilis* with fluorescent antibiotics. *Proc Natl Acad Sci U S A* **103**: 11033-11038.

Tonthat, N.K., Arold, S.T., Pickering, B.F., Van Dyke, M.W., Liang, S., Lu, Y., Beuria, T.K., Margolin, W., and Schumacher, M.A. (2011) Molecular mechanism by which the nucleoid occlusion factor, SlmA, keeps cytokinesis in check. *EMBO J* **30**: 154-164.

Trusca, D., Scott, S., Thompson, C., and Bramhill, D. (1998) Bacterial SOS checkpoint protein SulA inhibits polymerization of purified FtsZ cell division protein. *J Bacteriol* **180**: 3946-3953.

Typas, A., Banzhaf, M., van den Berg van Saparoea, B., Verheul, J., Biboy, J., Nichols, R.J., Zietek, M., Beilharz, K., Kannenberg, K., von Rechenberg, M., Breukink, E., den Blaauwen, T., Gross, C.A., and Vollmer, W. (2010) Regulation of peptidoglycan synthesis by outer-membrane proteins. *Cell* **143**: 1097-1109.

Uehara, T., Dinh, T., and Bernhardt, T.G. (2009) LytM-domain factors are required for daughter cell separation and rapid ampicillin-induced lysis in *Escherichia coli*. *J Bacteriol* **191**: 5094-5107.

Uehara, T., Parzych, K.R., Dinh, T., and Bernhardt, T.G. (2010) Daughter cell separation is controlled by cytokinetic ring-activated cell wall hydrolysis. *EMBO J* **29**: 1412-1422.

van den Ent, F., Amos, L.A., and Lowe, J. (2001) Prokaryotic origin of the actin cytoskeleton. *Nature* **413**: 39-44.

van den Ent, F., Johnson, C.M., Persons, L., de Boer, P., and Lowe, J. (2010) Bacterial actin MreB assembles in complex with cell shape protein RodZ. *EMBO J* **29**: 1081-1090.

van den Ent, F., Leaver, M., Bendezu, F., Errington, J., de Boer, P., and Lowe, J. (2006) Dimeric structure of the cell shape protein MreC and its functional implications. *Mol Microbiol* **62**: 1631-1642.

van den Ent, F., and Lowe, J. (2000) Crystal structure of the cell division protein FtsA from *Thermotoga maritima*. *EMBO J* **19**: 5300-5307.

van den Ent, F., Vinkenvleugel, T.M., Ind, A., West, P., Veprintsev, D., Nanninga, N., den Blaauwen, T., and Lowe, J. (2008) Structural and mutational analysis of the cell division protein FtsQ. *Mol Microbiol* **68**: 110-123.

Van Melderen, L., and Aertsen, A. (2009) Regulation and quality control by Lon-dependent proteolysis. *Res Microbiol* **160**: 645-651.

van Teeffelen, S., Wang, S., Furchtgott, L., Huang, K.C., Wingreen, N.S., Shaevitz, J.W., and Gitai, Z. (2011) The bacterial actin MreB rotates, and rotation depends on cell-wall assembly. *Proc Natl Acad Sci U S A* **108**: 15822-15827.

Varma, A., de Pedro, M.A., and Young, K.D. (2007) FtsZ directs a second mode of peptidoglycan synthesis in *Escherichia coli*. *J Bacteriol* **189**: 5692-5704.

Vats, P., and Rothfield, L. (2007) Duplication and segregation of the actin (MreB) cytoskeleton during the prokaryotic cell cycle. *Proc Natl Acad Sci U S A* **104**: 17795-17800.

Vega, D., and Ayala, J.A. (2006) The DD-carboxypeptidase activity encoded by *pbp4B* is not essential for the cell growth of *Escherichia coli*. *Arch Microbiol* **185**: 23-27.

Vicente, M., Rico, A.I., Martinez-Arteaga, R., and Mingorance, J. (2006) Septum enlightenment: assembly of bacterial division proteins. *J Bacteriol* **188**: 19-27.

Vicente, M., and Rico, A.I. (2006) The order of the ring: assembly of *Escherichia coli* cell division components. *Mol Microbiol* **61**: 5-8.

Vollmer, W., Blanot, D., and de Pedro, M.A. (2008) Peptidoglycan structure and architecture. *FEMS Microbiol Rev* **32**: 149-167.

Wachi, M., Doi, M., Okada, Y., and Matsuhashi, M. (1989) New *mre* genes *mreC* and *mreD*, responsible for formation of the rod shape of *Escherichia coli* cells. *J Bacteriol* **171**: 6511-6516.

Wachi, M., Doi, M., Tamaki, S., Park, W., Nakajima-Iijima, S., and Matsuhashi, M. (1987) Mutant isolation and molecular cloning of *mre* genes, which determine cell shape, sensitivity to mecillinam, and amount of penicillin-binding proteins in *Escherichia coli*. *J Bacteriol* **169**: 4935-4940.

Wadenpohl, I., and Bramkamp, M. (2010) DivIC stabilizes FtsL against RasP cleavage. *J Bacteriol* **192**: 5260-5263.

Wadsworth, K.D., Rowland, S.L., Harry, E.J., and King, G.F. (2008) The divisomal protein DivIB contains multiple epitopes that mediate its recruitment to incipient division sites. *Mol Microbiol* **67**: 1143-1155.

Walker, J.R., Kovarik, A., Allen, J.S., and Gustafson, R.A. (1975) Regulation of bacterial cell division: temperature-sensitive mutants of *Escherichia coli* that are defective in septum formation. *J Bacteriol* **123**: 693-703.

Wang, X., and Lutkenhaus, J. (1996) Characterization of the *ftsZ* gene from *Mycoplasma pulmonis*, an organism lacking a cell wall. *J Bacteriol* **178**: 2314-2319.

Ward, J.E., Jr., and Lutkenhaus, J. (1985) Overproduction of FtsZ induces minicell formation in *E. coli*. *Cell* **42**: 941-949.

Weart, R.B., Nakano, S., Lane, B.E., Zuber, P., and Levin, P.A. (2005) The ClpX chaperone modulates assembly of the tubulin-like protein FtsZ. *Mol Microbiol* **57**: 238-249.

Weidel, W., Frank, H., and Martin, H.H. (1960) The rigid layer of the cell wall of *Escherichia coli* strain B. *J Gen Microbiol* **22**: 158-166.

Weiss, D.S. (2004) Bacterial cell division and the septal ring. *Mol Microbiol* **54**: 588-597.

Weiss, D.S., Chen, J.C., Ghigo, J.M., Boyd, D., and Beckwith, J. (1999) Localization of FtsI (PBP3) to the septal ring requires its membrane anchor, the Z-ring, FtsA, FtsQ, and FtsL. *J Bacteriol* **181**: 508-520.

Weiss, D.S., Pogliano, K., Carson, M., Guzman, L.M., Fraipont, C., Nguyen-Disteche, M., Losick, R., and Beckwith, J. (1997) Localization of the *Escherichia coli* cell division protein Ftsl (PBP3) to the division site and cell pole. *Mol Microbiol* **25**: 671-681.

Wientjes, F.B., and Nanninga, N. (1991) On the role of the high molecular weight penicillin-binding proteins in the cell cycle of *Escherichia coli*. *Res Microbiol* **142**: 333-344.

Wissel, M.C., and Weiss, D.S. (2004) Genetic analysis of the cell division protein FtsI (PBP3): amino acid substitutions that impair septal localization of FtsI and recruitment of FtsN. *J Bacteriol* **186**: 490-502.

Wu, L.J. (2009) It takes two DNA translocases to untangle chromosomes from the division septum. *Mol Microbiol* **74**: 773-776.

Wu, L.J., and Errington, J. (1997) Septal localization of the SpoIIIE chromosome partitioning protein in *Bacillus subtilis*. *EMBO J* **16**: 2161-2169.

Wu, L.J., and Errington, J. (2004) Coordination of cell division and chromosome segregation by a nucleoid occlusion protein in *Bacillus subtilis*. *Cell* **117**: 915-925.

Wu, L.J., Ishikawa, S., Kawai, Y., Oshima, T., Ogasawara, N., and Errington, J. (2009) Noc protein binds to specific DNA sequences to coordinate cell division with chromosome segregation. *EMBO J* **28**: 1940-1952.

Wu, L.J., Lewis, P.J., Allmansberger, R., Hauser, P.M., and Errington, J. (1995) A conjugation-like mechanism for prespore chromosome partitioning during sporulation in *Bacillus subtilis*. *Genes Dev* **9**: 1316-1326.

Yan, K., Pearce, K.H., and Payne, D.J. (2000) A conserved residue at the extreme C-terminus of FtsZ is critical for the FtsA-FtsZ interaction in *Staphylococcus aureus*. *Biochem Biophys Res Commun* **270**: 387-392.

Yang, J.C., van den Ent, F., Neuhaus, D., Brevier, J., and Lowe, J. (2004) Solution structure and domain architecture of the divisome protein FtsN. *Mol Microbiol* **52**: 651-660.

Yim, L., Vandenbussche, G., Mingorance, J., Rueda, S., Casanova, M., Ruysschaert, J.M., and Vicente, M. (2000) Role of the carboxy terminus of *Escherichia coli* FtsA in self-interaction and cell division. *J Bacteriol* **182**: 6366-6373.

Yu, X.C., and Margolin, W. (1997) Ca^{2+}-mediated GTP-dependent dynamic assembly of bacterial cell division protein FtsZ into asters and polymer networks *in vitro*. *EMBO J* **16**: 5455-5463.

Appendices

Appendix A: Solutions, buffers and media

Name	Composition
Blocking buffer	5% Milk powder in PBS 0.1% Tween
CAA (casamino acids)	20% casamino acids
DNA loading dye	0.04% bromophenol blue in 50% glycerol
Fixative solution	2% formaldehyde 0.2% glutaraldehyde 32 mM NaH_2PO_4 adjust pH to 7.5
Staining solution	50% methanol 10% acetic acid 40% water 10 mg/l Coomassie R-250
Destaining solution	50% methanol 10% acetic acid 40% water
50x TAE buffer	2 M Tris pH 8 50 mM acetic acid 100 mM EDTA
Transfer Buffer (for semi dry transfer)	3 g Tris 14.4 g glycine 150 ml methanol fill up to 1 L with dH_2O

LB medium	10 g Tryptone 5 g Yeast extract 10 g NaCl adjust pH to 7 fill up to 1 L with dH_2O; autoclave
Nutrient Agar	28 g Oxoid Nutrient Agar fill up to 1 L with dH_2O; autoclave
2xTY	16 g Tryptone 10 g Yeast extract 5 g NaCl fill up to 1 L with dH_2O; autoclave
PEM buffer	50 mM PIPES pH 6.5 5 mM $MgCl_2$ 1 mM EDTA
X-Gal solution (2%)	0.2 g X-Gal dissolve in 10 ml dimethylformamide store at −20°C
5xM9 salts	40 g $Na_2HPO_4 \cdot 2H_2O$ 15 g KH_2PO_4 2.5 g NaCl 5 g NH_4Cl fill up to 1 L with dH_2O; autoclave
M9 minimal medium	1x M9 salts 1 mM $MgSO_4$ 0.1 mM $CaCl_2$ 0.1% CAA 1 µg/ml Thiamine
Malachite green solution	0.3 g malachite green oxalate 2 g sodium molybdate 0.5 g Triton X-100 dissolve in 1 L of 0.7 M HCl store in dark at 4°C

Appendix B: Oligonucleotides

Name	Sequence 5'-3'
ForZapB-RFP	TTTGGATCCATGACAATGTCATTAGAAGTG
RevZapB-RFP	AAAGAGCTCGCTTGCGACCTCTTCCATGCGACCCAG
ForFtsZ-GFP	TTTCCCGGGATGTTTGAACCAATGGAACTT
RevFtsZ-GFP	AAACCATGGCGCCGGGGATGCTATCAGCTTGCTTACGCAGGAA
zapA-1	CCCCCGTCGACGGATCCGATGTCTGCACAACCCGTCGA
zapA-2	CCCCCGGTACCTCATTCAAAGTTTTGGTTAG
zapA-3	CCCCCGGATCCAGGAGGAATTCACCATGTCTGCACAACCCGTCGAT
zapA-4	CCCCCAAGCTTTCATTCAAAGTTTTGGTTAG
Xa-zapA	TTTTTGGATCCATCGAGGGAAGGATGTCTGCACAACCCGTCGAT
EG47-For	CCCCCCCATGGGATCGCATCACCATCACCATCACAGAGGATCGCATC ACCATCACCATCACGGA
zapB-82	CCCCCGAATTCGTGTGCCTCGTCATAAAA
zapB-83	CCCCCGGATCCGAGAGGGTACCTCAGACCTCTTCCATGCGAC
pEG83-For	AAAAAGAATTCAGCTGTCATCGTTACCGC
pEG83-Rev	TTTTTGGATCCTCATTCAAAGTTTTGGTT
zapB-84F	TACTTTTGCTTCCAGCATACCTCTCCTGAATTGCAAGGCGTT
zapB-84R	CTGGAAGCAAAAGTACAGCAG
zapB-86F	ACCTCTCCTGAATTGCAAGGC
zapB-86R	GCCTTGCAATTCAGGAGAGGTATGACAATGTCATTA
zapB-86	CCCCCGGATCCGAGAGGGTACCTTACTTGTACAGCTCGTCCAT
zapB-88	CCCCCAGGCCTGAGAGGGTACCTTAATGATGATGATGATGATGGGAT CC
zapA-89R	GCCACCTTCCTGCTG
zapA-89F	CAGCAGGAAGGTGGCATGAGAGGATCTCACCAT
zapA-89	CCCCCCAGCTGTCATTCAAAGTTTTG

zapB-90	CCCCCGGATCCTTACTTGTACAGCTCGTCCAT
zapA-82	CCCCCGGTACCTCAGCAGGAGGAATCACCATGTCTGCACAACCCGTC GAT
zapA-83	CCCCCGGATCCTCATTCAAAGTTTTGGTTAG
zapA-N1	CCCCCAAGCTTGGAGGAATTCACCATGTCTGCACAACCCGTCGAT
zapA-N2	CCCCCGGATCCCCCGGGCAGTTCACACG
zapA-N3	CCCCCGGATCCCCGACTCTAGTGCGTTC
zapA-12	CCCCCGTCGACGGATCCGATGCCTGACCAAAGGGATGCGTTGA
zapA-13	CCCCCGTCGACGGATCCGATGACAAATACTGAACAGTTGGTC
zapB-6	CCCCCGTCGACGGATCCGATGACAATGTCATTAGAAGTG
zapB-61	CCCCCGTCGACGGATCCGATGCTGGAAGCAAAAGTACAG
zapB-62	CCCCCGTCGACGGATCCGATGACCATCACTCTGTTGCAG
zapB-63	CCCCCGTCGACGGATCCGATGGAGCTGAAAGAAAAAAAC
zapB-64	CCCCCGTCGACGGATCCGATGCAGGAAGTTCAAAATGCC
zapB-6b	CCCCCGTCGACGGATCCGATGACAATGGCCGCCGAAGTGTTT
zapB-6c	CCCCCGTCGACGGATCCGATGACAATGTCATTAGCCGCCTTTGAGAAA
zapB-6d	CCCCCGTCGACGGATCCGATGACAATGTCATTAGAAGTGGCCGCCAA ACTGGAA
zapB-6e	CCCCCGTCGACGGATCCGATGACAATGTCATTAGAAGTGTTTGAGGCC GCCGAAGCAAAA
zapB-7	CCCCCGGTACCTCAGACCTCTTCCATGCGACCC
zapB-71	CCCCCGGTACCTCAACGTTCCTGCCAGCCGTTCTG
zapB-72	CCCCCGGTACCTCACAGATGGTTGTTCTCACGCTC
zapB-73	CCCCCGGTACCTCAGCGCTGATGCTGGGCATTTTG
zapB-74	CCCCCGGTACCTCACGACAGTGAGTTGTTTTTTTC
zapA-up	CCTTCGCAGACCATGGGTCT
zapA-down	CAGGGGACTGGCCCGCTTGC
zapB-up	CGAACTTAAAATGTGTGTGCCTCG
zapB-down	GCTGGATATTGAATGATAAGAAAGG
zapC-up	CATCGCTGTTGCTTA

zapC-down	GAAGTCACGCCGCT
slmA-up	GCATCCGAATAACGTCATAAC
slmA-down	TATCGCGAAGAGTTTGGCGTT
minC-up	TCTGAATAAATGGGAGGG
minD-down	TGCAATGTTGGCTGTGTT
sulA-up	TGTTTTCCCGTCACCAAC
sulA-down	TCTTTTTTGTCAGCGACA
zapAqPCR-f	AAAGGGATGCGTTGAATCAG
zapAqPCR-r	CGCGTAGTCACGAGTCTTTG
zapBqPCR-f	TCTGTTGCAGATGGAAATCG
zapBqPCR-r	AGCCGTTCTGCTGTTCTTTC
rpsAqPCR-f	CTGGGTCTGAAACAGTGCAA
rpsAqPCR-r	TCCAAGCCGATGAAGATACC
rpoBqPCR-f	TCCGTATTCCCGATTCAGAG
rpoBqPCR-r	TCACCAGACGCAGTTTAACG
mut41	CCCCCATATGACAATGGCCGCCGAAGTGTTTGAGAAACTG
zapB-H17	AAAAACATATGCTGGAAGCAAAAGTACAG
zapB-H17R	AAAAAGGATCCGACCTCTTCCAT

Publications

Material contained within this thesis has been published in:

Ebersbach, G., **Galli, E.**, Moller-Jensen, J., Lowe, J., and Gerdes, K. (2008)
Novel coiled-coil cell division factor ZapB stimulates Z-ring assembly and cell division.
Mol Microbiol **68**: 720-735.

Galli, E., and Gerdes, K. (2010)
Spatial resolution of two bacterial cell division proteins: ZapA recruits ZapB to the inner face of the Z-ring.
Mol Microbiol **76**: 1514-1526.